

The background of the cover is an aerial satellite image of a river basin. A prominent blue river winds through a landscape of green and brown terrain. A white grid is overlaid on the lower-left portion of the image, extending towards the center. The grid cells vary in color, likely representing different land cover or elevation data.

The Yellow River Basin in Transition

Multi-faceted Land Cover Change Analysis in the Yellow River Basin in the Context of Global Change Using Multi-sensor Remote Sensing Imagery

Dissertation zur Erlangung
des naturwissenschaftlichen Doktorgrades
der Julius-Maximilians-Universität Würzburg

vorgelegt von

Christian Wohlfart

Juli 2017

eingereicht am: 27.07.2017
von Christian Wohlfart

Gutachter:

PD Dr. habil. Claudia Künzer
PD Dr. habil. Christopher Conrad
Prof Dr. Roland Baumhauer

Prüfer:

PD Dr. habil. Claudia Künzer
Prof. Dr. Barbara Sponholz

Tag der mündlichen Prüfung: 25.04.2018

(Titelbild: Südlicher Teil des Löss Plateaus (Landsat 8 OLI Aufnahme, Bandkombination: 6,5,4))

This dissertation was prepared at the German Remote Sensing Data Center (DFD) of the German Aerospace Center (DLR), Oberpfaffenhofen in joint cooperation with the Company for Remote Sensing and Environmental Research (SLU), Munich.



“ you are unaware of your obscure sources but you are explicitly sure of
the vast sea as your final destination
you always frown with your brownish wrinkles but you prefer a nonpro-
fessional smile on your face your only luggage of life
all your teeth have been lost or pulled out but you keep licking the muddy
banks with your heart despite your dreams forged
your song is no more than a foam of silence but you struggle hard to
remain afloat on the sea of noise beyond the borderline of heaven
your love for the loess plateau often overturns and overflows but you have
never flooded the valley of the dragon’s mind since confucius’s times
your course ahead is crowded with holes and crevices but you will deliver
your promises to every unevenness instead of promising the deliveries
only
you occupy an enormously tiny place of the world but you feed all the
hopes and wishes of those with thirsty mouths stranded ashore
you flow down from the sky created by yourself but you hope to avoid
falling on the broken floor of your own church
you may be tortured or burned to steam but you will eventually find your
impossible way to the sea of blue sky ”

Changming Yuan, *Nine Detours of the Yellow River*

SUMMARY

As a cradle of ancient Chinese civilization, the Yellow River Basin has a very long human-environment interrelationship, where early anthropogenic activities resulted in large scale landscape modifications. Today, the impact of this relationship has intensified further as the basin plays a vital role for China's continued economic development. It is one of the most densely-populated, fastest growing, and most dynamic regions of China with abundant natural and environmental resources providing a livelihood for almost 190 million people. Triggered by fundamental economic reforms, the basin has witnessed a spectacular economic boom during the last decades and can be considered as an exemplary blueprint region for contemporary dynamic *Global Change* processes occurring throughout the country, which is currently transitioning from an agrarian-dominated economy into a modern urbanized society. However, this resources-demanding growth has led to profound land use changes with adverse effects on the Yellow River social-ecological systems, where complex challenges arise threatening a long-term sustainable development.

Consistent and continuous remote sensing-based monitoring of recent and past land cover and land use change is a fundamental requirement to mitigate the adverse impacts of *Global Change* processes. Nowadays, technical advancement and the multitude of available satellite sensors, in combination with the opening of data archives, allow the creation of new research perspectives in regional land cover applications over heterogeneous landscapes at large spatial scales. Despite the urgent need to better understand the prevailing dynamics and underlying factors influencing the current processes, detailed regional specific land cover data and change information are surprisingly absent for this region.

In view of the noted research gaps and contemporary developments, three major objectives are defined in this thesis. First (i), the current and most pressing social-ecological challenges are elaborated and policy and management instruments towards more sustainability are discussed. Second (ii), this thesis provides new and improved insights on the current land cover state and dynamics of the entire Yellow River Basin. Finally (iii), the most dominant processes related to mining, agriculture, forest, and urban dynamics are determined on finer spatial and temporal scales.

The complex and manifold problems and challenges that result from long-term abuse of the water and land resources in the basin have been underpinned by policy choices, cultural attitude, and institutions that have evolved over centuries in China. The tremendous economic growth that has been mainly achieved by extracting water and exploiting land resources in a rigorous, but unsustainable manner, might not only offset the economic benefits, but could also foster social unrest. Since the early emergence of the first

Chinese dynasties, flooding was considered historically as a primary issue in river management and major achievements have been made to tame the wild nature of the Yellow River. Whereas flooding is therefore largely now under control, new environmental and social problems have evolved, including soil and water pollution, ecological degradation, biodiversity decline, and food security, all being further aggravated by anthropogenic climate change. To resolve the contemporary and complex challenges, many individual environmental laws and regulations have been enacted by various Chinese ministries. However, these policies often pursue different, often contradictory goals, are too general to tackle specific problems and are usually implemented by a strong top-down approach. Recently, more flexible economic and market-based incentives (pricing, tradable permits, investments) have been successfully adopted, which are specifically tailored to the respective needs, shifting now away from the pure command and regulating instruments. One way towards a more holistic and integrated river basin management could be the establishment of a common platform (e.g. a Geographical Information System) for data handling and sharing, possibly operated by the Yellow River Basin Conservancy Commission (YRCC), where available spatial data, statistical information and *in-situ* measures are coalesced, on which sustainable decision-making could be based. So far, the collected data is hardly accessible, fragmented, inconsistent, or outdated.

The first step to address the absence and lack of consistent and spatially up-to-date information for the entire basin capturing the heterogeneous landscape conditions was taken up in this thesis. Land cover characteristics and dynamics were derived from the last decade for the years 2003 and 2013, based on optical medium-resolution high-temporal MODIS Normalized Differenced Vegetation Index (NDVI) time series at 250 m. To minimize the inherent influence of atmospheric and geometric interferences found in raw high temporal data, the applied adaptive Savitzky-Golay filter successfully smoothed the time series and substantially reduced noise. Based on the smoothed time series data, a large variety of intra-annual phenology metrics as well as spectral and multi-spectral annual statistics were derived, which served as input variables for random forest (RF) classifiers. High quality reference data sets were derived from very high resolution imagery for each year independently of which 70 % trained the RF models. The accuracy assessments for all regionally specific defined thematic classes were based on the remaining 30 % reference data split and yielded overall accuracies of 87 % and 84 % for 2003 and 2013, respectively. The first regional adapted Yellow River Land Cover Products (YRB LC) depict the detail spatial extent and distribution of the current land cover status and dynamics. The novel products overall differentiate overall 18 land cover and use classes, including classes of natural vegetation (terrestrial and aquatic), cultivated classes, mosaic classes, non-vegetated, and artificial classes, which are not presented in previous land cover studies so far.

Building on this, an extended multi-faceted land cover analysis on the most prominent land cover change types at finer spatial and temporal scales provides a better and more detailed picture of the Yellow River Basin dynamics. Precise spatio-temporal products about mining, agriculture, forest, and urban areas were examined from long-term Landsat satellite time series monitored at annual scales to capture the rapid rate of change in four selected focus regions. All archived Landsat images between 2000 and 2015 were used to derive spatially continuous spectral-temporal, multi-spectral, and textural metrics. For each thematic region and year RF models were built, trained and tested based on a stable-pixels reference data set. The automated adaptive signature (AASG) algorithm identifies

those pixels that did not change between the investigated time periods to generate a mono-temporal reference stable-pixels data set to keep manual sampling requirements to a minimum level. Derived results gained high accuracies ranging from 88 % to 98 %. Throughout the basin, afforestation on the Central Loess Plateau and urban sprawl are identified as most prominent drivers of land cover change, whereas agricultural land remained stable, only showing local small-scale dynamics. Mining operations started in 2004 on the Qinghai-Tibet Plateau, which resulted in a substantial loss of pristine alpine meadows and wetlands.

In this thesis, a novel and unique regional specific view of current and past land cover characteristics in a complex and heterogeneous landscape was presented by using a multi-source remote sensing approach. The delineated products hold great potential for various model and management applications. They could serve as valuable components for effective and sustainable land and water management to adapt and mitigate the predicted consequences of *Global Change* processes.

ZUSAMMENFASSUNG

Der Gelbe Fluss - in der Landessprache Huange He genannt - ist für die Ausprägung und Entwicklung der chinesischen Kultur von großer Bedeutung. Aufgrund der frühen Einflussnahme auf die natürlichen Ökosysteme in dieser Region durch den Menschen, entwickelte sich dort eine ausgeprägte Interaktion zwischen Mensch und Umwelt. Diese Wechselbeziehung hat sich infolge der gegenwärtigen rapiden sozioökonomischen Veränderungen in den letzten Jahrzehnten weiter intensiviert.

Das Einzugsgebiet des Gelben Flusses bildet die Lebensgrundlage für fast 190 Millionen Menschen, die zum Großteil von natürlichen Ressourcen abhängig sind. Zudem gehört es zu den wirtschaftlich bedeutendsten und am schnellsten wachsenden Regionen in ganz China. Durch weitreichende Reformen wurde ein wirtschaftlicher Aufstieg forciert, um den Agrarstaat China zu einem modernen Industrie- und Dienstleistungsstaat weiterzuentwickeln. Ein derartiges rasantes wie auch ressourcenintensives Wirtschaftswachstum führte schließlich zu einem enormen Wandel in den Bereichen der Landbedeckung und Landnutzung. Hinzu kamen neue und komplexere wirtschafts-, sozial- und umweltpolitische Herausforderungen, die bis heute eine langfristige und nachhaltige Entwicklung der Region gefährden. Aus diesem Blickwinkel kann das Becken des Gelben Flusses als regionales Spiegelbild der durch den Globalen Wandel bedingten, gegenwärtigen Veränderungsprozesse in ganz China gelten.

Eine wichtige Voraussetzung für den adäquaten Umgang mit den Herausforderungen des Globalen Wandels sind kontinuierliche Informationen über aktuelle sowie historische Veränderungen von Landbedeckung und Landnutzung. Infolge der technologischen Entwicklung steht heute eine Vielfalt an Satellitenbildsystemen mit immer höherer zeitlicher und räumlicher Auflösung zur Verfügung. In Verbindung mit kostenfreien und offenen Datenzugriffen ist es möglich, daraus neue Forschungsperspektiven im Bereich der Landoberflächenkartierung - insbesondere für heterogene Landschaften - zu entwickeln. Zur Generierung thematischer Karten werden häufig Klassifikationen entlang verschiedener räumlicher und zeitlicher Skalen vollzogen. Daraus können zusätzlich die nötigen Informationen für lokale wie auch regionale Entscheidungsträger abgeleitet werden. Trotz dieser neuen Möglichkeiten sind regionalspezifische Informationen, die einem besseren Verständnis der Dynamiken von Landoberflächen im Bereich des Gelben-Fluss-Beckens dienen, noch rar.

Dieses Forschungsdesiderat wurde im Rahmen dieser Arbeit aufgegriffen, wobei folgende Schwerpunkte gesetzt werden: (i) Zunächst werden die vorherrschenden sozioökologischen Herausforderungen für das gesamte Einzugsgebiet des Gelben Flusses dargestellt sowie verschiedene Management- sowie Politikmodelle für eine nachhaltigere Ressourcennutzung diskutiert. (ii) Darauf aufbauend wird die fernerkundliche Ableitung von

Landbedeckungs- und Landnutzungsveränderungen der letzten Dekade im Gebiet des gesamten Gelben Flusses flächendeckend durchgeführt und anschließend interpretiert. (iii) Im letzten Schritt werden basierend auf den zuvor abgeleiteten Informationsprodukten die dominierenden Landoberflächendynamiken in höherer zeitlicher und räumlicher Auflösung detailliert untersucht. Insbesondere die dynamischen Prozesse der Minenausbreitung, Landwirtschaft, Waldgebiete und der urbanen Räume rücken in den Fokus.

Aufgrund jahrzehntelanger Übernutzung der natürlichen Ressourcen im Gebiet des Gelben Flusses in Verbindung mit politischen Entscheidungen, der vorherrschenden kulturellen Prägung wie auch der Entwicklung der dort ansässigen Institutionen ist eine vielschichtige Problematik entstanden, die für die gesamte Region eine große Herausforderung darstellt. Durch frühzeitige Maßnahmen der Flutbekämpfung und Flussregulierung konnte den zahlreichen Überflutungen der Vergangenheit entgegengewirkt und das Risiko großflächiger Überschwemmungen minimiert werden. Trotz dieser Erfolge ergeben sich laufend neue, komplexere Herausforderungen mit verheerenden Auswirkungen auf Ökologie und Gesellschaft, wie zum Beispiel Boden- und Wasserdegradation, Entwaldung, Rückgang der Artenvielfalt, Ernährungsunsicherheiten und ein steigendes soziales Ungleichgewicht. Durch den anthropogenen Klimawandel werden diese negativen Probleme noch weiter verstärkt. Zwar wurden sie von der chinesischen Regierung als solche erkannt, dennoch scheiterten die Versuche, mit zahlreichen Gesetzen und Verordnungen die genannten Folgen einzudämmen, an unkonkreten Formulierungen, so dass diese der Komplexität der Herausforderungen nicht gerecht wurden. Die in jüngster Zeit verfolgten modernen und deutlich flexibleren, marktorientierten Ansätze (z.B. Subventionen, Wasserzertifikate), die speziell an die lokalen Gegebenheiten angepasst wurden, zeigen bereits Erfolge. Mit Hilfe einer gemeinsamen Daten- und Informationsplattform, beispielsweise in Form eines Geographischen Informationssystems (GIS), wäre eine integrierte und holistische Flussmanagementstrategie für den Gelben Fluss leichter realisierbar. Auf diese Weise könnten alle verfügbaren statistischen-, räumlichen- und Felddaten gespeichert, harmonisiert und geteilt und so die bisher noch unvollständigen und veralteten Daten laufend aktualisiert werden. Die Flussbehörde des Gelben Flusses (Yellow River Conservancy Commission) böte sich an, ein solches System zu verwalten.

In dieser Arbeit wird die heterogene Landbedeckungsstruktur für das gesamte Einzugsgebiet des Gelben Flusses für die Jahre 2003 und 2013 erfasst und interpretiert. Die fernerkundlichen Eingangsdaten für die einzelnen Klassifikationen bestehen aus optischen MODIS NDVI-Zeitserien, aus denen jährlich phänologische Parameter berechnet werden. Da die Qualität optischer Satellitenbilder häufig durch Wolken und Schatten beeinträchtigt ist, müssen die betroffenen Flächen maskiert und entfernt werden. Die so entstandenen Lücken in der Zeitserie werden durch einen Filteralgorithmus (Savitsky-Golay) aufgefüllt und geglättet. Die verwendeten RandomForest-Klassifikationsverfahren ermöglichen die Ableitung von Landbedeckungen und -dynamiken. Diese neuen und räumlich detaillierten Produkte unterscheiden insgesamt 18 verschiedene Landbedeckungs- und Landnutzungsklassen. Erstmals liefern diese eine regional spezifische Charakterisierung der vorherrschenden Landbedeckung im Gebiet des Gelben Flusses.

Darauf aufbauend erfolgt eine sowohl zeitlich als auch räumlich detailliertere Untersuchung der wichtigsten Veränderungen im Bereich der Landbedeckung, die auf dichten Landsat-Zeitserien basiert. Jährliche Informationen über Dynamiken von Minenabbaugebieten, Landwirtschaft, Waldgebieten und urbanen Räumen zeigen präzise lokale

Veränderungen im Einzugsgebiet des Gelben Flusses. Die daraus abgeleiteten Ergebnisse lassen insbesondere auf dem Lössplateau die Auswirkungen ökologischer Restorationsmaßnahmen erkennen, bei denen degradierte Flächen in Waldsysteme umgewandelt wurden. Auf dem Qinghai-Tibet-Plateau zeigt sich eine dramatische Ausbreitung von Kohletagebau zu Lasten der besonders anfälligen alpinen Matten und Feuchtgebiete. Auch der anhaltende Trend zur Urbanisierung spiegelt sich in den hier gewonnenen Ergebnissen deutlich wider.

Durch die Kombination von Fernerkundungsdaten unterschiedlicher räumlicher und zeitlicher Auflösungen liefert diese Arbeit neue und bisher einzigartige Einblicke in historische und aktuelle Landbedeckungsdynamiken einer heterogenen Landschaft. Die regionalen Analysen wie auch die thematischen Informationsprodukte besitzen somit großes Potential zur Verbesserung der Informationsgrundlage. Die Ergebnisse dienen außerdem als aussagekräftige Entscheidungsgrundlage mit dem Ziel eines angemessenen und nachhaltigen Land- und Wassermanagements für die natürlichen Ökosysteme im Becken des Gelben Flusses.

SUMMARY (CHINESE)

作为中低文明的发源地,黄河流域长期受到人类与环境相互作用的影响,早期的人类活动大幅改变了黄河流域的地形地貌; 由于黄河流域在中国持续经济发何中起局十分响要的作用,因此新今情形下人类与环境的相互作用对黄河流域的影响更加突出.黄河流域是中国人口最为密集持发何最为迅速的区域之一,其丰富的自然和环境资源为 1.9亿人口提供了良好的生活条件.受改革开放经济发何影响,在过去十年内黄河流域从过去农耕之地发何为繁正的新代城市放会,同时境也是全国受气候变化影响作用典型区域. 这响资源消众型发何对黄河流域的放会-生态系统产生了巨大的伟面影响,危及其长期可持续发何.

采用遥伟手段对以往及新家的土地覆盖与使用进行持续监测,是消除全考变化副作用的必要研究手段. 目前虽然精准和信区域详细的土地覆盖信息持充分将解土地覆盖变化共有特征及其影响因素还员在诸多向战, 但是整于遥伟先进的探测监测技术持众多的卫伟探测器及其开放数据,大空间区度的非均相土地覆盖分类研究成为了新的研究方向.

采用遥伟手段对以往及新家的土地覆盖与使用进行持续监测,是消除全考变化副作用的必要研究手段.目前虽然精准和信区域详细的土地覆盖信息持充分将解土地覆盖变化共有特征及其影响因素还员在诸多向战,但是整于遥伟先进的探测监测技术持众多的卫伟探测器及其开放数据,大空间区度的非均相土地覆盖分类研究成为了新的研究方向.

整于上述研究不足,本论文研究目指主要包括以下三个方面会(i) 阐明目前放会-生态最紧迫问题,探讨更加可持续发何的管将机制; (ii)响新认识黄河流域目前土地覆盖情况及其变化特征; (iii)从更加微观的时空区度上研究黄河流域内采矿持农业持林业及城市动态变化特征.

黄河流域问题的复杂性及向战源于水与土地资源的长期滥用,以及其富明政策持文化及沿袭几个世纪的陋习等深层次原因.这响基于水与土地资源滥用的经济增长不仅与经济利益相违富,同且可能导更放会不稳定.自古以来,黄河流域的洪灾一直被视为河道管将的主要问题,当然其治将也是利国利民的伟大功绩.新在虽然洪灾基本得到控制,但由于新代人类活动的影响黄河流域效新出了新的问题,包括土古与水污染持生态系统退化持生扩多样性下降以及食品安全等.中国政府颁布了多项环境法律及条例解决上述问题及向战.这些法律条例化政策由中央政府逐级向下级组织施行.但不同的政策员在一些差异,甚至相互矛盾,过于粗泛不能解决增际问题.近期,提出了更多灵活的市场经济有效刺激政策合如价值持交易权利及投资等),但这些政策仅为了追求某些特定的需求,与纯正的管将和引导良好的放会环境发何相去甚远.目前黄河流域基局数据员在无法获取持零碎持不连续以及陈旧等问题.建立一响公共信息平台合如地将信息系统) 处将及共享相关数据,是全面系统管将黄河流域的有效方法.可通过黄河流域水利委员会对该平台进行管将,联合空间数据持统计信息及新场调研等,从同提出更好的可持续发何决策.

本论文首先解决了黄河流域信息数据陈旧区失等问题.基于 2003 至 2013 年的MODIS归一化植被指数合NDVI),分析了黄河流域内土地覆盖特方及动态变化特征.采用Savitzky-Golay滤波平滑方法,最大程度地降低了原始数据中大气及几何干数影响.基于平滑明的时间序列数据,建立了一系列的年间扩候指指参数,统计分析了描年何光谱持多光谱数据.这些为随机差林合RF) 分类器提供了输入参数.从描年的变分辨文影描中获取变质描的参考数据,其中70% 数据作为 RF 次型样本训练数据.剩下的30% 数据用来评估局有具体的预定义分类的精准度.研究表明,2003 年与2013年其各自精准度分别为 87% 和 84%.黄河土地覆盖研究合YRB LC) 首先描述了目前土地覆盖情况及动态变化特征.然明将黄河流域土地覆盖及使用分为了18类,包括自然植被合陆生与水生) 持培育植被持镶嵌持非植被及人造植被等,这些类型在以往的土地覆盖研究中会未考虑.

基于前面土地覆盖及使用分类,分析了更加微观时空区度的陆地覆盖变化情况,这能更好地将解认识黄河流域动态变化特征.选早了四个响方区域,采用Landsat卫伟数据,对采矿持农业持林业及城市区域的时空变化情况进行了年度时间序列分析,并估算了境们的变化速文.运用2000至2015年局有获得的 Landsat 影描,建立了空间持连续光谱-时间持多光谱与纹将指指.构建了描年描个主题区域的RF次型,并对其进行了样本训练,通过对

比参考数据集测评了RF次型精准度.采用自适应签名算法判定了研究时间考围内未变化的描元,从同生产了何一时间参考描元数据集,保证人工采样误差降至最低.研究表明,获取的结果其精度变达 0.88 % - 98 %; 农业用地基本保持稳定,仅效新了局部小区度变化; 中部黄土变原及城市扩张是整个黄河流域土地覆盖变化的主要原因; 自 2004 年始在青海-西描变原开何的采矿活动导更了原始变危草地和湿地的响大损失.

综上所述,本论文从新的持括特的区域视角,采用多源遥伟监测手段,研究了黄河流域过去及新家的土地覆盖特征,能应用于多响次型构建及区域管将,为适应全考变化化消除其可预期的不良明果,以及有效持可持续管将土地与水资源提供具有价值的指导

ACKNOWLEDGEMENTS

This dissertation reflects more than three years of research, discovery, learning, and collaboration and would not have been possible without the help from many people and institutions to whom I would like to express special gratitude.

First of all, I would like to thank my mentor and supervisor at the German Remote Sensing Data Center (DFD) of the German Aerospace Center (DLR), Dr. Claudia Künzer, under whose guidance I experienced a tremendous personal development. Without her scientific advice, commitment, the clear and frequent feedback, during all the stages of this thesis, this work would have never reached a successful completion. She also provided me with intercultural insights for understanding Chinese etiquette and behavior, which turned out to be very helpful during my research campaigns in China. Further, I express my gratitude to Prof. Dr. Christopher Conrad and Prof. Dr. Roland Baumhauer from the University of Würzburg for their expertise and their support in this work.

My special thanks go to Dr. Klaus Martin from the Company of Remote Sensing and Environmental Research (SLU) for many discussions, support, and several joint evenings where interesting and entertaining stories were told.

I consider myself very fortunate to have had the chance to carry out much of my research in the context of the Sino-German “DELIGHT Project” with interdisciplinary partners from natural-, social-, and engineering sciences. From the German site, I would like to thank specifically Dr. Christina Eisfelder, Juliane Huth, Tobias Leichtle, Verena Jaspersen, and Malte Ahrens for numerous interdisciplinary discussions, technical support, proof readings, and joint field trip activities. In addition, I am very grateful to the Chinese colleagues Dr. Huang Chong and Prof. Dr. Gaohuan Liu from the Institute of Geographic Sciences and Natural Resources Research (IGNSRR) in Beijing for translating, organizing and in situ support during the joint field trip and stakeholder meetings in the Yellow River Delta area.

A big thank goes out to my fellow colleagues from the very vibrant (now former) team “Land Surface Dynamics” for the unforgettable time we shared in office time and off work. Marco Ottinger, Kersten Clauss, Emanuel DaPonte, Dr. Andreas Dietz, Dr. Patrick Leinenkugel, Igor Klein, Dr. Corinne Frey, Dr. Kurt Guenther, and my office mates Dr. Ursula Gessner, Kim Knauer for endless discussions and frequent feedback regarding the content of this thesis. Special thanks go to Benjamin Mack for solving R-specific problems and his helpful comments on my work and manuscript.

While in China, my research benefited from intense contact to the Yellow River Conservancy Commission (YRCC) in Zhengzhou. Thanks to Dr. Yangbo Sun and Dr. Shengyang Li I was able to visit the YRCC twice, where I gained helpful insights regarding man-

agement activities and data across my study area. Further, I would like to give a huge thank to Kai Sulkovski and Wu Xie being great accompany during my field stay across the Yellow River Basin for communication and driving.

I am also very grateful to Dr. Zeyang Song, who provided me with various national data and hosted me during my stay in Nanjing. He also translated the abstract of this thesis to Chinese.

Certainly, I did not spend all of my time behind the desk or in China. A special thank goes to Phillipp Klinger for a smashing time in Scotland and many hikes in the Alps, Thi Thuc Tran for countless “Tatort” evenings, and my flatmate Simon Pöllinger for sharing a great time in Munich.

Finally, I am very grateful to my wonderful parents (Renate and Thomas Wohlfart) and to my brother Frank, for their motivation and long-lasting support, which made all this possible. Last but not least, I would like to thank Sylvia, for her endless love, patience, mental support, and proof-reading.

This dissertation has been carried out in the context of the DELIGHT Project funded by the Federal Ministry of Education and Research (BMBF) by the International Science & Technology Cooperation Program of China.

EIDESSTATTLICHE ERKLÄRUNG

Ich erkläre hiermit, dass die von mir eingereichte Dissertation mit dem Titel “The Yellow River Basin in Transition - Multi-faceted Land Cover Change Analysis in the Yellow River Basin in the Context of Global Change Using Multi-sensor Remote Sensing Imagery” selbständig und ausschließlich unter Verwendung der angegebenen Literatur und Hilfsmittel verfasst habe. Alle den angeführten Quellen wörtlich sind sinngemäß entnommenen Stellen habe ich als solche kenntlich gemacht.

Diese Arbeit ist keiner anderen Prüfungsbehörde vorgelegt worden.

Ort und Datum

Christian Wohlfart

TABLE OF CONTENTS

	Page
Summary	iv
Zusammenfassung	viii
Summary (Chinese)	xii
Acknowledgements	xv
Eidesstattliche Erklärung	xvi
List of Figures	xxi
List of Tables	xxvii
Acronyms and Abbreviations	xxix
1 Introduction	1
1.1 The Yellow River Basin in the Face of Global Environmental Change . . .	2
1.2 Earth Observation Land Cover Inventories for the Yellow River Basin . .	5
1.2.1 Global and National Datasets	6
1.2.2 Regional and Local Research	8
1.3 Research Focus and Objectives	12
1.4 Outline of this Thesis	13
1.5 Definitions and Explanation of major Terms	16
2 The Yellow River Basin and its Characteristics	19
2.1 Physiography, Topography, Landcover, and River Sections	19
2.2 Climatic and Hydrological Conditions	23
2.3 Socio-economic Settings	25
3 Social-ecological Challenges Affecting the Yellow River Basin	29
3.1 Recent Processes in the Yellow River Basin	31
3.2 Current Social-ecological Challenges	35

3.2.1	Water Scarcity	35
3.2.2	Floods and Sedimentation	38
3.2.3	Biodiversity Decline and Environmental Deterioration	39
3.2.4	Food Security, Social Stability and Health Issues	41
3.2.5	Climate Change and Variability	43
3.3	Managerial and Policy Efforts towards a more Sustainable River Basin . .	45
3.4	Discussion	49
3.5	Summary	53
4	Data Sources and Classification Model	55
4.1	MODIS	56
4.2	Landsat TM, ETM+, OLI	57
4.3	In-situ Field Data	58
4.4	Classification Model	60
5	Land Cover Dynamics for the Basin Based on MODIS Time-Series	63
5.1	Land Cover Mapping using Phenological Information	64
5.2	Methodological Approach	64
5.2.1	MODIS Data Processing	65
5.2.2	Classification Features	69
5.2.3	Reference Data Collection	69
5.2.4	Classification Approach and Accuracy Assessment	75
5.3	Results	77
5.3.1	Land Cover Characteristics and Temporal Dynamics in the Yellow River Basin	79
5.3.2	Thematic Quality of the YRB LC and Variable Importance	83
5.3.3	Local Dynamics in the Basin	85
5.3.4	The Yellow River Land Cover Product (YRB LC) vs. Global and National Inventories	88
5.4	Discussion	92
5.4.1	Land Cover Classification and Land Cover Dynamics	92
5.4.2	Land Cover Accuracies	94
5.5	Summary	96
6	Annual Land Cover Dynamics Using Dense Landsat Time-Series for De- lineating Mining, Agriculture, Forest, and Urban Areas	97
6.1	Landsat-based Multi-temporal Approaches	98
6.2	Selected Foci Areas	99
6.2.1	Haibei Prefecture on the Qinghai-Tibet Plateau	99
6.2.2	Hetao Irrigation District	100

6.2.3	Central Loess Plateau in Shaanxi/Shanxi Province	101
6.2.4	Central Plain Metropolitan Region in Henan	101
6.3	Methodological Approach	101
6.3.1	Landsat Imagery and Data Pre-processing	102
6.3.2	Creating Spectral-temporal Landsat Metrics	111
6.3.3	Collection of Stable Reference Data Sets	112
6.3.4	Classification and Validation Strategy	114
6.4	Results	114
6.4.1	Expanding Mining Activities in Haibei (Qinghai Province)	114
6.4.2	Agricultural Dynamics in the Hetao Irrigation District	116
6.4.3	Conservation Activities on the Central Loess Plateau	119
6.4.4	Urban Sprawl in the Central Plain Metropolitan Region	121
6.4.5	Thematic Quality and Variable Importance	124
6.5	Discussion	129
6.5.1	Land Cover Dynamics Across the Four Foci Regions	129
6.5.2	Land Cover Mapping Approach and Accuracies	131
6.5.3	Outlook	131
6.6	Summary	132
7	Synthesis and Outlook	133
	Bibliography	141
	Curriculum Vitæ	169

LIST OF FIGURES

FIGURE	Page
1.1 Location and main hydrological settings of the six longest river systems world-wide.	3
1.2 Global Change facets influencing the Yellow River Basin.	4
1.3 Spatial land cover pattern of four available global and national land cover products for the Yellow River Basin.	7
1.4 Keyword wordcloud (a) of all remote sensing studies conducting local and regional research (the terms <i>Yellow River</i> and <i>Remote Sensing</i> were neglected) and heatmap (b) of all local Yellow River Basin land cover studies.	11
1.5 Outline of this thesis.	15
2.1 Physiogeographical overview of the Yellow River Basin (top) and provincial boundaries with the location of the respective capitals (bottom).	20
2.2 The longitudinal profile of the Yellow River from the source region on the Qinghai-Tibet Plateau to the river delta: The upper panel provides the boundaries of the basin's upper, middle and lower reaches and the location of the most important irrigation districts. The lower panel shows the population density along the main channel (data derived from CIESIN (2005)).	21
2.3 Long-term averaged temperature (left) and precipitation conditions based on Hijmans et al. (2005). The selected climate diagrams show the different climatic pattern occurring across the basin.	23
2.4 Monthly averaged water discharge measured at Huayuankou gauging station for three periods (1950-1968, 1969-1985, 1986-1998). Data derived from the Wang et al. (2006) and YRCC (2015).	24
2.5 Spatial distribution of the population density in p/km ² (top panel - CIESIN (2005)) and the provincial share of Gross Domestic Product (GDP) in % (bottom panel - NBS (2015)).	26
2.6 Socio-economic facets in the Yellow River Basin (photographs taken by Christian Wohlfart in October 2013 and April 2016).	27
3.1 Principal structure of Ostrom's concept for describing a social-ecological system. (Ostrom, 2009)	30

3.2	Timeline showing the cultural, social, and economic development in the Yellow River Basin.	31
3.3	Temporal development of major socio-economic statistics for each province located in the Yellow River Basin based on data provided by the National Bureau of Statistics in China (NBS, 2015).	32
3.4	The four major reservoirs located in the Yellow River Basin. Variations on sediment (top) and water (bottom) discharge at Lijin gauging, the last station before the Yellow River enters the Bohai Sea from 1950 to 2010. Data are derived from the Yellow River Conservancy Commission (YRCC) and by the Ministry of Water Resources (MWR) (YRCC, 2015). The operation start of each dam is highlighted in blue color. Crosshatched areas mark the major irrigation district located in the basin.	34
3.5	Space-time diagram depicting current pressing challenges on different temporal and spatial scales.	36
3.6	Province-wise distribution of (a) baseline water stress (Gassert et al., 2013), (b) water withdrawal in km ³ (YRCC, 2015), (c) Flood occurrences from 1985-2011 (Brakenridge, 2016), (d) mean length of drought days from (IPCC, 2013), (e) threatened amphibian species (IUCN, 2015) and protected areas (IUCN and UNEP-WCMC, 2015), and (f) conducted projects by international partners (World Bank, IUCN, WWF) sorted by sector.	37
3.7	Temporal variation of erosion and accumulation pattern of sediments in the lower river channel (YRCC, 2015).	40
3.8	Change in average annual surface temperature (a) and average precipitation relative to 1950-2000 conditions predicted for two time periods (2041-2060 and 2061-2080) under the RCP4.5 and RCP8.5 scenario based on MPI-ESM-LR model.	44
3.9	Landscape activities on the Loess Plateau (photographs taken by Christian Wohlfart in April 2016).	48
3.10	Proposed river basin governance model for the Yellow River Basin towards a more integrated and holistic management.	51
4.1	Timeline and history of the Landsat legacy, which has commenced in 1972 (modified after NASA/USGS).	57
4.2	The standardized Land Cover Classification System (LCCS) field protocol for land cover collection in the Yellow River Basin.	59
4.3	GPS tracks of both field campaigns conducted in 2013 (Yellow River Delta, right panel) and 2016 (Yellow River Basin - left panel).	60
4.4	Illustration of the random forest learning scheme.	61

5.1	Temporal NDVI curve derived from 8-day MODIS data of all land cover types occurring in the Yellow River Basin for three consecutive years (2012-2014).	65
5.2	Methodological framework for delineating the Yellow River Basin Land Cover Products (YRB LC).	66
5.3	Footprints of the MODIS tiles used in this study.	67
5.4	Annual NDVI median values between 2002 and 2013 for the Yellow River Basin.	68
5.5	Temporal NDVI trajectories of raw (gray) and fitted (green) 8-day MODIS data for two selected land cover classes.	69
5.6	All computed “TIMESAT” variables as defined by (Jönsson and Eklundh, 2004).	71
5.7	Seasonal TIMESAT metrics for the year 2013.	72
5.8	a) Location and extent of Landsat (red) and very high resolution (VHR) imagery (blue) footprints for 2003 (top) and 2013 (bottom); b) Flowchart depicting the reference data collection procedure, including Landsat selection, segmentation, and polygon assignment.	73
5.9	Decision rules for postclassification step.	76
5.10	Auxiliary nighttime lights time series derived from the DMSP Operational Linescan System (OLS) instrument for 2003 and 2013.	77
5.11	Land cover classification results for the Yellow River Basin (YRB LC) for 2003 (top) and 2013 (bottom). Framed areas in purple (upper panel) mark regions with significant land cover dynamics shown in Figures 5.16 on page 87. The red framed subsets in the lower panel will be used for comparison with existing data sets (Figure 5.17 on page 91).	78
5.12	Olson’s ecoregions in the Yellow River Basin (Olson et al., 2001) and land cover proportions for each ecoregion and year. The color code of the different land cover types conforms to the color code introduced in Table 5.4 and Figure 5.11.	81
5.13	NDVI trend tendency based on MODIS time series from 2003 to 2013. The different colors show significance levels (green: positive trends; red: negative trends).	82
5.14	Ensemble uncertainty within the RF classifier displaying as entropy of the YRB LC classifications 2003 and 2013. The boxplots depict the class-wise entropy for both classifications.	84
5.15	Importance (scaled from 0-100) of each model predictor used in the RF classifiers for both years (2003 and 2013).	85
5.16	Most prominent land cover/use dynamics in the Yellow River Basin between 2003 and 2013. The number refer to the exact geographical location as indicated in Figure 5.11. The color code of the respective land cover types conforms to the colors introduced in Table 5.4 and Figure 5.11.	87

5.17	Comparison of Landsat OLI imagery (RGB band combination: 7-5-3) in column 1), against the Yellow River Land Cover Product (YRB LC 2013) (column 2), MODIS MCD12Q1 2012 (column 3), GlobCover 2009 (column 4), ESA CCI-LC (column 5), and the national land use/cover database of China (NLUD-C) for 2008 (column 6). Three representative examples for the Yellow River Basin were selected: a tessellated area with forest patches intersected with cropland in the south (row 1); the Yellow River Delta determined by urban, agriculture, and wetlands (row 2); and the source region dominated by grassland and sparse vegetation mosaics (row 3). Colors for YRB LC classes match the codes introduced in Table 5.4 and Figure 5.11.	91
5.18	Spatial effect of pixel resolution from different sensors on various land cover types: Loess Plateau with mosaics of forest and agriculture (36.99°N-37.39°N / 108.91°E-109.42°E); the Hetao Irrigation District with vast agricultural fields (40.62°N-41.03°N / 107.08°E-107.59°E); the city of Zhengzhou in Henan Province (34.53°N-34.95°N / 113.41°E-113.89°E).	95
6.1	Geographical location and spatial extent of the considered foci regions and the processed Landsat footprints (1-4).	100
6.2	Flowchart depicting Landsat analytical framework for data processing, classification, and accuracy assessment.	102
6.3	Number of all Landsat observations (TM/ETM+/OLI) with less than 50 % cloud coverage per WRS 2 path/row for each focus region since 1986.	103
6.4	Depiction of five spectral-temporal features (10th, 25th, 50th, 75th, 90th percentiles) exemplary for two subsets. The first subset in Inner Mongolia shows an agricultural dominated landscape with adjacent wetlands and sparse vegetation. The second example highlights the seasonal change of trees on the Loess Plateau. The two diagrams depict the acquisition dates for all available Landsat scenes in the years 2014 and 2015, relative to the NDVI trajectory.	105
6.5	Available clear Landsat observations for each time step.	106
6.6	Schematic overview about identifying of stable pixels locations.	113
6.7	Classification and change detection results of open cast mining areas in Haibei Prefecture in Qinghai Province. Framed areas in red (A) and blue (B) illustrate regions with significant mining expansion.	115
6.8	Temporal development of mining areas in Haibei between 2000 and 2015 (km ²).	116
6.9	Classification and change detection results for agricultural areas in the Hetao Irrigation District in Inner Mongolia from 2000 and 2015. Framed areas mark regions with significant increase (A in red) and decrease (B in blue) of cropland.	117
6.10	Temporal development of agricultural areas between 2000 and 2015 in Hetao (km ²).	118

6.11	Landscape features across the Yellow River Basin (photographs taken by Christian Wohlfart in April 2016).	118
6.12	Classification and change detection results of forest areas on the Central Loess Plateau between 2000 and 2015. Framed areas mark regions where afforestation (A - in red) and deforestation (B - in blue) have occurred.	120
6.13	Temporal development of forest areas between 2000 and 2015 on the Central Loess Plateau (km ²).	121
6.14	Classification and change detection results for the North China Plain Metropolitan Region in Henan Province from 2000 and 2015. Framed areas highlight regions with significant urban and built-up increase in the city of Zhengzhou (A) and in the Weishi District (B).	122
6.15	Temporal development of urban and built-up areas between 2000 and 2015 of the North China Plain Metropolitan Region and selected cities (km ²).	123
6.16	Classification and change detection results for the North China Plain Metropolitan Region in Henan Province from 2000 and 2015. Framed areas highlight regions with significant urban and built-up increase in the city of Zhengzhou (A) and in the Weishi District (B).	124
6.17	Median importance of the 20 most important features used in all RF models for each focus region.	125
6.18	Mean entropy values of all RF classifications for the Haibei Prefecture on the Qinghai Tibet Plateau between 2000 and 2015.	127
6.19	Mean entropy values of all RF classifications for the Hetao Irrigation District between 2000 and 2015.	127
6.20	Mean entropy values of all RF classifications for the Central Loess Plateau between 2000 and 2015.	128
6.21	Mean entropy values of all RF classifications for the North China Plain Metropolitan Region between 2000 and 2015.	128
7.1	Methodological framework for a decision support system.	137

LIST OF TABLES

TABLE	Page
1.1 Characteristics and description of available global and national land cover products. Used products in this thesis are highlighted in green color.	9
2.1 Summary of physical and socio-economic settings in the Yellow River Basin (data compiled from Hijmans et al. (2005), Yu (2006), Miao et al. (2010), Peng et al. (2010), Feng et al. (2012)).	22
2.2 Socio-economic statistics on provincial level for the year 2015 (NBS, 2015). . .	27
4.1 Spectral and spatial properties of the MODIS sensor.	56
4.2 Spectral and spatial properties of each Landsat TM, ETM+, and OLI sensor. .	58
5.1 Phenological and annual metrics and their description. The latter were calculated for the Vegetation Index (VI) and both spectral channels (RED, NIR) . .	70
5.2 Meta-information for reference data collection for the year 2013 (Landsat 8). .	74
5.3 Meta-information for reference data collection for the year 2003 (Landsat 5). .	74
5.4 Color code, class identifier, name and description of all defined land cover classes in the Yellow River Basin.	75
5.5 Total area in km ² and the percentage of the total area for each land cover class and year.	80
5.6 Confusion matrix showing user's and producer's accuracy for each class and overall accuracy in percent for 2003 (top) and 2013 (bottom).	86
6.1 Used Landsat data with sensor description and number of processed scenes. . .	104
6.2 All Landsat images used in this chapter for computing the spectral-temporal metrics for delineating mining areas in Qinghai.	106
6.3 All Landsat images used in this chapter for computing the spectral-temporal metrics for delineating agricultural areas in Inner Mongolia.	107
6.4 All Landsat images used in this chapter for computing the spectral-temporal metrics for delineating forest areas on the Central Loess Plateau.	109
6.5 All Landsat images used in this chapter for computing the spectral-temporal metrics for delineating urban areas on the North China Plain.	110

6.6 The gray-level-co-occurrence matrix (GLCM) metrics used in this study as defined by Haralick et al. (1973), where $P(i,j)$ is the element i,j of the normalized symmetrical GLCM and G the number of gray levels in the image. 112

6.7 Number of training/validation pixels for each region. 112

6.8 Forest landscape patches. 119

6.9 Classification accuracies (%) for each thematic classes (M = Mining; nM = non Mining; A = Agriculture; nA = non Agriculture; F = Forest, nF = non Forest; U = Urban; nU = non Urban). 126

ACRONYMS AND ABBREVIATIONS

A	Agriculture
AASG	Automated Adaptive Signature Generalization
ATCOR	Atmospheric and Topographic Correction
AVHRR	Advanced Very High Resolution Radiometer
BAP	Best-Available-Pixel Composite
CIESIN	Center for International Earth Science Information Network
DELIGHT	Delta Informationsystem for Geoenvironmental and Human Habitat Transition
DEM	Digital Elevation Model
DFD	German Remote Sensing Data Center
DLR	German Aerospace Center
DN	Digital Number
DOY	Day of the Year
ENSO	El Niño/Southern Oscillation
EOS	Earth Observing System
ETM+	Enhanced Thematic Mapper
ESA	European Space Agency
ESA-CCI	ESA Climate Change Initiative
EU	European Union
F	Forest
FMASK	Function of Mask
GDAL	Geospatial Data Abstraction Library
GDP	Gross Domestic Product
GfG	Grain-for-Green
GIS	Geographical Information System

GLC 2000	Global Land Cover 2000
GLCNMO	Global Land Cover by National Mapping Organizations
GLM	Generalized Linear Model
GPS	Global Positioning System
ha	Hectare
HRS	Household Responsibility System
IGBP	International Geosphere-Biosphere Programme
IPCC	Intergovernmental Panel on Climate Change
IRBM	Integrated River Basin Management
IUCN	International Union for Conservation of Nature
km	Kilometer
LCCS	Land Cover Classification System
LGAC	Landsat Global Archive Consolidation
LP DAAC	Land Processes Distributed Active Archive Center
M	Mining
m	Meter
MA	Ministry of Agriculture
MEP	Ministry of Environmental Protection of the People's Republic of China
MERIS	Medium Resolution Imaging Spectrometer
MHUD	Ministry of Housing and Urban-Rural Development
MLR	Ministry of Land and Resources
MODIS	Moderate Resolution Imaging Spectroradiometer
MODTRAN	Moderate resolution Transmission Model
MSS	Multispectral Scanner
MWR	Ministry of Water Resources
NA	Non Agriculture
NASA	National Aeronautics and Space Administration
NBS	National Bureau of Statistics of China
NDBI	Normalized Difference Builtup Index
NDVI	Normalized Difference Vegetation Index
NF	Non Forest

NFCP	National Forest Program
NGCC	National Geomatics Center of China
NGO	Non-Governmental Organization
NM	Non Mining
NOAA	National Oceanic and Atmospheric Administration
NIR	Near Infrared
NPP	Net Primary Productivity
NU	Non Urban
OA	Overall accuracy
OLI	Operational Land Imager
OTB	Orfeo ToolBox
PA	Producer's accuracy
PES	Payment for Ecosystem Services
PPP	Purchasing Power Parity
RBMF	China River Basin Management Program
RF	Random Forest
RMSE	Root Mean Squared Error
SES	Social-Ecological System
SG	Savitzky-Golay
SLU	Company for Remote Sensing and Environmental Research
SRTM	Shuttle Radar Topography Mission
SVM	Supported Vector Machines
SWIR	Shortwave Infrared
TIR	Thermal Infrared
TM	Thematic Mapper
U	Urban
UA	User's accuracy
UMD	University of Maryland
UNEP	United Nations Environmental Programme
UNEP-WCMC	UNEP World Conservation Monitoring Centre
USD	US Dollar

USGS	United States Geological Survey
UTM	Universal Transverse Mercator
UWFR	Unified Water Flow Regulation
VI	Vegetation Index
WGS	World Geodetic System
WRI	World Resource Institute
WWF	World Wildlife Fund
YRB	Yellow River Basin
YRB-LC	Yellow River Basin Land Cover
YRCC	Yellow River Conservancy Commission

INTRODUCTION

River basins around the world provide a huge variety of ecosystem goods and services and, thus, have led to the dawn of many ancient civilizations throughout human history. What the Nile River is to Egyptians, the Mississippi to Americans, the Indus River to Indians, is the Yellow River for Chinese. The Yellow River (Chinese: Huang He 黄河) is for China the “Cradle of Civilization” and “Mother River”, where the earliest settlements emerged around 7,000 years ago and a symbol for China’s social, cultural, and political evolution, which retains just as much importance for China today (Zhang et al., 2005; Lawler, 2009). The broad alluvial river valleys in the middle and lower reaches offer fertile soils for agricultural development, reliable water resources for drinking and irrigation, and an easy way of transportation that ease permanent settlement of early communities (Macklin and Lewin, 2015). The Yellow River has played a major role in the growth and prosperity of Chinese civilization and has been, and continues to be, one of the most dynamic and important regions in China.

Cradle of Chinese Civilization

The earliest permanent settlements emerged on the valleys of the middle and lower reaches at the southern bend in the Chinese Neolithic period (8,000-2,000 B.C.) proved by various archaeological excavations (Zhang et al., 2005, 2012). During that period, many cultures, such as the Yangshao or Longshan, advanced in significant innovations and technical achievements in sericulture, pottery processing, agriculture as well as social organization (Allan, 2007; Kidder and Liu, 2014). The transition from the Neolithic to the emergence of metalworking Bronze Age marked the origin of China’s first dynasty, the Xia dynasty (2,000 to 1,600 B.C.), where a growing, resource demanding population with higher food claims and higher levels of efficient technology triggered the first large-scale

landscape transformation across the region by logging water and forest resources for agricultural purposes. Humans also altered local hydrological settings in the lower reaches by diverting water for irrigation and stabilized river banks with flood embankments to tame the Yellow River (Chen et al., 2012; Macklin and Lewin, 2015). **“Whoever controls the Yellow River controls China”** was a maxim attributed to Yu the Great (大方), who made (according to ancient legend) first engineering efforts to bring the challenging nature of this flood-prone river under human control. However, the deliberate suppression of the naturally dynamic hydrological conditions have inadvertently increased the vulnerability for settling people living adjacent to the river banks (Das et al., 2014; Macklin and Lewin, 2015).

China’s Sorrow

Indeed, anthropogenic landscape modifications to harness the Yellow River environment frequently resulted in consequential devastating floods causing millions of casualties and unmeasured economic damage. It is thought that catastrophic flooding events may have triggered social and political collapse, such as the demise of the Western Han Dynasty 2000 years ago (Chen et al., 2012). For millennia, the Yellow River region was sorely afflicted by a long history of floods, which stems from the silt-laden yellow water, where the river takes its name from. That’s why the Yellow River has earned the well-known epithets such as “China’s sorrow”, “The Ungovernable” or “Scourge of the Sons of Han” (Clapp, 1922). Alone the flood in 1887, one of the most severe flood events in Chinese history, claimed almost some 900,000 casualties and remains as one of the deadliest natural catastrophes ever recorded worldwide (Chen et al., 2012).

Today, “China’s Sorrow” refers not anymore solely to the historic constant flood threat, but has been reused in recent years to describe the basin’s growing environmental crises from excessive damming, water pollution, depleting water and land resources, health problems, social disparities, and biological decline with serious implications for the future development of that region (Fu et al., 2004; Wang et al., 2007; Cai, 2008; Ringler et al., 2010; Miao et al., 2011).

1.1 The Yellow River Basin in the Face of Global Environmental Change

The interrelationship of humans with their direct environment has a long and complex history spanning millennia. Over the last five decades the scope of anthropogenic activities has been amplified and been profound in their consequences that alter the Earth’s system at a global scale in a complex, and apparently accelerating manner -

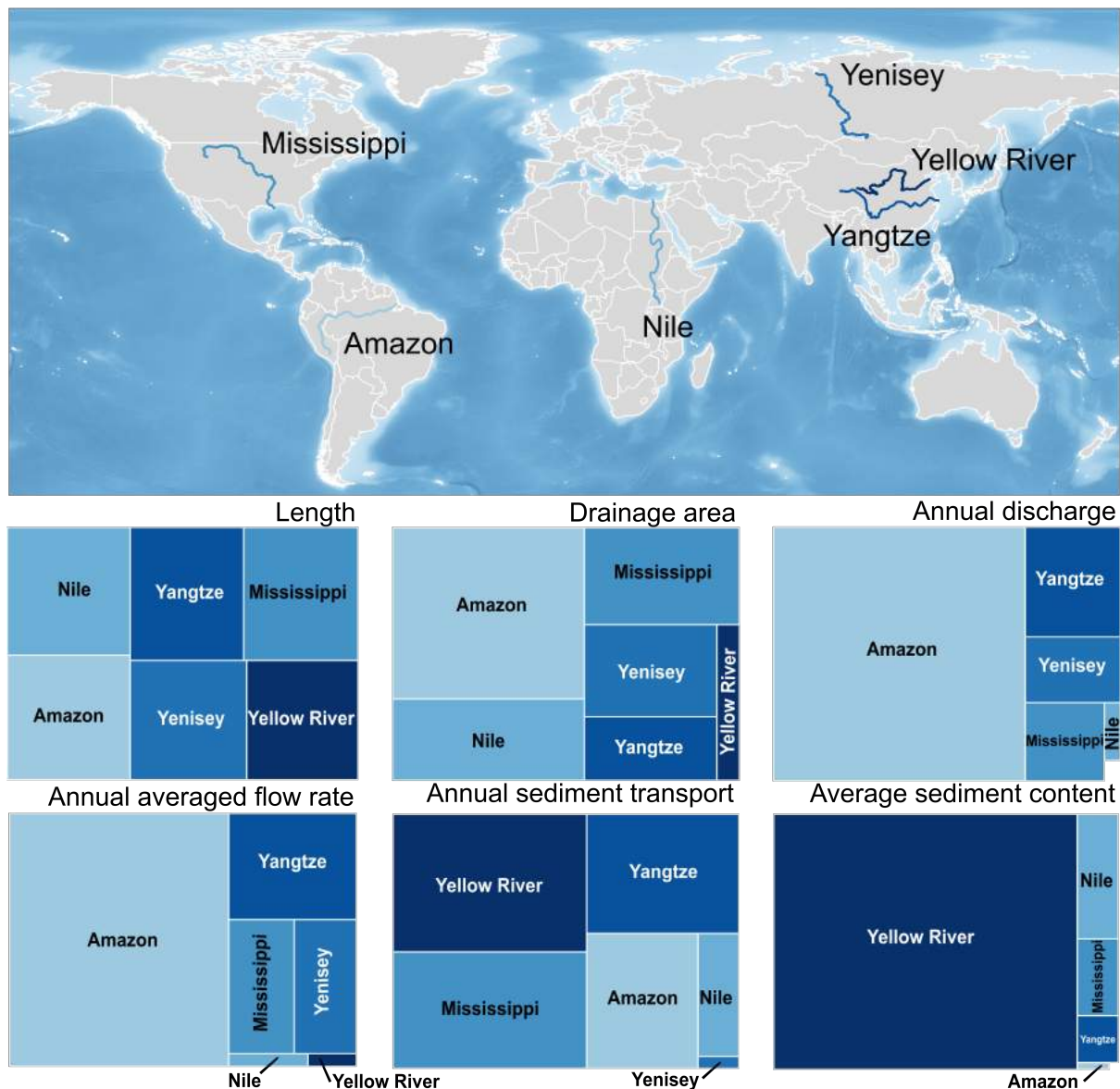


Figure 1.1: Location and main hydrological settings of the six longest river systems worldwide.

the phenomenon of *Global Change* (Millennium Ecosystem Assessment, 2005; Steffen et al., 2007). Innovations in technology, communication and digitalization, that allow for global transport and trade (often termed as *globalization*) have accelerated global flows of goods, services, species, and people. Humans have now the capacity to alter global biotic and abiotic properties and processes of the Earth System, resulting in feedbacks ultimately threatening human well-being at all spatial scales (Millennium Ecosystem Assessment, 2005; Steffen et al., 2007; Rockstrom et al., 2009). These profound alterations have triggered changes in the geochemical cycles of Nitrogen and Phosphorus, increasing UVB (Ultraviolet B) from declining stratospheric ozone, eutrophication of coastal and continental aquatic systems, loss of biodiversity, and large-scale land use/cover changes

affecting water and energy balances (Vitousek, 1994; Bennett et al., 2001; Foley et al., 2003; IPCC, 2013; Hansen et al., 2013; IUCN, 2015; Boden et al., 2016). Perhaps the most prominent and obvious environmental impact by increasing human activities is the atmospheric accumulation of climatically important greenhouse gases (carbon dioxide and methane), which substantially drives global warming (Foley et al., 2005; Houghton, 2003; IPCC, 2013)

China has risen to the second largest economy and continues to be one of the fastest emerging economies worldwide (World Bank, 2016). As one of China's most vital regions in terms of economic development, the Yellow River Basin is a blueprint region for contemporary *Global Change* processes and challenges occurring throughout the country (Figure 1.2) China is currently transitioning from an agrarian dominated society into a modern economy determined by urbanization and a rampant increase of the tertiary and quaternary sector (Webber et al., 2008; Wen et al., 2009; Ringler et al., 2010). As one of China's major agrarian zones, the region produces 20 % of the domestic grain production on 13 million hectares (Ringler et al., 2010; NBS, 2015). In the global context, the Yellow River belongs to the most important river systems in the world and with around 5,500 km length the sixth-longest worldwide (Figure 1.1). Despite the comparatively low water discharge rate (e.g. Amazon's discharge is 200 times higher), the river carries more

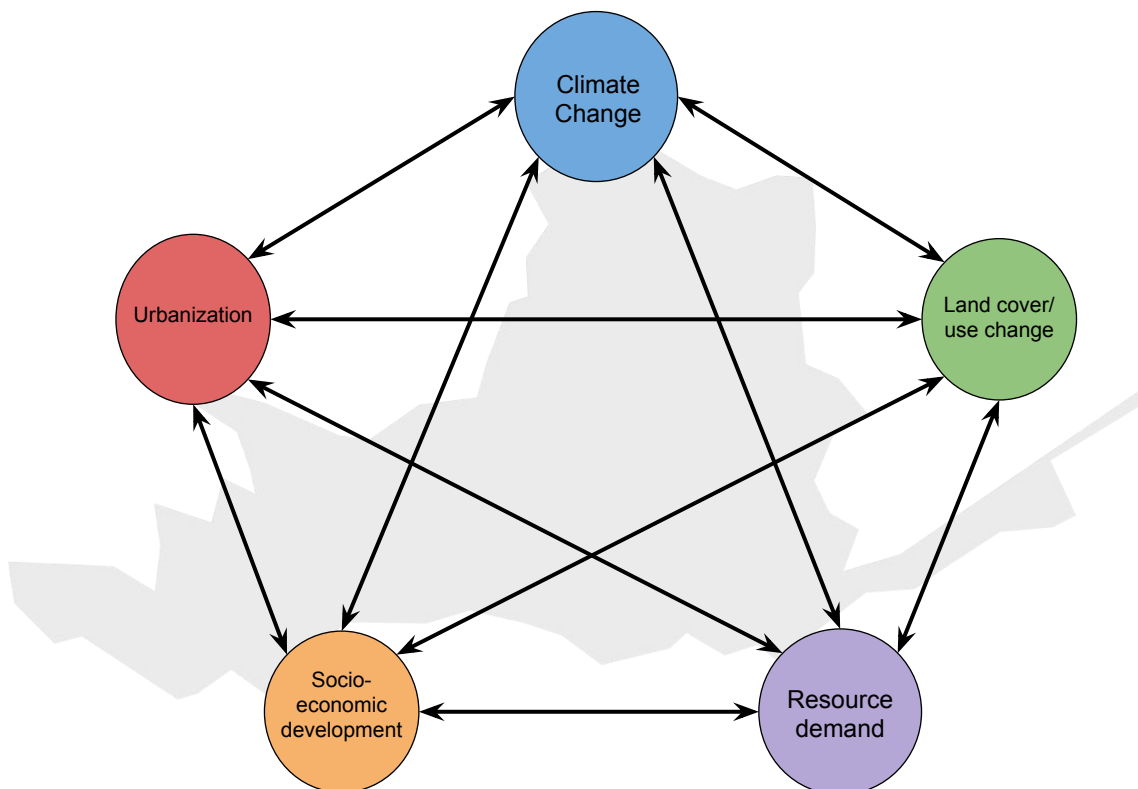


Figure 1.2: Global Change facets influencing the Yellow River Basin.

sediment than any other major river system in the world and contributes around 6 % of the global sediment budget to the oceans (Miao et al., 2010; Wang et al., 2016).

Impacted by rapid and profound industrialization and intensification processes, agricultural and mining encroachment, population and urban growth, as well as anthropogenic-induced climate change, the basin has undergone tremendous land cover dynamics during the past decades. They are pressuring and diminishing prevailing natural ecosystems and their providing services, including water purification, pollination, regional and global climate and flux regulation, on which humans heavily depend on (Daily et al., 2000; DeFries et al., 2004; Millennium Ecosystem Assessment, 2005; Turner et al., 2007; Zhen and Zhang, 2011). To mitigate the adverse effects of land cover change on future ecosystem functioning, it is crucial to have precise spatio-temporal information about prevailing land surface dynamics. It helps to understand the underlying drivers of change, which can either appear as direct/proximate or indirect/root causes (Ojima et al., 1994; DeFries et al., 2004; Foley et al., 2005; Nagendra et al., 2013b). Proximate drivers of land cover change are linked to local scales affecting the direct transformation of land cover, whereas root causes operate more diffusely from regional to even global scales determined by complex social, political, economic, and biophysical variables that modulate proximate causes (Lambin et al., 2003; Miyamoto et al., 2014). Such an understanding remains a challenging task as land cover change in a river basin operates at various spatial and temporal scales, which are often interlinked, because sufficient data is commonly not available over large spatial for longer time periods (Lambin and Geist, 2006). This dissertation makes a contribution towards filling these knowledge gaps.

In summary, land cover information is a central component of *Global Change* research. There is high demand for precise spatio-temporal information on land use/cover dynamics from local to global scales, which is a prerequisite for creating more sustainable and holistic management perspectives in a river basin system. In addition, a better understanding of what drives land cover dynamics is essential for acting stakeholders to anticipate future developments and mitigate ecosystem degradation.

1.2 Earth Observation Land Cover Inventories for the Yellow River Basin

Since the 1970s, the domain of remote sensing applications has greatly advanced in terms of sensor variety and derived products to exploit new fields of application to understand Earth system processes (Lillesand and Kiefer, 2000; Xie et al., 2008; Kuenzer et al., 2014c). Today, a fleet of various remote sensing sensors observe the surface of the earth temporally and spatially explicit providing thematic detailed information capturing biotic

and abiotic properties at various spatial scales with different temporal and spectral properties. Mapping land cover with remote sensing tools is a way of portraying the physical surface of the earth and is one of the most important agents in *Global Change* research (Justice et al., 1998; Foley et al., 2005; Hansen et al., 2013; Esch et al., 2013). Based on this multitude of sensors, various land cover and land cover change products on global and regional level have been developed for the Yellow River Basin, which are introduced in this section.

1.2.1 Global and National Datasets

During recent decades various global and national remote sensing based products have evolved from different initiatives providing information on land surface characteristics. They cover the Yellow River Basin mainly using medium to coarse resolution sensors ranging from 300 m to 8,000 m. An overview about all freely available global and national land cover maps is given in Table 1.1. The first attempts to delineate global land cover using satellite imagery produced maps at 8,000 m and 1 ° spatial resolution based on NOAA (National Oceanic and Atmospheric Administration) AVHRR (Advanced Very High Resolution Radiometer) sensor for 1984 and 1987, respectively (Defries and Townshend, 1994; Defries et al., 1998). Following these efforts, the initiative of the International Geosphere-Biosphere Programme Data and Information System (IGBP – DISCover) and the University of Maryland (UMD) provided two global datasets on a much finer resolution (1 km), based on AVHRR Normalized Difference Vegetation Index (NDVI) composites covering 1992-1993 (Loveland et al., 2000; Hansen et al., 2000). The Global Land Cover 2000 Project (GLC 2000) provided a harmonized land cover database at 1 km resolution for the year 2000 using daily acquisitions over 14 months from the VEGETATION instrument aboard the SPOT 4 satellite (Bartholomé and Belward, 2005). Since the launch of the Moderate-resolution Imaging Spectroradiometer (MODIS) in 2000, this sensor was often used to produce global thematic maps. The initial product based on MODIS acquisitions provided global land cover information at 1 km spatial resolution for 2002 (Friedl et al., 2002). The same spatial resolution offers the 2003 global land cover map by the Global Land Cover by National Mapping Organizations (GLCNMO) based on MODIS (Tateishi et al., 2011). With 300 m pixel resolution, the GlobCover maps (2005-2006/2009) provided by the European Space Agency (ESA) improve substantially spatial accuracy showing the most detailed global land cover characteristics when published (Arino et al., 2008; Bicheron et al., 2010). These products were generated from time-series Medium Resolution Imaging Spectrometer (MERIS) instruments on board of ESA's ENVISAT platform. The initial MODIS land cover dataset at 1 km spatial resolution was updated in 2010 by introducing the Collection 5 global land cover product (MOD12Q1 and MCD12Q1) with refined algorithms and new data input at 500 m spatial resolution, providing a four-fold

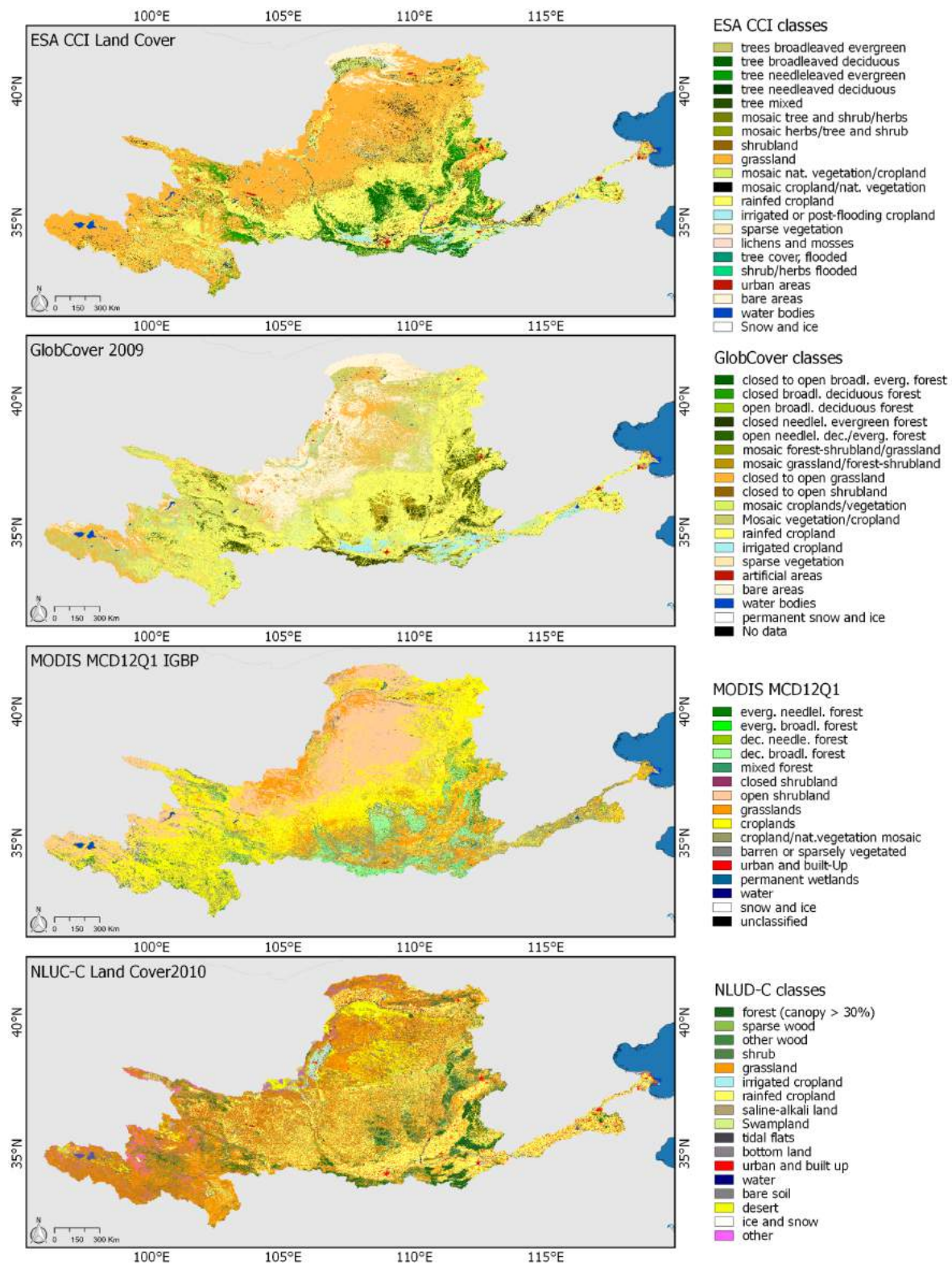


Figure 1.3: Spatial land cover pattern of four available global and national land cover products for the Yellow River Basin.

increase in resolution relative to previous versions (Friedl et al., 2010). The MODIS products are available at annual scales since 2001. The ESA Climate Change Initiative

(CCI) Land Cover (CCI-LC) is ESA's successor of the GlobCover project and creates global land cover products (2000/2005/2010) from various remote sensing instruments initialized to meet requirements for the climate change community at 300 m (Defourny et al., 2014). The most recent global products at finer Landsat resolution is provided from the National Geomatics Center of China (NGCC), which developed the GlobeLand30 dataset for 2000 and 2010 at 30 m spatial resolution (Chen et al., 2015). As a national product, the National Land use/cover Database of China (NLUD-C) was specifically designed to capture history land cover/use dynamics within China and is so far available for three time steps (2000, 2005, 2010) (Zhang et al., 2014). These multi-temporal products are based on Landsat acquisitions at 30 m spatial resolution.

Global land cover products are designed to reflect global land cover pattern; their suitability, however, for regional applications is not always given. The obvious spatial disagreement of four selected national and global product is illustrated in Figure 1.3. Often, these products are used to answer regional specific land-use related questions that will help to support sustainable land management policies and practices. Much research has been focusing on validating and comparing global products to regional scale and consistently show poor spatial agreement to regionally adapted land cover products or statistics (Sedano et al., 2005; McCallum et al., 2006; Fritz and See, 2008; Fritz et al., 2010; Colditz et al., 2012; Kuenzer et al., 2014a; Gessner et al., 2015). China specific comparative studies assessed and evaluated the thematic quality for several land cover types over China (Wu et al., 2008a; Ran et al., 2010; Bai et al., 2014; Yang et al., 2017). Basically, all studies concluded evident discrepancies and low agreement when applied at regional scales. Spatially and spectrally homogeneous landscapes, such as the Qinghai-Tibet Plateau show higher classification accuracies compared to landscapes that are endowed with inherent spatial heterogeneities (e.g. Loess Plateau) and not captured by the defined standard classification schemes of global products (Yang et al., 2017). Further, differences and inconsistencies in classification schemes hamper a direct comparison and synergistic use of available maps (Herold et al., 2008).

1.2.2 Regional and Local Research

The above-mentioned spatial inconsistencies, uncertainties, and inaccuracies make the use of global land products problematic and have fostered regional and localized land cover studies across the Yellow River Basin, which are adapted to the specific research question. In this section, exclusively internationally published research from peer-reviewed literature is considered and discussed, meaning an exclusion of publications in Chinese language as well as studies from common gray literature. Basin-wide land cover studies providing precise "wall-to-wall" information about land surface characteristics and dynamics are rare. As one of the first regional Yellow River Basin land cover products,

Table 1.1: Characteristics and description of available global and national land cover products. Used products in this thesis are highlighted in green color.

Land cover map	Sensor	Input data	Spatial resolution	Time of acquisition	Classification method	Classification scheme	Reference
IGBP DISCover	NOAA AVHRR	12 monthly composites	1 km	1992-1993	Unsupervised clustering	IGBP 17 classes	Loveland et al. (2000)
UMD	NOAA AVHRR	41 spectral metrics from NDVI, 5 bands monthly to 3 monthly NDVI composites	1 km	1992-1993	Supervised classification tree	IGBP 14 classes	Hansen et al. (2000)
GLC 2000	SPOT VGT	16 day composites	1 km	2000	Optimal classification methods	LCCS 22 classes	Bartholomé and Belward (2005)
MODIS LC	MODIS	16 day composites	1 km	2001	Supervised classification trees	IGBP, UMD, other	Friedl et al. (2002)
GLCNMO	MODIS	16 day composites of NDVI and 7 bands	1 km	2003	Supervised classification trees	LCCS 20 classes	Tateishi et al. (2011)
GlobCover	MERIS	Bi-monthly from 10 day composites	300 m	2005-2006	(Un)Supervised spatio-temporal clustering	LCCS 22 classes	Arino et al. (2008)
MODIS 5	MODIS	Monthly EVI, LST, 7 bands from 8 day composites	500 m	2001-2013	Supervised classification tree boosting	5 different classification schemes	Bicheron et al. (2010) Friedl et al. (2010)
ESA CCI-LC	ENVISAT MERIS	MERIS t day composites	300 m	2000, 2010	(Un)Supervised spatio-temporal clustering	LCCS 22 classes	Defourmy et al. (2014)
GlobeLand30	Landsat TM/ETM+, HJ-1	Landsat bands, MODIS and HJ-1 time series	30 m	2010	Pixel and object-based classification	10 classes	Chen et al. (2015)
NLUD-C	Landsat TM/ETM	Landsat bands	30 m	2000, 2005, 2010	Supervised classification trees	10 classes	Zhang et al. (2014)

Daofeng et al. (2004) provided a 1 km resolution map based on monthly NOAA AVHRR data from the Pathfinder dataset spanning a 12 months period from April 1992 to March 1993. Despite the low spatial resolution, this attempt defined 25 region specific classes using unsupervised ISODATA approach that captures the prevailing heterogeneous land surface conditions in the basin, but lacks a comprehensive accuracy assessment of the delineated product. Wang et al. (2009) performed a multi-temporal land cover analysis comparing dynamics between 1990, 1995, and 2000 at finer spatial resolution derived from 30 m using Landsat TM imagery. Based on the final multi-temporal thematic maps, several landscape FRAGSTATS metrics were computed. By defining only 6 major land cover types, the thematic detail is comparable low and is not sufficient to reflect spatially heterogeneous conditions. Both studies are outdated and not applicable for analyzing current land and pressing land cover dynamics within the Yellow River Basin.

A mere of localized small-scale land cover studies on sub-basin level covering only small parts exist in international published literature. Across the Yellow River Basin three geographically confined focus regions can be identified as displayed in Figure 1.4b, where the spatial distribution of all conducted land cover studies is illustrated. The majority of past research is concentrated in the fast-emerging Yellow River Delta investigating mainly wetland dynamics (Hui and Haijun, 2004; Yue et al., 2003, 2004; Zhao et al., 2004; Li et al., 2007; Ottinger et al., 2013; Kuenzer et al., 2014b), followed by spatial analysis across the Qinghai-Tibet Plateau in the source region of the Yellow River (Feng et al., 2005; Guo et al., 2008; Dong et al., 2009; Song et al., 2009). Another geographical research hotspot includes the Central Loess Plateau (Wang et al., 2013; Gao et al., 2015; Zhai et al., 2015). Conducted environmental research within the Yellow River Basin emphasized on topics related to wetland and grassland dynamics in the delta and source region as well as on desertification and salinization processes on the arid Ordos Plateau (Wu et al., 2008a; Yan et al., 2009; Zhou et al., 2012; Liang and Yang, 2016). Sedimentation and erosion control played a major role in past research as can be seen from the wordcloud in Figure 1.4, where mapped land cover products served as input for hydrological models predicting and estimating local erosion fields. Conclusively, there is urgent need for high quality land cover change information to better understand the prevailing spatio-temporal dynamics that are currently shaping the surface of the Yellow River Basin at unprecedented speeds.

1.3 Research Focus and Objectives

Contemporary socio-economic processes in combination with the long and intense human-environment interrelationship, the Yellow River Basin has experienced and will continue to experience tremendous pressure on ecological and societal resources threatening a long-term sustainable development. The Yellow River Basin offers a unique research opportunity to study how global environmental change has influenced recent land transformation on the regional land system in China, but remains comparatively understudied. Remote sensing technology is a key tool for land use change monitoring and the fleet of various sensors and data products offer great potential for new detailed spatial and historic analytic approaches. Yet, the required spatial information is not available and regional land cover change pattern is not well understood over the Yellow River Basin. In view of this, three major objectives are defined as follows:

Objective 1

As first objective (chapter 3 of this thesis), current and most pressing social-ecological challenges affecting the Yellow River Basin will be determined and a possible governance model towards a more sustainable and holistic management will be developed.

To approach this objective a sound review of existing scientific literature but also considering technical reports and statistics from national and international agencies, such as the World Bank and the Yellow River Conservancy Commission (YRCC), the main river basin authority, will be performed. The latter institution was personally visited twice, where fruitful discussions with scientists and local stakeholders from various disciplines allowed new and deeper insights into current and future challenges across the Yellow River Basin.

Objective 2

The secondary object of this thesis (chapter 5) is to gain a comprehensive land cover pictures of the Yellow River Basin to determine the current land surface characteristics and the most dynamic processes that have influenced the basin.

This objective addresses the urgent need for consistent and multi-temporal land information by delineating regionally-adapted land cover products for the years 2003 and 2013 that capture the basin's spatially complex landscape heterogeneity. The spatial

dynamics will be explicitly investigated. Technically, the classification takes the advances of phenology-based metrics derived from high temporal remote sensing data at medium spatial resolution of 250 m. Finally, the generated land cover data are compared to the previously described existing global and national inventories to demonstrate the necessity of delineating regional specific land cover products.

Objective 3

The final objective, which is presented in chapter 6 of this thesis, includes a spatially and temporally more detailed thematic change detection analysis of the most prominent land cover dynamics across the Yellow River Basin related to mining, agriculture, forest, and urban areas.

To approach this objective, land cover analysis and change mapping will be extended at finer temporal and spatial resolution by focusing on the most prominent historic land cover dynamics to better understand rates and spatial pattern. Spectral-temporal, multi-spectral, and textural features are computed using dense Landsat time series to derive eight bi-annual composite maps from 2000 to 2015. The semi-automated classification approach is further combined with a stable pixels analysis to collect a mono-temporal reference data set, that remained the same during the study period.

1.4 Outline of this Thesis

This thesis consists of seven chapters, including this Introduction Chapter. The outline of the subsequent chapters is presented in Figure 1.5.

Chapter 1 highlights briefly the cultural importance of the Yellow River Basin as blessing and curse in the Chinese cultural development, followed by a section describing the basin in the face of Global Environmental Change. Further, Chapter 1 presents a review about conducted research related to land cover, completed by the definition of the research focus, final objectives, and general outline of this thesis.

Chapter 2 provides comprehensive information about the Yellow River Basin and its three river reaches by summarizing the main contemporary hydro-physical, climatic, and socio-economic facets.

Chapter 3 elaborates the current challenges affecting the Yellow River Basin social-ecological system. It aims at introducing recent and current dynamic processes, both

natural and anthropogenic and summarizes taken measures to enhance river basin management towards more sustainability. Finally, a potential river basin model is suggested and discussed.

Chapter 4 gives an overview and short description of the various remote sensing based data used in this thesis. Further, Chapter 4 introduces the main methodological principle of the applied Random Forest algorithm.

Chapter 5 presents the results of “wall-to-wall” land cover change products for the entire Yellow River Basin for the years 2003 and 2013. The introduced methodological approach using high-temporal MODIS time series allows for the accurate delineation of heterogeneous landscapes at large spatial scales. Furthermore, local hotspot regions of change and a direct comparison of the regional adapted land cover product to existing global land cover inventories is presented and discussed.

Chapter 6 extends the land cover change analyses for the Yellow River Basin using dense Landsat time series and a stable pixels approach to generate annual change maps related to mining, agriculture, forest, and urban areas.

Chapter 7 summarizes and concludes the results of the thesis obtained from Chapter four to six. This chapter also includes a brief outlook and recommendation for future studies.

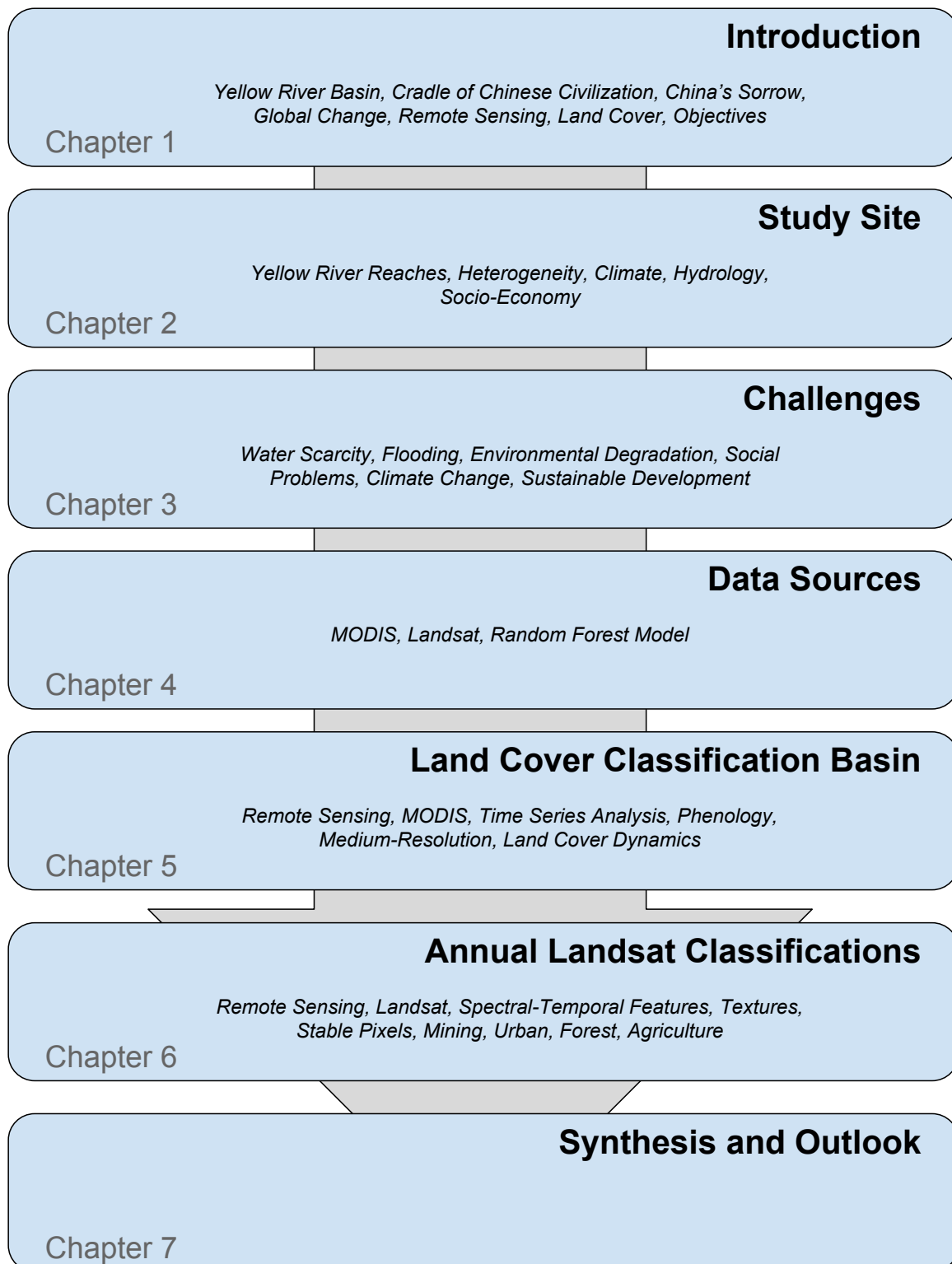


Figure 1.5: Outline of this thesis.

1.5 Definitions and Explanation of major Terms

This section provides the reader with short explanations and definitions of major terminologies that are used in this thesis to better understand the underlying concepts and theories.

Socio-economics

The concept of socio (or social)- economics is a branch of economics that focuses on the relationship between social behavior and economics. It examines how social norms, ethics and other social philosophies influence consumer behavior and shape an economy. Socio-economics uses history, politics, cultural attitude, and other social sciences to predict potential results of changes for society or economy (Eatwell et al., 1989).

Social-ecology

Social-ecology expands the concept of socio-economics by the component “ecology” and was originally developed by Murray Bookchin. In this thesis, the modern approach of Elinor Ostrom describing social-ecological systems was applied, which describes intricately linked systems of humans and nature (Ostrom, 2009). This conceptual framework is described in more detail in chapter 3.

Sustainability

The term has been widely used in various disciplines, however, there is in fact no universally definition on what sustainability means. The basic concept of sustainable development appeared first as common term at the World’s first Earth Summit in Rio 1992, which was based on the Brundtland Report (Brundtland et al., 1987). The original definition: “*Development that meets the needs of the present without compromising the ability of future generations to meet their own needs*”.

Governance

In this thesis, the term governance has been often used particularly when it comes to sustainable river basin governance. Generally, governance describes all processes, which are undertaken by the members of a governing body of an organization within a given geopolitical boundary. In this thesis, I propose a river basin governance model towards a more integrated management to meet current and future challenges (chapter 3).

Ecosystem services

In the early 200s, the concept of ecosystem services became very popular, in particular through the Millennium Ecosystem Assessment (MA). Ecosystem services are the direct and indirect contributions of ecosystems to human well-being (Daily, 1997) According to the MA, four major categories of ecosystem services can be distinguished: (1) supporting services; (2) provisioning services; (3) regulating services; (4) cultural services.

Food security

Food security is also a flexible concept and constitutes of many definitions in research and policy. Perhaps the most accepted definition was adopted at the 1996 World Food Summit: *“Food security, at the individual, household, national, regional and global levels [is achieved] when all people, at all times, have physical and economic access to sufficient, safe and nutritious food to meet their dietary needs and food preferences for an active and healthy life”* (FAO, 1996).

THE YELLOW RIVER BASIN AND ITS CHARACTERISTICS

The Yellow River can be counted as one of the world's most significant river systems, spanning almost 5,500 km, and contains a great environmental heterogeneity as a result of the large geographical extent (32°N-42°N/96°E-119°E). With a size of 751,869 km², the Yellow River Basin encompasses more than double the size of Germany. This chapter aims to introduce the key characteristics and gives a comprehensive overview about geophysical and socio-economic conditions.

2.1 Physiography, Topography, Landcover, and River Sections

Located in the north of Central China, the Yellow River Basin originates in the Bayan Har and Kunlun Mountains at an altitude of 4,500 m on the vast Qinghai-Tibet Plateau. This plateau is the world's largest and highest plateau and known as Asian's "water tower", where all major river systems in Asia rise, including the Yangtze, Brahmaputra, Mekong, Indus, Ganges, and the Yellow River. From there, the river flows almost 5,500 km crossing nine Chinese provinces (or autonomous regions): Qinghai, Sichuan, Gansu, Ningxia, Inner Mongolia, Shaanxi, Shanxi, Henan, and Shandong. The river flows eastwards through the Ordos and Loess Plateau as well as the North China Plains and discharges into the Bohai Sea, an embayment of the Yellow Sea, where a fast-growing delta is formed (Figure 2.1). According to its distinct geomorphological and climatic characteristics, the Yellow River is commonly separated into three major sections: the upper, middle, and lower reaches. A summary of major physical conditions for each river section is given in Table 2.1

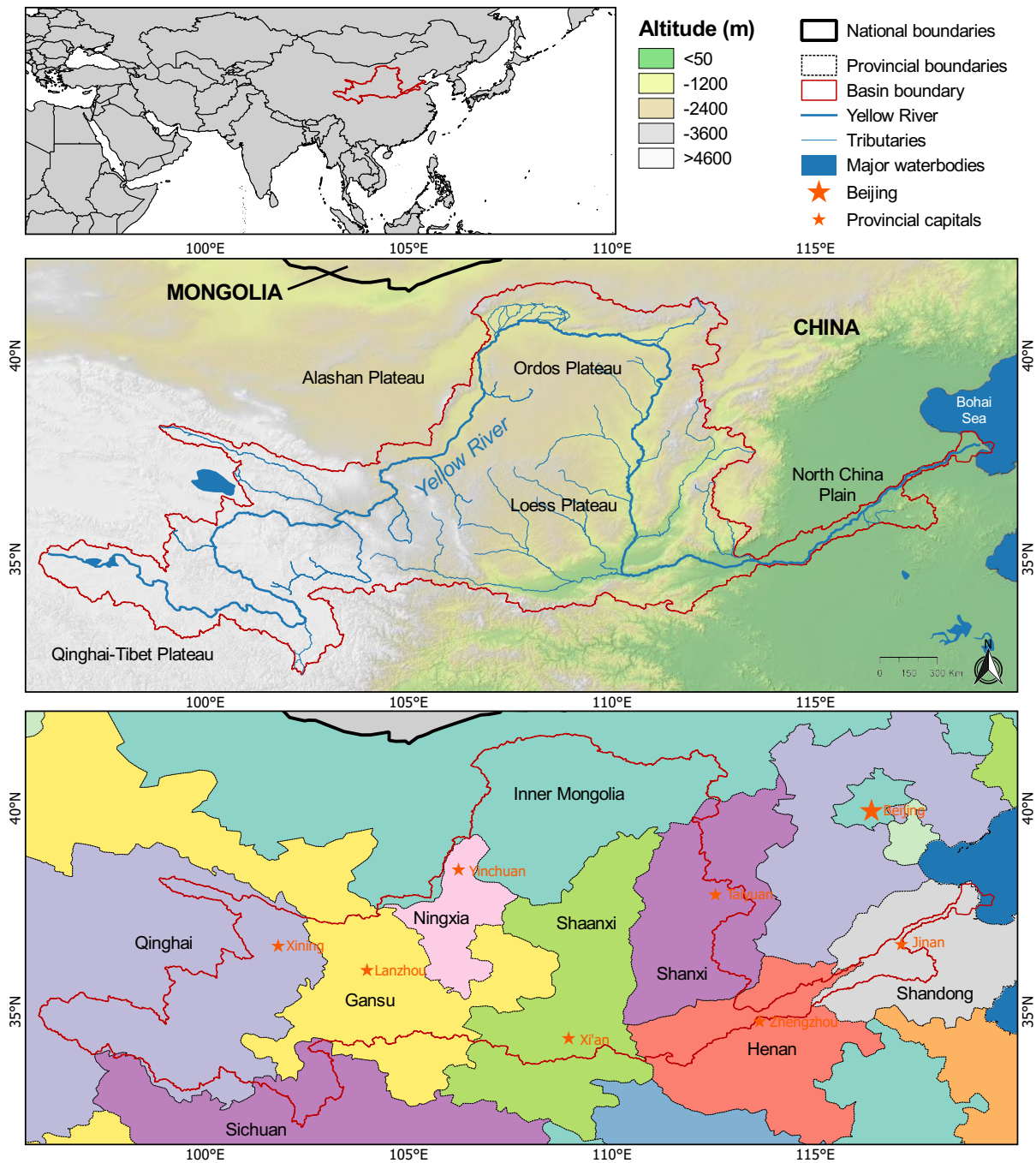


Figure 2.1: Physiogeographical overview of the Yellow River Basin (top) and provincial boundaries with the location of the respective capitals (bottom).

The Headwaters and Upper Reaches

The upper reaches range from the river's source region in the Bayan Har Mountains (4,500 m) in Qinghai to the Toudaoguai gauging station near Datong in Inner Mongolia (1,000 m), traversing the provinces Qinghai, Gansu, Ningxia, and Inner Mongolia. Covering a total drainage area of 367,898 km² and a river length of approximately 3,500 m, the upper reaches comprise more than 50 % of the entire basin area (Table 2.1). Much

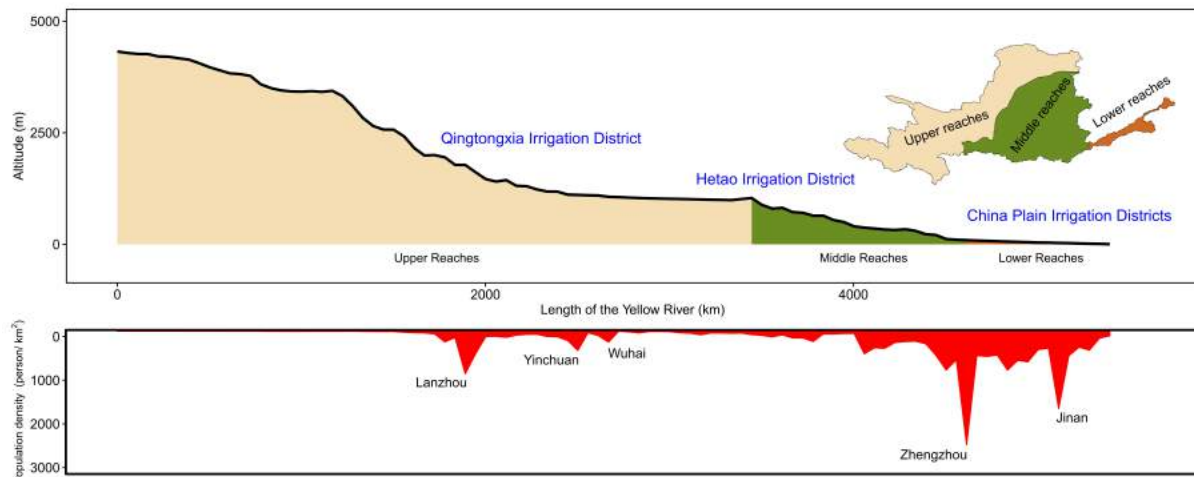


Figure 2.2: The longitudinal profile of the Yellow River from the source region on the Qinghai-Tibet Plateau to the river delta: The upper panel provides the boundaries of the basin's upper, middle and lower reaches and the location of the most important irrigation districts. The lower panel shows the population density along the main channel (data derived from CIESIN (2005)).

of the upper reaches is defined by the Qinghai-Tibet Plateau ecoregion that is covered by vast alpine swamp meadows offering habitats to a unique composition of faunal and floral species, where nomadic pastoralism is still widespread (Li et al., 2012). Trees only occur in riparian areas of the south-eastern Tibetan Plateau. On the plateau, the Yellow River is fed by three major tributaries, namely the Huangshui River, Datong River, Tao River, and Buha River. After passing Lanzhou, the Yellow River turns northwards into the Ningxia/Inner Mongolia plains (Ordos Plateau) and flows through the expanses of the Gobi desert. Large-scale irrigation districts along the main stem, such as the Qingtongxia District (Ningxia) or the Hetao District (Inner Mongolia) enable the intensive production of crops, such as wheat and oil bearing crops as well as various plantations (tea, melons, and pears) (NBS, 2015). The Daxia River in Gansu Province belongs to the most important tributary in the upper reaches that is not embedded on the Qinghai-Tibet Plateau. The great potential for hydro-electric power generation has led to the construction of several major reservoirs, such as the Lijiaxia and Longyangxia reservoir.

The Middle Reaches

The middle reaches (Shanxi and Shaanxi) drain a total area of 362,138 km² and continue from Toudaogui to Huayuakou (Table 2.1) crossing the Loess Plateau at a length of around 1,200 m. At Toudaogui, the Yellow River bends to the south and flows with an average gradient of 7.4 ‰ through dissected and highly erosive hills on the central part of the Loess Plateau. This human-dominated landscape is endowed with a high abundance of fertile, but erosive soils, which can reach vertical extents up to 300 m (Chen et al., 2007),

Table 2.1: Summary of physical and socio-economic settings in the Yellow River Basin (data compiled from Hijmans et al. (2005), Yu (2006), Miao et al. (2010), Peng et al. (2010), Feng et al. (2012)).

	Upper reaches	Middle reaches	Lower reaches	Entire basin
Area (km ²)	367,898	362,138	21,138	751,869
Length (m)	3472	1206	786	5464
Altitude (m)	4480 - 1000	1000 - 95	95 - 0	4480 - 0
Gradient (m/km) (‰)	10.1	7.4	1.2	8.2
Precipitation (mm/year)	396	516	648	520
Average temperature range (°C)	1 - 4	8 - 14	12 - 14	1 - 14
Number of primary tributaries (°C)	43	30	3	76
Population density (p/km ²)	70	210	750	230
Urbanization rate (%)	39	35	39	39

allowing for agricultural cultivation. At the eastern margins of the basin, the Lüliang mountain range divides the Fen River valley, one of the major tributaries in the middle reaches, from the Yellow River. Further south-west, the Ziwuling and Yunwu Mountains cover a large part of the Loess Plateau, which are still dominated by natural mixed forests. The Qinling Mountains delimit the Yellow River Basin to the south and force the river to flow eastwards into the North China Plain, where the lower river section starts. There, the largest tributary joins the Yellow River, the Wei River with a length of around 800 km. Also the middle reaches are intersected with large reservoirs. The Sanmenxia reservoir, constructed with Russian aid, was the basin's first major dam, which began operating in 1957. The last realized dam, the multi-purpose Xiaolangdi reservoir, started in 1999.

The Lower Reaches and the Yellow River Delta

Downstream from Huayuankou gauging station, the Yellow River flows on the flat North China Plain to the mouth a distance of almost 800 km. From here, the alignment of the river is confined to a series of artificial levees now as it flows in a relatively stable and narrow channel in north-easterly direction to the coast Bohai Sea, just north of the Shandong Peninsula. With only 21,000 km², the lower reaches are the smallest Yellow River section. The high concentration of eroded material from the Loess Plateau carried by the river accompanied with reduced velocity and water discharge resulted in sediment deposition in the lower reaches and have raised the riverbed up to 10 m above the immediate surrounding alluvial plains (Wang et al., 2007; Peng et al., 2010). This unforeseen phenomenon is known as “suspended” or “hanging” river (Zhu et al., 2003; Yu, 2002). As a consequence, the water inflow is hampered and hardly any tributaries can join the Yellow River, except for the Yiluohe and Qinhe Rives in the most upper part of the lower reaches (Zhu et al., 2004). The present Yellow River Delta area, one of the largest river deltas in China, is about 7,870 km² equating to less than five percent of the total area. The high sediment quantities and deposition rates create a very dynamic and fast growing natural delta at the river mouth with diverse wetland ecosystems

holding a unique assemblage of various species (Cui et al., 2009). The fertile alluvial soils distributed by the Yellow River provide a fertile basis for intensified, mainly irrigated, agricultural crop production in the lower reaches.

2.2 Climatic and Hydrological Conditions

On account of the large geographical extent, the Yellow River Basin is characterized by a large-scale climatic gradient contributing to a great variety of environmental conditions (Figure 3.8). The basin's climate is influenced by the East Asian continental monsoon circulation system and transits from cold alpine (ET) and arid desert (Bw) climate to temperate climates (Cw) according to Köppen climate classification (Peel et al., 2007; Yancheva et al., 2007). While the southeasterly winds bring a insignificant amount of precipitation in late June, the wind regime shifts in winter and northeastern monsoon transports relatively cold and dry air flows (Yancheva et al., 2007). As depicted in Figure 3.8 and Table 2.1, the current average precipitation in the entire basin equals 520 mm, but is unevenly distributed in space and time (Hijmans et al., 2005; Zhao et al., 2008). Generally, rainfall decreases from southeast to northeast and is mainly concentrated in the summer season from July to September. The southeasterly monsoon

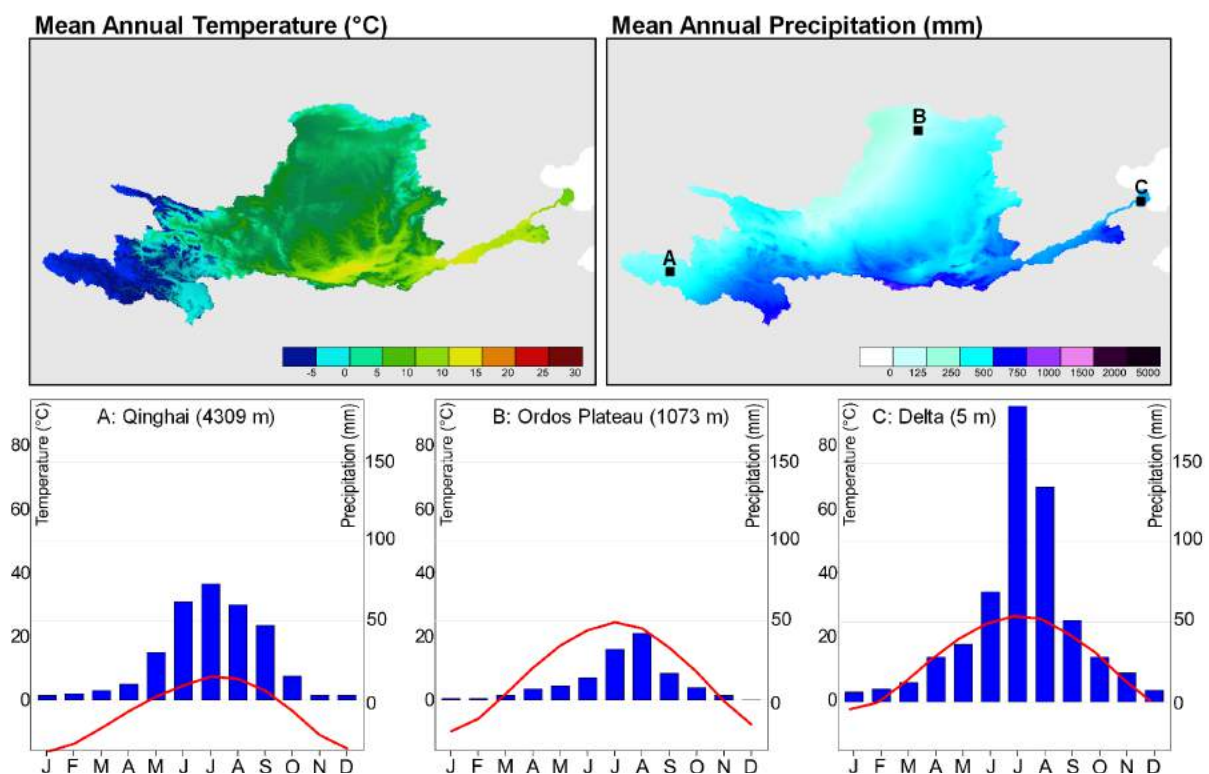


Figure 2.3: Long-term averaged temperature (left) and precipitation conditions based on Hijmans et al. (2005). The selected climate diagrams show the different climatic pattern occurring across the basin.

loses much of its moisture when it reaches the northwestern part of the Loess Plateau and annual precipitation drops from 500 mm to less than 250 mm. The period from December to March is generally the driest.

Even though the Yellow River is ranked as the second largest river basin area in China, the water discharge is comparatively low. The Yellow River produces an annual runoff of 2,571 m^3/s , a small figure compared to the 30,166 m^3/s of the Yangtze River, China's largest river system (YRCC, 2015; CWRC, 2016). The intra-annual discharge follows the precipitation pattern and more than 40 % of annual runoff is generated in August as can be seen in Figure 2.4. (Wang et al., 2006; Zhuo et al., 2016). Numerous built dams and reservoirs have influenced and weakened the intra-annual water variability. A detailed overview about the temporal development of water and sediment discharge in the last decades will be further explained in section 3.1 on page 31.

The Qinghai-Tibet Plateau region is characterized by harsh environmental conditions with low annual temperatures ranging from 1 to 4 °C and annual precipitation averaging around 400 mm (Figure 3.8, diagram A). The climatic characteristics in the upper reaches experience two counteracting hydro-climatic processes. The mountainous high-altitude Qinghai-Tibet Plateau above Lanzhou is dominated by a cold semi-arid climate with low evapotranspiration rates and significant precipitation values, that create abundant river runoff and contribute 56 % of the basin's water resources. As opposed to this, the region northwards from Lanzhou, where the Yellow River turns into the semi-arid and arid regions of the Ordos Plateau and Gobi Desert, the evapotranspiration rates exceed precipitation values by far, making this region a net consumer of water resources

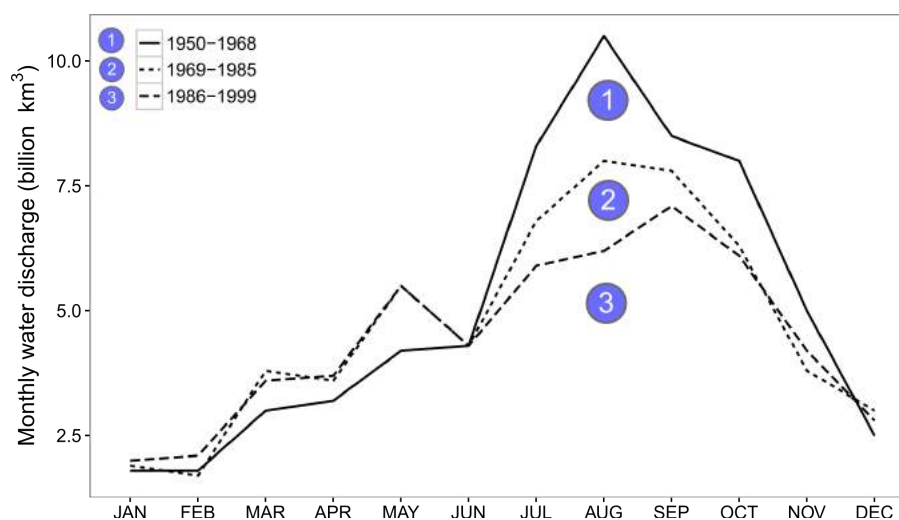


Figure 2.4: Monthly averaged water discharge measured at Huayuankou gauging station for three periods (1950-1968, 1969-1985, 1986-1998). Data derived from the Wang et al. (2006) and YRCC (2015).

(Figure 3.8, diagram B). The humidity brought by the southeastern monsoon is not able to reach this area, where annual precipitation drops to 100 mm or even less.

The middle reaches's climate is determined by semi-humid and humid with higher mean annual temperatures and precipitation than those of the upper reaches with 8 to 14 °C and 516 mm, respectively (Table 2.1). A large number of tributaries drain into the main stream and are responsible for 47 % of the water resources within the basin. Intensive rainfall events in summer combined with low vegetation coverage lead to high water erosion rates. Here, 90% of the river's total sediment load are generated (Wei et al., 2006; Chen et al., 2007).

The highest precipitation falls in the lower reaches and the Yellow River Delta area, where the southeast monsoon brings sufficient humid and warm air from the Pacific during summer months (July -September) (Figure 3.8, diagram C). Despite the humid climate with around 750 mm and mild temperatures, the water contribution is relatively low with and contribute only 3 % to the river's total water resources. As described in the previous section, the elevated river bed greatly reduces the water inflow from the alluvial North China Plain.

2.3 Socio-economic Settings

The basin provides water and land resources for around 110 million people, representing 9 % of China's total population. This figure would increase to almost 190 million if the flood plains in the North China Plain were included. The region plays a vital core for China's remarkable economic growth and resource intense development. Along its courses, particularly in the middle and lower reaches, rich quantities of natural resources are abundant, such as oil, gas, and coal resources, which are increasingly becoming important for China's economic boom. Raw coal and oil extraction in the basin accounts for 50 and 25 % of domestic production, respectively (NBS, 2015). The delta area with China's second largest oilfield, the Shengli oilfield, belongs to an important base for oil exploitation, where reserves >4.6 billion tons are buried (Figure 2.5 b). Further, the basin is a key region for China's food production and harvested 10 million tons of grain in 2013, equivalent to 20 % of the total domestic grain production. The central government has maintained the emphasis on producing as much food domestically as possible to achieve food self-sufficiency (Ghose, 2014). The majority of the cropland areas are irrigated in large-scale irrigation districts, scattered in all river reaches. Besides grain products, agricultural commodities produced in the basin include oil-bearing crops, cotton, fruits and vegetables (NBS, 2015). The long-term development goal of the government is to transform China from a nation of peasant farmers into a modern and urbanized country. However, economic transition towards an industrialized society has not occurred equally

throughout the basin. As can be seen in Figure 2.5, coastal provinces show a higher degree of economical development than the hinterland, causing social and economic disparities. As a result of favorable environmental and commercial conditions as well as cultural heritage, industrialization and urbanization occurred mainly in Shandong province in the lower reaches, but also in Henan, Shanxi, and Shaanxi in the lower parts of the middle reaches (Figure 2.2). The largest and most populous city is Xi'an, the provincial capital of Shaanxi province with almost 14 million inhabitants, followed by Jinan (Shandong - 13 million), Zhengzhou (Henan - 8.6 million), Lanzhou (Gansu - 2.5 million), and Baotou located in Inner Mongolia (2 million). By contrast, the provinces in the upper reaches, particularly the provinces Qinghai, Ningxia, and Gansu, exhibit a low degree of agricultural and industrial development and remain sparsely populated with around 70 persons living per km² (Table 2.1) and still rely on agriculture and remain poorly developed as indicated in Table 2.2. Only the provincial capitals Xining and Lanzhou, the most populous settlements, mark a regional hub for a strong regional

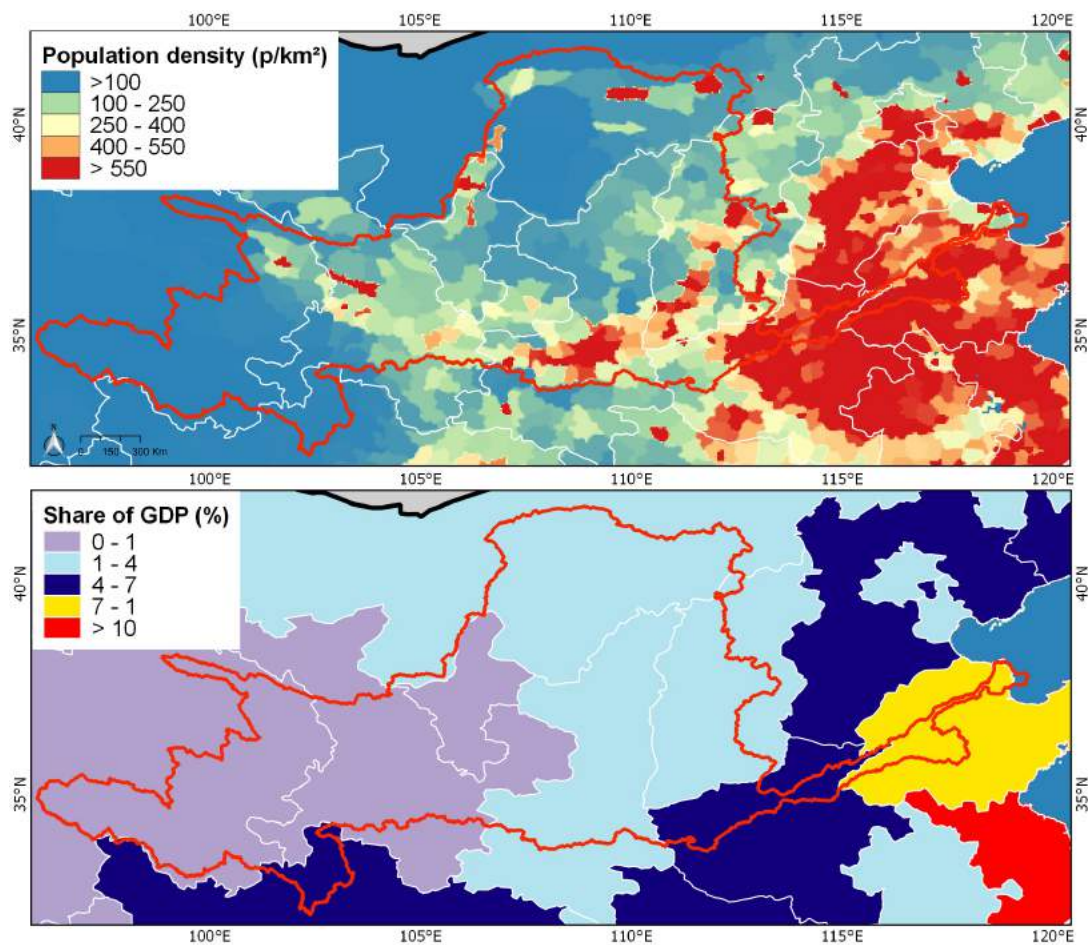


Figure 2.5: Spatial distribution of the population density in p/km² (top panel - CIESIN (2005)) and the provincial share of Gross Domestic Product (GDP) in % (bottom panel - NBS (2015)).



Figure 2.6: Socio-economic facets in the Yellow River Basin (photographs taken by Christian Wohlfart in October 2013 and April 2016).

economy with higher population numbers. Basinwide, migration from rural to urban areas can be observed. Today, according to the statistics provided by the National Bureau of Statistics of China, almost 40 % of the population lives in an urbanized environment (NBS, 2015). A more detailed view about temporal development of socio-economic aspects are given in the next chapter 3 on page 29. Within the economic sectors, agricultural share of Gross Domestic Product (GDP) has been reduced, as secondary and tertiary sector have been developed faster. In terms of employment, however, agriculture is still the dominant working sector throughout the basin (NBS, 2015).

Table 2.2: Socio-economic statistics on provincial level for the year 2015 (NBS, 2015).

	Qinghai	Sichuan	Gansu	Ningxia	Inner Mongolia	Shaanxi	Shanxi	Henan	Shandong
Area proportion in the basin (%)	7.44	9.16	7.11	26.81	8.45	6.77	4.83	18.82	10.82
Population (in 100,000)	5.8	82.04	26.00	6.68	25.11	37.93	36.63	94.80	98.47
GDP (PPP) total (1000 USD)	38	853	192	82	511	515	363	1,049	1,786
GDP (PPP) per capita (USD)	6.623	5,914	4,201	7,033	11,544	7,710	5,622	6,283	10,302
Real growth (%)	8.2	7.9	8.1	8.0	7.7	8.0	3.1	8.0	8.0
GDP share of primary sector (%)	8.61	12.23	14.05	8.14	9.01	8.86	6.13	11.37	7.90
Foreign direct investments (100 million USD)	7.4	88.41	7.66	8.97	35.14	51.57	41.10	68.71	219.334
Electricity consumption (100 million kwh)	658	1992	1098	878	2542	1221	1737	2879	5117
Life expectancy at birth (years)	69.96	74.75	72.23	73.38	74.44	74.68	74.92	74.57	76.46
Birth rate (births per 1000 persons)	14.72	10.22	12.36	12.62	7.72	10.10	10.81	12.70	12.55
Death rate (death per 1000 persons)	6.17	7.02	6.15	4.58	5.32	6.28	5.93	7.05	6.67

SOCIAL-ECOLOGICAL CHALLENGES AFFECTING THE YELLOW RIVER BASIN*

With the first agricultural societies having appeared 7,000 years ago, the Yellow River has always played an important role in China's social, economical, and political development and is therefore characterized by a strong and intense human-environment relationship (Zhang et al., 1990; Lawler, 2009). For millennia, humans have altered the river's landscape and hydrological settings by deforesting hill slopes on the Loess Plateau for agricultural production and large parts of the riverbanks along the lower reaches were stabilized with dikes for taming the Yellow River's unstable course (Wu et al., 2004; Ongley, 2009). Although new opportunities for economy and food provision have been created, these measures have led to serious soil erosion, environmental degradation, and a rising riverbed in the downstream (Shi and Shao, 2000; Chen et al., 2007).

Today, the basin is facing an even more tremendous social-economic change. Economic and industrial growth, urbanization, accompanied with population growth expansion and rising affluence have accelerated based on radical exploitation of water and natural resources (Webber et al., 2008). In conjunction with dam and reservoir construction, as well as increasing water and environmental pollution, which have greatly affected the natural dynamic conditions of the river, are posing now new environmental and social threats on the complex Yellow River social-ecological system (Wang et al., 2007; Kuenzer, 2007; Bi et al., 2011).

These complex environmental and social problems require interdisciplinary solutions.

* This chapter is based on: Wohlfart, C., Kuenzer, C., Chen, C. and Liu, G. (2016b). Social-ecological challenges in the Yellow River basin (China): a review. *Environmental Earth Sciences*, 75 (13), 1-20

During the last decade, many interdisciplinary frameworks considering all interactions between social, economic, and ecological systems have been advanced and were applied to different problems and regions (Carr et al., 2007; Ostrom, 2009; Scholz et al., 2011; Binder et al., 2013). The Yellow River Basin, as other river basins worldwide, can be used as a case study for a strong coupled human-natural system, also termed as social-ecological systems (SES). The basin is comprised of a vast divergence of many social, economic, and ecological facets, almost all facing challenges on different scales, where some are more of regional nature and others more localized. The concept of SES describes intricately linked systems of humans and nature, while emphasizing that the separation of both systems is artificial and arbitrary (Berkes and Folke, 1998; Anderies et al., 2004; Folke et al., 2005). Further, SES are not just linked but also interconnected and co-evolving across multiple scales. That makes such systems as well as their management and governance inherently complex, necessitating a consistent and comprehensive framework to describe them. Ostrom's SES framework is one approach describing complex SES (Figure 3.1) and has been applied to different regional and local systems, such as forestry, agriculture, fishery, and watersheds demonstrating the applicability of this framework to a wide range of different systems operating over a number of scales (Blanco, 2011; Parrott et al., 2012; Nagendra et al., 2013a; Ban et al., 2013). This chapter gives an overview about recent dynamics that have occurred in the Yellow River Basin during the last decades. Further, the key challenges affecting the social-ecological system will be summarized and introduced efforts in management and policy will be highlighted and discussed. Finally, a governance model towards a more sustainable river basin management will be introduced.

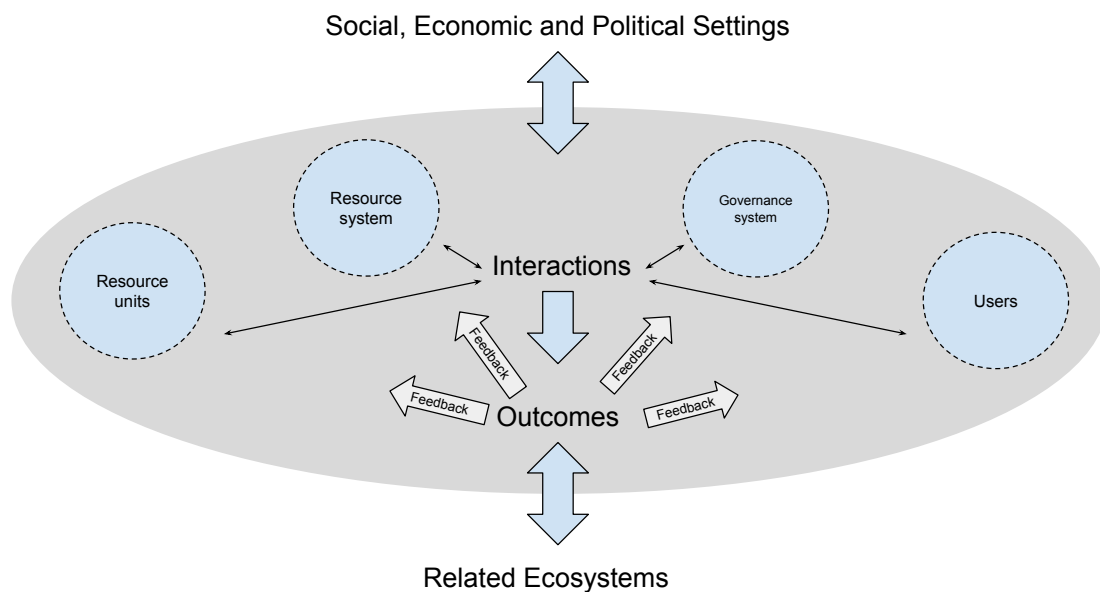


Figure 3.1: Principal structure of Ostrom's concept for describing a social-ecological system. (Ostrom, 2009)

3.1 Recent Processes in the Yellow River Basin

Just like all of China, the Yellow River Basin has witnessed incredible developments during recent decades (Figure 3.2). In the Post-Mao Era, the late 1970s, fundamental economic reforms introducing a more liberalized market-oriented system and a privatized economy have boosted Chinese economy at unprecedented speed (Webber et al., 2008). The opening to international markets have been rewarded with increasing foreign investments and import of new technologies. These investments induced a remarkable expansion of the economy, fostering industrialization, agricultural intensification, urbanization, and affluence in the basin (UNDP, 1999; Tisdell, 2009). In order to sustain food security, the collective principle within the agricultural sector was dissolved, which is also known as household responsibility system (HRS) (Chinese: 家庭联产使包责任制). In the new decentralized structure motivated farmers to take responsibility for their own revenues and losses, which triggered an intensified and increased agrarian production, as well as rural urbanization and welfare (Webber et al., 2008). As a result, average grain production almost tripled from 2 to 5 tons/ha since 1971 (Piao et al., 2010). These reforms were urgently needed to maintain an adequate food supply to match the needs of growing demands of an increasing population and rising affluence. Besides the new initiated policies in land tenure, increasing production of agricultural commodities has been also achieved through the increased use of organic and inorganic fertilizer, which has increased by approximately 70 % since 2005 (NBS, 2015). Through the expansion large-scale irrigation networks by installing channels, wells, and reservoirs, water resources were developed for agriculture during low water conditions, allowing for multiple yields per year. The largest districts include the Qingtongxia (upper reaches), the Hetao (upper reaches), and the North China Plain Irrigation District in the lower reaches (Figure 3.4).

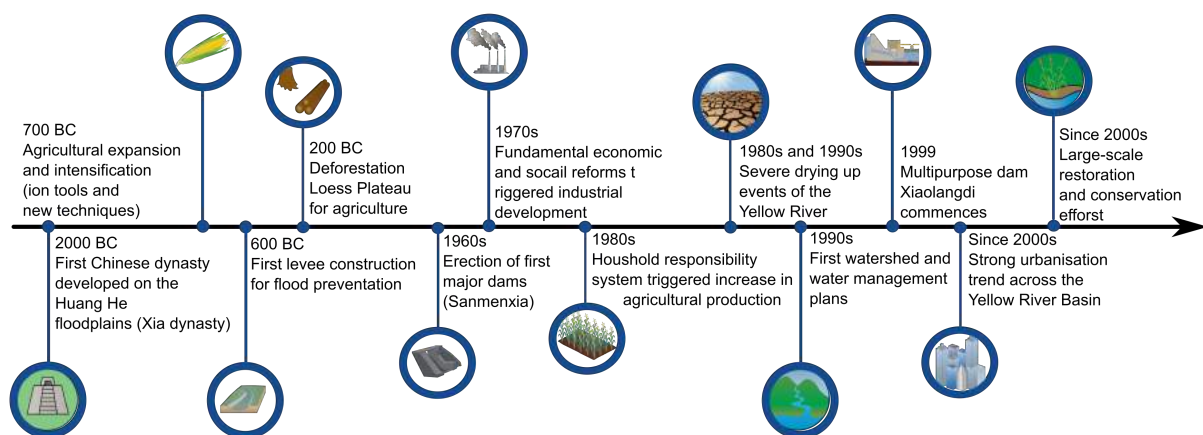


Figure 3.2: Timeline showing the cultural, social, and economic development in the Yellow River Basin.

The earliest irrigation facilities date back several centuries primarily in the upper and middle reaches, but the majority of large-scale irrigation districts with areas larger than 20,000 ha were established during the last 50 years (Fu et al., 2004; Yang and Ishidaira, 2010). The irrigated area of arable land expanded from 8,000 km² in 1949 to around 75,100 km² by 2000, an increase of more than 800 %, of which 50 % is under irrigation (Cai and Rosegrant, 2004; Nakayama, 2011). This number is expected to continue to rise over the next decades. Amongst the provinces, Shandong and Henan province in the lower reaches have experienced a significant intensification of agrarian production as can be seen in Figure 3.3, where grain production incremented by 25 % during the last 15 years (NBS, 2015). The North China Plain's vast flat terrain, fertile soils, and its proximity to potential markets near the coast enable an intensive agricultural development (Webber et al., 2008).

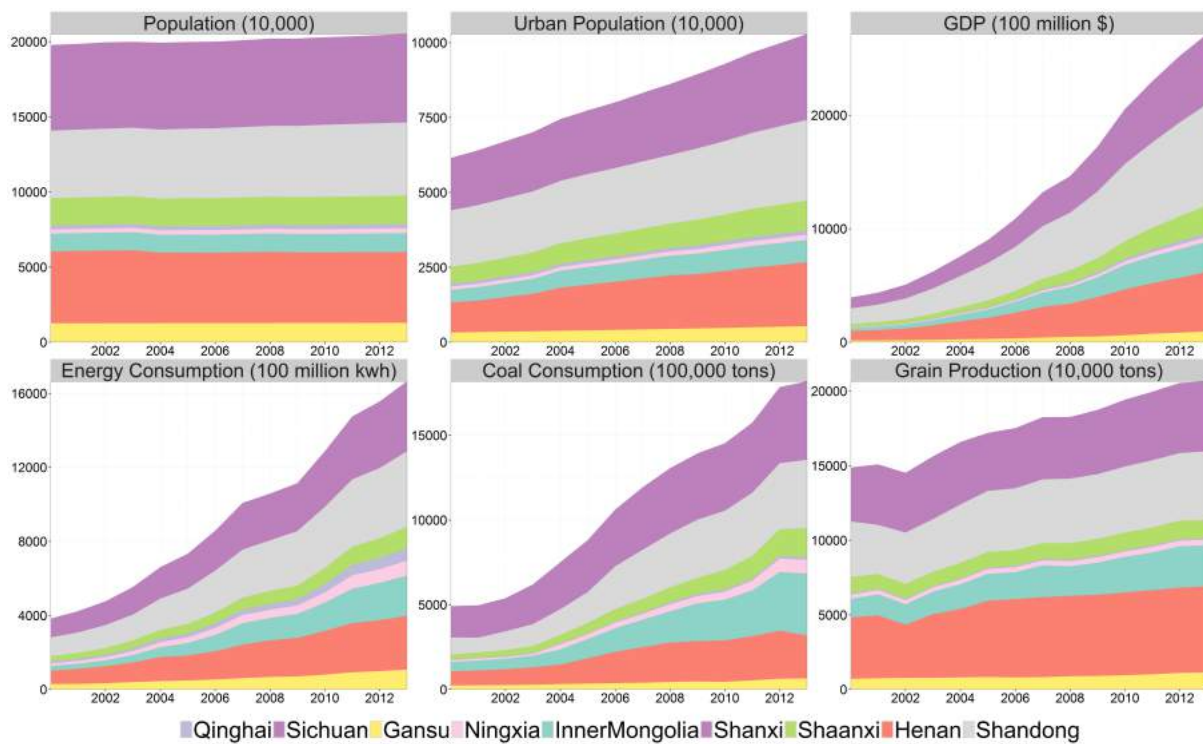


Figure 3.3: Temporal development of major socio-economic statistics for each province located in the Yellow River Basin based on data provided by the National Bureau of Statistics in China (NBS, 2015).

Within the economic sectors, agricultural share of GDP has been reduced, since the industrial and service sectors have developed faster. In 1990, the agricultural sector accounted for 30 % of the basin's GDP, whereas by 2015 this figure had declined to less than 10 % (NBS, 2015). Industrialization and hence GDP in the basin has tremendously changed and increased from 11 billion USD (1980) to 21.2 billion USD (given the price constant since 2003) in 2015 at annual growth rates between 7 % and 10 %. Basically,

economic development was present across all provinces as depicted in Figure 3.3, but strongest in Shandong and Henan. The provinces in the upper and middle reaches remain poorly developed. In the past 100 years, the population in the Yellow River Basin has more than quadrupled from 50 to around 190 million, but remained more or less stable in the last two decades (Figure 3.3), whereas urbanization rates doubled since the 1980s (NBS, 2015). A more urbanized lifestyle tends to raise consumption and increase the demand for higher-value food, such as meat, dairy products, fruits, vegetables, and other commodities. These changes, in turn, indirectly influence landscape transformation in rural areas (Lambin et al., 2001).

These tremendous socio-economic processes and the increased demand for land and water resources have altered the basin's landscape features. During recent decades a cascade of dams and reservoirs have been constructed scattered in the main stem and tributaries of the Yellow River, which are mainly located in the river's upstream catchment (Figure 3.4). In 2007, a total number of 3,147 registered reservoirs were counted with a total storage capacity of 72 km³, exceeding the natural annual water discharge by far, which is around 25 km³ at Lijin gauging station (Ran and Lu, 2012; YRCC, 2015). These facilities generate 33.55 billion kWh of electricity every year (Fu et al., 2004). Dams and large reservoirs fundamentally change water and sediment discharge pattern resulting in profound physical, geomorphological, and ecological impacts on the lower reaches, the coastal area including the delta, and the Bohai Sea (Li et al., 1998a,b; Wang et al., 2007; Cui and Li, 2011; Kuenzer et al., 2013). The direct impact on water and sediment discharge is highlighted in Figure 3.4 and shows clearly the changes on the hydro-physical settings after the operation start of each dam.

Perceiving the environmental and social costs of the unsustainable land resource management, the Chinese government launched several land use policies that have greatly modified the landscape features within the Yellow River Basin. First measures to counteract degradation processes include the *Loess Plateau Watershed Rehabilitation Program* launched in 1996, which was funded by the World Bank, followed by national state-funded schemes, such as the *Grain-for-Green Program* (GfG), or the *National Forest Conservation Program* (NFCP). All initiated conservation programs target specifically degraded landscape to enhance the ecological status, also taking social aspects into consideration. A detailed overview about the sustainable management efforts will be explained in section 3.3 on page 45. Direct anthropogenic land cover and use activities have been comparatively weak in the upper reaches and have progressed rather slowly. Currently, the upper part and headwaters are more affected by variability of natural conditions, such as temperature and precipitation (Ni, 2011). There, desertification trends became apparent, which affect and deteriorate the extremely fragile grassland ecosystems. The adjacent deserts have expanded annually by approximately 2 % (Dong et al., 2009; Hao

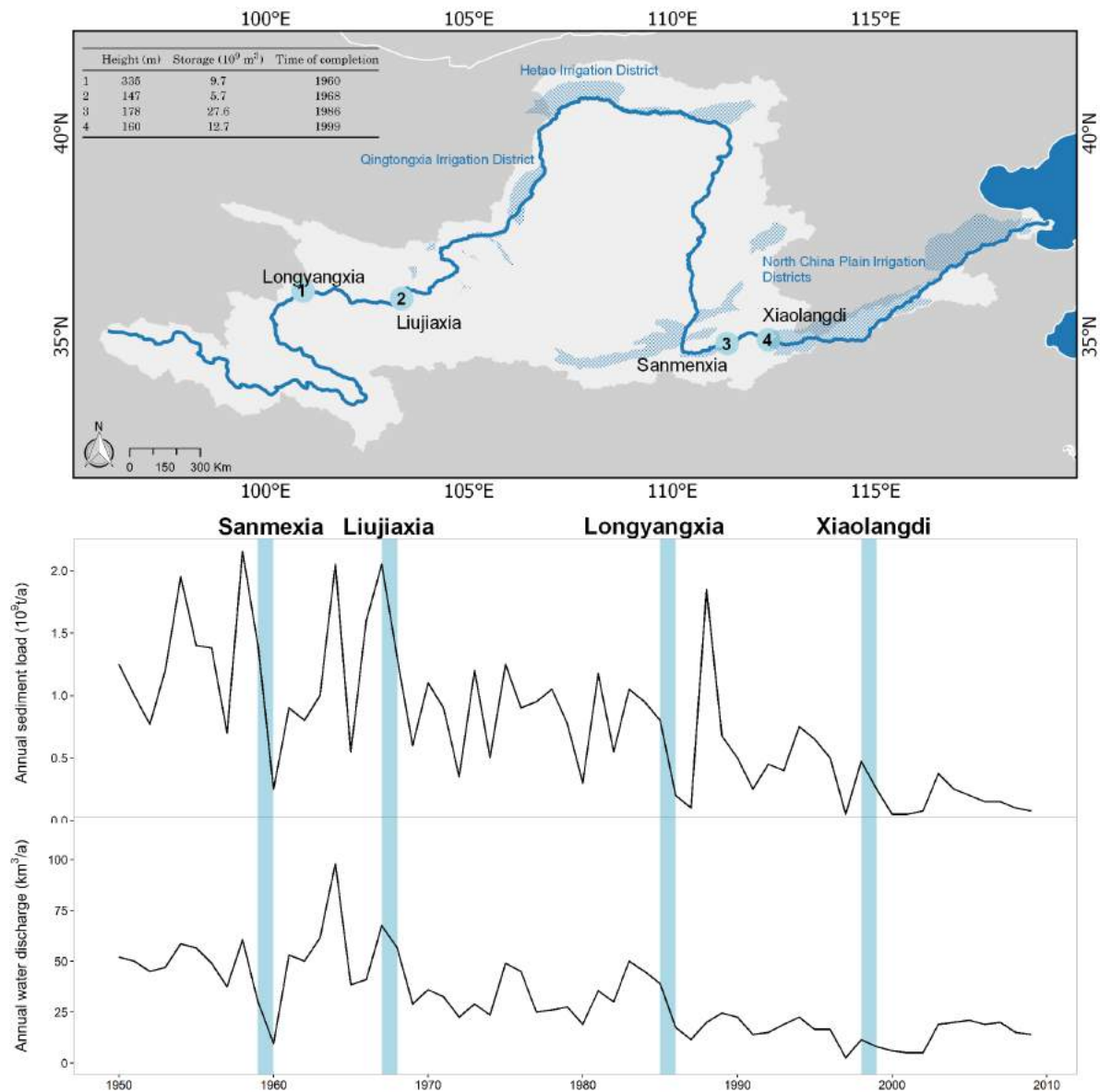


Figure 3.4: The four major reservoirs located in the Yellow River Basin. Variations on sediment (top) and water (bottom) discharge at Lijin gauging, the last station before the Yellow River enters the Bohai Sea from 1950 to 2010. Data are derived from the Yellow River Conservancy Commission (YRCC) and by the Ministry of Water Resources (MWR) (YRCC, 2015). The operation start of each dam is highlighted in blue color. Crosshatched areas mark the major irrigation district located in the basin.

et al., 2012).

Climatic variations and the increasing water allocation have resulted in a continuous decline of water discharge over the past 50 years (Figure 3.4). Human water extraction activities are mainly determined by water use for irrigated agricultural and industrial purposes, hydropower, water and soil conservation practices, and higher demand from

increased wealth (Wang et al., 2007; Piao et al., 2010; Miao et al., 2011). In 1949, the basin's people consumed 7.4 km³ for agriculture, industry, and domestic use only, whereas this figure increased to more than 30 km³ in 2014 (YRCC, 2015). Likewise, sediment load experienced a steady decline in the last decades as can be seen in Figure 3.4 (Peng et al., 2010). Sediment interception by dams and massive soil conservation practices to reduce erosion in the Loess Plateau contributed mainly to the decline of sediment load in the river. Changes in precipitation pattern had only a minor influence. Estimations show that the transported sediment quantities have been reduced by around 90 % since the 1960s level from 1.09 to 0.15 gigatons per year (Milliman and Meade, 1983; Wang et al., 2007). The current sediment load is similar to the pristine levels of the middle Holocene (6000 BP), prior to human intervention (Milliman et al., 1987). Similar trends in declining water discharge and sediment load can be obtained in other major river systems in China, such as the Yangtze or Pearl River, albeit not to the same extent as in the Yellow River (Zhang et al., 2006; Wu et al., 2012).

3.2 Current Social-ecological Challenges

The current challenges affecting the Yellow River system are resulting on the one hand from an intense long-term human-environment interaction and on the other hand from recent tremendous socio-economic dynamics, posing various and complex challenges to both the environment and society. Those can be of local nature or encompass large time and spatial scales (Figure 3.5). In the last years, the Yellow River has even received international attention as several articles reported about the complex social-ecological situation and challenges that are currently occurring. Phrases such as *The Dying River* in National Geography or the New York Times's *China's Troubled River* and *Cancer Villages* were used to describe the prevailing problems. In terms of economic progression, the enacted reforms can be considered as a great success story leading to emerging local industries and even rural farmers have increased their merits through the HRS. However, this rigorous focus on economic growth and the consequent over-exploitation of natural resources have taken their toll posing various threats to the environment and society and might offset the economic benefits and threaten social stability.

3.2.1 Water Scarcity

The Yellow River Basin is a large catchment that is sensitive to drying trends and one of China's most water-stressed regions (Figure 3.6 a). The water scarce basin represents only 2 % of the freshwater resources, but supplies up to 15 % of China's total population (Xia and Pahl-Wostl, 2012). Today, the per capita water availability in the basin averages only 430 km³, which is by definition far beyond the 1,000 km³ threshold for chronic

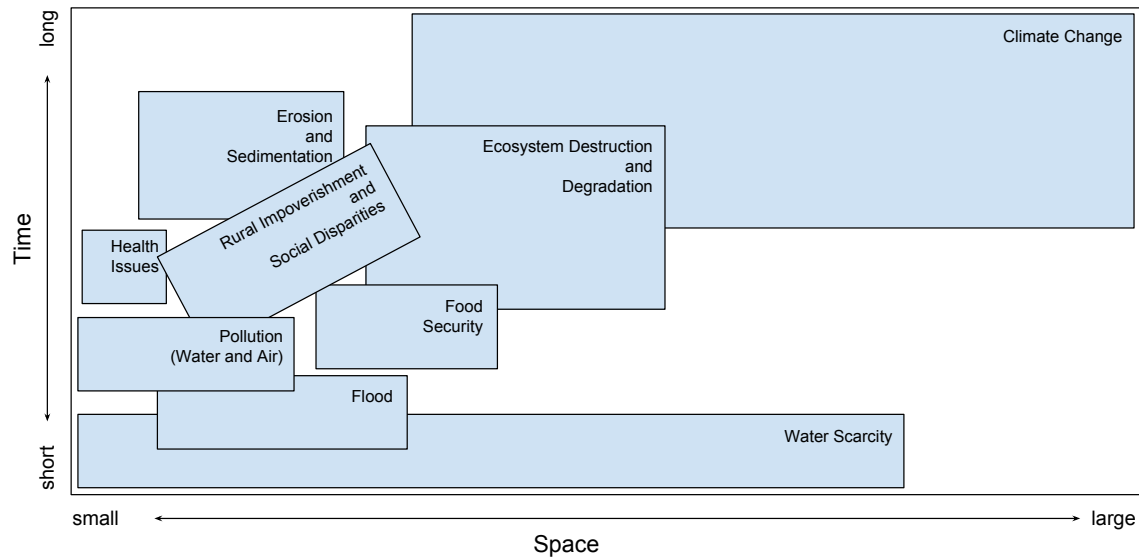


Figure 3.5: Space-time diagram depicting current pressing challenges on different temporal and spatial scales.

water stress (Falkenmark and Widstrand, 1992; Ringler et al., 2010). The region is naturally water scarce due to the prevailing climatic and hydrological settings, showing a distinct spatial and seasonal pattern as introduced in Figures 3.8 and 2.4. But more importantly, water demand and consumption have increased due to the rapid socio-economic developments and water resources have become severely scarce by irrational extraction and unsustainable water management. This causes regional bottlenecks for sustainable developments in the basin affecting agricultural and industrial production as well as livelihoods. Between 1950 and 2015, the total annual water withdrawal almost tripled from 12 billion m^3 to 35.1 billion m^3 , which resulted in a declining water discharge, particularly in the lower reaches (YRCC, 2015) (Figure 3.4). Owing to the unsustainable water extraction, the Yellow River experienced a novel situation in the 1970s: the main stem of the river ceased to flow in the lower reaches during the irrigation period in spring (Yang et al., 2004). This situation became even worse in the 90s, when the lower river channel dried up constantly every year, which peaked in 1997 with 226 consecutive days of no-flow (Cai and Rosegrant, 2004). The river desiccated at a total length of 700 km from the river mouth, even failing to reach Shandong province. These low-flow and no-flow events, however, are of national concern, as they cause serious negative repercussions for basin functions affecting the lower reaches and the delta region. Access to drinking water for 1.3 million people was restricted and agricultural and industrial production suffered severe economic losses. Many industrial facilities, such as the oil wells in the delta region, were forced to close, resulting in an estimated direct economic loss of almost 1 billion USD (Li, 2005).

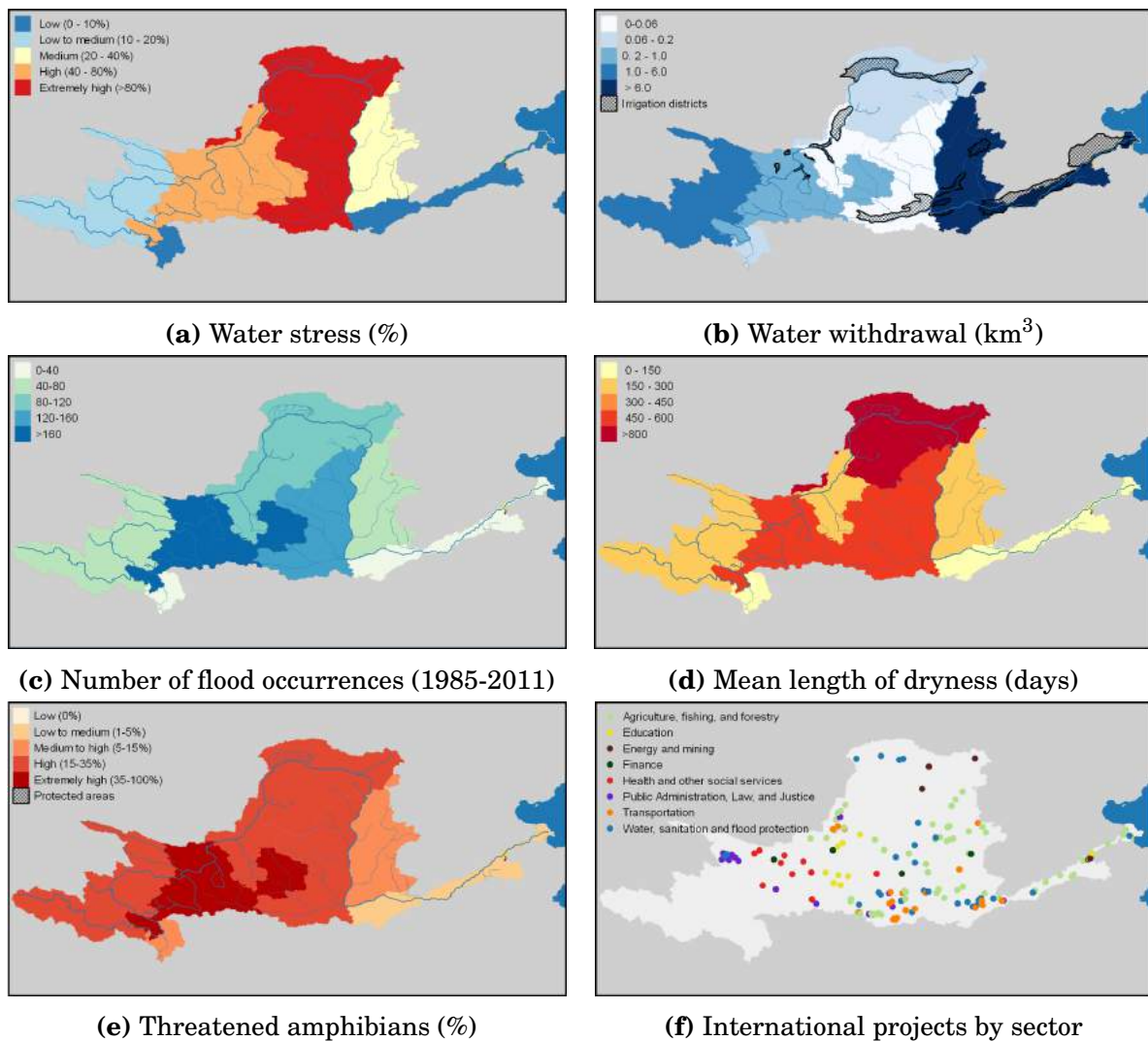


Figure 3.6: Province-wise distribution of (a) baseline water stress (Gassert et al., 2013), (b) water withdrawal in km³ (YRCC, 2015), (c) Flood occurrences from 1985-2011 (Brakenridge, 2016), (d) mean length of drought days from (IPCC, 2013), (e) threatened amphibian species (IUCN, 2015) and protected areas (IUCN and UNEP-WCMC, 2015), and (f) conducted projects by international partners (World Bank, IUCN, WWF) sorted by sector.

Given the spatial imbalance between water supply and demand, the Yellow River Basin can be seen as a classic example of an upstream-downstream water allocation problem. The majority of the water is generated in the upper reaches, but population, urbanization, and economical development there is poor, which is mainly based on agricultural production. There, the high abundance of water resources leads to the water wastage in agricultural production, as farmers have constructed their own canal and irrigation system and are unwilling to divert or save water since their production would be affected adversely. Basin-wide, the agricultural sector, as major water consumer, allocates around 75 % of the entire used water. Farmers allocate more water to their own production than they are entitled to by law (Lohmar et al., 2003; Cai, 2008). Consequently, the downstream

users with a higher share of industrial and domestic demands suffer severely from water shortage and annual flow interruptions. While the river does not cross international borders, the Chinese provinces themselves pursue divergent objectives and interests, leading to sharp competition between upstream and downstream users (Barnett et al., 2006). In fact, a decline in irrigation withdrawal can be observed due to several water allocation policies in recent years; however the water consumption of non-agricultural water users tended to increase at the same time instead (Cai, 2008; YRCC, 2015). This suggests that the provincial conflict is shifting more towards a conflict between sectors (agriculture vs. industry vs. ecology) when it comes to allocating water resources. Competing demands trigger conflicts between geographical regions on the one hand and economic sectors on the other.

3.2.2 Floods and Sedimentation

Historically, the Yellow River area is prone to flooding events, where the most disastrous floods in China caused millions of casualties, weakened social stability, and diminished national prosperity. In the last 4,000 years more than 1,000 major floods have been recorded (Chen et al., 2012). As soon as humans settled down in the vicinity along the river banks, they soon began to construct artificial flood levees and embankments adjacent to the lower reaches to restrain its wild nature and to protect their villages and cities. However, these embankments reduced the sediment carrying capacity of the river due to its lower water velocity and volume. The riverbed inside the flood levees began to rise several centimeters a year and formed a super-elevated riverbed. Large efforts in flood control and mitigation have been made. This includes the raising and reinforcement of existing levee structures (levees have been heightened four times in recent decades), the expansion of flood retention areas in the lower reaches, the construction and operation of large reservoirs in the basin such as the Xiaolangdi and Sanmenxia reservoir in the middle reaches, and soil erosion and sedimentation control on the Loess Plateau (Wu et al., 2004; Li, 2005). Nowadays, the flood risk has been reduced and contemporary flood events are of rather small-scale and localized nature, which were either induced by heavy rainfall events in summer or by ice jams in early spring (Jiang et al., 2008; Chen et al., 2012). Since 1985, more than 120 floods in Shaanxi and 160 in Gansu province have been counted in the middle and upper reaches (Figure 3.6 c).

Flood prevention is closely related to sedimentation control activities, which requires comprehensive bio-technical measures, combining engineering and biological approaches. Therefore, part of the basin-wide strategy is the reduction of sediment loads, particularly that of the Loess Plateau. Since the late 1970s, large efforts in soil conservation and ecosystem restoration have been implemented by the Chinese government, in consultation with international partners (Zhou et al., 2006). First measures included the building of

check dams, and creation of level terraces, followed later by vegetation restoration, either by selective tree planting or natural recovery by land closure (Chen et al., 2007; Miao et al., 2010, 2011). Until 2011, a total area of 20,000 km² sloped land was converted to terraces (Miao et al., 2012). By altering the micro-topography, intercepting precipitation and improving the infiltration rate, the surface runoff and sediment transport into the river has been reduced. These land cover practices in the middle reaches, in combination with the successful joint operation of the Sanmenxia and Xiaolangdi reservoir of flushing water and sediment annually, the so-called *Water and Sediment Regulation Scheme*, have stopped the strong deposition tendency in the lower reaches and channel scouring can be observed instead Figure 3.7. However, the high suspended sediment load has been the dominant factor controlling the delta evolution over the last 150 years. Prior to the 1970s, the delta extended rapidly into the Bohai Sea (Li et al., 1998b). Reduced sediment supply in turn has increased coastal erosion, and decelerating and even stopping delta progradation altogether (Kuenzer et al., 2014b). Sediment load is expected to decline even further in the future. Therefore, it is important to find a balance between controlling deposition in the lower river channel on the one hand ensuring that a sufficient amount of sediment is conserved, on the other that tide and wave erosion keeping at a minimum in the Yellow River Delta.

The implemented measures successfully reduced the flood frequency in the basin. This, however, motivated local farmers to move into the floodplains and make use of their fertile soils for intensive agriculture. In 1996, more than 2 million people lived within the artificial flood levees. The farmers constructed new inner levees inside the floodplain, which are called “agricultural” or “production” dikes (Yu, 2006). In recent years, the declining sediment carrying capacity of the Yellow River has resulted furthermore in a constant raise of the riverbed within the “agricultural” dikes by 3-5 meters. This development changes the “old hanging” river into a “secondary hanging” river with a current length of around 300 km. Hence, the major challenge for river planners is integrating the dual utilization of the floodplain: it is important to maintain and restore the function of the floodplain as a retention area and the utilization of the floodplains for agricultural purposes has to be allowed.

3.2.3 Biodiversity Decline and Environmental Deterioration

The large geographical extent of the Yellow River Basin and the complexity and heterogeneity form a wide range of different and fragile ecoregions containing a unique floral and faunal species variety, many of them endangered (Olson et al., 2001; IUCN, 2015). The long history of deforestation and overgrazing, particularly on the Loess Plateau, has turned vast areas into degraded and fragmented landscapes, which used to be covered by dense temperate mixed forest ecosystems (Guobin, 1999). The recent socio-economic

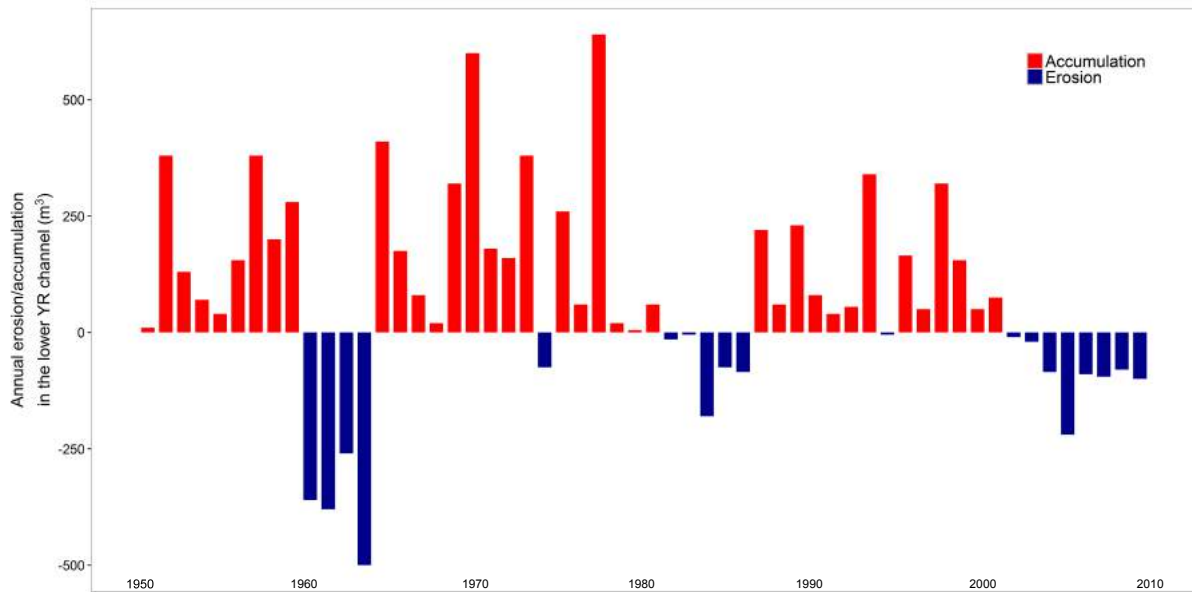


Figure 3.7: Temporal variation of erosion and accumulation pattern of sediments in the lower river channel (YRCC, 2015).

intensification, as well as anthropogenic climate change are currently threatening the remaining ecosystems and species.

Four large connected mixed deciduous forests, namely the Lüliang mountain range (2,800 km²), the Ziwuling (1,000 km²), Yunwu (1,300 km²) and Qinling Mountains (3,000 km²) remain in the Yellow River Basin, all located in the middle reaches (Shanxi and Shaanxi province). Forest patches disappeared from agricultural expansion, infrastructure development, and encroaching mining sites. The Qinling Mountains provide habitats for a significant number of endangered giant pandas. Habitat loss and fragmentation are the most serious threats to pandas. The remaining population accounts for 200 species, which is restricted to few isolated patches (Loucks et al., 2003).

Wetland ecosystems are also very dominant ecosystem features in the basin, which consist of seven internationally important Ramsar wetlands sites, such as the Shandong Yellow River Delta Wetland (1,530 km²), Eling or Ngoreng Lake in Qinghai province (610 km²), or the Zhaling or Gyaring Lake, both located in Qinghai province. As shown in Figure 3.6e, amphibian species, which depend heavily on intact wetlands, are listed by the International Union for Conservation of Nature (IUCN) as critically endangered **??**. Also avian species, such as the red-crowned crane (*Grus japonensis*, which is among the rarest cranes worldwide, require connected and healthy wetland resources (Xu et al., 2004; Wang et al., 2012a). Particularly, the lower reaches and the delta region, where the anthropogenic influence has been most prominent, experienced the strongest decline and deterioration of natural wetland ecosystems, including those of central and coastal

wetlands with a decline of more than 50 % since 1995 (Ottinger et al., 2013). Not only did direct land cover transformation, but also landscape fragmentation processes accelerated. Species connectivity was reduced and even lost through infrastructure development and the construction of industrial facilities, such as oil and gas pumps, which almost quadrupled from 340 to 1,150 in the last 20 years (Yue et al., 2003; Bi et al., 2011; Kuenzer et al., 2014b).

Facing the need to balance levels of sustained economic development in accordance with environmental conservation, large and numerous protected areas have been established to protect the remaining ecological resources. Nowadays, 100,000 km² are under protection, which equals 7 % of the basin's area (IUCN and UNEP-WCMC, 2015) (Figure 3.6e). In 1992, the Yellow River Delta Nature Reserve was founded by the Chinese government to restore and protect the remaining and still-prograding wetlands with their rare and endangered bird and plant species. Since 2013, this area is listed as a protected Ramsar site (Kuenzer et al., 2014b). Another major conserved area is the Sanjiangyuan National Nature Reserve on the Qinghai-Tibet Plateau, which was established in 2000. With covering a total area of appropriately 152,000 km², it is the second largest terrestrial protection site worldwide to protect the prevailing sensitive alpine swamp meadows and their unique wildlife with an emphasis on promoting local sustainable economic development in the region (Li et al., 2012). The predominant grassland ecosystems are extremely fragile and their capacity for regeneration is low. However, the increasing demand for cheap energy fosters coal extraction and mining activities that even encroached on this protected area (Xu et al., 2012). Ecosystems are further harmed by the release of various pollutants like oil, detergents, heavy metals, nitrogen and phosphate from fertilizer (Xia et al., 2002; Hui et al., 2009; YRCC, 2015). The loss of wetlands is even more worrisome, as this ecosystem type regulates biochemical processes, stabilizes riverbanks and coastlines, and enhances soil and water quality, but loses many of these ecosystem functions through human activities.

3.2.4 Food Security, Social Stability and Health Issues

In China food security and food self-sufficiency is a major subject of concern in the national agricultural policy to reduce dependencies on international trade markets (Ghose, 2014). Although major achievements in agricultural production have been made, domestic market prices are very susceptible to year-to-year fluctuations. The majority of the cropland is irrigated and a reduction of sufficient water causes heavy financial losses for peasant farmers, who rely on the resources water for generating income. Rural people usually have fewer alternatives for revenue generation than urban dwellers. However, the increasing demand from the industrial and domestic sector triggers conflicts between different water users. Local authorities tend to privilege industrial and domestic water

users compared to agriculture since the latter has a comparatively low economic power (Lohmar et al., 2003). There has been a transfer of water, labor, and capital towards industrialized provinces and therefore, away from the primary sector and hinterland without any compensation by the government. The majority of the population is employed in the primary sector and depends heavily on stable harvests for their livelihoods. Fish and seafood is a reliable and essential source of protein on which many locals in the Yellow River Basin depend. In recent years, fish population has declined by 30 %, fish catch even by 40 % (Li, 2005) due to overfishing, water pollution, and disruptive dams, which prevent natural migration of fish. Recent achievements in food production growth (increase by 20 % since 2000) can be seen in Figure 3.3. As one of China's main agricultural production zones, the Yellow River Basin faces great challenges of feeding the increasing demand of its population where water and land resources decline from environmental degradation, pollution, and from seizure of competing non-agricultural users. Further, the high food production and price volatility has negative impacts on food security.

Nowadays, the water of the Yellow River is heavily polluted and water quality has deteriorated rapidly by increasing industrial, agricultural, and domestic waste. Many sections are far below minimum standards. According to the latest annual report published by the Yellow River Conservancy Commission (YRCC), the main river basin authority, more than 70 % of the river's water resources are polluted and even a third are 'unsafe for any use', including drinking, agricultural, or industrial use (YRCC, 2015). Although water treatment has improved, a large quantity of effluents are still directly drained into the river system, due to lack of adequate treatment facilities and high treatment costs (Kuenzer, 2007). Further, the declining water discharge has substantially reduced the dilution capacity of wastewater causing irreparable damages to the riverine environment. Very often the Ministry of Environmental Protection (MEP) has tried to shut down polluting factories close to the main stem, but its power is limited because local environmental protection bureaus are under the control of local governments, which pursue local economic development.

Water pollution not only damages environment, but also harms the health of humans. Water pollution may not damage human health immediately, but lead to serious health impacts after long-term exposure. Industrial waste, often carcinogenic, contains many toxic compounds that threaten riparian people, who consume the contaminated water directly or eat seafood that is contaminated with heavy metals through the trophic food transfer (Cui and Li, 2011). As a consequence, the rise of the so-called 'cancer villages' along the Yellow River has even received international attention. These circumstances mainly affect the local poor, who heavily depend on the water resources for their drinking, washing, and cooking. It is believed that toxins from water and air pollution are mainly responsible for the high occurrences of cancer. However, non-point source pollution is

also considered as an critical pollution factor in the basin, as those are more difficult to control. Non-point source pollution usually stems from agricultural production by applying organic and inorganic fertilizer and pesticides on their fields. Particularly during heavy rainfall events in summer, large residues are polluting the river causing an increase in aerobic algae and depletes oxygen from the water column (Chen et al., 2003; Ju et al., 2004; Zhao et al., 2009). All in all, the aforementioned factors could threaten economic growth and fuel social instability, which has culminated in public, sometimes even violent, demonstrations (Delang, 2016).

3.2.5 Climate Change and Variability

Human-induced climate change and variability is increasingly affecting many aspects of human livelihoods and environmental conditions in the basin and exacerbates all previously mentioned social and ecological challenges. Consistent with the global trend, temperatures have increased by more than 1 °C since the 1960s, even more on the high-elevated Qinghai-Tibet Plateau (Tang et al., 2008; Hu et al., 2012; IPCC, 2013). There, permafrost is constantly degrading and a continuous thawing may lead to increasing emissions of greenhouse gases (Li et al., 2008; Wu et al., 2015). Rainfall patterns have also changed throughout the basin. Generally, the amount of precipitation has decreased, but mainly concentrates on the Loess Plateau in the middle reaches, whereas the Yellow River's source region has even received higher quantities (Tang et al., 2008).

In Winter 2015/2016, one of the strongest occurrences of the El Niño/Southern Oscillation (ENSO) event ever recorded has tremendously influenced China's weather conditions (Zhai et al., 2016). Summer precipitation has significantly reduced in the middle and lower reaches, particularly in Inner Mongolia with serious drought events. This global phenomenon influences precipitation patterns, causing a strong variability in regional climatic patterns. In the basin, strong and moderate ENSO events can be directly linked to years with low rainfall (Wang et al., 2006). There has been an apparent trend of increasing frequency of ENSO activities within the basin in the last 30 years (Wang et al., 2006).

The fifth Assessment Report of the Intergovernmental Panel on Climate Change (IPCC) reported that average temperature may increase between 2-3 °C in the RCP4.5 pathway (emission peak in 2040) and even 4-5 °C in the RCP8.5 pathway with continued emissions by 2070 (Figure 3.8) (Hijmans et al., 2005; IPCC, 2013). Rising temperatures will be more prominent in the high alpine Qinghai-Tibet Plateau and in the very arid Ordos Plateau. Precipitation trends differ depending on the greenhouse trajectory, but predict consistently a further drying of the alpine headwater region (Figure 3.8). This trend is alarming as the majority of the water resources is generated in this region and could

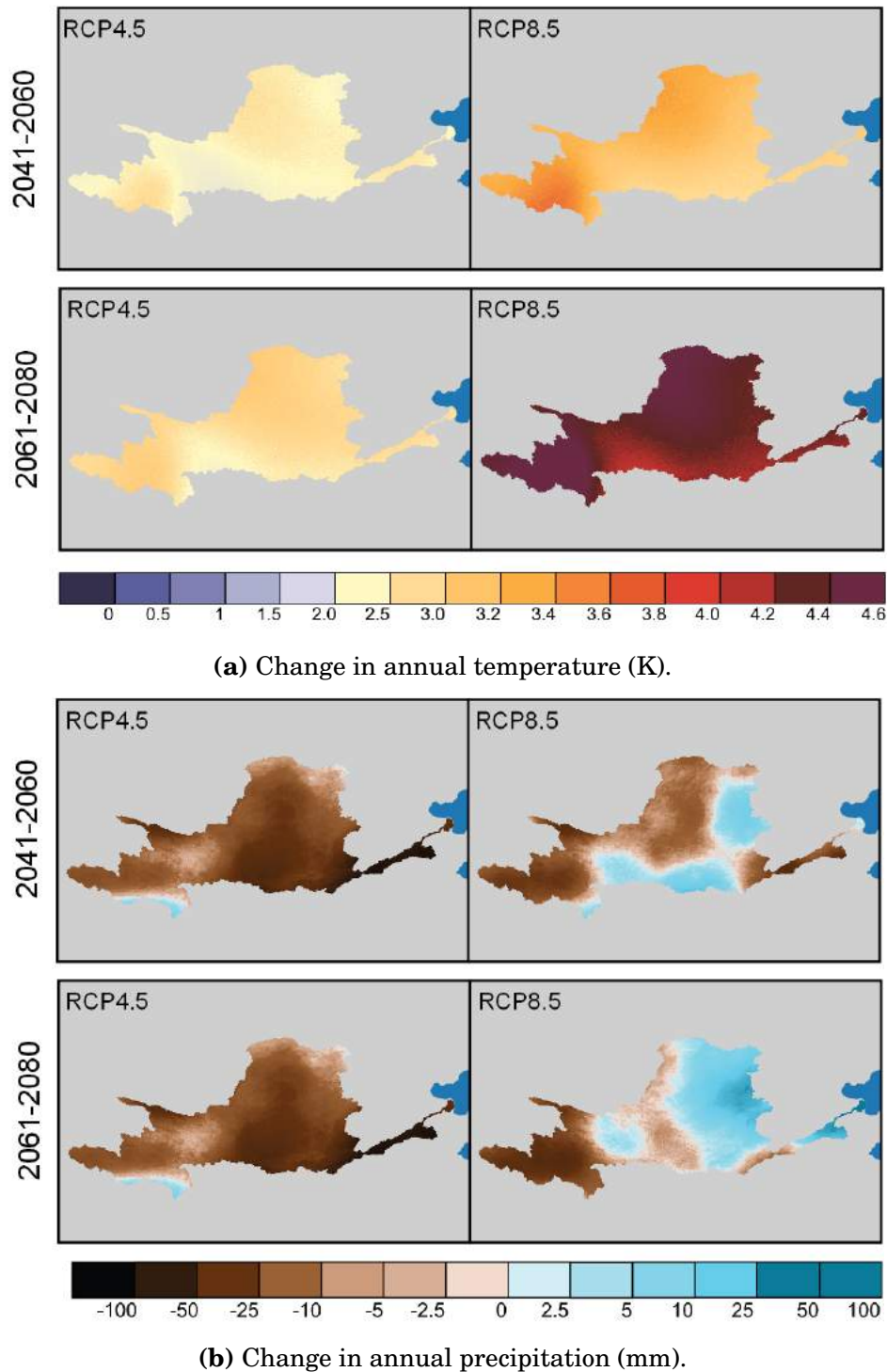


Figure 3.8: Change in average annual surface temperature (a) and average precipitation relative to 1950-2000 conditions predicted for two time periods (2041-2060 and 2061-2080) under the RCP4.5 and RCP8.5 scenario based on MPI-ESM-LR model.

result in a further decline of the river's water discharge, which is already at a critical level. Climate change may alter seasonal variability of rainfall and foster extreme events more frequently.

The direct impacts of Global Warming are diverse. The basin is a very important base for domestic food production and many rural people depend on agriculture for living. There are contradictions about climate change effects related to agricultural production in China. Tao et al. (2008) concluded a reduced agricultural yield between 10 and 20 %, whereas warmer temperatures in winter could increase yields of winter wheat (Tao and Zhang, 2013). Extreme weather events, such as heat waves, heavy rainfall events accompanied with flooding, and storms are expected to increase with adverse effects on agrarian production (IPCC, 2013). As a consequence, climate change could put result in increasing rural impoverishment as those people usually only have limited capacity to adapt to the negative impacts.

The delta region of the Yellow River is on the front line of climate change and extremely vulnerable to resulting and expected impacts. Land subsidence, resulting from groundwater withdrawal, in combination with sea level rise is an immediate threat to the dense population and economy (Syvitski et al., 2009; Kuenzer et al., 2014b). Models suggest an increase of 35 cm until 2050 (IPCC, 2013). Intact coastal wetlands are the first defense against storm surges and erosion processes, making the protection of such essential.

3.3 Managerial and Policy Efforts towards a more Sustainable River Basin

Facing serious environmental and social challenges, numerous stakeholders in the Yellow River Basin are now seeing the consequences of the long-term irrational exploitation of land and water resources. They will worsen, unless management strategies and policies are adopted in the near future. To counteract, several national management plans and policies have been issued at almost all hierarchical levels, from national to local, to address the complex and diverse problems that are currently affecting a sustainable development within the basin (Liu et al., 2012). China's oblong political and social heritage has preferred regulatory mechanism by legislation as major policy instrument. However, it seems that China's policy is currently undergoing a sizable paradigm shift towards bottom-up approaches, e.g. tackling pollution problems and is shifting away from pure command and regulating instruments (Zhang and Wen, 2008). Already in the 1970s, environmental policy frameworks have been initiated by adapting more than 30 environmental laws and regulations. A major trigger for increasing environmental awareness was the Yangtze flood in 1998 with almost 4,000 casualties and an economic loss of 24 billion USD, which urged the need of restoring and conserving ecosystems (Ye and Glantz, 2005). In recent past, the *Law on Water Pollution Control* (1984), the *Environmental Protection Law* (1989), the *Soil and Water Conservation Law* (1991), and the *Water Law* in 2002 can be considered as the most important national laws attempting to ensure an improvement of

environmental quality (Zhang and Wen, 2008). So far, China's policies have tended to be more in a reactionary, responding to environmental crises instead of pro-actively avoiding them (Turner, 2005).

The frequently desiccated Yellow River showed the need to manage water quantities and withdrawal in a more sustainable way. The State Council of the People's Republic of China responded with the *Yellow River Water Allocation Scheme*, also known as *1987 Scheme* to manage water shortage and scarcity approved in 1987. This tool regulates water withdrawal quota for all riparian provinces and assigns the Yellow River Conservancy Commission (YRCC) as responsible institutional organ. The YRCC was established in 1929 as institution for flood management and for development of new water resources. The novelty of this program was that environmental water requirements were taken into consideration to maintain ecosystem health and services particularly in the lower reaches. Despite this measure, drying out events didn't stop, in fact, they have even become worse. Reasons are the violations of national laws by the provincial governments due to the weakness in law enforcement of the YRCC. Provinces often institute their own laws considering only personal benefits, causing heterogeneity in policy (Zhu et al., 2003; Xia and Pahl-Wostl, 2012). To address the shortcomings of the *1987 Scheme*, the adaptive Unified Water Flow Regulation (UWFR) was initiated by the YRCC. In this adaptive scheme monthly water thresholds released by dams are calculated based on the prevailing reservoir storage, weather forecast, and water demand (Ringler et al., 2010). Further, the YRCC established provincial water bureaus that can better monitor water allocation and manage the operation of large reservoirs. Since the enforcement of the UWFR, the Yellow River has not ceased to flow. The weakness of law enforcement of the YRCC has been tackled with the implementation of the innovative *New Water Law* from 2002, which is the outcome of negotiations between state, river basin authorities, and provincial officials. It has strengthened the river basin commission as a formal river basin authority and was set above province level, with mandates to implement reforms and create regional river basin bureaus. Now the YRCC defines critical thresholds for water discharge and water abstractions are constrained or even stopped if water river's discharge falls below the critical value. Furthermore, it received more financial resources.

Inspired by the theory of economic instruments, the Chinese government has recently started to introduce economic and market-based instruments. If they are well designed, economic-based instruments internalize environmental costs from production and consumption and should influence consumptive behavior as well as the production of polluters. Common mechanisms include the use of pricing mechanisms (taxes, subsidies, pollution charges, payments for ecosystem services), tradable permits for pollutants or emissions, and investment incentives for greener technologies or environmental protection and restoration (Dinar et al., 1997; Starvins, 2000). In the Yellow River Basin water is consid-

ered under-priced despite recent pricing reforms (Webber et al., 2008; Ringler et al., 2010). Higher prices could reduce water wastage towards higher water use efficiency. Pricing mechanism influence consumption attitude and works usually well for industrial and domestic users, but hits predominantly agricultural water users, as they only produce economically low-value commodities with relatively low income (Ringler et al., 2010). Their livelihoods depend heavily on the use of water for irrigating their crops. Charging higher prices would result in a direct reduction of farmer's revenue with tremendous social repercussions. Therefore, pricing reforms need appropriate water prices for farmers to avoid adverse social consequences, such as impoverishment of the rural population. At the same time reforms are necessary to achieve gains in water use efficiency (Cai, 2008). Besides pricing reforms, water-use rights as tradable permits establish rights and responsibilities for users to allocate resources from low-value to high-value production. Currently, there is no formal water market established in the basin. The YRCC experimented with local-level water rights transactions between industry and agricultural irrigation districts in upstream regions in Inner Mongolia (Xia and Pahl-Wostl, 2012). The basis idea of this experiment was that industry financed water conservation infrastructure, which received in turn the water quantities saved by the new infrastructure. This concept was later successfully extended to other provinces.

The need for ecological restoration within the Yellow River Basin to restore ecosystem functions, such as carbon sequestration, hydrological functions, and soil retention capacity, has become a major goal for various local and regional stakeholders. In 1996 the *Watershed Rehabilitation Program*, which was supported by the World Bank, targeted specifically degraded areas in the Loess Plateau with low vegetation coverage (Figure 3.9c). One objective was to foster sustainable crop production on terraced slopes and to stabilize the highly erosive soils by planting trees and shrubs to reduce soil loss (Figure 3.9b). This project also aimed to support local farming structures and improve the living and working conditions to reduce the increased impoverishment in rural areas.

Following the international trend, the payments for ecosystem services (PES) instruments are becoming more important in China, where a number of national and regional policies have been initiated in the last years (Zhen and Zhang, 2011). Most of the PES programs conducted in the basin are targeted to improve water quality and quantity, to control soil erosion, and to promote biodiversity. Amongst others, the two previously mentioned (in section 3.1 on page 31) programs are the NFCP and GfG programs. The former one has aimed to protect natural forests particularly in the upper and middle reaches through logging restrictions and afforestation incentives. Logging companies were financially compensated for their economic losses for allowing forest regeneration. The second initiative, the GfG program, which is one of the largest conservation projects worldwide, compensated farmers for converting sloped cropland (>25°) to grassland or forest. This



(a) Ecologically restored Loess Plateau in Shaanxi.



(b) Newly created terraced fields for agricultural cultivation.



(c) Still degraded and sparsely vegetated Loess Plateau in Gansu.



(d) Planted square grass mats.



(e) Pine nursery in the valleys of the Loess Plateau for afforestation.

Figure 3.9: Landscape activities on the Loess Plateau (photographs taken by Christian Wohlfart in April 2016).

measure was taking place mainly on the Loess Plateau in order to maintain and improve the ecological status of the basin and to promote sustainable regional development.

Farmers were either provided with direct financial compensation or received grain as replacement for each hectare of cropland they converted. The project started in 1999 and contributed to a significant increase in vegetation coverage. Around 82,700 km² were subjected to GfG (Zhou et al., 2009). However, the initially proposed period of eight years of financing might not be enough to guarantee a long-term effective ecosystem recover, as farmers tend to convert back their land to cropland if payments cease. Therefore, the Chinese government approved the extension to an additional eight year cycle, which ends now end of 2016. Large-scale restoration effects can be seen in Figure 3.9 a.

Apart from these two policy instruments, various other tools exist, such as capacity training and education of local people to raise public awareness, self-regulation, consultation and negotiation, or community involvement. All these tools complement to each other well and no single measure could possibly solve all of the existing problems in the basin given the complexity of the occurring challenge in the basin. Another important issue is that policies should target social inequality in the basin by integrating the concerns of rural people. So far, the benefits of growth have not necessarily touched the poorest.

3.4 Discussion

River basins are complex social-ecological systems in which humans interact strongly with their biogeophysical environment. In the Yellow River Basin, these interdependencies can be dated back several millennia, but under the tremendous economic boom in recent decades, their intensity has increased dramatically creating manifold, complex social-ecological challenges. The majority of the contemporary problems facing the basin stem from long-term and rigorous abuse of the prevailing natural resources and underpinned by policy choices, cultural attitude, and institutions that have evolved over the centuries in China. To deal with these complex and multi-faceted challenges, it was suggested in several studies that it is more important to change the existing governance and institutional settings towards a more adaptive and holistic river management, rather than changing the Yellow River's biogeophysical condition itself (Habron, 2003; Myint, 2003; Moss, 2004; Lebel et al., 2013). So far, research has put more of an emphasis on issues related to the biogeophysical environment, whereas studies dealing with river governance hardly received any scientific attention.

China has created a complex hierarchical but also vertical and inflated bureaucratic structure to manage the river system. The different levels often have divergent interests and therefore slow down the implementation of efficient policies (Lieberthal and Lampton, 1992; Lohmar et al., 2003; Barnett et al., 2006). Certainly, many individual environmental laws and regulations have been enacted by different ministries, but they often pursue different and contradictorily goals. In the current government structure, there are many

ministries with their own program and interests: e.g. surface water conservation (Ministry of Water Resources - MWR); ecological preservation and pollution reduction (Ministry of Environmental Protection - MEP), fisheries, livestock and farming (Ministry of Agriculture - MA), oil and coal extraction and groundwater (Ministry of Land and Resources - MLR), and urban development (Ministry of Housing and Urban-Rural Development - MHURD) (Ringler et al., 2010; Wang et al., 2011). In the context of water management, it is odd that issues relating to surface and groundwater are treated by different national ministries. Also, the responsibilities for water quality management fall into the scope of duties of two ministries, the MWR and MEP (Ongley and Wang, 2004). Many ministries have overlapping and unclear defined responsibilities and furthermore tend not to share data and information with each other (Song et al., 2010). Often, ministries gather and publish contradictory results as they implement different and non-standardized monitoring and information systems. Horizontal policy integration and coordination remains weak in the basin. Besides the national-level ministries, the nine provincial bureaus are main river stakeholders and at the subprovincial level, there are bureaus on prefecture, county, and township levels (Lohmar et al., 2003; Barnett et al., 2006). However, vertical coordination between these authorities and provinces remains poor or even non-existent. Another problem is that many responsibilities are primarily delegated to the provincial level, such as water and pollution management. The lack of data and information exchange between provincial governments also becomes apparent. These tend to make decisions based on self-interest and local considerations, without taking the needs of other players into consideration, and sometimes even ignoring national policy (Liu et al., 2012).

At present, river basin management lacks a unified strategy to deal with issues as a whole. To resolve these complex challenges in the basin, a more integrated and holistic basin management is required and should incorporate all different needs and users (Varis and Vakkilainen, 2001; Lohmar et al., 2003). Sustainable development won't happen if not all involved facets are working together. River basins are dynamic over space and time, and changes in any single component can influence the whole basin. Certainly, there is a trans-provincial river commission, the YRCC, which should act as an independent agency and not determined by any political or provincial boundaries. But this is not really true for the YRCC. Basically, the YRCC is an arm of the Ministry of Water Resources and hence follows the strategy dictated by the Ministry more and is therefore unable to represent collective interests. A river commission properly speaking should be more of a committee of different ministerial bureaus representing various interests and different provinces and all vertical tiers, working together with one common aim: to use the prevailing resources in a long-term sustainable manner (Barrow, 1998; Griffiths, 2002) (Figure 3.10). Another problem of the YRCC is the lack of enforcement power in the basin, as it is simply a regional agency on a low administrative level. Only a strong and powerful

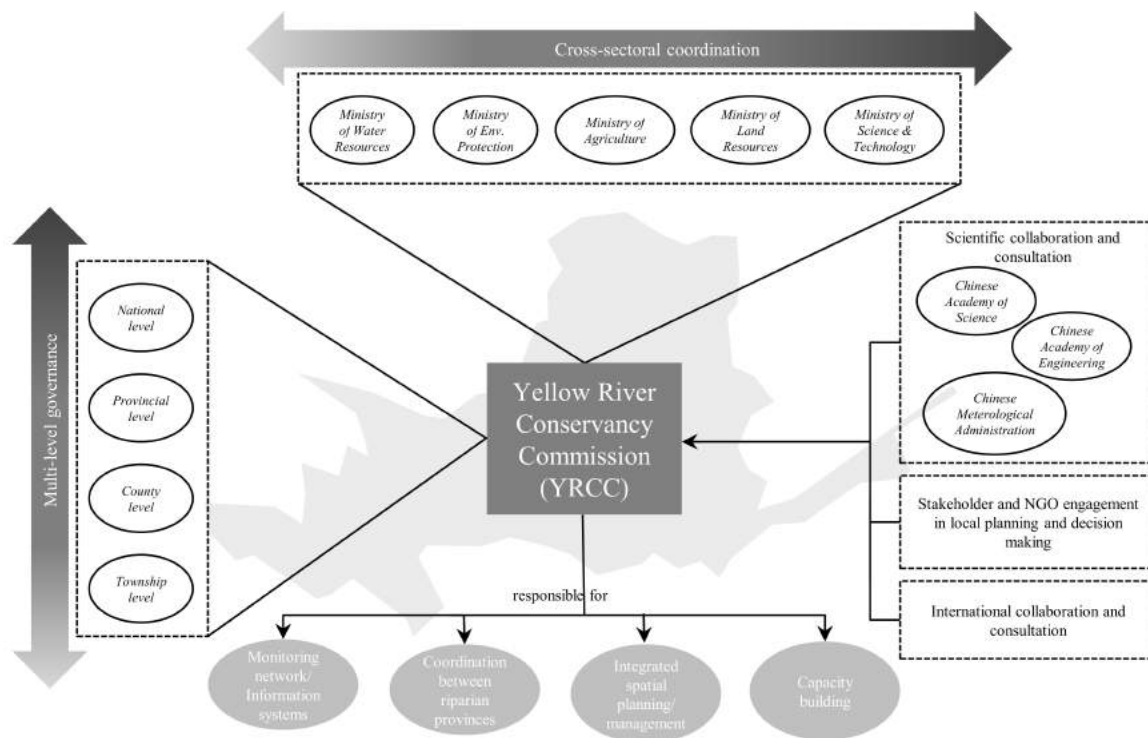


Figure 3.10: Proposed river basin governance model for the Yellow River Basin towards a more integrated and holistic management.

established river basin commission can address the complex challenges by overcoming institutional and provincial inertia. Initially, the YRCC was established as an institution for flood control and water resources development. The early management strategies were dominated by pure supply-driven and engineering-dominated approaches, but are now shifting towards more holistic and demand-based strategies not only linking social and economic development but also considering the conservation of natural ecosystems (Boxer, 2001). Despite this current transition within the YRCC, there has to be a continuing institutional change. The first step towards a stronger river commission was taken in 2002, when the YRCC was set above provincial level in order to improve cross-provincial coordination.

Yet the main obstacle in dealing with the complex challenges is the current mono-centric governance system that has such a strong vertical top-down approach (Xu, 1999; Zhang and Wen, 2008). This approach is usually quite successful in dealing with simple and clear challenges. For example, the YRCC succeeded in developing efficient flood management plans, based on the traditional top-down and mainly technically driven model. When it comes to more complex social-ecological situations, however, such approaches remain insufficient to respond comprehensively to all challenges facing river management. Therefore, localized management and a better vertical and horizontal that ideally incorporates all different needs and interests of all users helps to ensure that the complex issues are

addressed in new policies, specifically tailored to solve the particular problems faced (Figure 3.10). Further, strong top-down approaches impede local community involvement; as a consequence local people often show little to no interest in following national governance. A more bottom-up approach, where local stakeholders are included and incorporated into the decision-making and planning process, is essential for improving the quality and coherence of public policy and must be strengthened within the basin. This is mainly the task of a strong and properly designed river basin commission to balance and coordinate all specific needs with mutual benefits, also those of poorer locals.

Besides the strong consideration of locals in the decision making and planning process, national NGOs can serve as a powerful consultative body, as these organizations are often a useful proxy for the concerns of local and regional stakeholders. But China's NGOs are affected by legal and political constraints and therefore lack experience and financial resources (Economy 2010). Today, China is trying to work more closely with the international community in the field of water governance and integrated river basin management (IRBM). In 2006, the EU - China River Basin Management Program (RBMP) has been initiated, which involves Chinese ministries (e.g. MWR, MEP), the YRCC, and all riparian provinces, supported by leading experts from the EU who enhance IRBM policies and practices by sharing EU experience. The successful EU water framework directive, which is one of the most innovative and powerful legislative instruments, served as an inspiring policy example for China and the basin managers in the field of water policy and water resource management (Moss 2004). The regulatory directive has more ecosystem-based objectives and all EU member states have committed to achieving a good qualitative and quantitative status of all water bodies. The EU experts also included local communities and stakeholders as well as NGOs designing a proper and realistic management plan to meet the present and future demands of society, while maintaining environmental and ecological quality. However, to guarantee the successful implementation of such an integrative approach, there is a strong need for high vertical and horizontal integration, which currently still does not exist in the basin. Indeed, the YRCC started to establish regular meetings on various topics to bring all involved stakeholders together. In place since 2003, the biannual International Yellow River Forum is a large international conference and serves as an exchange and communication platform where governmental entities, scientific institutions, NGOs, and industry share their experience in river basin management to jointly develop management strategies for the Yellow River Basin. This forum is the first step towards a better horizontal integration. Information sharing, data harmonization, science and technology support, and public participation should be prioritized and accomplished by a strong river basin commission. An effective integrated river basin management also demands basin-wide precise and consistent information about biophysical, environmental, and socio-economic situations,

which is necessary for strategic decision-making. As already stated, the current data management within the basin is either difficult to access, fragmented, inconsistent or outdated. One possibility of handling and sharing data could be the establishment of a common platform for spatial information in form of an inter- and transdisciplinary geographical information system (GIS), maintained e.g. by the YRCC on which various data on socio-economic aspects, such as hydro-meteorological, water and quality data, and land use/cover characteristics are provided. This information can be retrieved by either in situ monitoring, modeling techniques, or with remote sensing techniques. The latter has the capability to monitor timely consistent environmental dynamics on large spatial scales and to derive various thematic maps. In conjunction to remote sensing information, a well-developed set of various simulation models in hydro-meteorological or even socioeconomic context can further optimize and support planning and management strategies and scenarios for future development. Such systems have already been successfully implemented in other river basins globally, but always need to be tailored to the respective requirements of the stakeholders in the Yellow River basin.

3.5 Summary

- ❶ This chapter provided the reader of this thesis with an executive summary of current dynamic processes and consequent challenges affecting the Yellow River social-ecological system and the difficulties of find a long-term sustainable solution for such a dynamic and vulnerable system.
- ❷ In recent decades, the Yellow River Basin has faced a spectacular socio-economic boom, which has mainly achieved at the expenses of environmental and social resources.
- ❸ Water scarcity, flooding, pollution, and ecological degradation, the considered key challenges, have been further aggravated by anthropogenic-induced climate change.
- ❹ Many conservation policies and management plans have been issued, often consulted by international partners, to address the prevailing social-ecological challenges.
- ❺ Despite major success, further policy and institutional reforms are still required to enable a long-term sustainable development.
- ❻ An integrative and holistic river basin management could be supported by a common data platform (e.g. GIS), where various data forms are stored and shared.

DATA SOURCES AND CLASSIFICATION MODEL

This chapter outlines the multiple remote sensing data sources used for assessing land surface dynamics in the Yellow River Basin in China. Further, a detailed description about the applied classification model is given.

The Moderate-resolution Imaging Spectroradiometer (MODIS) monitors earth's surface since 2000 at a spatial resolution of 250 m. The high temporal resolution of this sensor allows for the delineation of seasonal features on which the land cover/use classification is based. With a pixel size of 30x30 m, Landsat TM (Thematic Mapper), ETM+ (Enhanced Thematic Mapper Plus), and OLI (Operational Land Image) data provide a spatially more detailed view and are better suited for depicting the complex and heterogeneous character that is present in the Yellow River Basin. Detailed information about the MODIS and Landsat data processing steps will be explained in the sections 5.2 and 6.3 on pages 64 and 101, respectively. Besides, remote sensing products, such as the SRTM (Shuttle Radar Topography Mission) Digital Elevation Model (DEM) or the Nighttime Lights Time Series derived from the DMSP Operational Linescan System (OLS) instrument served as auxiliary data sets for improving classification results of the Yellow River Basin.

For each delineated land cover/use product, the thematic quality is assessed by using very high resolution data (VHR) provided in virtual globe software, such as Google Earth and the Chinese pendant Mapworld, where freely VHR data are available. The VHR imagery available in the Yellow River Basin stems mainly from Quickbird and IKONOS data. As this data were only used as a visually source and were not further processed, a description of such data was intentionality excluded. In addition, accuracy assessment was supported by *in-situ* data from two field campaigns in 2013 and 2016.

Finally, the Random Forest (RF) classification model will be introduced, which has often

been applied in many remote sensing studies for land cover/use applications.

4.1 MODIS

The launch of the MODIS in December 1999 inaugurated a new era in hyperspectral remote sensing. Besides the Landsat legacy, MODIS is one of NASA's (National Aeronautics and Space Administration) Earth Observing System (EOS) key instruments aboard the Terra and Aqua satellites as it provides a continuous measurement of many environmental parameters (land surface temperatures, fire products, snow and ice cover, vegetation properties and dynamics, surface reflectance and emissivity, cloud and aerosol properties, atmospheric temperature and water vapor, ocean color and pigments and ocean biological parameters). The first MODIS sensor went into orbit with the launch of the Terra (formerly known as EOS AM) on December 2000. With the launch of Aqua (EOS PM) on May 2002, MODIS Terra and Aqua are observing the entire Earth's surface with near daily coverage (Barnes et al., 2003).

MODIS is a 36 band spectrometer providing a global data set every 1-2 days with swath dimensions of 2,330 km (cross track) by 10 km (along track at nadir). It provides data with high radiometric sensitivity (12 bit) in a spectral range from 405 μm to 14,385 μm at moderate spatial resolution. Two bands (red and NIR) are imaged at a nominal resolution of 250 m at nadir, with five bands (visible to short-wave infrared) at 500 m, and the remaining 29 bands at 1000 m (visible to thermal infrared). A detailed overview for the 36 spectral channels of MODIS is given in Table 4.1.

Based on MODIS observations a suite of higher-level products describing different terrestrial, ocean, and atmospheric features have been generated, for a wide range of users in support of *Global Change* research (Justice et al., 2002). More than 70 standardized MODIS land products are distributed to the scientific and application community via the Land Processes Distributed Active Archive Center (LP DAAC), where specifically level-2 or higher processed data can be downloaded. All higher-level MODIS products are

Table 4.1: Spectral and spatial properties of the MODIS sensor.

band	bandwidth (μm)	spatial resolution (m)
1 Red	620 - 670	250
2 NIR	841 - 876	250
3 Blue	459 - 479	500
4 SWIR	545 - 565	500
5 - 7	1230 - 2155	500
8 - 19	405 - 965	1000
20 - 36	3660 - 14,385	1000

delivered in sinusoidal projection in 1200x1200 tiles (Huete et al., 2002). Most MODIS standard products contain a pixel-wise quality assurance (QA) information embedded in a Scientific Data Set (SDS) array. The QA layer provides information on cloud coverage, atmospheric disturbances, viewing angle, and confidence levels of the product. Since the launch of Terra, there have been several MODIS data “collections” (or versions) processed. Basically, a MODIS collection is a MODIS data version, where new and improved data algorithms have been developed, implemented and distributed as new “collections” (Justice et al., 2002).

In this thesis, the MODIS surface reflectance product **MOD09Q1** (collection 5 data) served as backbone remote sensing data for classifying the land cover/use characteristics of the Yellow River Basin. The MOD09Q1 product are provided at 250 m nominal spatial resolution as a level-3 gridded product in the HDF-EOS format. The SDS array has three layer including MODIS bands 1 & 2 reflectance, which contains the best possible observation during an 8-day period as selected on the basis of high observation coverage, low view angle, the absence of clouds or cloud shadow, and aerosol loading, and a 250 m reflectance band quality rating.

4.2 Landsat TM, ETM+, OLI

With the launch of the first sensor in 1972, the Landsat mission provides the world’s longest continuous earth observation record of multi-spectral data (Williams et al., 2006). Since that, seven Landsat-bound sensors (Landsat 1-5 and Landsat 7-8) have successfully been launched and facilitate the collection of terrestrial imagery (Figure 4.1). The TM (Thematic Mapper) on board the Landsat-4 and Landsat-5 acquired spectrally richer data from 1982 until 2013 at a much wider range of wavelength with seven spectral bands and spatial resolutions of 30 m and 120 m (TIR) (Table 4.2), compared to its predecessor the

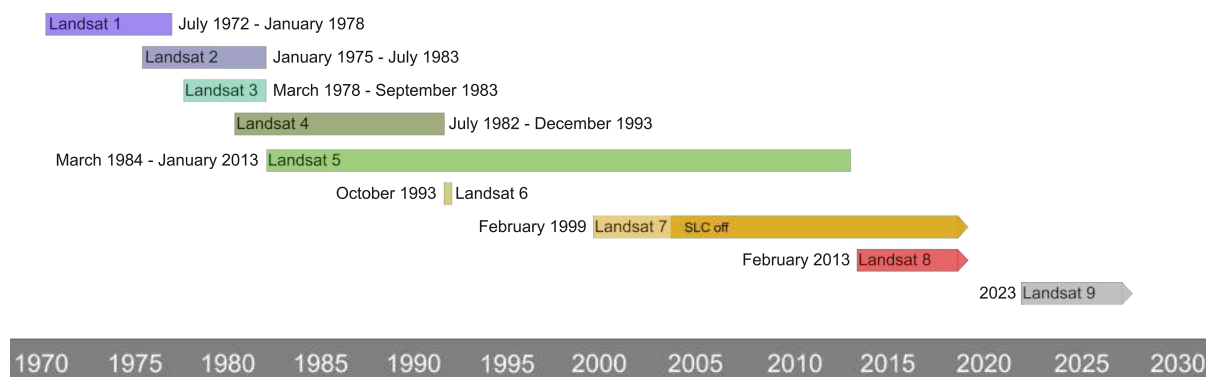


Figure 4.1: Timeline and history of the Landsat legacy, which has commenced in 1972 (modified after NASA/USGS).

Table 4.2: Spectral and spatial properties of each Landsat TM, ETM+, and OLI sensor.

Landsat TM			Landsat ETM+			Landsat OLI		
band	bandwidths (μm)	resolution (m)	band	bandwidths (μm)	resolution (m)	band	bandwidths (μm)	resolution (m)
1 Blue	0.45 - 0.52	30	1 Blue	0.441 - 0.514	30	1 Coastal/Aerosol	0.435 - 0.451	30
2 Green	0.52 - 0.60	30	2 Green	0.519 - 0.601	30	2 Blue	0.452 - 0.512	30
3 Red	0.63 - 0.69	30	3 Red	0.631 - 0.692	30	3 Green	0.533 - 0.590	30
4 NIR	0.76 - 0.90	30	4 NIR	0.772 - 0.898	30	4 Red	0.636 - 0.673	30
5 SWIR 1	1.55 - 1.75	30	5 SWIR 1	1.547 - 1.740	30	5 NIR	0.851 - 0.879	30
						6 SWIR 1	1.566 - 1.651	30
						10 TIR 1	10.60 - 11.19	100
						11 TIR 2	11.50 - 12.51	100
6 TIR	10.40 - 12.50	120	6 TIR	10.31 - 12.36	60	7 SWIR 2	2.107 - 2.294	30
7 SWIR 2	2.08 - 2.35	30	7 SWIR 2	2.064 - 2.345	30	8 PAN	0.503 - 0.676	15
		15	8 PAN	0.515 - 0.896	15	9 Cirrus	1.363 - 1.384	30

Multispectral Scanner (MSS), which only captured reflected radiation from the visible and near infra-red (NIR) wavelength. Since 1984 the second TM sensor (Landsat-5 platform) was released into orbit. The following ETM+ aboard Landsat-7 continues to provide datasets at the same spectrum of wavelength as TM (blue, green, red, near-infrared (NIR) and mid-infrared (MIR) with 30 m resolution. ETM+ added a panchromatic band with 15 m ground resolution and improved ground resolution of TIR with now 60 m. The eighth Landsat mission launched in 2013, featuring the Operational Land Imager (OLI) and the Thermal Infrared Sensor (TIRS) with 100 m resolution (Table 4.2). Combined these two instruments generate eleven total spectral bands. OLI expands the spectral range offered by TM and ETM+, including additional bands for enhanced atmospheric correction and cloud masking (Irons et al., 2012). The Landsat program was not running without any trouble. The Landsat 6 mission equipped with ETM, launched in 1993, didn't reach orbit. Luckily, data continuity was ensured by the unforeseen lifespan of the Landsat-5 TM sensor. In May 2003, a failure in the Scan Line Corrector (SLC) on board the ETM+ sensor resulted in data gaps with an approximately 22 % loss of data but are still useful and maintain the same radiometric and geometric corrections as data collected prior to the SLC failure (Maxwell et al., 2007). NASA and USGS (United States Geological Survey) are currently working on the Landsat-9 mission for an expected launch in 2023. Landsat-9 will extend Landsat program's record length to half a century, which provides consistent images of the Earth and basically replicates its predecessor Landsat 8 (Figure 4.1). In 2008, a new era of open-access satellite imagery commenced. The USGS released the entire Landsat archive for free public use, which is the world's largest collection of satellite imagery (Woodcock et al., 2008). This open policy creates new prospects for environmental monitoring.

4.3 In-situ Field Data

Two field campaigns in the Yellow River Basin were conducted to gain additional *in-situ* measurements to complement the comprehensive reference dataset for training and testing the classification model Figure 4.3. Ground-based land cover field surveys are

essential and further support the interpretation and analysis of what is being sensed, as the synoptic view of remote sensing imagery shows a different perspective of the prevailing landscape conditions (Wohlfart et al., 2016a). The classes and sampling procedure was based according to the Land Cover Classification System (LCCS) defined by the Food and Agriculture Organization of the United Nations (FAO) (Di Gregorio, 2005). This system is a comprehensive and standardized a priori classification system, designed to retrieve consistent and harmonized samples for land cover/use classification. In the field, reference sites with a minimum size of 250x250 m containing homogeneous land characteristics were determined and field surveys were carried out following the field form as shown in Figure 4.2.

Field survey May 2014		Surveyor			
		Date			
		Location			

Point Measures		
Point ID		Sketch
Waypoint ID		
Sample Size		
Lat		
Lon		
Distance		
Azimuth		

Object measures					
Landuse/Landcover type	Level 1 - LCCS	Level 2 - LCCS	Level 3	Level 4	Level 5
	<input type="checkbox"/>	<input type="checkbox"/>	<input type="checkbox"/>	<input type="checkbox"/>	<input type="checkbox"/>
Homogeneity	<input type="checkbox"/> Dense	<input type="checkbox"/> Sparse	<input type="checkbox"/> Open	<input type="checkbox"/> None	
Growing Stage	<input type="checkbox"/> High	<input type="checkbox"/> Medium	<input type="checkbox"/> Low	<input type="checkbox"/> None	
Shape	<input type="checkbox"/> Compact	<input type="checkbox"/> Linear	<input type="checkbox"/> Fragmented	Min-Diameter [m]	
				<input type="checkbox"/>	

Conditions				Temperature [°C]
Clouds	<input type="checkbox"/> High	<input type="checkbox"/> Medium	<input type="checkbox"/> Low	<input type="checkbox"/> None
Rain	<input type="checkbox"/> High	<input type="checkbox"/> Medium	<input type="checkbox"/> Low	<input type="checkbox"/> None
Accessibility		<input type="checkbox"/> Easy	<input type="checkbox"/> Difficult	<input type="checkbox"/> None
Soil Moisture	<input type="checkbox"/> High	<input type="checkbox"/> Medium	<input type="checkbox"/> Low	<input type="checkbox"/> None
Soil Salinity	<input type="checkbox"/> High	<input type="checkbox"/> Medium	<input type="checkbox"/> Low	<input type="checkbox"/> None

Photographs / image names		
	A (GPS)	5
	B (Plot)	6
	1 (→N)	7
	2 (→E)	8
	3 (→S)	
	4 (→W)	

Comments

Figure 4.2: The standardized Land Cover Classification System (LCCS) field protocol for land cover collection in the Yellow River Basin.

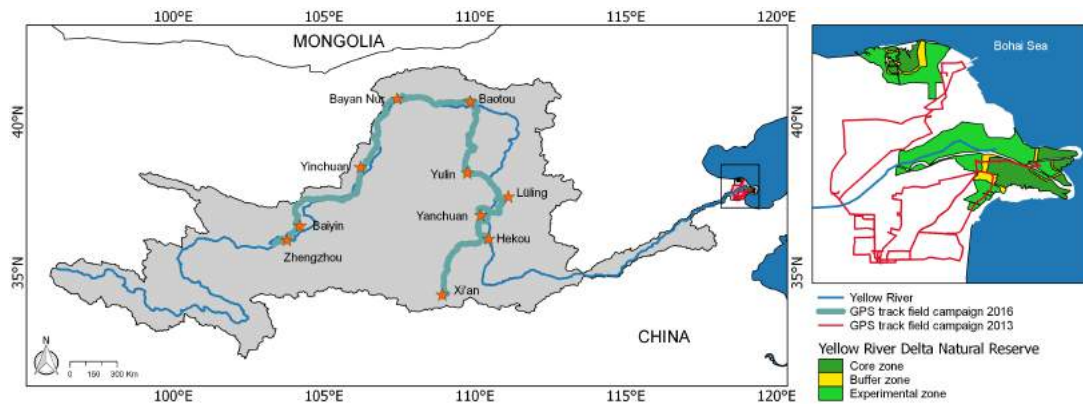


Figure 4.3: GPS tracks of both field campaigns conducted in 2013 (Yellow River Delta, right panel) and 2016 (Yellow River Basin - left panel).

In the first two-week field campaign in October 2013 (07. Oct to 21. Oct) the land surface characteristics in the Yellow River Basin with focus particularly on agriculture and natural wetland ecosystems were sampled. The second field trip in April 2016 (04. Apr to 28. Oct) to the study region encompassed the entire Yellow River Basin to cover and sample all land cover entities that occur in the basin. The journey started in Xi'an following the Yellow River upstream crossing the Loess and Ordos Plateau until Lanzhou was reached. During both field campaigns a total number of around 450 field samples were acquired.

4.4 Classification Model

In the domain of land cover applications various classification models using multi-spectral data exist, including generalized linear models (GLM), support vector machines (SVM), or decision tree learning, among others. Decision tree-based classifiers, such as random forests (RF), have been successfully and extensively applied to land cover studies and tend to yield higher accuracies than other conventional classifiers, including maximum likelihood and standard trees (Gislason et al., 2006; Chan and Paelinckx, 2008). Aside from the high performance, RF is robust to noise and overfitting, and the algorithm is comparably quicker than methods based on boosting (Breiman, 2001). Further, the handling of the classifier is user-friendly, as the model can be run without much tuning of the parameters. RF algorithms are used to construct multiple decision trees, which are built independently, using a bootstrap sample of the dataset (Breiman, 2001). RF searches for a random sample of the predictors and chooses the best split amongst the predictors. The final classification is based on the majority vote of the ensemble (Figure 4.4).

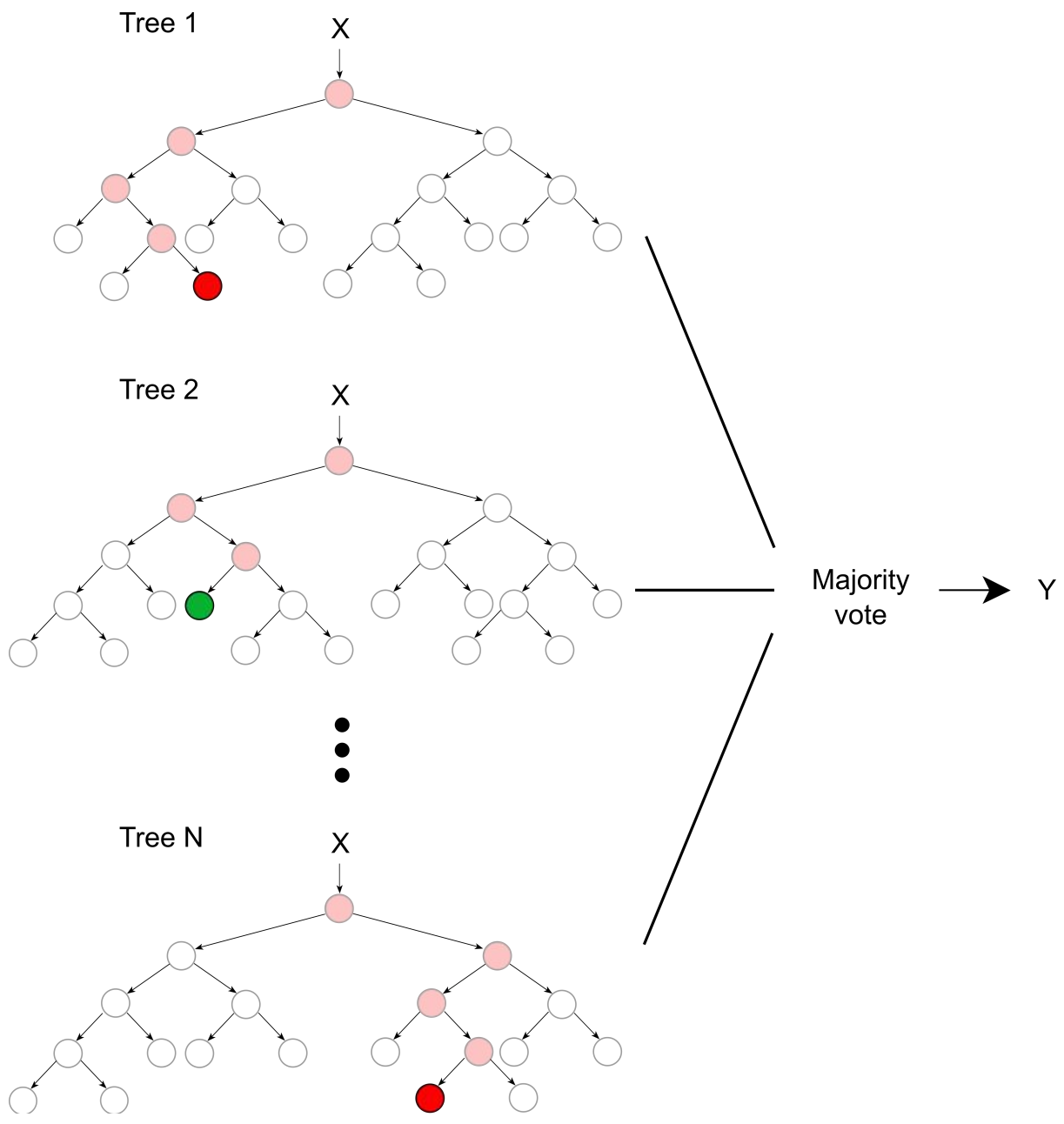


Figure 4.4: Illustration of the random forest learning scheme.

LAND COVER CHANGE DYNAMICS FOR THE YELLOW RIVER BASIN BASED ON MODIS TIME-SERIES*

As stated in the previous chapter, a holistic river basin management requires reliable, consistent, multi-temporal spatial “wall-to-wall” information as baseline information for the involved stakeholders to support a more sustainable regional management plans and decisions. Despite the urgent need for such information, there is a surprising lack of precise thematic land products showing the current dynamics of land cover and use for the entire basin. The availability of precise and up-to-date regional land cover change information is crucial to better understand the prevailing dynamics and underlying factors influencing the current processes in the complex Yellow River Basin social-ecological system and can additionally serve as a valuable component for modeling and decision making. As already shown in section 1.2.1 on page 6, remote sensing research for the Yellow River Basin was conducted localized on small spatial scales with a strong geographical focus on Qinghai-Tibet Plateau (Guo et al., 2008; Dong et al., 2009; Song et al., 2009; Liang et al., 2012), the highly erosive and impacted Loess Plateau (Chen et al., 2009; Zhai et al., 2015) or the fast emerging Yellow River Delta region (Wang et al., 2012b; Ottinger et al., 2013; Kuenzer et al., 2014b).

In this chapter, land cover change dynamics will be delineated for two time steps (2003 and 2013) to show the very recent dynamic processes that have influenced the Yellow River Basin. The bi-temporal thematic maps are derived from a semi-automated supervised classification approach using phenological information based on high-temporal medium-resolution MODIS data time series for the whole basin. A detailed description of the

* This chapter is based on: Wohlfart, C., Liu, G., Huang, C. and Kuenzer, C. (2016c). A river basin over the course of time: Multi-temporal analyses of land surface dynamics in the Yellow River basin (China) based on medium resolution remote sensing data. *Remote Sensing*, 8 (3), 186

thematic quality of each land cover product is provided. Further the underlying driving forces that have fostered the dynamic processes are exemplarily explained by choosing local subsets. The last section includes direct comparison of the Yellow River Land Cover Product (YRB LC) to existing global and national land cover datasets by selecting local case study sites representing the basin's inherent heterogeneous land cover structure. This chapter is finally complemented by a section discussing the final maps and potential errors.

5.1 Land Cover Mapping using Phenological Information

This chapter uses MODIS as primary sensor (detailed sensor description is given in section 5.2 on page 64). Despite the medium spatial resolution, the high temporal resolution of daily or near-daily global acquisition of this sensor provides the basis for continuous time series that allows for detailed analyses of intra-annual phenological features. The advantages of using phenological and intra-annual metrics derived from high-temporal time-series at medium spatial resolution remote sensing imagery as predictors for land cover classification have been demonstrated in many broad-scale land cover studies with heterogeneous landscape conditions (Hansen et al., 2003; Klein et al., 2012; Leinenkugel et al., 2013; Kiptala et al., 2013; Wohlfart et al., 2014; Gessner et al., 2015; Knauer et al., 2017). Every land cover class consists of its individual intra-annual temporal spectral trajectory, which is represented in the computed phenological metrics for land cover classification, as shown in Figure 5.1. This inherent intra-annual pattern allows for a clear separation of different land cover classes.

5.2 Methodological Approach

The methodological framework for classifying the land cover characteristics of the Yellow River Basin is based on high-temporal remote sensing at an medium spatial resolution of 250 m. The MODIS data processing and reference data procedure are presented in Figures 5.2 and 5.8. The feature space for the classification consists of spectral, multi-spectral, seasonal and annual statistics based on MODIS derived time series. The final classifications for the Yellow River Basin were based on a random forest classifier, trained by reference samples from high and very high-resolution imagery. For assessing the quality of the two final thematic maps a 30 % reference data split was used. Data processing and classification chain was done in an automated fashion; only the reference data sampling required manual labor. All data processing steps, classification, and

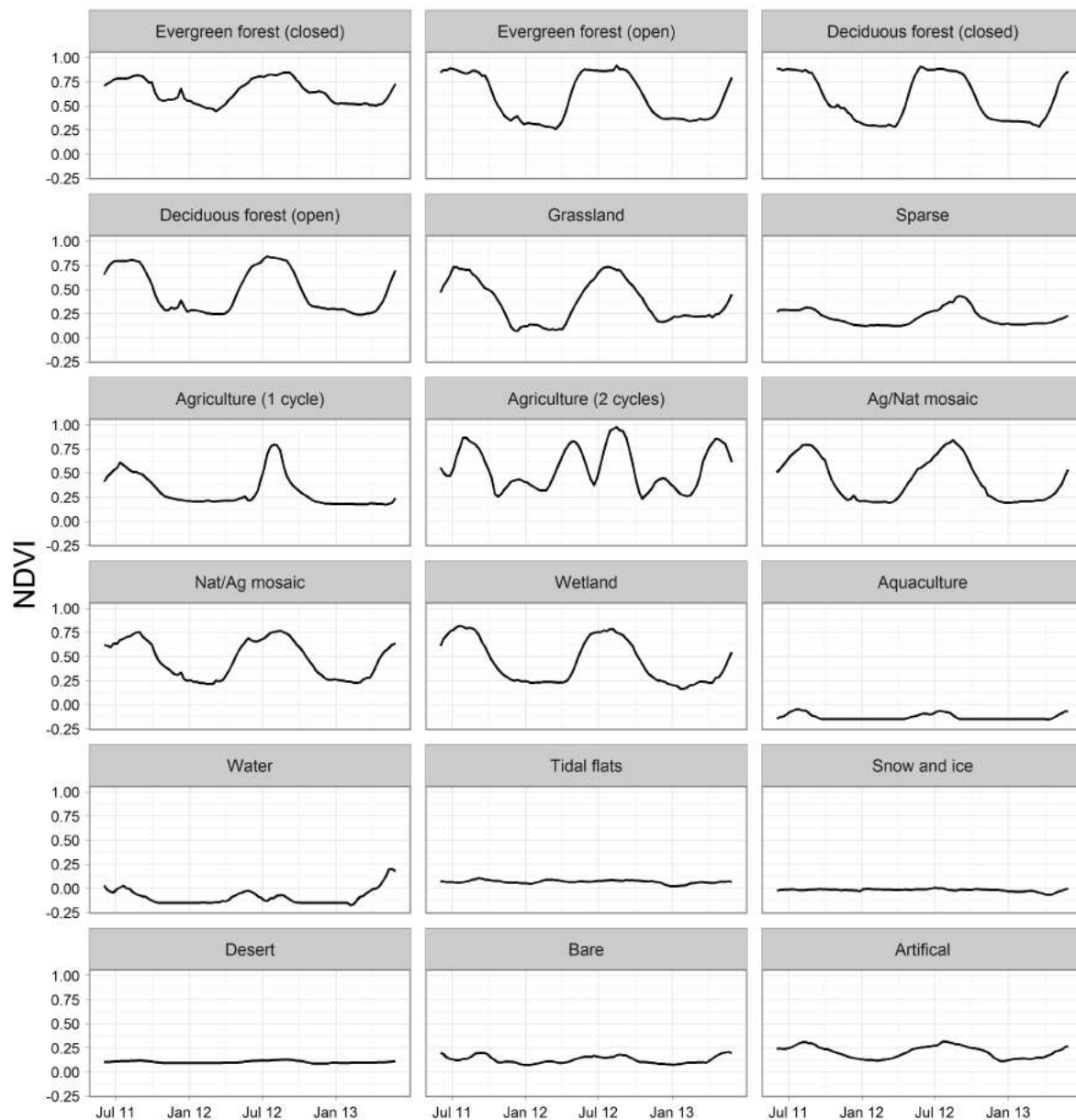


Figure 5.1: Temporal NDVI curve derived from 8-day MODIS data of all land cover types occurring in the Yellow River Basin for three consecutive years (2012-2014).

statistical analyses were prepared solely with freely available open source software tools using the statistical programming language R, Quantum GIS, GRASS GIS, and GDAL.

5.2.1 MODIS Data Processing

Spectral and spatial properties of the MODIS data base for delineating land surface characteristics in the Yellow River Basin have been introduced in section 5.2 on page 64. The MODIS 8-day surface reflectance product MOD09Q1, which is provided at a nominal

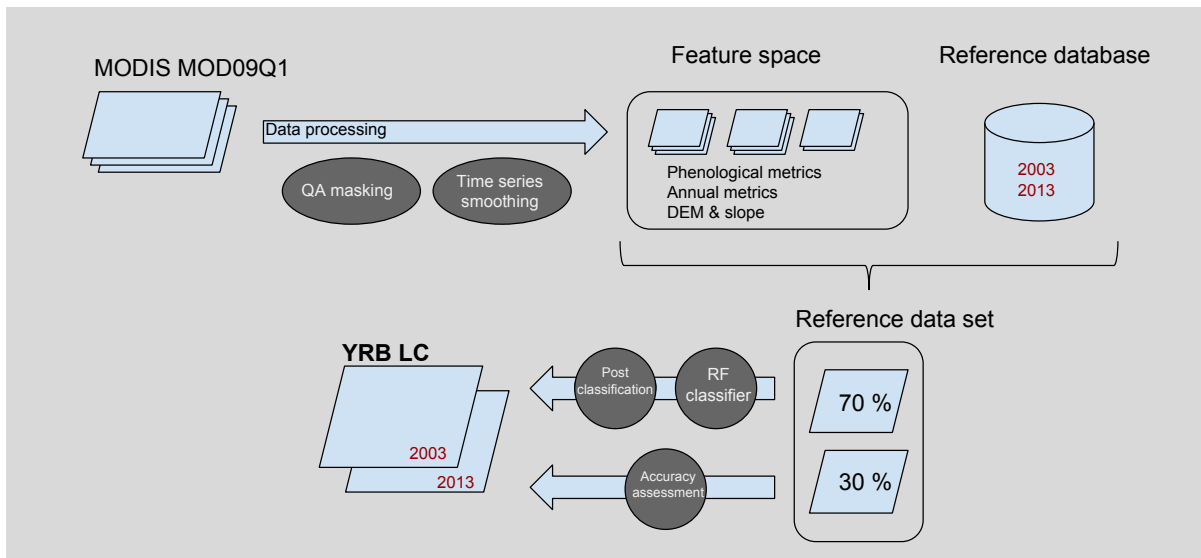


Figure 5.2: Methodological framework for delineating the Yellow River Basin Land Cover Products (YRB LC).

spatial resolution of 250 m, was acquired and processed for two time spans: from January 2002 until December 2004 and from January 2012 until December 2014. All provided layers by MOD09Q1 were used: MODIS band 1 (red channel, 620-670 nm), band 2 (NIR channel, 841-876nm) and the QA (Quality Assurance) layer. Although only the years 2003 and 2013 were classified, it was necessary to process the complete time series of three consecutive years to guarantee the precise calculation of the start and end of the season of the central year. For a full spatial coverage of the basin, five MODIS tiles were processed (h25v04, h25v05, h26v04, h26v05, h27v05) (Figure 5.3).

MODIS preprocessing steps and feature generation is depicted in Figure 5.2. The first step involves product acquisition and download. This has been done with the package *MODIS* (version 0.10-34) in the statistical programming language R, which incorporates automatic download and initial processing functions, including reprojection, tile mosaicking, and subsetting (Mattiuzzi, 2016; R Core Team, 2016). Each since was reprojected from its native Sinusoidal to the geographical latitude/longitude (WGS84 datum), keeping the spatial resolution of 250 m. Very often, high-temporal time series are inherently influenced by cloud contamination and atmospheric variability (Leinenkugel et al., 2013; Wohlfart et al., 2014). Therefore, a pixel-based quality assessment was performed to reduce such effects. Low quality pixels were masked out using the quality information provided by the MODIS QA layer. Based on the cleaned surface reflectance bands, the Normalized Difference Vegetation Index (NDVI) was calculated for the full time series with 46 images per year (Figure 5.4). The NDVI is a proxy of plant “greenness” or photosynthetic activity. Photosynthetically active vegetation absorbs most of radiation in the visible red and reflects very well in the near infrared part of the spectrum. By taking the ratio of red and

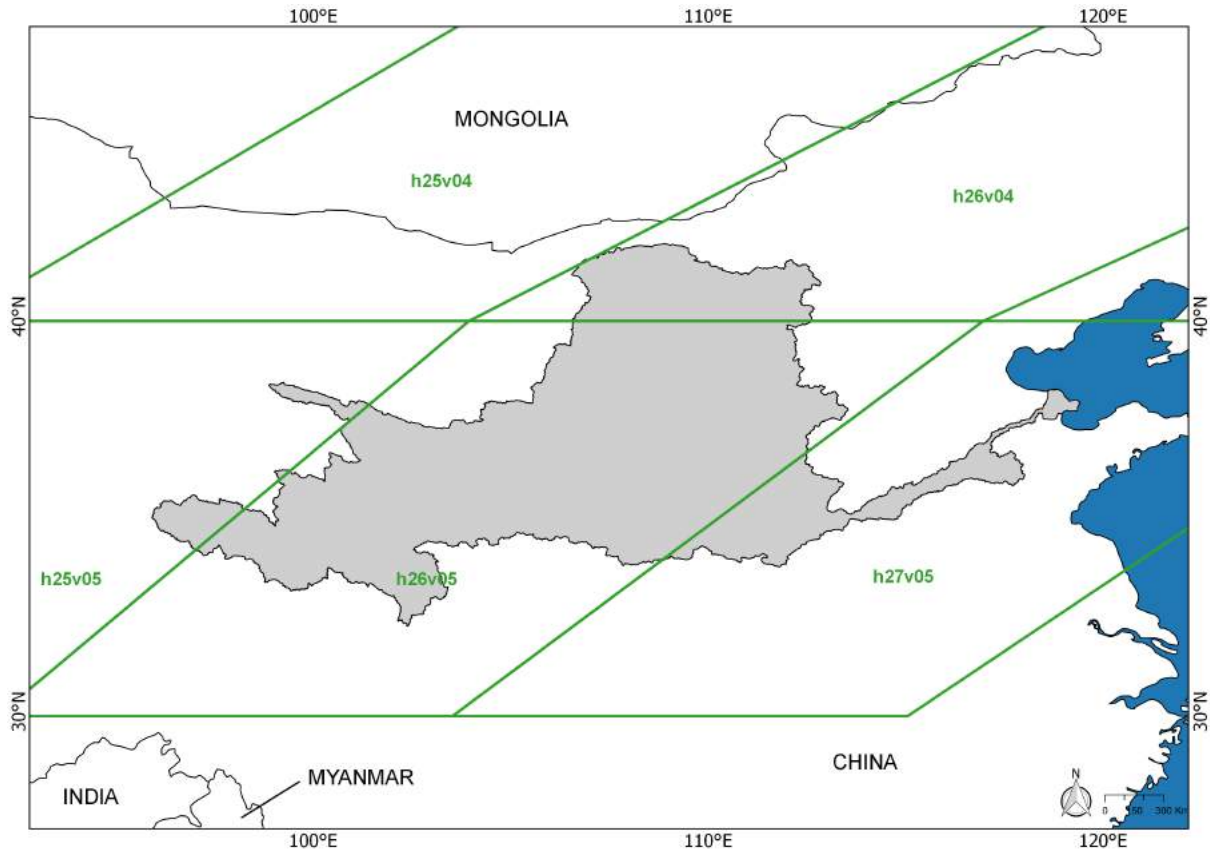


Figure 5.3: Footprints of the MODIS tiles used in this study.

NIR bands from a remotely-sensed image, an index can be defined:

$$(5.1) \quad NDVI = \frac{(NIR - RED)}{(NIR + RED)}$$

where NIR and RED are the spectral reflectance measurements in the red (MODIS band 1) and near-infrared (MODIS band 2) regions (Tucker, 1979).

The resulting data gaps in the time series from the masking procedure were removed by applying an adaptive Savitzky-Golay (SG) interpolation filter. The SG filter is a moving window approach that performs a polynomial least-squares fit of a certain degree to all points in a specific window and replaces the central point with the value of the polynomial (Savitzky and Golay, 1964). For this interpolation step and further noise reduction with the SG-filter the TIMESAT software was applied (Jönsson and Eklundh, 2004). In TIMESAT, the SG algorithm is implemented in a newly-adapted form. Sometimes, the globally defined window size does not capture the rapid dynamics in high-temporal NDVI trajectories. In these cases, it is necessary to locally decrease the window size (Jönsson and Eklundh, 2002), which follows the rapid changes within the time series and captures fast changing phenology cycles.

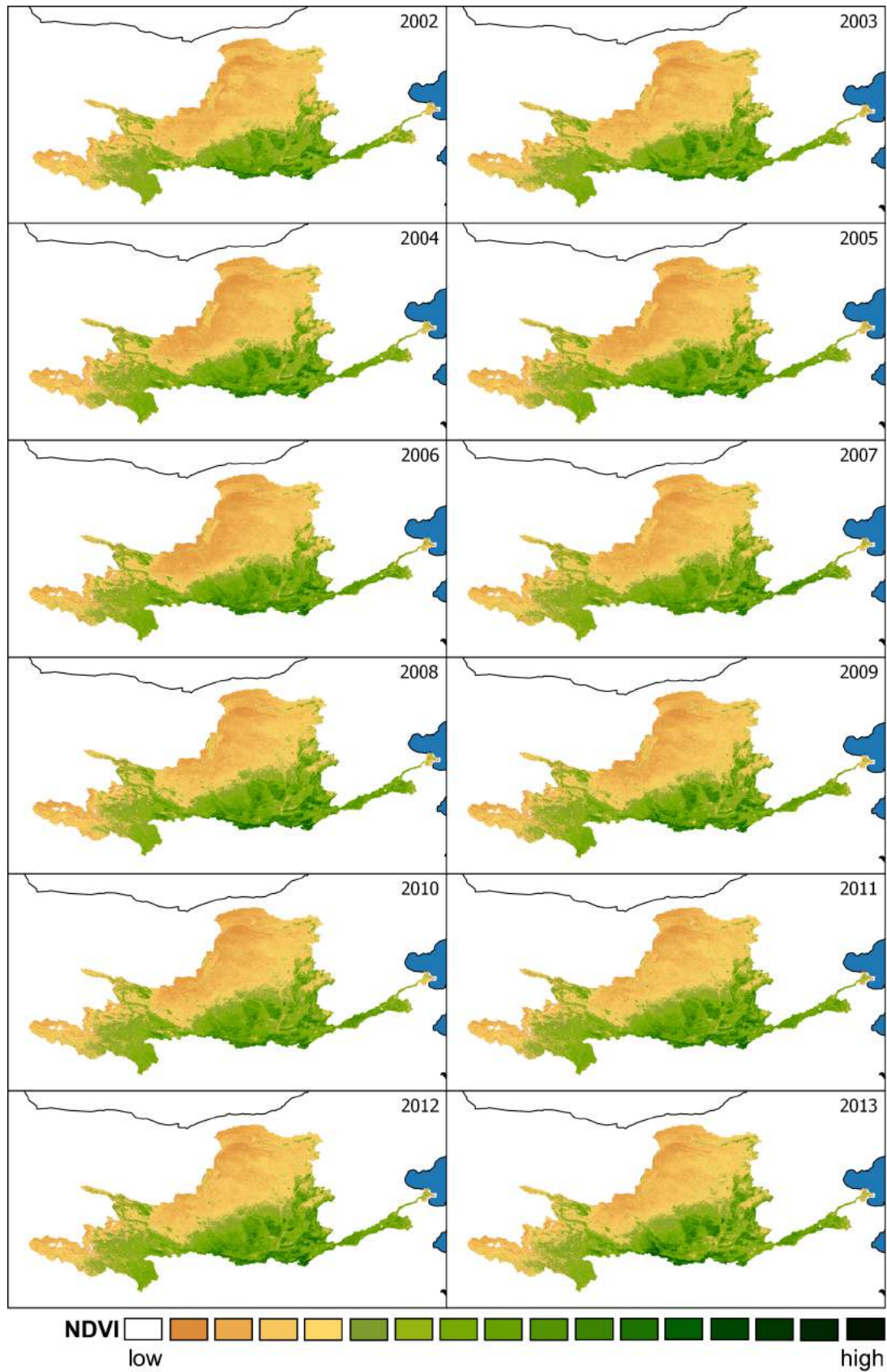


Figure 5.4: Annual NDVI median values between 2002 and 2013 for the Yellow River Basin.

In this thesis a rather small window size of five was defined. In Figure 5.5 two smoothed NDVI (and raw) trajectories are exemplary shown for two-season crop and deciduous forests.

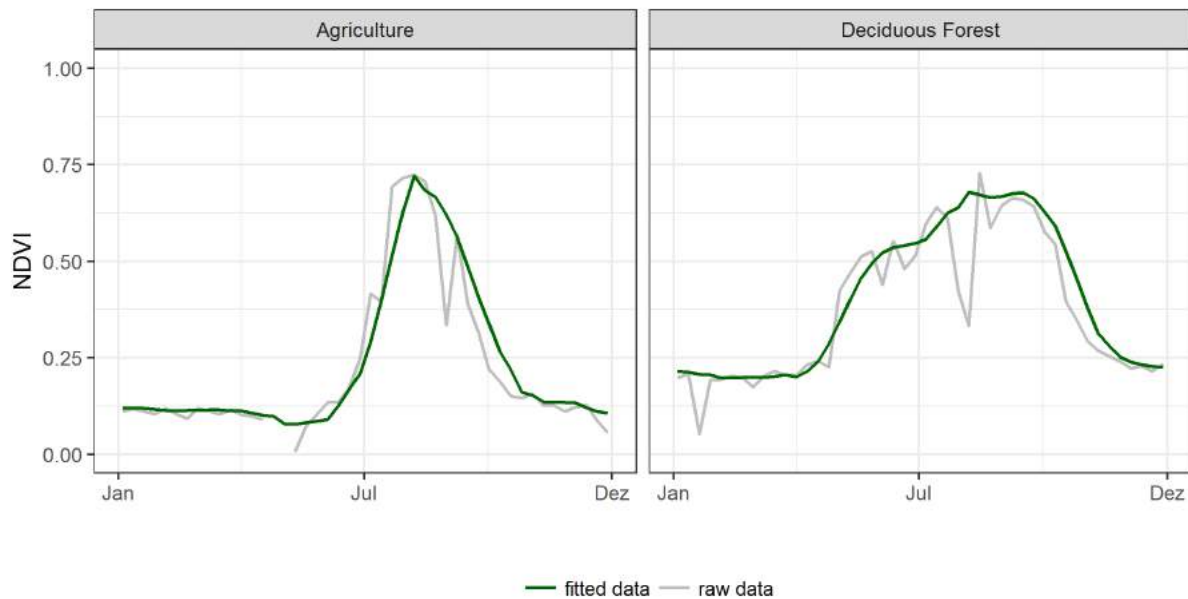


Figure 5.5: Temporal NDVI trajectories of raw (gray) and fitted (green) 8-day MODIS data for two selected land cover classes.

5.2.2 Classification Features

In section 5.1, the advantages of using phenological information derived from high temporal medium spatial resolution remote sensing imagery as classification input feature for large regions with heterogenic conditions were explained. Based on the previously smoothed NDVI time series, a total number of eleven seasonal phenology metrics were generated from TIMESAT, which characterize the growing and biological cycle throughout the year. The exact definition of each metric is described in Jönsson and Eklundh (2002) and summarized in Table 6.6 and Figure 5.6. In addition, annual statistical image metrics, such as the median, standard deviation, percentiles (10, 25, 75, 90 %), and their differences, were obtained individually for the NDVI and both spectral MODIS bands (NIR and red). As auxiliary information a digital elevation model (DEM) and the calculated slope was added to the classification model. In total, the entire feature space consists of 37 input predictors for the final land cover/use classification (Table 6.6).

5.2.3 Reference Data Collection

Remote sensing-based land cover analysis relies on a high quality reference database for training and testing (Stehman and Czaplewski, 1998; Olofsson et al., 2014). A faulty and

Table 5.1: Phenological and annual metrics and their description. The latter were calculated for the Vegetation Index (VI) and both spectral channels (RED, NIR)

	Metrics	Description	
seasonal metrics	Start of season	Time for which the left edge has increased to 40 % of the seasonal amplitude measured from the left minimum level	
	End of the season	Time for which the right edge has decreased to 40 % of the seasonal amplitude measured from the right minimum level	
	Length of the season	Time from the start to the end of the season	
	Base level	Average of the left and right minimum values	
	Mid of the season	Mean value of the times for which the left edge has increased to the 80 % level and the right edge has decreased to the 80 % level	
	Peak value	Largest value between start and end of the season	
	Seasonal amplitude	Difference between peak value and base level	
	Rate of increase at the beginning of the season	Ratio of the difference between the 20 % and 80 % levels and the corresponding time difference	
	Rate of decrease at the end of the season	Ratio of the difference between the right 20 % and 80 % levels and the corresponding time difference	
	Large seasonal integral	Integral of all values between start and end of the season	
	Small seasonal integral	Integral of all values from start to end of the season minus base level	
	annual metrics	Median	Median value derived from annual multi-temporal statistics
		Standard deviation	Standard deviation from annual multi-temporal statistics
10 percentile		10 percentile value from annual multi-temporal statistics	
25 percentile		25 percentile value from annual multi-temporal statistics	
75 percentile		75 percentile value from annual multi-temporal statistics	
90 percentile		90 percentile value from annual multi-temporal statistics	
Diff 90-10 percentile		Difference between 90 and 10 percentile	
Diff 75-25 percentile	Difference between 75 and 25 percentile		

inappropriate sampling scheme might introduce systematic error to the final classification, reducing the reliability of the thematic products (Wohlfart et al., 2016a). Despite the two field campaigns conducted in the Yellow River Basin and Yellow River Delta, it was not possible to collect a valid amount of *in situ* reference data due to the large geographical extent (750,000 km²) of the basin. Therefore, high-resolution data stemming from Landsat TM/OLI sensors and complementary freely available VHR data, provided by Google Earth and Mapworld, were used to generate a comprehensive reference dataset for training the model and validating the classification results. Adequate thematic land cover classes for the Yellow River Basin (see Table 2) by interpreting various sources and databases, including existing region-specific land cover descriptions, expert knowledge and VHR imagery in combination with geo-referenced photographs. A detailed description of each defined class is given in Table 5.4.

The procedure for finding adequate reference sites is illustrated in Figure 5.8. It consists of three main steps and was carried out independently for 2003 and 2013. First, suitable, fairly cloud-free and spatially and temporally consistent Landsat scenes between June and

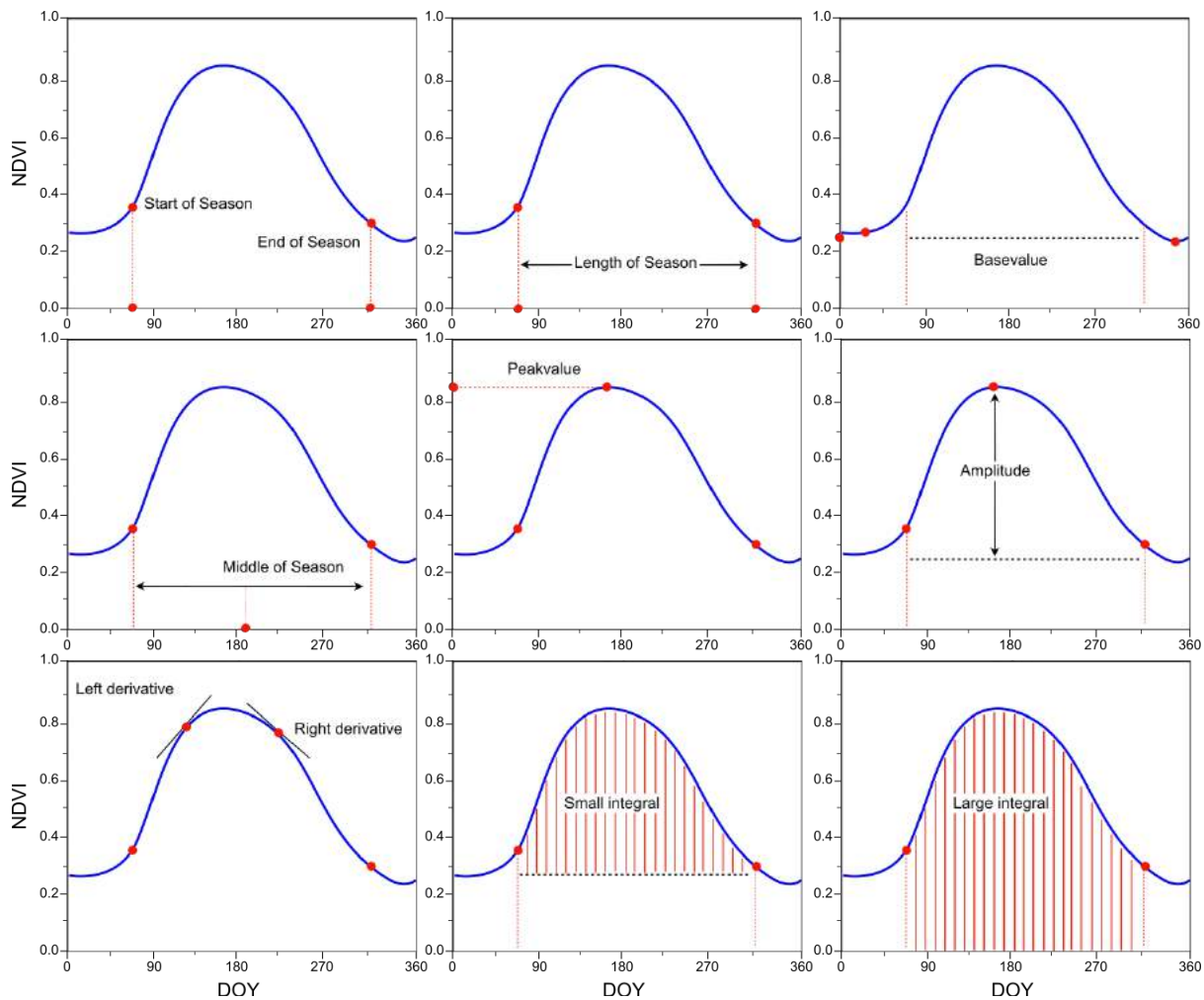


Figure 5.6: All computed “TIMESAT” variables as defined by (Jönsson and Eklundh, 2004).

August were acquired for 2003 and 2013. In this period, vegetation characteristics are fully established allowing for a clear visual interpretation of the prevailing land cover types. To capture all land cover entities, a total number of 14 Landsat tiles were equally distributed across the study area (Figure 5.8 and Table 5.2 and 5.3). As second step, spectrally- and texturally homogeneous objects were retrieved with the Orfeo ToolBox (OTB), which is implemented in Quantum GIS software (Q-GIS). OTB is a library for processing remote sensing imagery and consists of a performant multi-spectral segmentation application. The implemented mean-shift segmentation algorithm groups objects with similar spectral and textural properties based on all Landsat spectral bands plus the computed NDVI. As a minimum sampling unit, only objects encompassing an area of at least nine MODIS pixels, equivalent to $562,500 \text{ m}^2$, were chosen. This figure was suggested by Congalton and Green (2009). The marginal areas of each polygon might still be influenced by mixed pixels. A negative buffering of one MODIS pixel excluded the transitional pixels to further guarantee homogeneous reference objects. As a clear visual interpretation of the

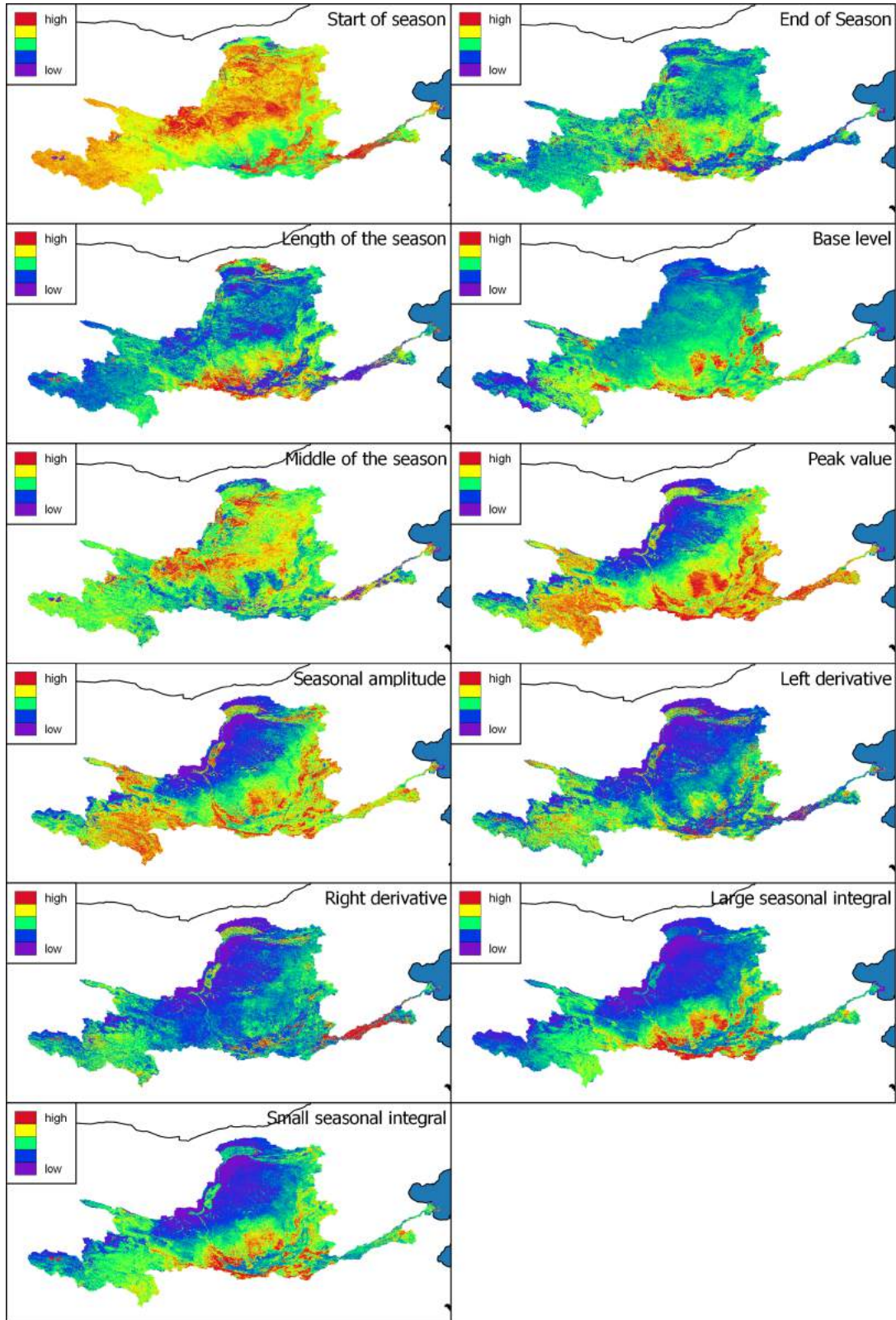
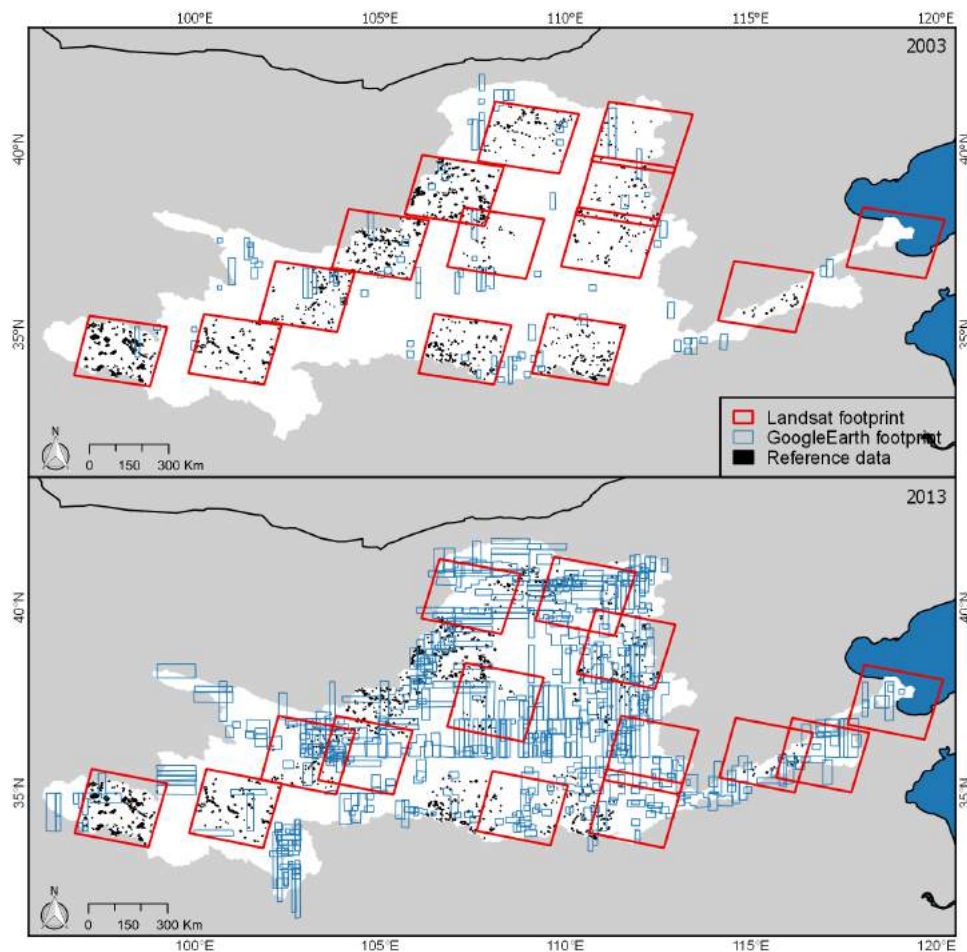
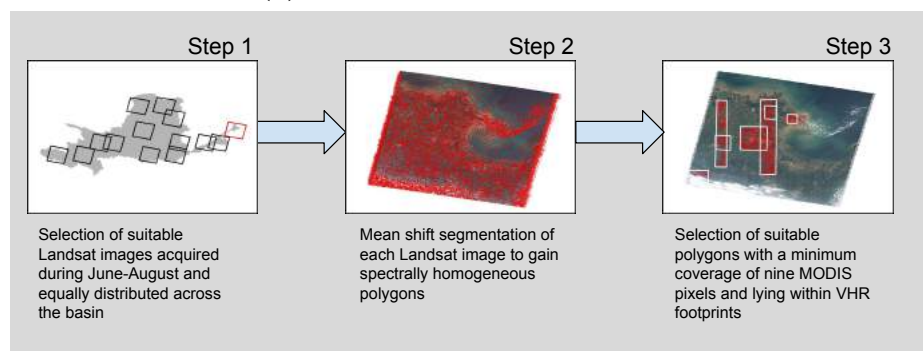


Figure 5.7: Seasonal TIMESAT metrics for the year 2013.

prevailing land cover is only feasible with high quality and high resolution data, polygons embedded in available VHR Google Earth and Mapworld data were selected as potential



(a) Location of the reference data.



(b) Reference data collection procedure

Figure 5.8: a) Location and extent of Landsat (red) and very high resolution (VHR) imagery (blue) footprints for 2003 (top) and 2013 (bottom); b) Flowchart depicting the reference data collection procedure, including Landsat selection, segmentation, and polygon assignment.

reference data (Step 3 in Figure 5.8). From those, 2500 randomly selected polygons were extracted across the basin. Simple random sampling is meant to be an unbiased sampling technique, since all parts of the study area have an equal chance of being selected (Stehman, 2009; Olofsson et al., 2014; Wohlfart et al., 2016a). To get a representative and statistically-valid representation of the complex landscape conditions, at least 100

Table 5.2: Meta-information for reference data collection for the year 2013 (Landsat 8).

Sensor	Acquisition date	Path/Row	Center location
Landsat 8 OLI	2013-06-30	121/34	37.5°N/119.0°E
Landsat 8 OLI	2013-06-21	122/35	36.0°N/116.9°E
Landsat 8 OLI	2013-06-13	123/35	36.0°N/115.4°E
Landsat 8 OLI	2013-08-30	125/35	36.1°N/112.3°E
Landsat 8 OLI	2013-08-05	126/33	34.6°N/111.9°E
Landsat 8 OLI	2013-08-12	127/32	38.9°N/111.5°E
Landsat 8 OLI	2013-06-25	127/36	34.5°N/108.8°E
Landsat 8 OLI	2013-08-03	128/34	37.5°N/108.0°E
Landsat 8 OLI	2013-08-01	130/35	40.3°N/107.2°E
Landsat 8 OLI	2013-08-08	131/35	36.0°N/102.9°E
Landsat 8 OLI	2013-08-15	132/36	34.6°N/101.1°E
Landsat 8 OLI	2013-08-13	134/36	34.5°N/97.9°E


















Table 5.3: Meta-information for reference data collection for the year 2003 (Landsat 5).

Sensor	Acquisition date	Path/Row	Center location
Landsat 5 TM	2003-08-07	121/34	37.5°N/119.0°E
Landsat 5 TM	2003-06-18	123/35	36.1°N/115.1°E
Landsat 5 TM	2003-07-09	126/32	40.0°N/112.1°E
Landsat 5 TM	2003-06-07	126/33	38.9°N/111.5°E
Landsat 5 TM	2003-06-23	126/34	37.5°N/111.1°E
Landsat 5 TM	2003-06-23	126/36	34.5°N/110.3°E
Landsat 5 TM	2003-06-05	126/36	40.3°N/108.9°E
Landsat 5 TM	2003-06-05	128/34	37.5°N/108.1°E
Landsat 5 TM	2003-06-05	128/36	34.6°N/107.2°E
Landsat 5 TM	2003-06-12	129/33	38.9°N/106.9°E
Landsat 5 TM	2003-06-19	130/34	37.4°N/104.9°E
Landsat 5 TM	2003-07-17	134/36	34.5°N/97.9°E

samples for each thematic class were selected as suggested by several studies (Congalton, 1991; Congalton and Green, 2009). A distance criterion was implemented in the random sampling strategy. To avoid spatial autocorrelation, a minimum sampling distance of 30 MODIS pixels was set. Dominant land cover/use classes and those classes with inherent variability and complexity have been sampled with a minimum number of 100 polygons (Congalton, 1991). Finally, a class-specific ID code, as defined in Table 5.4, was assigned to each polygon by visual interpretation. The drawback of simple random sampling is, however, the underrepresentation of small and rarely-occurring areas, because they are not uniformly distributed across the landscape. This problem has also appeared in our sampling strategy. Therefore, underrepresented classes were additionally sampled until at least 100 samples had been taken. The final reference dataset for training and testing contained a total of 2340 objects for 2003 and 2232 for 2013. The spatial distribution of

each reference object across the Yellow River Basin can be obtained in Figure 5.8.

Table 5.4: Color code, class identifier, name and description of all defined land cover classes in the Yellow River Basin.

Color code	ID	Class name	Description
	1	Evergreen needle-leaved forests (closed)	Forest with predominant evergreen needle-leaved tree species, covering at least 65 % and height exceeding 2 m
	2	Evergreen needle leaved shrub & woodland (open)	Evergreen needle leaved forests covering 15-40 % and mixed with grassland and/or shrub entities.
	3	Deciduous broadleaved forests (closed)	Forest with predominant broadleaved deciduous tree species, covering at least 65 % and height exceeding 2 m
	4	Deciduous broadleaved shrub & woodland (open)	Deciduous broadleaved forests covering 15-40 % and mixed with grassland and/or shrub entities
	5	Grassland	Herbaceous vegetation layer with less than 10 % woodland and shrub coverage
	6	Sparse vegetation	Sparse shrub and herbaceous vegetation entities covering 5-15 %
	7	One season cropland	Agricultural areas with one harvest per year
	8	Two season cropland	Agricultural areas with two harvests per year
	9	Natural vegetation/agriculture mosaics	Predominant natural vegetation entities (grassland, shrub, woodland), accompanied with cropland
	10	Agriculture/natural vegetation mosaics	Predominant cropland, accompanied with natural vegetation entities
	11	Aquaculture	Water ponds used for aquaculture production, mainly for fish, crustaceans, and turtles, usually surrounded and intersected with grassland
	12	Wetlands	Areas, saturated with salt or fresh water with a permanent mosaic of water and herbs or woodland
	13	Water bodies	Areas covered with either fresh or salt water
	14	Tidal flats	Coastal wetlands exposed to tidal amplitude consisting of unconsolidated sediments
	15	Snow and ice	Areas permanently covered by snow or ice
	16	Deserts (sandy)	Barren area covered by sand dunes
	17	Bare areas	Barren land with natural vegetation less than 5 %
	18	Artificial areas	Built up areas and associated areas

5.2.4 Classification Approach and Accuracy Assessment

Using the sampled reference data set, two independent RF models (2003 and 2013) were employed to delineate the land cover characteristics for the Yellow River Basin based on seasonal and annual MODIS metrics. Model building and testing was carried out using the R with the package *randomForest*, where Breiman's algorithm is implemented (Liaw and Wiener, 2002). For the final classifications, RF models with 300 individual trees were built, as prior testing showed a stabilization of the mean squared error (MSE) and a higher number of trees classification would not gain further improvements. The *mrtv* parameter was set to the default value, defined as \sqrt{p} , where p represents the number of input predictors for the RF model (Liaw and Wiener, 2002). Prior to fitting the model, the Boruta algorithm was applied (Kursa and Rudnicki, 2010). This algorithm tests if a variable is expected to be less important than random samples. Here, no variable was deemed to be unimportant. As training input served a 70 % polygon-wise split of the entire reference data set. The remaining 30 % proportion was used as independent test data set for assessing thematic accuracy of each land cover product. According to

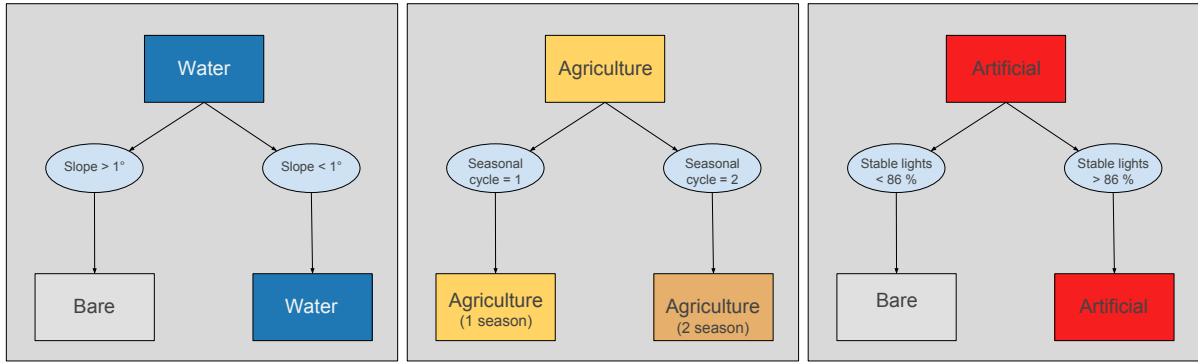


Figure 5.9: Decision rules for postclassification step.

Adelabu et al. (2015), the 70/30 % split option performs best using RF algorithms. By means of confusion matrices the accuracy of both products is presented, which contains class-specific user's, producer's and overall accuracy (Foody, 2002; Congalton and Green, 2009). Further, *randomForest* integrates a measure of variable importance to see which predictor is seen as most informative in making decisions for class separation. Besides looking at confusion metrics, the spatial component in the accuracy assessment should not be neglected (see section 4.4 on page 60, therefore the concept of entropy was used to display spatial uncertainties and potential errors. The Shannon entropy is defined as follows:

$$(5.2) \quad - \sum_{i=1}^M p_i \log p_i$$

with p being the probability of each class i , summed up over all classes M .

In pixel-based land cover classifications, the resulting products are often influenced by isolated pixels and noise, known as the so-called “salt-and-pepper” effect or speckled appearance. By applying the GDAL (Geospatial Data Abstraction Library) sieve majority filter smooths the output and improves quality. The separation of some thematic classes is ambiguous, as they consist of similar spectral and temporal features. Therefore, several logical decision rules using ancillary remote sensing data were defined to further improve the classified accuracy. The defined rules can be obtained from Figure 5.9. For instance, mountain shadows lead often to the misclassification as water. To correct this issue, the classification result was superimposed with slope layer calculated from a DEM. All water pixels with an inclination $> 1^\circ$ were edited to the bare class, as lentic water is not present on slopes. Also the spectral differentiation between barren land on slopes and artificial surfaces remain a challenging classification task. With the help of the Nighttime Lights Time Series (Version 4) product, which is derived from the DMSP Operational Linescan System (OLS) instruments, it was possible to indicate urban and built-up structures

(Figure 5.10). A threshold of 87 % was applied to detect lighted urban areas (Small et al., 2005). Double cropping agriculture is very common in the Yellow River Basin, particularly in the vast irrigation districts on the North China Plain (Li et al., 2014b). When processing the seasonal metrics, TIMESAT provides an additional mask with information about the number of intra-annual vegetation cycles. This layer was used to specify the agriculture class in single and double cropping cycles.

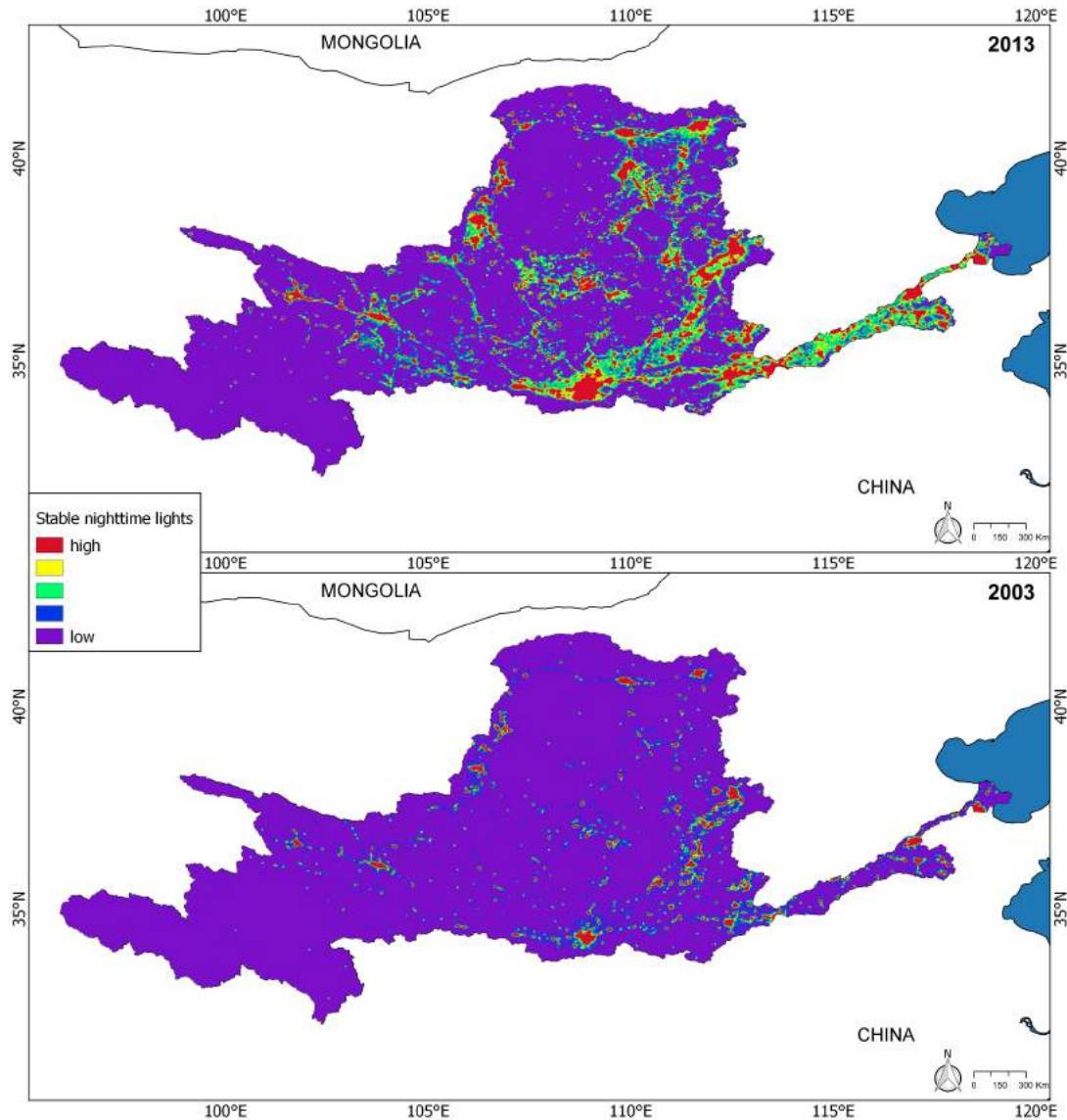


Figure 5.10: Auxiliary nighttime lights time series derived from the DMSP Operational Linescan System (OLS) instrument for 2003 and 2013.

5.3 Results

The results presented in this chapter comprise three major parts. As first step, the bi-temporal land cover characteristics and dynamic processes for the Yellow River Basin

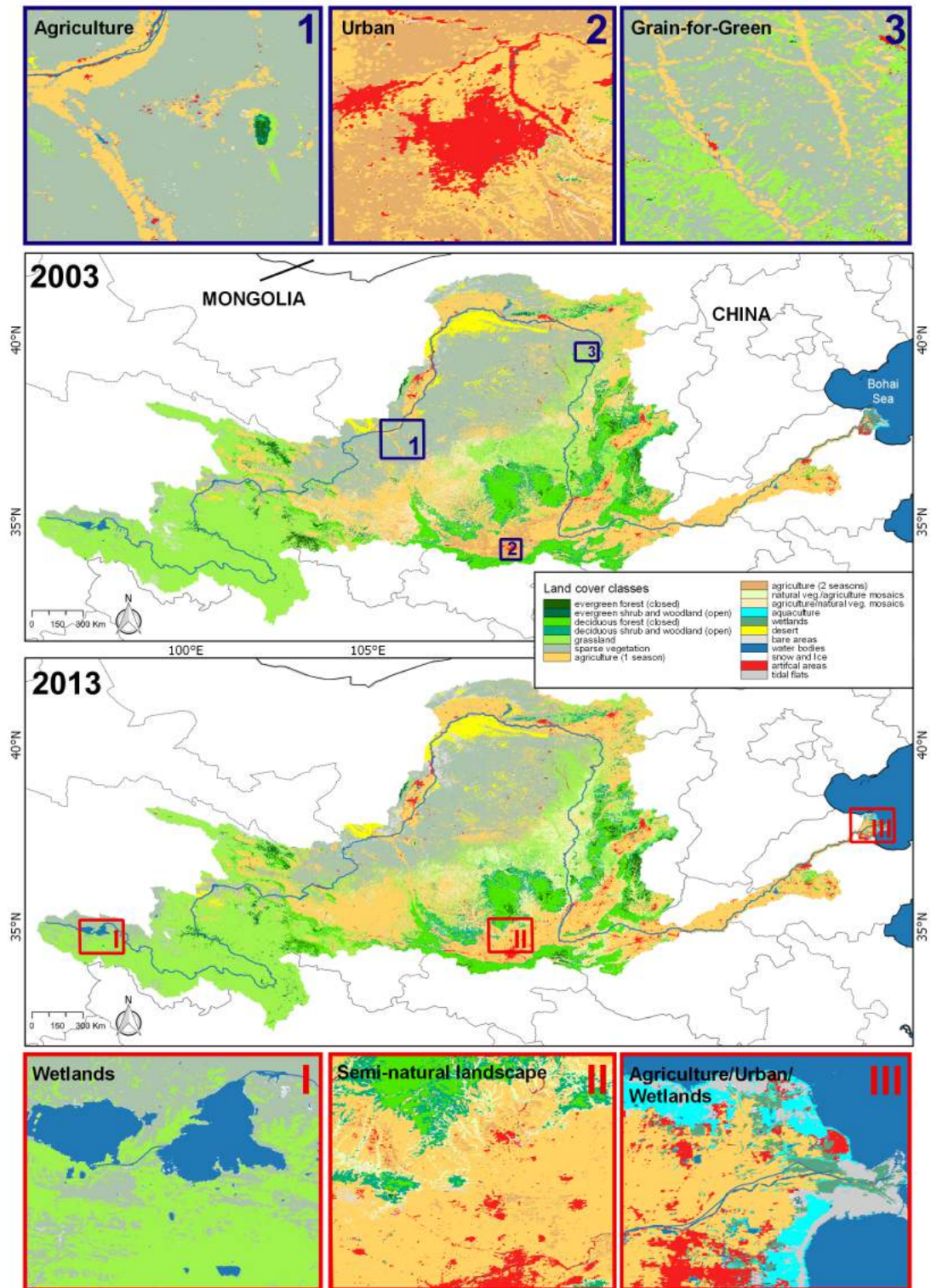


Figure 5.11: Land cover classification results for the Yellow River Basin (YRB LC) for 2003 (top) and 2013 (bottom). Framed areas in purple (upper panel) mark regions with significant land cover dynamics shown in Figures 5.16 on page 87. The red framed subsets in the lower panel will be used for comparison with existing data sets (Figure 5.17 on page 91).

are explained quantitatively and qualitatively, focusing specifically explained on each of Olson's ecoregions (Olson et al., 2001). Further, the thematic quality of both novel products is highlighted and the feature importance of each RF model is summarized. The next step involves the direct comparison of local dynamic regions, including urbanization, agricultural encroachment, and ecological restoration, with a detailed description of the underlying drivers of change. To show the out-performance of the regionally adapted Yellow River land cover maps, the resulting classifications are compared to existing global and national land cover inventories, which are often applied as management and modeling baseline for regional decision making processes. Representative examples of the basin's heterogeneous examples from the Qinghai-Tibet Plateau, the Loess Plateau, and the Yellow River Delta were chosen.

5.3.1 Land Cover Characteristics and Temporal Dynamics in the Yellow River Basin

The final classification results of the Yellow River land cover products (YRB LC 2003 and 2013) can be obtained from Figure 5.11. The delineated maps present a detailed view of the current land cover characteristics and the most recent dynamics that have shaped the basin. To reflect the realistic heterogeneous landscape conditions 18 different thematic classes were adapted and defined specifically for the Yellow River Basin, including classes of natural vegetation (terrestrial and aquatic), cultivated classes (e.g. agriculture), mosaic classes, natural sparsely, non-vegetated classes (ice, bare rock) and artificial classes (Table 5.4). The obvious landscape modifications are resulting from the aforementioned socio-economic development coupled with large-scale land policies as stated in chapter 3. Throughout the basin, the three most abundant land cover types are grassland systems (30 %), sparse vegetation (20 %), and agricultural areas with almost 25 %, together encompassing around 550,000 km², equivalent to two-thirds of the entire basin area. Detailed information (total area and percentage share) is summarized in Table 5.5.

In the subsequent sections, a detailed description is compiled for each Olson ecoregion of the prevailing land cover facets and their main dynamics as displayed in Figure 5.12. Each of the four ecoregions, namely the Qinghai-Tibet Plateau, the Ordos and Loess Plateau, and the North China Plain in the Yellow River Basin pose distinct geographical characteristics in geology, geomorphology, vegetation and fauna, climate, hydrology, and soils forming complex heterogeneous conditions across the basin (Olson et al., 2001).

5.3.1.1 The Qinghai-Tibet Plateau

With more than 2.5 million km², the Qinghai-Tibet Plateau is the largest and highest plateau and source of Asia's major rivers (see chapter 2 on page 19). The high elevated

Table 5.5: Total area in km² and the percentage of the total area for each land cover class and year.

Class ID	2003		2013	
	Area (km ²)	Area (%)	Area (km ²)	Area (%)
1	6,158	0.81	6,146	0.83
2	4,100	0.54	5,171	0.70
3	47,745	6.33	52,226	7.31
4	24,718	3.28	23,456	3.65
5	225,728	29.95	225,308	30.44
6	167,427	22.24	150,605	20.34
7	161,370	21.42	171,620	23.18
8	1,3573	1.80	2,219	0.29
9	30,681	4.07	32,456	4.38
10	30,070	3.99	26,170	3.54
11	623	0.08	1,777	0.24
12	1,734	0.23	1,035	0.13
13	4,523	0.60	4,534	0.60
14	506	0.05	507	0.07
15	537	0.04	521	0.06
16	14,299	1.89	15,135	2.04
17	13,234	1.75	10,030	1.39
18	6,437	0.85	11,030	1.49

landscape is dominated by relatively homogeneous alpine grassland tundra intersected with areas of sparse and bare vegetation. Approximately 65 % or 45,000 km² of the plateau is vegetated by alpine grassland, which remained fairly stable between 2003 and 2013 (Figure 5.12). Desertification at the costs of grasslands occurred in the vicinity of the Gyaring and Nyoring Lakes, the two largest freshwater lakes in the basin (1,000 km²). The glacier remnants in the A'nyê Magên Mountains show no retreat by covering an area of around 500 km² in both years. Despite the relatively small spatial share of 0.07 %, those glaciers are crucial for China's water supply. Harsh environmental conditions with low temperatures and few rainfall prohibit large-scale agricultural activities on the plateau, where nomadic pastoralism is still the dominant life form. In low altitude valleys at the plateau's eastern margins with a milder climate, subsistence farming is possible to produce wheat and vegetables on small fields (NBS, 2015; Wohlfart et al., 2016c). Although agrarian output could be increased by 10 % (NBS, 2015), agricultural fields remained stable at 6,600 km². Artificial and built-up structures play a minor role on the Qinghai-Tibet Plateau with a slight decrease from 150 to 156 km². However, expanding mining activities in the Haibei Prefecture could be detected, where alpine swamp meadows were replaced.

5.3.1.2 The Ordos Steppe

Vegetation form and characteristics on the Ordos Plateau differ significantly from the Qinghai-Tibet Plateau as climatic conditions become more arid. Therefore, dry-adapted

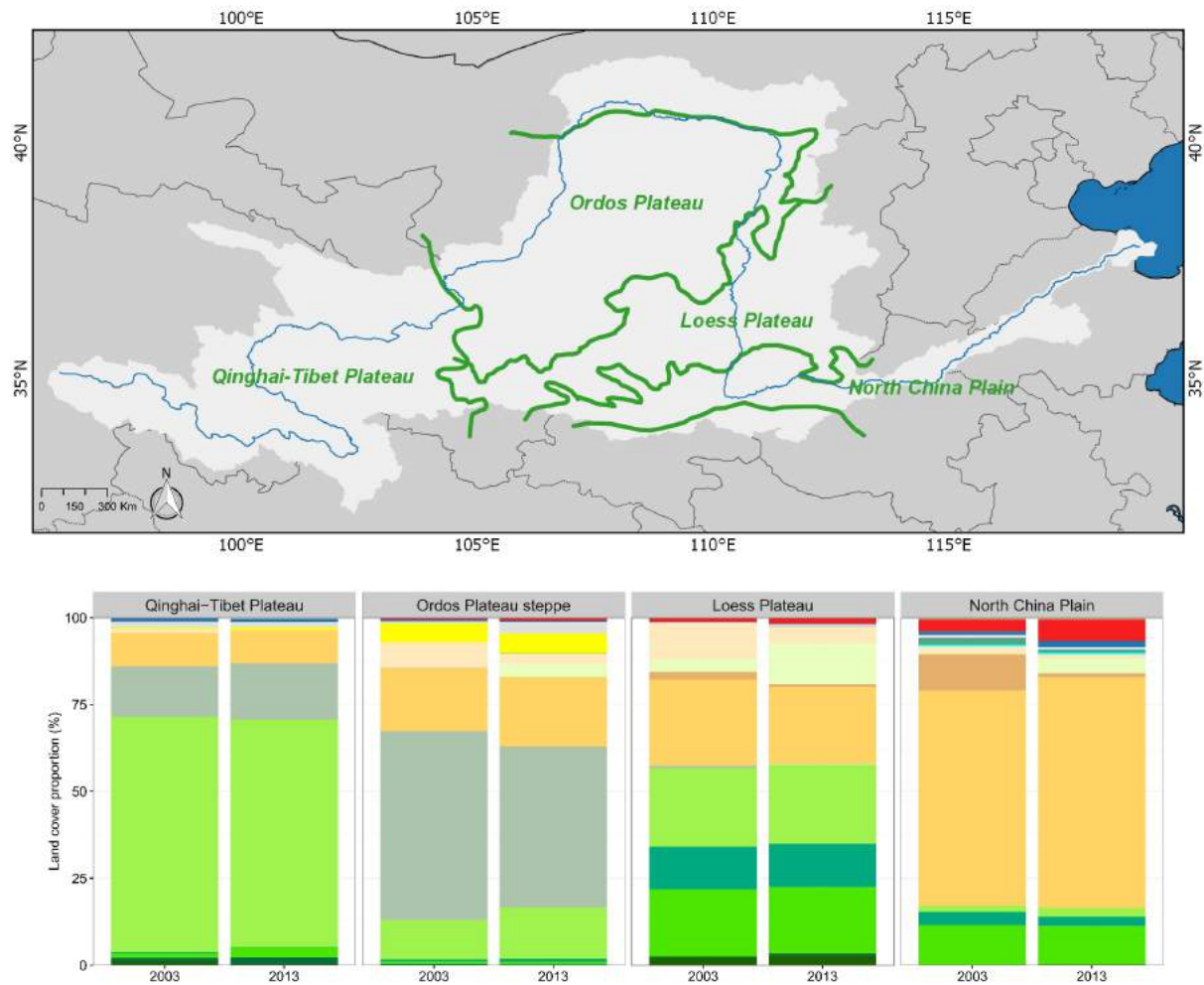


Figure 5.12: Olson's ecoregions in the Yellow River Basin (Olson et al., 2001) and land cover proportions for each ecoregion and year. The color code of the different land cover types conforms to the color code introduced in Table 5.4 and Figure 5.11.

xeric or desertic plants are the predominant vegetation type, forming a sparse vegetated steppe. However, the sparse and barren land has been reduced from 37,000 km² (2003) to 31,000 km² in 2013 by planting a “Green Great Wall” of shrubs and forest strips to minimize and stop the progradation of the Gobi desert, known as the *Three-North Shelter Forest Program* (Chinese: 三北防护林) (Figure 5.12). This nationwide program has commenced its fourth phase in 2003. Besides the Gobi Desert at the western margins of the Yellow River Basin, the Ordos Plateau contains two large sandy deserts, the Kubugi Desert (north) and the Maowusu Desert further south with an area of 6 % or 3,880 km². This figure has not changed since 2003. Agricultural cultivation is limited by the lack of precipitation in conjunction with poor soils. Arable zones on the Ordos steppe include the large-scale irrigation districts along the river banks, e.g. the Qingtongxia and Hetao

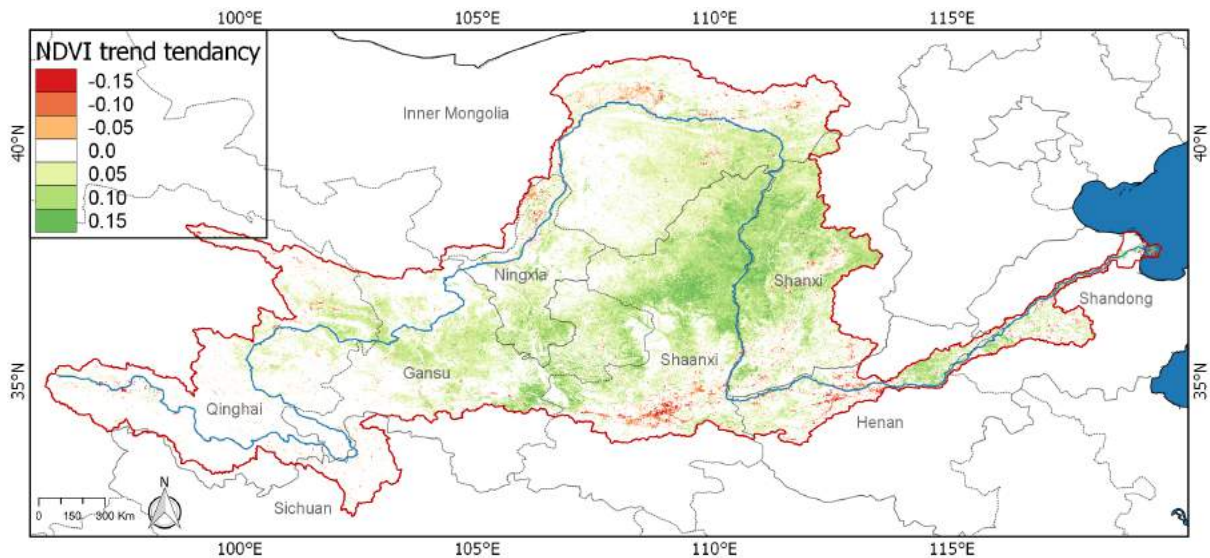


Figure 5.13: NDVI trend tendency based on MODIS time series from 2003 to 2013. The different colors show significance levels (green: positive trends; red: negative trends).

District (Figure 3.4 on 34), where sufficient water and fertile soils guarantee rich harvests. Oases scattered throughout the Ordos steppe are another base for planting crops. Between 2003 and 2013, agricultural fields increased from 12,442 km² to 13,885 km², an 11 % expansion. Urban and built up structures sprawled by more than 50 % from 436 km² to 641 km², including the major cities of Lanzhou, Yinchuan, Baotou, Bayan Nur, and Wuhai.

5.3.1.3 The Loess Plateau

The Loess Plateau, natively covered by extensive temperate open and closed deciduous (oak, birch) and in higher altitudes evergreen (spruce, mountain-ash) forest species has experienced a long history of deforestation and over-grazing, turning this region into a degraded landscape with highest soil erosion rates. The Yellow River and many tributaries cut the hilly and easy erodible, non-vegetated area into numerous narrow ridges and mounds creating a rugged and uneven surface (Figure 3.9 on page 48). Persistent continuous forest remnants on the Loess Plateau include the Lu Liang Mountains at the eastern margins of the basin (Shanxi Province) and the Ziwuling and Yunwu Mountains in Shaanxi Province. Presently, forest and woodland structures (land cover classes 1 – 4) encompass a total area of 16,242 km², equivalent to around 30 % of the Loess Plateau. In 2003, this figure was considerably lower with 15,000, meaning a 7 % growth of woody vegetation. The central part is covered by small mosaics of natural vegetation and agricultural fields, which have significantly increased, while sparse vegetation and the mosaic class “agricultural/natural vegetation” with a predominant share of natural vegetation had

dwindled until 2013 (Figure 5.12). The proportion of agriculture cultivated land slightly decreased by 3 % from 16,242 km² to 15,100 km². Many land use policies, such as the GfG and the NFCP (see section 3.3 on page 45) aim to green slopes on the Loess Plateau to mitigate the massive soil erosion. This “greening” effect is nicely reflected in Figure 5.13, where the NDVI trend tendency based on annual median values is depicted. The economic boom and increasing demand for fossil fuel resources across the Yellow River Basin has led to noticeable mining encroachments mainly in Shaaxi Province. Urban and built up structures have tremendously grown by almost 50 % from 487 km² to 725 km².

5.3.1.4 The North China Plain and Delta

The degree and extent of cultivation processes throughout the basin climaxes in the fertile and flat alluvial North China Plain, where greater part of the land surface is dominated by agriculture. In the south, the Yellow River basin is delimited by the Qinling Mountain Range, which is dominated by temperate deciduous forest forms. Forest and woody vegetation remained stable between 2003 and 2013 with around 3,770 km² (15 %). Around 19,000 km², representing more than 60 % of the North China Plain, are cultivated for agricultural purposes producing commodities such as wheat, corn, sorghum, and cotton. Large-scale irrigation districts in combination with extreme fertile alluvial soils allow for intensified multi-seasonal crop production in this region. Despite increasing crop output of 22 % since 2003 (NBS, 2015), agrarain fields only expanded by 5 % since 2003 (NBS, 2015). The densely-populated regions (Henan and Shandong Provinces) faced strong urbanization processes and built up areas sprawled by 80 % from 895 km² to 1,652 km² (Figure 5.12). The delta area, a key region of China’s economic development, has tremendously evolved during the last decade. Urban and industrial expansion, the digging of aquacultural ponds, and agricultural intensification have harnessed the ecologically-sensitive wetland ecosystems, where only few remnants of 170 km² remain.

5.3.2 Thematic Quality of the YRB LC and Variable Importance

With an overall accuracy of 87 % and 84 % for 2003 and 2013, respectively, both land cover classifications gained satisfactory results, given the spatial heterogeneity and extent. Overall, accuracies (OA), class-specific user’s (UA) and producer’s accuracies (PA) for each year are summarized in Table 5.6. Class-wise entropy values and spatial distribution are displayed in Figure 5.14.

Highest class-wise accuracies are present in the defined closed evergreen and deciduous forest structures (class ID 1 and 3), with PA and UA >90 %. For those classes entropy values rank among the lowest around 0.35. In contrast, open woody vegetation (ID 2 and 4) are attributed with higher error and entropy. Classification errors remain lower

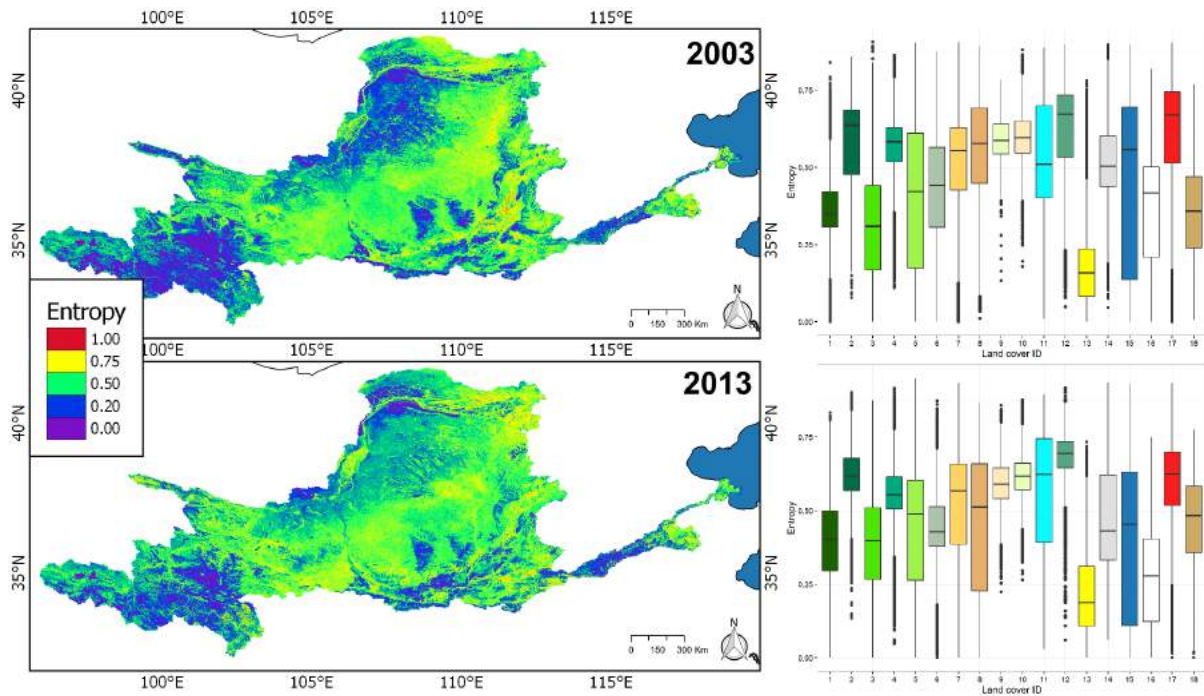


Figure 5.14: Ensemble uncertainty within the RF classifier displaying as entropy of the YRB LC classifications 2003 and 2013. The boxplots depict the class-wise entropy for both classifications.

in rather homogeneous non-vegetated classes, such as water, ice, sparse, and barren surfaces, as well as the sandy desert class, all with high PA and UA exceeding 90 % and low entropy values (Table 5.6 and Figure 5.14). Wetlands (ID 12) are also delineated in high thematic detail, showing only minor misclassification with grasslands, but are attributed with relatively high spatial uncertainty (entropies around 0.75). Grassland is delineated well on the Qinghai-Tibet Plateau, where high entropies for both years can be observed, whereas grassland on the Loess Plateau shows higher spatial uncertainties, resulting in overall lower PA (78 % and 82 %) and UA (64 % and 69 %). From Figure 5.14 the lowest entropy is visible on the Loess Plateau, where the small-scale tessellated landscape structure of agriculture, grass- and woodland patches lead to high confusion and spatial uncertainty with accuracies beneath 80 %. The prediction accuracy increases for the homogeneous agricultural fields on the North China Plain, where entropy is lower compared to the Loess Plateau. Urban and artificial classes (ID 18) received accuracies in the lower spectrum with PA values of 78 % and 82 %, respectively. UA range around 90 % with a rather high entropy >of 0.75.

The variable importance measures from both RF classifications (2003 and 2013) of the entire features space are presented in Figure 5.15, ordered descending from most to least important. For both years similar pattern can be obtained. The most relevant metrics for land cover class differentiation include seasonal metrics, such as the *base level*, the

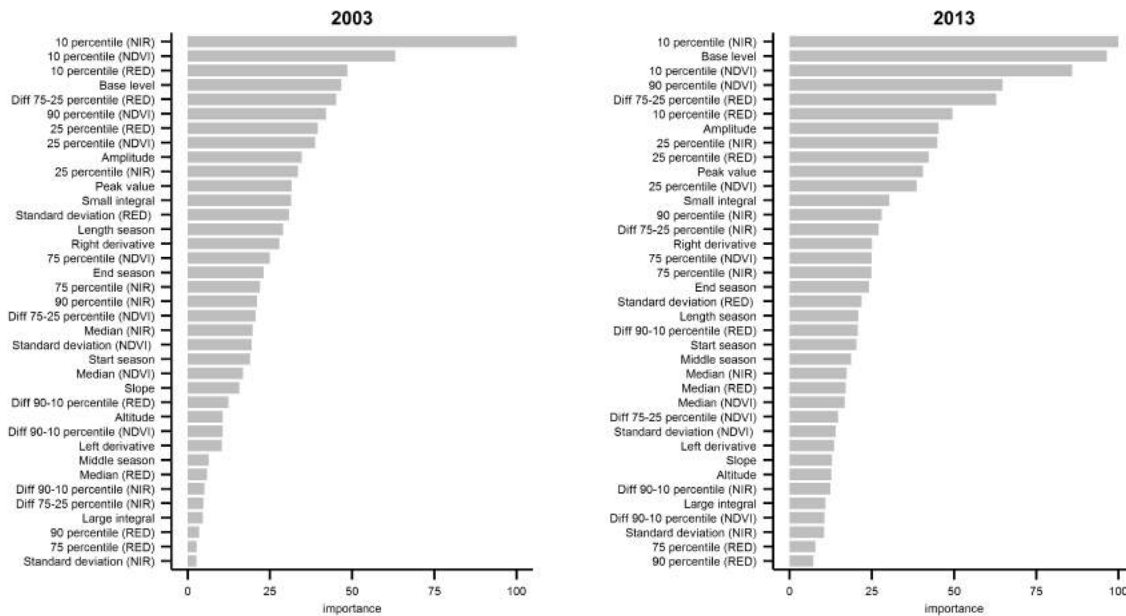


Figure 5.15: Importance (scaled from 0-100) of each model predictor used in the RF classifiers for both years (2003 and 2013).

amplitude, or the *peak value* as well as small value percentiles (10 % and 25 %) for the NDVI and both spectral bands (RED and NIR). In contrast, the seasonal metrics *left derivative*, *middle season*, and the *large integral* are determined as least important variables. Likewise, slope and altitude, and the 50 % and 75 % (RED and NIR) percentiles play only a minor role (Wohlfart et al., 2016c).

5.3.3 Local Dynamics in the Basin

Both classified maps (Figure 5.11) show the tremendous land cover dynamics that have happened during the last decades. Socio-economic developments can be seen as major triggers of these dynamics, which fostered urbanization and industrialization accompanied with infrastructure development across the Yellow River Basin. Agriculture is the most important land cover asset within the basin and many local expansion and intensification processes can be observed. As already stated in section 3.3 on page 45, various land use policies and management plans have been issued, which have influenced the basin's land surface characteristics on large spatial scales. In the subsequent sections, three selected subsets, as depicted in Figure 5.11, were chosen to highlight exemplary the aforementioned most prominent land cover dynamics since 2003.

Table 5.6: Confusion matrix showing user's and producer's accuracy for each class and overall accuracy in percent for 2003 (top) and 2013 (bottom).

		Reference																		UA (%)
		1	2	3	4	5	6	7	9	10	11	12	13	14	15	16	17	18		
2003	Classification	1	89.15	9.52	0	1.06	0.26	0	0	0	0	0	0	0	0	0	0	0	0	89.15
		2	14.18	82.53	0.46	2.30	0.23	0	0	0	0	0	0	0	0	0	0	0	0	82.53
		3	3.61	1.45	92.29	1.69	1.3	0	0	0	0	0	0	0	0	0	0	0	0	92.29
		4	0.22	3.23	0	78.06	3.36	0	1.29	5.26	3.2	0	0	0	0	0	0	0	0	78.06
		5	0	0.60	0	7.01	69.14	0	0	7.21	5.01	0	5.21	0.20	5.01	0	0	0.60	0	69.14
		6	0	0.72	0	0	1.67	83.73	0.48	0	0	0	0	0	0	0	0	3.59	6.46	83.73
		7	0	0	0	0	0.45	0	82.21	5.63	10.14	0.23	1.13	0	0	0	0	0.23	0	82.21
		9	0	0	0	7.6	7.04	0.29	4.40	79.77	0.3	0	0	0	0	0	0	0	0.29	79.77
		10	0	0	0	1.13	0.91	0.45	8.14	1.58	87.10	0	0	0	0	0	0	0	0	87.10
		11	0	2.5	0	0	0	0	0	0	0	94.00	0	5.99	0	0	0	0	0	94.00
		12	0	0	0.43	0	0	0	1.10	0	0	0.82	97.3	0.55	0	0	0	0	0	97.30
		13	0	0	0	0	0.23	0	0	0	0	11.9	0.35	82.00	0	5.69	0	0	0	82.00
		14	0	0	0	0	0	0	0	0	0	3.5	0.23	96.26	0	5.69	0	0	0	96.26
		15	0	0	0	0	0	0	0	0	0	0	0	1.05	0	98.94	0	0	0	98.94
		16	0	0	0	0	0	1.12	0	0	0	0	0	0	0	0	98.92	13.09	0	98.92
		17	0	0	0	0	0.23	5.25	0	0	0	0	0	0	2.94	3.15	0	77.73	5.46	77.73
		18	0	0	0	0	1.21	5.84	0	0	0	0.25	0	0.73	3.65	0	3.15	0.49	87.59	87.59
		PA (%)		81.01	84.47	90.97	80.67	84.14	85.99	85.28	76.40	81.57	87.31	88.33	90.68	88.41	92.16	90.23	82.96	86.96

		Reference																		UA (%)
		1	2	3	4	5	6	7	9	10	11	12	13	14	15	16	17	18		
2013	Classification	1	94.04	4.70	1.25	0	0	0	0	0	0	0	0	0	0	0	0	0	0	94.04
		2	5.91	89.83	0.47	0.95	2.36	0	0.24	0.24	0	0	0	0	0	0	0	0	0	89.83
		3	0.48	1.45	91.04	5.57	0.48	0	0	0	0.24	0	0.73	0	0	0	0	0	0	91.04
		4	1.66	13.39	6.98	65.96	2.99	0	0	11.87	1.06	0	0	0	0	0	0	0	0	65.97
		5	0	0.92	0.23	10.30	64.32	0.23	5.72	5.95	9.34	4.15	0	0.23	0	0	0	0.69	0.12	64.32
		6	0	0	0	0	0.97	71.07	1.94	0.39	0.19	0	4.47	0.19	0	0	1.75	12.62	6.21	71.07
		7	0	0	0	0.25	1.27	0	90.93	1.01	1.01	3.54	0.76	0.51	0	0.19	0	0	1.10	90.93
		9	0	0.44	0.22	5.01	8.71	0.65	1.09	76.25	6.97	0	0	0	0	0	0	0.22	0.44	76.25
		10	0	0	0	0.84	2.51	0.42	9.41	12.55	74.27	0	0	0	0	0	0	0	0	74.27
		11	0	0	0	0	0	0	0.48	0	0	92.36	0	5.97	1.19	0	0	0	0	92.36
		12	0	0	0.53	0.26	0	0	2.65	0.26	0	2.38	92.59	0.26	0.53	0	0	0	0.53	92.59
		13	0	0	0	0	0	0	0	0	0	12.27	0	87.50	0	0	0	0	0	87.50
		14	0	0	0	0	0	0	0	0	0	0.27	0	0	98.94	0	0	0	0	98.94
		15	0	0	0	0	0.25	0	0.23	0	0	1	0	0	0	98.15	0	0	0	98.15
		16	0	0	0	0	0	1.26	0	0	0	0	0	0	0	0	97.47	1.27	0	97.47
		17	0	0	0	0	0	8.88	0.51	0	0	0	0.91	1.27	2.54	2.1	2.5	76.14	9.4	76.14
		18	0	0	0	0	0	3.05	.910	0	0	0.30	0.80	2.13	2.13	0	0	1.22	91.50	91.50
		PA (%)		90.36	84.07	92.38	71.23	78.68	86.73	77.48	71.57	80.32	79.30	90.91	90.17	90.17	98.30	95.54	79.37	81.08

5.3.3.1 Agricultural Expansion and Intensification

Covering almost 30 % of the basin's area, agricultural and cultivated areas (Class ID 7 – 10) are the most dominating landscape features in the Yellow River Basin. In the investigated time period, the absolute numbers remained stable at 200,000 km² (Table 5.5). Despite the fairly stable conditions in absolute terms, localized dynamics are present, when investigating smaller subsets. One example of new developed agricultural fields is located in the arid northern part of Ningxia Province, near the city of Zhongwei as depicted in Figure 5.16 (subset 2), where new irrigation facilities allow cropping in a relatively dry region. Throughout the basin, other local examples of encroaching fields include the Hetao Irrigation District in Inner Mongolia and small groundwater-fed oases located in the Kubuqi Desert on the Ordos Steppe.

5.3.3.2 Urbanization

Total population numbers remained more less stable within the Yellow River Basin, whereas urbanization rate almost doubled in the last 15 years (see Figure 3.3) on page 32.

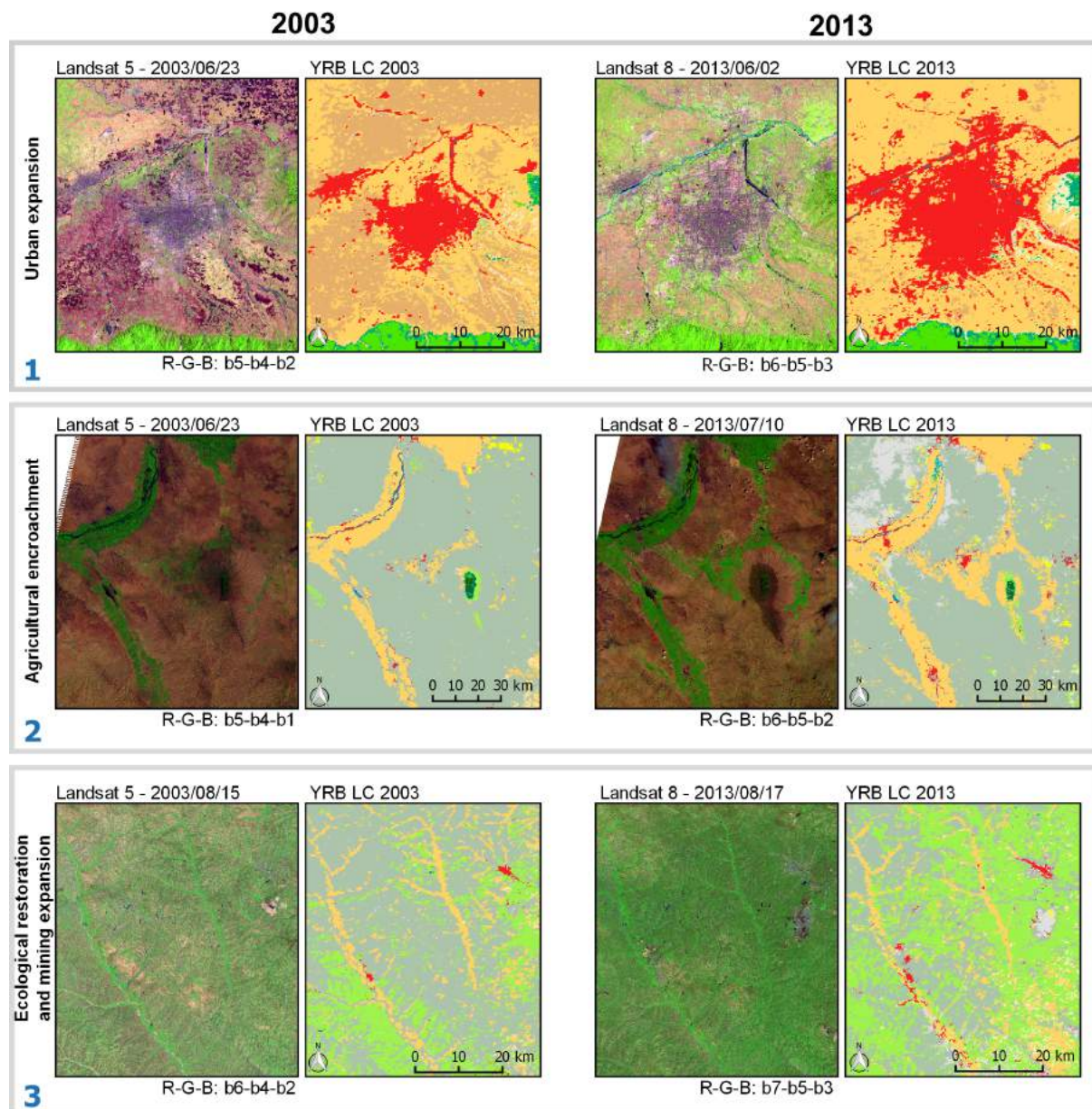


Figure 5.16: Most prominent land cover/use dynamics in the Yellow River Basin between 2003 and 2013. The number refer to the exact geographical location as indicated in Figure 5.11. The color code of the respective land cover types conforms to the colors introduced in Table 5.4 and Figure 5.11.

As one of the major cities in Northwest China, the city of Xi'an is one of China's most emerging megacities (Figure 5.16 2) and belongs to the *China Western Development* (Chinese: 西部大开发) region. It is specifically tailored to attract foreign investments and funds to foster regional economies and employment in western China. Xi'an has re-emerged as an important industrial and educational center of the central-northwest region, with facilities for research and industrial development. In ancient times, Xi'an was assign as capital city of the Qin dynasty (Chinese: 秦朝), the first dynasty of Imperial

China. Today, the city holds a population of appropriately 8.5 million, which sprawls with annual rates around 4 % (NBS, 2015). Artificial and built-up structures have expanded along the river banks of the Wei River and in peri-urban settlements in the irrigation districts. In 2013, the city of Xianyang was integrated into the Xi'an metropolitan area. Throughout the basin, artificial and built-up structures increased from around 35,000 km² to 87,000 km², equivalent to a 35 % increase, between 2003 and 2013 (Table 5.5).

5.3.3.3 Ecological Restoration

The long-term abuse of land and water resources has turned large parts of the Central Loess Plateau into a degraded landscape. Once covered by mixed forests and shrubland, agricultural cultivation replaced, already centuries ago, those forest ecosystems, which have stabilized the highly erosive Loess soils, resulting in a severe soil erosion and deterioration. In order to “green up” the bare and sparse vegetation areas, various policies and sustainable management programs have been launched. As one of the world's largest restoration activity, the *Loess Plateau Watershed Rehabilitation Program* (see section 3.3 on page 45) targeted specifically the degraded areas susceptible to soil erosion in the Yellow River Basin. The primary objective was not only to restore natural vegetation on gulch slopes, but also to include social aspects by supporting local and small-scale farming practices to raise agricultural production and income. This program was implemented from 1996 until 2005 by the World Bank and many international partners. An even larger influence on the transformation of the Loess Plateau can be attributed to the nationwide launched *GfG* program with the main goal to increase vegetation coverage on steep slopes, which started in 1999. Subset 3 in Figure 5.16, embedded in Shanbei region (Shaanxi Province) depicts the obvious expansion of grassland coverage on previous cropland or spare land. From the computed NDVI trend tendency in Figure 5.13, the “greening” of the Loess Plateau can also be nicely seen.

5.3.4 The Yellow River Land Cover Product (YRB LC) vs. Global and National Inventories

As global land cover products have been designed for mapping land cover/use pattern on global scales, their applicability for regional specific applications is not necessarily given. In order to show the out-performance of a regional adapted land cover map, the YRB LC is directly compared to the often used MODIS MCD12Q1 IGBP (Friedl et al., 2010), the GlobCover2009 (Bicheron et al., 2010), and the ESA-CCI-LC 2010 (Defourny et al., 2014). Further, the NLUD-C (Zhang et al., 2014), a national inventory, that should incorporate better regional characteristics of the Chinese land cover was inspected. As a visual reference image, a high-resolution Landsat 8 OLI scene with 30x30 m pixel resolution was taken, which depicts the complex and heterogeneous landscape features of

the Yellow River Basin at higher spatial detail. The first example subset is illustrated in **row 1** in Figure 5.17 and shows alpine grasslands in Qinghai Province. As second subset a human-dominated landscape with semi-natural and agricultural vegetation coverage was chosen with disjunct mixed forest patches located in Shaanxi Province (**second row** in Figure 5.17). The third and last example for comparison is the Yellow River Delta (Shandong Province) as can be seen in **row 3** of Figure 5.17. This region is shaped by strong human activities, but still contains vast biodiverse wetland ecosystems at the river mouth. The geographical extent and distribution of each subregion is depicted in Figure 5.11's lower panel.

The first subregion on the Qinghai-Tibet Plateau in the upper reaches of the Yellow River encompasses rather homogeneous alpine grassland steppes vegetation interspersed with barren and sparse vegetated mountain ranges (**row 1** of Figure 5.17). Two large freshwater lakes (the Gyaring and Nyoring lake) and several small brackish water bodies are scattered across the area. Also a narrow sandy desert stripe can be seen at the western margins of the subset. Despite the more or less homogeneous landscape pattern, the considered maps show diverging classification schemes. Only the large water bodies are delineated consistently in all maps. Looking at the higher-resolution Landsat imagery, it is evident that the regional adapted YRB LC 2013 follows the spatial pattern of the reference imagery. The MODIS MCD12Q1 classifies all terrestrial areas as grassland, neglecting the non and sparsely vegetated structures on mountain ridges. Desert is also not delineated. In contrast, the GlobCover 2009 product captures at least barren land, but introduces non-existing cropland/vegetation mosaics and irrigated cropland. Same misclassification applies to the ESA CCI-LC, where grassland vegetation is assigned to cropland-related classes. In this harsh environment with infertile soils and cold temperatures, agricultural production is not possible. The national NLUD-C does not delineate cropland in this area, but overestimates the occurrence of desert structures.

The second subregion is a human dominated landscape in the floodplains of the Wei River in Shaanxi Province (**row 2**, Figure 5.17). This region encompasses a much more complex and heterogeneous landscape character with disjunctive small-scale deciduous and evergreen forest patches surrounded by intensified agricultural fields. At the forest edges, transitional and fragmented areas of semi-natural vegetation are present, where small-scale farming practices cut forests into small mosaics. Besides vegetated areas, urban and peri-urban structures are scattered across the Wei floodplain. At the south-eastern margins the city of Xianyang is present, close to the provincial capital Xi'an. From the Landsat imagery, these complex landscape facets are reflected well by the YRB LC 2013, which delineates even the small-scale mosaics of natural and semi-natural vegetation. The large continuous mixed forest formations in the northern part are classified in all land cover maps, except for the NLUD-C product. MODIS IGBP land

cover tends to overestimate forest area and fails to differentiate between forest types. In contrast, GlobCover underestimates forest patches, but separates between deciduous and evergreen forest types. Despite the lower class accuracies for open shrub- and woodland and for the mosaic classes, their distribution is clearly discernible in the YRB LC 2013 map, considering this heterogeneous semi-natural landscape. Surprisingly, the national NLUD-C performs worst: Forest and shrubs are confused with grassland and agriculture. The coarser spatial resolution of 1 km is not sufficient to illustrate the small-scale landscape facets in high spatial detail. Only ESA CCI-LC reflects the tessellated pattern in similar spatial detail. Looking at the artificial class, our YRB LC 2013 map is exclusively able to delineate complex and small-scale urban structures.

In terms of complexity, a similar landscape is the Yellow River Delta (**row 2** in Figure 5.17). Strong anthropogenic activities have resulted in tremendous landscape modifications. Large coastal wetlands and temporally flooded tidal flats can still be found at the river mouth, which are an important base for various bird species. Numerous aquaculture ponds intersect the near coastal zone and produce mainly fish and crustaceans. The inner delta is dominated by agriculture and small patches of urban settlements. Dongjing is the sole major city located in the southern delta region. Exclusively, the YRB LC 2013 consists of a thematic class aquaculture, which is depicted congruently with the Landsat OLI imagery. The other maps identified aquaculture incorrectly as either grassland, rain-fed cropland or water bodies. While wetlands are often misclassified as grassland or irrigated cropland, cropland areas are depicted correctly in almost all land cover maps, except for ESA CCI-LC, where evident cropland areas are assigned to grassland. In the MODIS MCD12Q1 product, large parts of the wetland and tidal flats areas are cut out and classified as water. The highly dynamic tidal flats are only classified in the YRB-LC 2013 and not defined in the other considered maps, except for the NLUD-C. It can be further noted that urban areas seem to be better detected compared to the previous subset. GlobCover still greatly underestimates urban and built up structures and the NLUD-C is not able to map these structures. Once again, YRB LC 2013 delineates these dispersed areas in higher spatial detail.

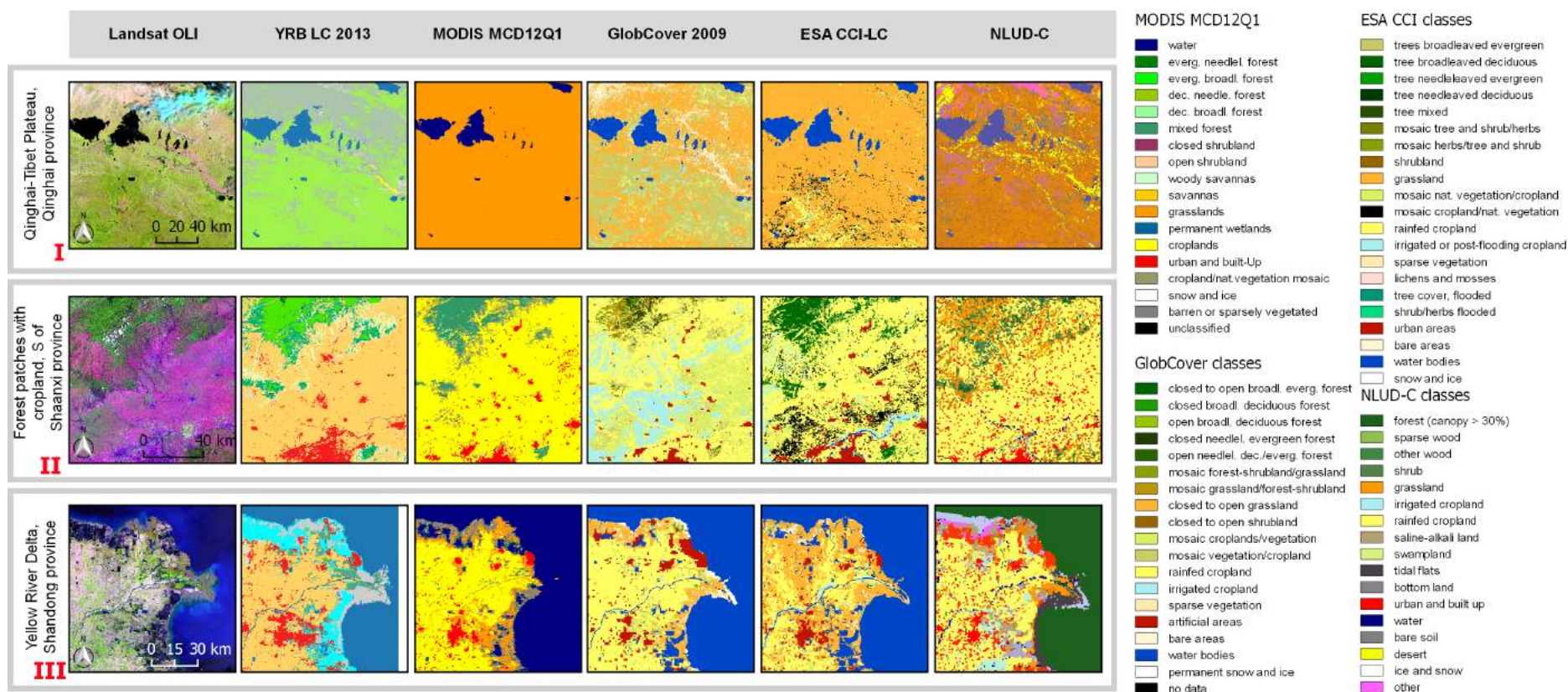


Figure 5.17: Comparison of Landsat OLI imagery (RGB band combination: 7-5-3) in column 1), against the Yellow River Land Cover Product (YRB LC 2013) (column 2), MODIS MCD12Q1 2012 (column 3), GlobCover 2009 (column 4), ESA CCI-LC (column 5), and the national land use/cover database of China (NLUD-C) for 2008 (column 6). Three representative examples for the Yellow River Basin were selected: a tessellated area with forest patches intersected with cropland in the south (row 1); the Yellow River Delta determined by urban, agriculture, and wetlands (row 2); and the source region dominated by grassland and sparse vegetation mosaics (row 3). Colors for YRB LC classes match the codes introduced in Table 5.4 and Figure 5.11.

5.4 Discussion

The previous chapters of this thesis have demonstrated the urgent need for updated, thematically detailed, consistent, and multi-temporal “wall-to-wall” information about regional landscape characteristics. These information can be used by many local stakeholders as decision making support, as well as by researchers for climatic and hydrological modeling. In this chapter, novel land cover change products have been generated for this very dynamic basin and the underlying factors have been determined. Following the methodological procedure as described in section 5.2 on page 64, a straightforward semi-automated supervised classification approach was developed using high-temporal medium-resolution MODIS time series, which is capable of delineating heterogeneous landscapes at large spatial scales.

This section discusses the apparent dynamic processes and their underlying factors in section 5.4.1. The subsequent section 5.4.2 discusses the quality and potential errors in the final thematic maps. Further, a short outlook for possible research is included.

5.4.1 Land Cover Classification and Land Cover Dynamics

In this chapter, two land cover maps in high thematic detail were presented for the years 2003 and 2013, on which the most dynamic processes were analyzed and the underlying factors described. Due to its large geographical extent and high altitudinal gradient, the Yellow River Basin consists of diverse bioclimatic and environmental conditions, requiring a regional adapted classification strategy. In line with many studies working on medium resolution scale (Clark et al., 2012; Klein et al., 2012; Blanco et al., 2013; Kiptala et al., 2013; Leinenkugel et al., 2013; Wohlfart et al., 2014; Gessner et al., 2015), this study demonstrates the advances of using high-temporal phenological information for land cover differentiation. During the last 15 years, the Yellow River Basin’s landscape was mainly affected by large-scale restoration activities, agricultural dynamics, and sprawling cities.

The most apparent landscape dynamics occurred on the Loess and Ordos Plateau. There, **ecological restoration** efforts have recovered vegetation structures on large spatial scales to combat the long-lasting environmental deterioration to recreate lost ecosystem goods and services, such as carbon sequestration, hydrological services, and soil retention. The results as described in sections 5.3.1.3 and 5.3.3.3 reveal enhancing ecological conditions by replanting barren and sparse surfaces and by transforming slopping farmland to grass- or woodland. The results presented in this chapter are analogues to various earth observation studies investigating local landscape dynamics, also revealing large scale improvements of ecology and environment on the Loess Plateau (Chen et al., 2009; Miao et al., 2012; Liu et al., 2013; Gao et al., 2015; Zhai et al., 2015). However, these studies only depict dynamics on rather small geographical extent and do not provide a compre-

hensive picture of the prevailing dynamics. The tremendous “greening” of the basin (see Figure 5.13) was also identified by studies investigating the net primary productivity (NPP), commonly used as proxy for vegetation productivity and carbon fluxes (Feng et al., 2013; Eisfelder and Kuenzer, 2015). Human-induced effects on the landscape are thought to be the main driver of the greening, as a correlation analysis from Zhai et al. (2015) showed no significant pattern with precipitation.

As one of China’s bread-baskets supplying much of the domestic crop production, **agriculture** is the dominant landscape feature across the basin, covering one third of the entire area. The national government promotes the goal of food self-sufficiency to be economically independent from international trade markets (see chapter 3 on page 29). A rising and more affluent society requires high quality food products, but puts pressure on the agricultural sectors to fulfill national production benchmarks, particularly considering the progressive degradation of water and land resources, as highlighted in section 3.2.4 on page 41. Between 2003 and 2013, the absolute area of cultivated land remained fairly stable, while crop output experienced a 25 % growth (Figure 3.3 on page 32) by means of irrigation, improved farming practices, increased fertilizer and pesticide consumption, and a higher degree of advanced machinery (Matson et al., 1997; Tilman et al., 2001; Rudel et al., 2009; Siebert et al., 2010). Published numbers from the National Bureau of Statistics of China reveal a substantial increase of chemical fertilizers by 10 % in Shandong and even 32 % in Henan Province, both major production zones within the Yellow River Basin (NBS, 2015). Likewise, pesticides applied on agricultural fields experienced rose by more than 25 % (NBS, 2015). Despite no detected trends in absolute values, various local spatial dynamics become obvious, when investigating smaller scales. The decline of cultivated areas has mainly appeared in Shaanxi and Shanxi Province, where the *GfG* program took large areas out for cultivation (Wang et al., 2013). A retreat can also be seen in the vicinity of expanding urban areas, such as Xi’an or Bayan Nur, which are embedded in large irrigation districts. Cultivated areas have proliferated in arid regions, such as Northern Gansu, Ningxia, or Inner Mongolia, where the Yellow River and its tributaries provide water resources for irrigation activities. To increase crop intensity and harvest without area expansion, multi-seasonal cropping is commonly practiced in the Yellow River Basin, particularly in the North China Plain Irrigation District, located in the floodplains of the Wei River and the North China Plain (Li et al., 2014b). There, corn, wheat, oil-bearing crops, cotton, vegetables, and fruits are produced. Between 2003 and 2013, cropping cycles decreased considerably in the Yellow River Basin. This pattern is in accordance with data provided by the National Bureau of Statistics of China, which reveals a decrease in total sown area of winter wheat, replaced by more profitable commodities, such as fruits or oil crops, showing an inverse trend (NBS, 2015). However, this drop of two-season crops is not fully represented in the national statistics.

One explanation could be the practice of different crop cycles, periodically rotating from three harvests in two years to annual harvests (Meng et al., 2006).

Urban and artificial areas have tremendously sprawled, encroaching on surrounding agriculture or natural vegetation. Shandong and Henan Province encompass highest urbanized population exceeding 60 % at annual growth rates up to 4 % (NBS, 2015). However, even less developed provinces in the upper reaches, including Qinghai, Ningxia, or Gansu, grow annually at relative urbanization rates exceeding 10 %. More and more poor rurals are moving to the centers of development as those are the loci of employment and opportunities. Besides expanding cities, built-up structures have significantly expanded along the river banks, where local industries and infrastructure emerged. A more urbanized society demands higher energy levels. Currently China's energy generation is mainly built on coal, which supplies two-thirds of China's energy use (NBS, 2015). Since 2003, coal production for domestic and international markets has increased by 25 % mainly in Shanxi Province, the leading coal producer within the basin, which has more coal mines than any other province in China (NBS, 2015). Opencast mines and excavations have recently appeared and expanded on the Qinghai-Tibet Plateau in Haibei Prefecture, replacing fragile and sensitive alpine grasslands meadows.

5.4.2 Land Cover Accuracies

Given the complex and heterogeneous landscape facets encompassing the Yellow River Basin in conjunction with the vast geographical extent, the attained overall accuracies of 84 % and 87 % for 2003 and 2013, respectively are satisfactory and in a comparable range to other equally changing land cover studies across the globe (Clark et al., 2010; Colditz et al., 2011; Klein et al., 2012; Leinenkugel et al., 2013; Gessner et al., 2015). The included seasonal metrics, derived from high-temporal time-series, are ranked as most important features in delineating land cover classes.

Basically, thematic classes receive class-specific accuracies in a quality range. However, classification challenges remain in this classification framework. Defined land cover classes containing various vegetation types, such as mosaic and open woodland classes (class IDs 2, 4, 9, 10), show highest confusion, mainly with grassland, and high entropy. This error pattern is analogous for both years. These classes often comprise a significant proportion of grassland areas, thus possessing similar spectral-temporal trajectories leading to false class allocation. When working on medium spatial resolution scale it is necessary to define such land cover mosaics to enhance thematic precision to represent the inherent spatial heterogeneity in the basin, albeit risking lower accuracies and increasing confusion. Indeed, misclassification is attributed to the occurrence of mixed pixels, particularly when conventional hard pixel classifiers are applied on medium-resolution

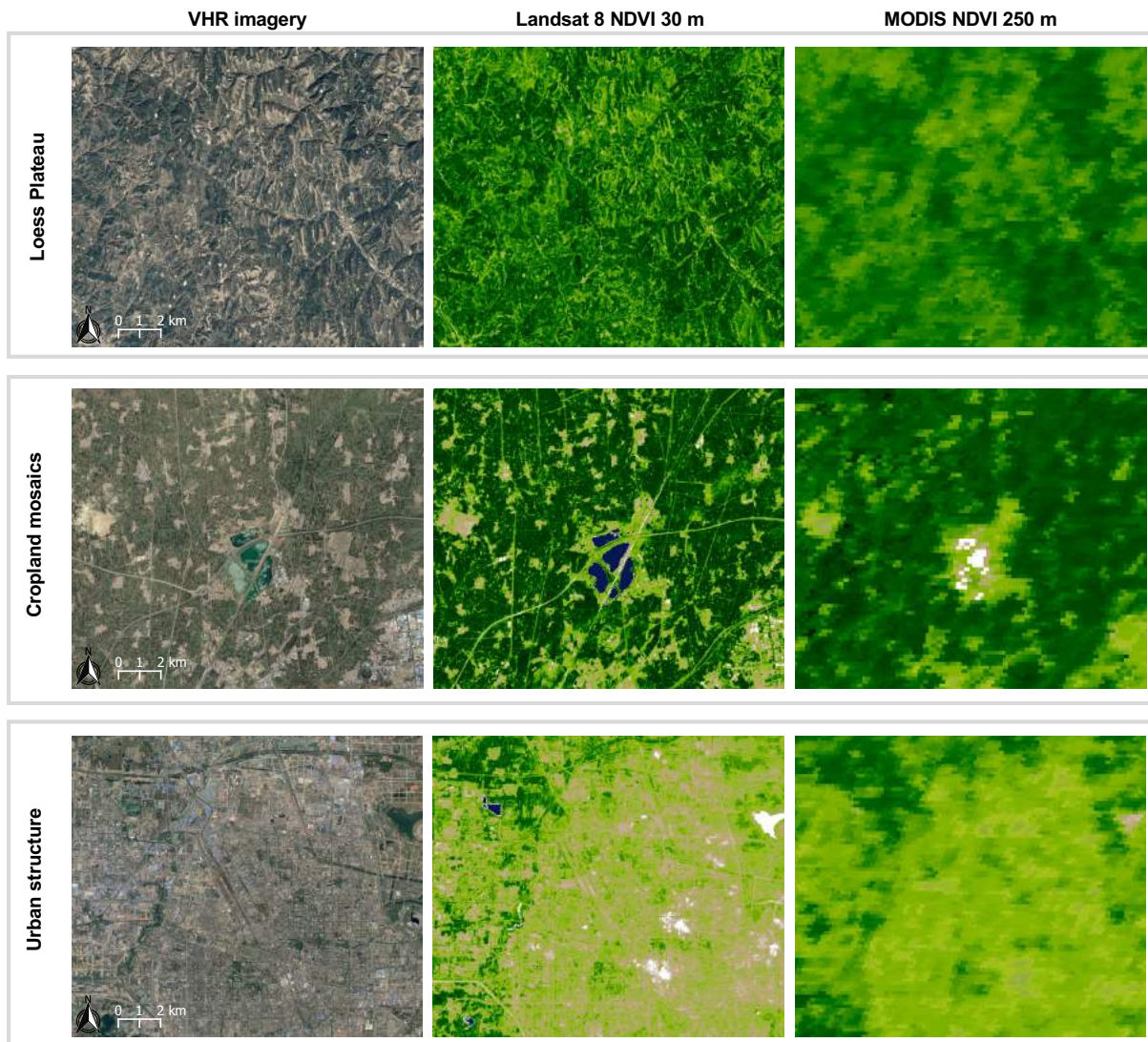


Figure 5.18: Spatial effect of pixel resolution from different sensors on various land cover types: Loess Plateau with mosaics of forest and agriculture (36.99°N - 37.39°N / 108.91°E - 109.42°E); the Hetao Irrigation District with vast agricultural fields (40.62°N - 41.03°N / 107.08°E - 107.59°E); the city of Zhengzhou in Henan Province (34.53°N - 34.95°N / 113.41°E - 113.89°E).

data. Delineating the fractional cover on a sub-pixel level could substantially improve classification performance for transitional and heterogeneous landscape structures (Fernandes et al., 2004; Gessner et al., 2013; Leinenkugel et al., 2014; Wohlfart et al., 2014). Working on a higher spatial resolution, e.g. Landsat resolution of 30 m, gives a spatially clearer picture of the prevailing landscape, even in ambitious environments, such as the Loess Plateau or urban structures (Figure 5.18).

Contrary to this, spatially homogeneous classes, including dense and closed forest types (evergreen and deciduous), water bodies, desert, snow, and tidal flats tend to hold higher chances of being predicted successfully, as these classes encompass distinct spectral-

temporal properties. Classification error appears to happen in separating aquacultural ponds from water bodies, barren land from desert, and barren land from built-up and artificial surfaces. The latter case is an ambitious classification task. Therefore, the application of ancillary nighttime lights information substantially improved the final classification result.

5.5 Summary

- ❶ This chapter presented novel, consistent, and thematically detailed land cover products, which represent the heterogeneous landscape characteristics for the Yellow River Basin for the years 2003 and 2013.
- ❷ From the bi-temporal information, major land cover changes have been extracted in this dynamic region.
- ❸ The final classifications were based on a random forest classifier using a large variety of spectral, multi-spectral, seasonal, and ancillary features.
- ❹ Accuracy assessment yielded satisfactory results achieving overall accuracies of 87 % and 84 % for 2003 and 2013, respectively.
- ❺ Major land surface dynamics include agricultural expansion and intensification, urbanization, and large-scale ecological restoration activities on the Loess Plateau.
- ❻ Medium-resolution data fail in delineating spatially heterogeneous and transitional landscape structures, such as those occurring on the Loess Plateau.
- ❼ The delineated “wall-to-wall” products provide essential information to support local and regional decision making for sustainable land and water management and can be used as primary input variable for hydrological and climate modeling.

ANNUAL LAND COVER DYNAMICS USING DENSE LANDSAT TIME-SERIES FOR DELINEATING MINING, AGRICULTURE, FOREST, AND URBAN AREAS*

In the previous chapter a comprehensive “wall-to-wall” analysis was presented based on MODIS time-series and provided an enhanced picture of the prevailing landscape characteristics and major dynamics influencing the Yellow River Basin in recent years. However, the spatial resolution of 250 m is not sufficient in dealing with heterogeneous landscape types requiring higher spatial detail. Spatially high-resolution datasets, such as Landsat with 30x30 m pixel resolution, balance the trade-offs involving spatial and temporal resolution, areal coverage, and availability of long historical data of more than 45 years (Wulder et al., 2011; Griffiths et al., 2014; Kuenzer et al., 2014c). The opening of the USGS Landsat archive for free automatically orthorectified imagery (L1T-product) (see section 4.2 on page 57) has created new unprecedented opportunities of regional land cover applications at higher temporal frequencies and more spatial detail (Woodcock et al., 2008; Hansen and Loveland, 2012). Aside from the spatial aspect, the magnitude of change that is currently present in the Yellow River Basin requires monitoring at annual steps to capture the rapid rate of change to fully understand the underlying factors.

A summary of Landsat based research conducted in the Yellow River Basin was already given in section 1.2.2 on page 8. So far, a mere of multi-temporal high-resolution remote sensing studies exist, which investigated diverse localized spatial pattern including

* This chapter is based on: Wohlfart, C., Mack, B., Liu, G., C. and Kuenzer, C. (2017). Multi-faceted land cover and land use change in the Yellow River Basin based on dense Landsat time series: exemplary analyses in mining, agriculture, forest, and urban areas. *Applied Geography*, 85, 73-88

grassland dynamics on the Qinghai-Tibet Plateau (Dong et al., 2009), forest dynamics on the Loess Plateau (Guo and Gong, 2016), urban sprawl (Schneider, 2012), or the Yellow River Delta (Ottinger et al., 2013). However, comparatively few scientific work has analyzed historic land cover changes on annual steps and detailed regional thematic information is not existent.

This chapter addresses this knowledge gap and delineates the most prominent land cover dynamics on higher spatial and temporal level. The annual land cover maps are derived in a semi-automated fashion using spatially continuous spectral-temporal, multi-spectral, and textural features based on dense Landsat stacks in conjunction with a stable pixels approach to generate a reliable and time-consistent reference dataset. The following spatio-temporal dynamics for the time period between 2000 and 2015 have been analyzed:

- ❶ Sprawling mining activities on the Qinghai-Tibet Plateau
- ❷ Agricultural dynamics in the largest irrigation district located in Inner Mongolia
- ❸ The extent of the ecological restoration measures on the Central Loess Plateau
- ❹ Urban and peri-urban encroachment in the largest metropolitan region in Henan Province

Prior to the analysis of the different land cover facets, a short summary of existing Landsat-based multi-temporal approaches is provided. It is followed by a short introduction of the four selected focus regions and an explaining Methods section, where data processing and classification steps are presented. Finally, this chapter is rounded off with a detailed discussion section and a short summary of the main findings.

6.1 Landsat-based Multi-temporal Approaches

Landsat-based time-series approaches on regional spatial scales have recently taken their cues from multi-temporal methods developed with coarse resolution datasets (Kennedy et al., 2010; Hansen et al., 2014; Franklin et al., 2015; DeVries et al., 2015; Hermosilla et al., 2015; Mack et al., 2017). A myriad of different analytical frameworks for performing change detection and mapping of land change with Landsat imagery have progressed greatly, particularly since the opening of the Landsat archive (Woodcock et al., 2008). Traditional land cover/use change detection approaches focus on one or several single-date pairs of images (Coppin et al., 2004; Lu et al., 2004; Kennedy et al., 2007). Such two-date methodological approaches have several drawbacks because detailed spatial and temporal aspects of change remain unclear proved by many comparative studies (Broich et al., 2011; Gómez et al., 2014; Franklin et al., 2015). A simple comparison of single-date

imageries, which only represent a specific phenological state within a year, is associated with radiometric and phenological variability between years - particularly for strong seasonally influenced land cover classes - that could introduce confusion when performing change detection analysis. Another limitation of single-date many change detection approaches is the reliance of available cloud-free imagery. Precipitation events across the Yellow River Basin are concentrated in the summer months July and August, which makes it difficult to obtain high quality images for this period. Recognizing these obstacles, Landsat time series compilations of long data sequences enhanced the interpretation of various land cover dynamics at more detailed spatial scales, which have begun to flourish with the opening of the USGS Landsat archive in conjunction with increasing computational power (Goodwin et al., 2008; Woodcock et al., 2008; Vogelmann et al., 2009; Kennedy et al., 2010; Huang et al., 2010). So far, research using Landsat-based time series has created annual cloud-free surface reflectance composites (e.g. Best-Available-Pixel composite - BAP) for a wide range of different land cover applications on large spatial scales (Broich et al., 2011; Griffiths et al., 2013; White et al., 2014; Thompson et al., 2015; Gómez et al., 2016). Intra-annual time series metrics offer great potential for land cover delineation in a complex environment, which are dominated by a distinct phenological trajectory. A direct characterization of phenological metrics as illustrated in the previous chapter 5 is challenging due to temporal irregularity and cloud contamination (Kovalskyy and Roy, 2013). These spectral-temporal metrics should capture the salient phenological information characterizing distinct land cover types.

6.2 Selected Foci Areas

Four representative thematic foci regions across the basin were selected in this chapter, reflecting the previously mentioned dynamic processes (Figure 6.1). The first region is embedded on the northeastern part of the Qinghai-Tibet Plateau in the Haibei Prefecture, where recent mining operations have commenced. The Hetao Irrigation District as second focus region located in Inner Mongolia encompasses the largest network in the basin. The challenging Loess Plateau was chosen, where remarkable conservation and restoration have taken place. One of the major centers of urban and economic development was picked as a generic example for demonstrating urbanization processes: the Central Plain or Zhongyuan Metropolitan Region.

6.2.1 Haibei Prefecture on the Qinghai-Tibet Plateau

The considered region ($37.45^{\circ}\text{N} - 38.30^{\circ}\text{N}/98.90^{\circ}\text{E} - 100.87^{\circ}\text{E}$) spans a total area of almost $17,000 \text{ km}^2$ covering around 50 % of Haibei Tibetan Autonomous Prefecture, elevated between 3,200 and 3,700 m (Figure 6.1, 1). It is located at the northeastern edges of the

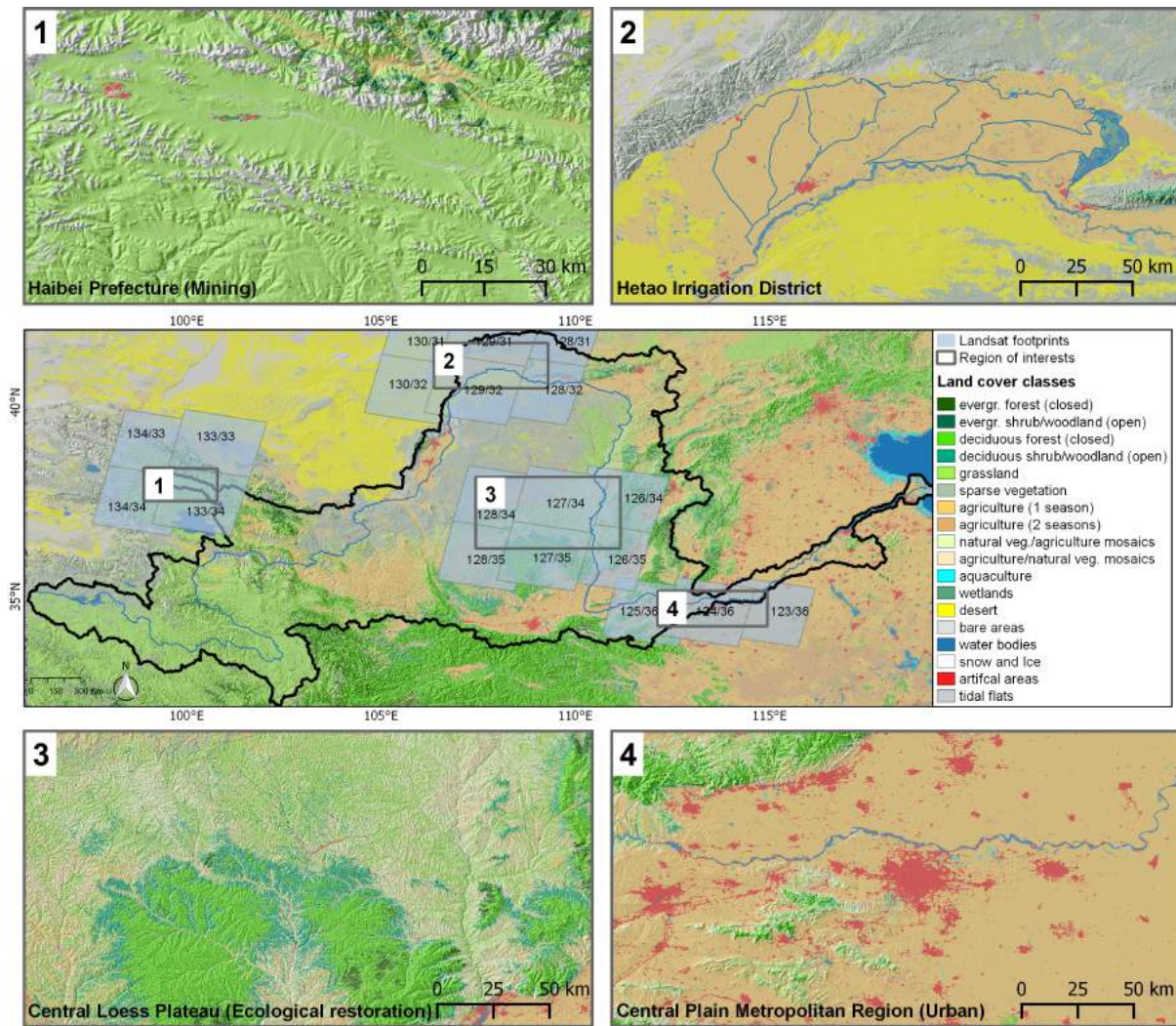


Figure 6.1: Geographical location and spatial extent of the considered foci regions and the process Landsat footprints (1-4).

Qinghai-Tibet Plateau, where the Qilian Mountains form the northeastern escarpment of the plateau. Influenced by harsh environmental conditions of low temperatures and few rainfall, Haibei's landscape is characterized by unique alpine swamp meadows, offering habitats to various adapted wildlife (Li et al., 2012). The Datong and Shule River, major tributaries of the basin's upper reaches are originating in Haibei. Although sparse populated with 6.56 inhabitants/km² (for comparison: Shandong Province 750 persons/km²) and poorly economically developed, the coal rich plateau has been recently discovered by coal companies, which started large open-pit coal excavation activities.

6.2.2 Hetao Irrigation District

With a total core area of 10,000 km² of which 60 % is irrigated with Yellow River water and more than 20,000 branches, the Hetao Irrigation District encompasses the most

extensive canal network across the Yellow River Basin (Figure 6.1, 2) (Wu et al., 2008b; Borruso et al., 2017). It is located in the southwestern part of Inner Mongolia on the Ordos Plateau and lies to the north of the *Great Bend*, also known as *Ordos Loop* (39.66°N – 41.70°N/106.05°E – 109.55°E). The flat alluvial terrain at an altitude of around 1,000 km² is characterized by paleochannels, oxbow lakes, sand dunes, lake marshes and hollows (Wu et al., 2008b). Hetao is bound by the Lang Mountains or Lang Shan, which is part of the Yin Mountains range, to the north, and surrounded by the extensive Gobi desert to the west and southwards by the Kubuqi Desert, the seventh largest desert of China. The arid climate with precipitation prevails less than 100 mm/year (Hijmans et al., 2005) requires intense irrigation measures for crop production. There, 10 % of the total Inner Mongolian grain crops are cultivated (NBS, 2015).

6.2.3 Central Loess Plateau in Shaanxi/Shanxi Province

The Loess Plateau in China stretches an area of 640,000 km² of which 90,000 km² were considered for detailed analysis (35.88°N – 37.81°N/107.59°E – 111.53°E) (Figure 6.1, 3). In this area located in Shanxi and Shaanxi Provinces, which still contain remnants of natural continuous forest patches (Lu Liang and Ziwuling Mountains), major restoration and afforestation activities are ongoing, fostered by PES and conservation programs, such as the *GfG*. Centuries of degradation and erosion have created the typically hilly and gullied surface structure (Figure 3.9).

6.2.4 Central Plain Metropolitan Region in Henan

The Central Plain (or Zhongyuan) Metropolitan Region in Henan Province (33.88°N – 35.29°N/111.46°E – 115.46°E) is embedded in the flat alluvial floodplains of the lower Yellow River (Figure 6.1, 3). This region is one of the ancient centers, where the Chinese civilization has evolved 4,000 years ago. Today almost 38.5 million people live in the metropolitan region, distributed across three major cities, namely Luoyang, Zhengzhou, and Kaifeng. These cities form a hub of outstanding economic development facilitated by abundant natural resources and fertile land. The investigated area includes around 25,000 km².

6.3 Methodological Approach

The analytic framework in this chapter for delineating spatio-temporal dynamics of four different land cover types (mining, agriculture, forest vegetation, and urban structures) is based on higher resolution dense Landsat time-series involving a spatial resolution of 30 m. Each RF classifier was fed by biannual composed spectral-temporal metrics combined with textural metrics between 2000 and 2015. To minimize reference data

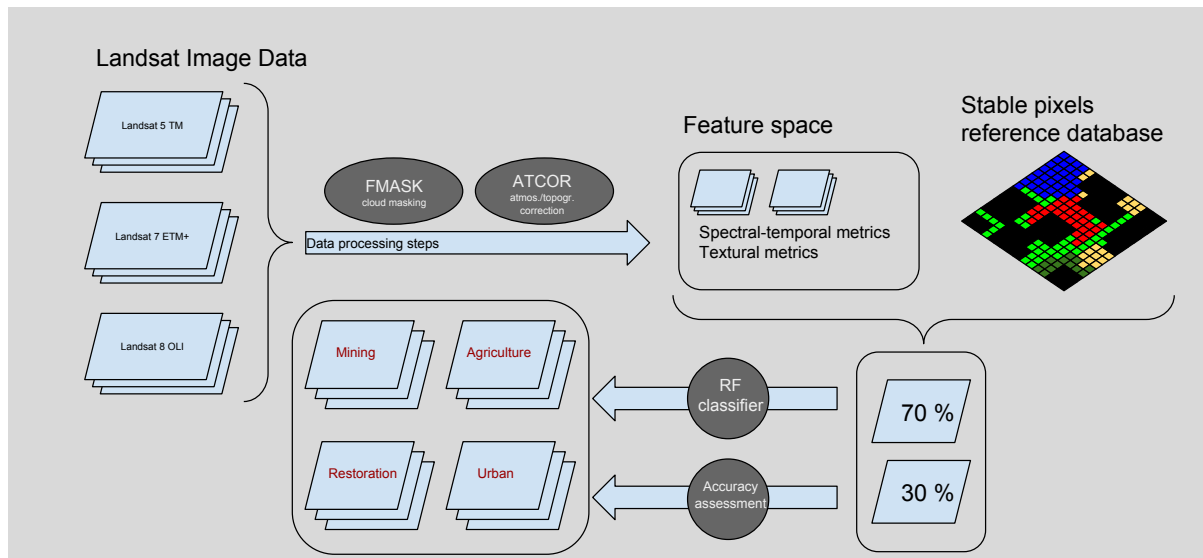


Figure 6.2: Flowchart depicting Landsat analytical framework for data processing, classification, and accuracy assessment.

collection to a minimum, a stable pixel approach was applied to identify those pixels that did not change between the considered time period. It generated a mono-temporal reference dataset using as training and validation measure for each time step. The automated Landsat data processing chain and semi-automated stable pixels collection procedure are presented in Figures 6.2 and 6.6). Again, 30 % of the reference data was split to assess thematic quality of each product. From the derived multi-temporal thematic maps, detailed land cover/use dynamics were analyzed quantitatively and qualitatively for each thematic region. Same as the MODIS analysis in the previous chapter, only freely available data and software resources were used for processing, classification, and statistical analysis.

6.3.1 Landsat Imagery and Data Pre-processing

For the analysis in this chapter all available precision and terrain corrected Level-1 standard products (L1T) data resources from Landsat 5 TM, Landsat 7 ETM+, and Landsat 8 OLI across the four foci regions with less than 50 % cloud coverage per scene were acquired, which are ingested in the USGS Landsat archive. This resulted in a total number of 4,520 Landsat scenes being processed. L1T products are processed to standard parameters, and distributed as scaled and calibrated digital numbers (DN). All bands, except for thermal bands were selected (Table 6.1). The temporal window of the analysis was restricted from 2000 to 2015 and could not be expanded further back in time. Prior, the amount of Landsat scenes was not sufficient to create reliable dense Landsat time series stacks for high quality spectral-temporal features (Figure 6.3). After 2003, the SLC failure on board Landsat 7 was luckily compensated by a large number of available

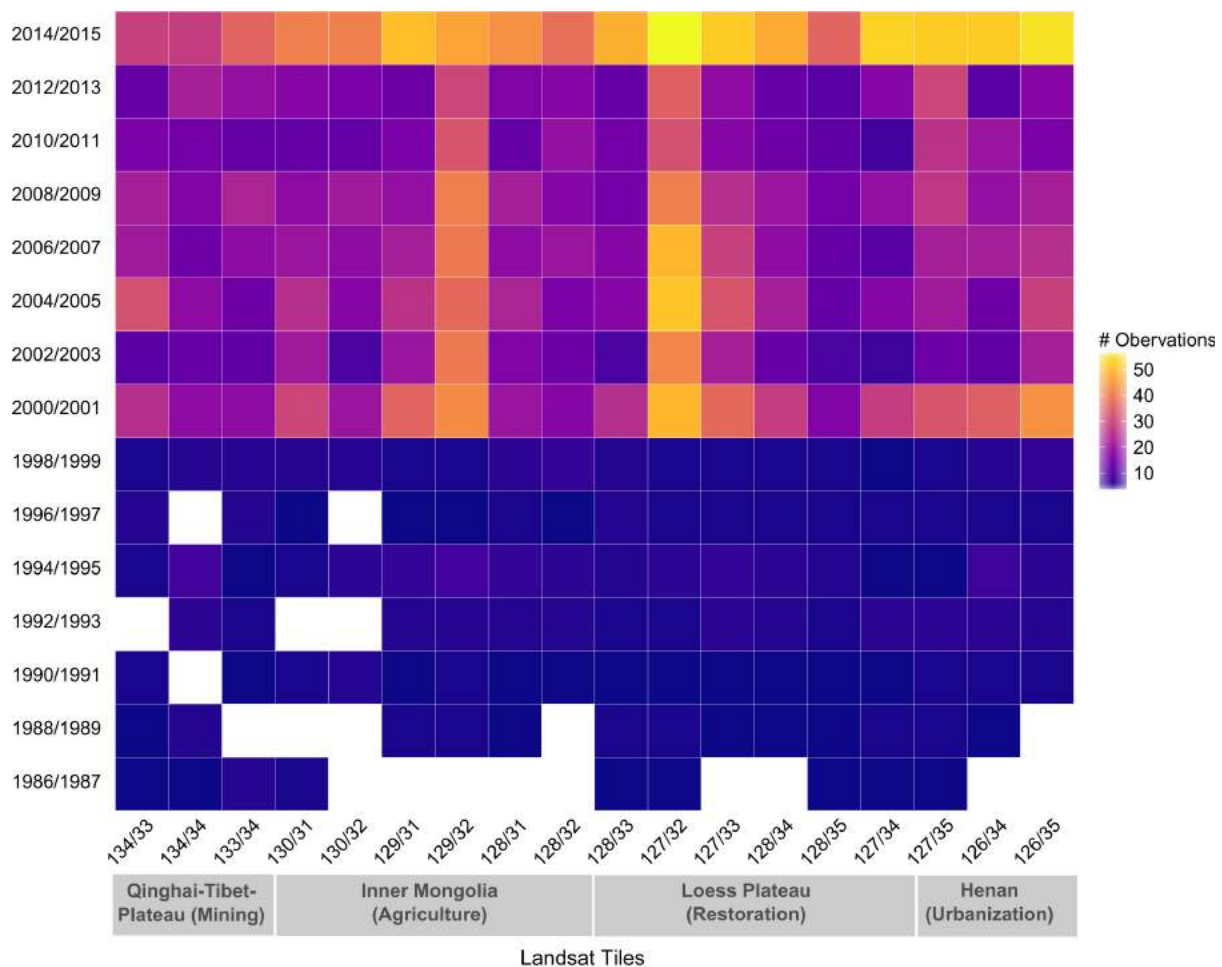


Figure 6.3: Number of all Landsat observations (TM/ETM+/OLI) with less than 50 % cloud coverage per WRS 2 path/row for each focus region since 1986.

Landsat TM scenes. However, the decommissioning of Landsat 5 at the end of 2011 caused a decrease in data density particularly for the years 2012 and 2013. To further reduce the potential effects of noise from cloud and cloud-shadow masking and other atmospheric distortions, intra-annual image frequency was further increased by merging available data of two years to achieve a denser temporal data coverage. Statistics and spatial coverage for the number of clear-sky observations available per year are shown in Figure 6.5 and Tables 6.2, 6.3, 6.4, 6.5. After screening of all images, the available data were still reasonably dense forming a continuous time-series since 2000. The total number of raw images ranged between 124 and 3456. From the often applied *FMASK* algorithm (Function of MASK), clouds and related shadows were detected for each scene and masked out and excluded from further processing (Zhu and Woodcock, 2012; Zhu et al., 2015). This rule-based algorithm was designed for automatically detecting clouds and cloud shadows by taking spectral and temporal information based on probabilistic scores into account. Here, all masks were produced using conservative values to capture as many clouds and cloud shadows as possible. Subsequently, DN of the raw imagery were converted

Table 6.1: Used Landsat data with sensor description and number of processed scenes.

Sensor	Range of acquisition	Spectral bands	Number of scenes
OLI	2013/04/11 – 2015/12/31	2 (blue) 3 (green) 4 (red) 5 (NIR) 6 (SWIR)	757
ETM+	2000/01/22 – 2015/12/31	1 (blue) 2 (green) 3 (red) 4 (NIR) 5 (SWIR)	1715
TM	2000/01/02 – 2011/09/29	1 (blue) 2 (green) 3 (red) 4 (NIR) 5 (SWIR)	2048

to atmospherically corrected surface reflectance for all considered Landsat bands using the *ATCOR 3* processor (Atmospheric and Topographic Correction), which also includes topographic correction procedure through the inclusion of elevation information based on SRTM data (Richter, 2007). *ATCOR* reduces atmospheric and illumination effects by using various atmospheric look up tables calculated with the *MODTRAN5* radiative transfer code, covering a wide range of various atmospheric conditions, to retrieve earth's surface reflectance (Berk et al., 1998). Due to the large geographical extent of the Yellow River Basin, Landsat scenes are spread across different UTM zones. The UTM zone of the central Landsat tile was chosen as reference projection zone and adjacent scenes from different zones were reprojected accordingly (Region 1 - Mining: WGS 84 UTM 47 North; Region 2 - Agriculture: WGS 84 UTM 48 North; Region 3 - Forest and 4 - Urban: WGS 84 UTM 48 North).

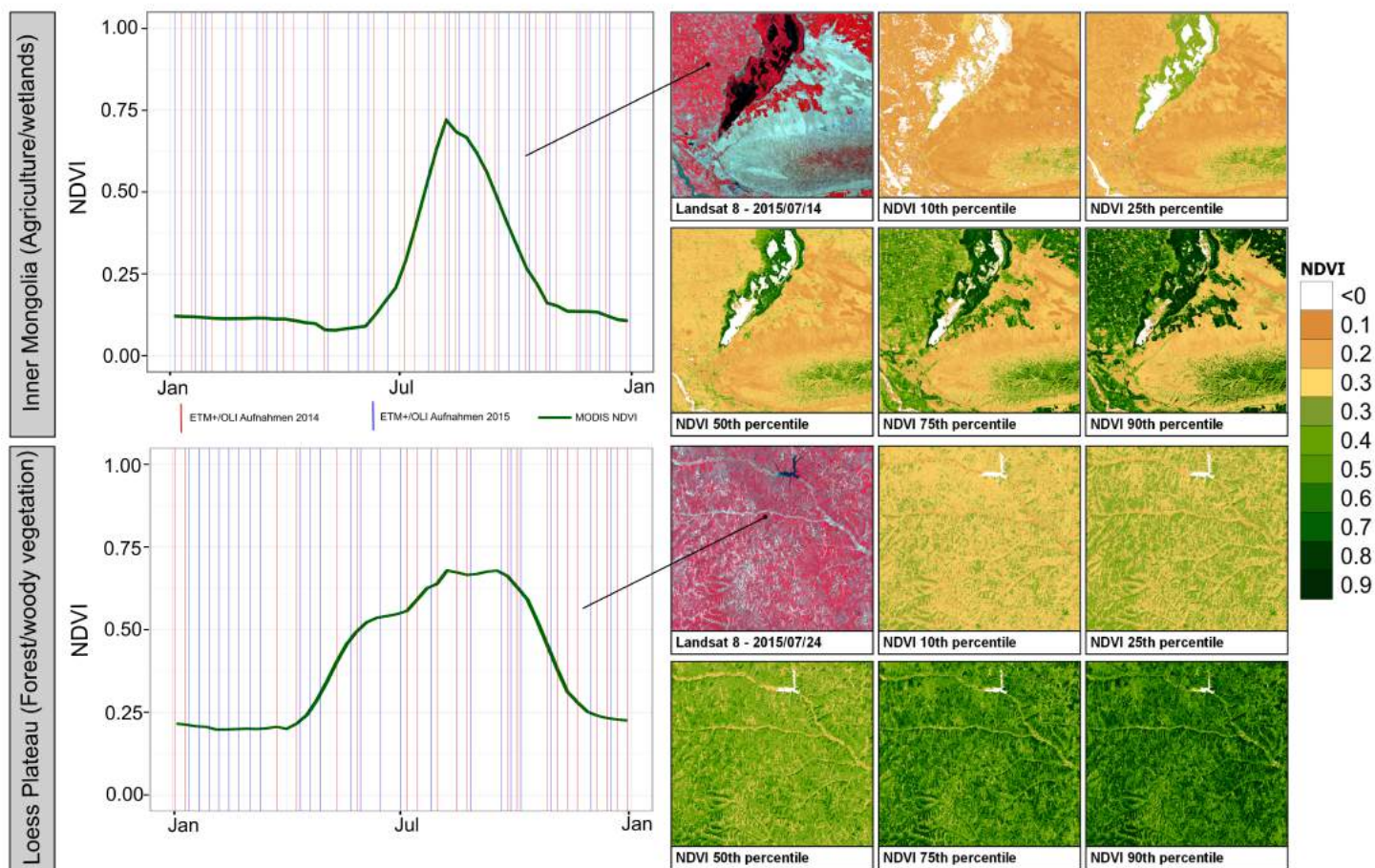


Figure 6.4: Depiction of five spectral-temporal features (10th, 25th, 50th, 75th, 90th percentiles) exemplary for two subsets. The first subset in Inner Mongolia shows an agricultural dominated landscape with adjacent wetlands and sparse vegetation. The second example highlights the seasonal change of trees on the Loess Plateau. The two diagrams depict the acquisition dates for all available Landsat scenes in the years 2014 and 2015, relative to the NDVI trajectory.

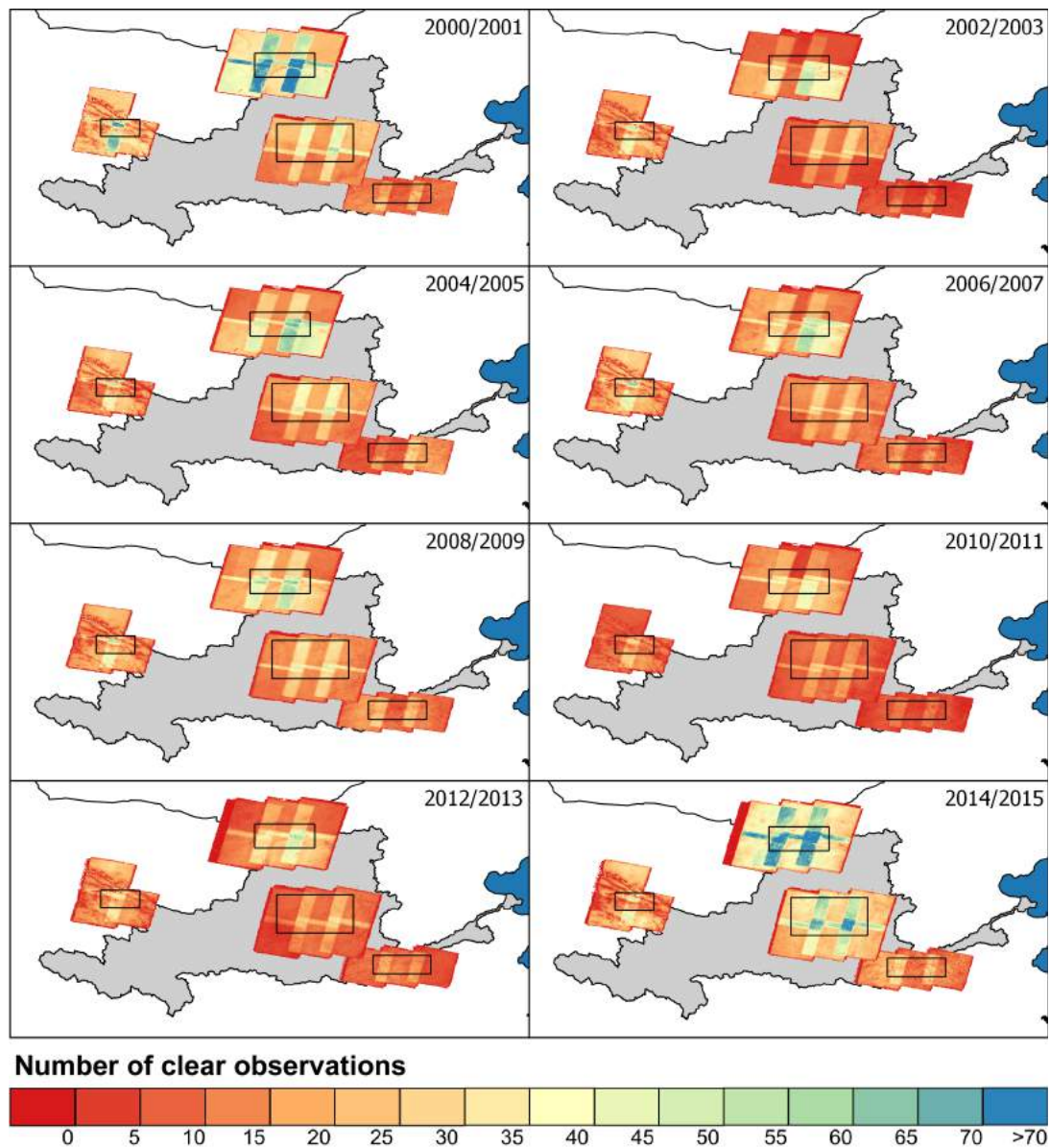


Figure 6.5: Available clear Landsat observations for each time step.

Table 6.2: All Landsat images used in this chapter for computing the spectral-temporal metrics for delineating mining areas in Qinghai.

Time period	Path	Row	Sensor	Number of images	Mean cloud coverage (%)
2000/2001	134	33	TM/ETM+	33	18.27
2002/2003	134	33	TM/ETM+	22	13.67
2004/2005	134	33	TM/ETM+ (SLC off)	34	10.48
2006/2007	134	33	TM/ETM+ (SLC off)	35	15.14
2008/2009	134	33	TM/ETM+ (SLC off)	29	17.66
2010/2012	134	33	TM/ETM+ (SLC off)	11	17.71
2012/2013	134	33	ETM+ (SLC off)/OLI	31	9.22

Table 6.2 – continued from previous page

Time period	Path	Row	Sensor	Number of images	Mean cloud coverage (%)
2014/2015	134	33	ETM+ (SLC off)/OLI	52	16.22
2000/2001	134	34	TM/ETM+	33	22.27
2002/2003	134	34	TM/ETM+	20	20.61
2004/2005	134	34	TM/ETM+ (SLC off)	21	13.75
2006/2007	134	34	TM/ETM+ (SLC off)	27	15.27
2008/2009	134	34	TM/ETM+ (SLC off)	16	24.11
2010/2012	134	34	TM/ETM+ (SLC off)	43	16.13
2012/2013	134	34	ETM+ (SLC off)/OLI	30	16.51
2014/2015	134	34	ETM+ (SLC off)/OLI	43	16.85
2000/2001	133	34	TM/ETM+	39	19.75
2002/2003	133	34	TM/ETM+	34	23.39
2004/2005	133	34	TM/ETM+ (SLC off)	39	21.42
2006/2007	133	34	TM/ETM+ (SLC off)	31	16.02
2008/2009	133	34	TM/ETM+ (SLC off)	33	20.27
2010/2012	133	34	TM/ETM+ (SLC off)	31	19.37
2012/2013	133	34	ETM+ (SLC off)/OLI	30	16.51
2014/2015	133	34	ETM+ (SLC off)/OLI	55	19.42

Table 6.3: All Landsat images used in this chapter for computing the spectral-temporal metrics for delineating agricultural areas in Inner Mongolia.

Time period	Path	Row	Sensor	Number of images	Mean cloud coverage (%)
2000/2001	130	31	TM/ETM+	35	6.53
2002/2003	130	31	TM/ETM+	11	7.45
2004/2005	130	31	TM/ETM+ (SLC off)	13	4.87
2006/2007	130	31	TM/ETM+ (SLC off)	22	10.35
2008/2009	130	31	TM/ETM+ (SLC off)	19	7.32
2010/2012	130	31	TM/ETM+ (SLC off)	20	9.28
2012/2013	130	31	ETM+ (SLC off)/OLI	10	5.18
2014/2015	130	31	ETM+ (SLC off)/OLI	53	7.65
2000/2001	130	32	TM/ETM+	44	7.55
2002/2003	130	32	TM/ETM+	22	5.77
2004/2005	130	32	TM/ETM+ (SLC off)	29	7.29
2006/2007	130	32	TM/ETM+ (SLC off)	25	15.26

Table 6.3 – continued from previous page

Time period	Path	Row	Sensor	Number of images	Mean cloud coverage (%)
2008/2009	130	32	TM/ETM+ (SLC off)	22	8.85
2010/2012	130	32	TM/ETM+ (SLC off)	15	4.65
2012/2013	130	32	ETM+ (SLC off)/OLI	17	2.34
2014/2015	130	32	ETM+ (SLC off)/OLI	56	7.47
2000/2001	129	31	TM/ETM+	28	4.47
2002/2003	129	31	TM/ETM+	6	3.95
2004/2005	129	31	TM/ETM+ (SLC off)	17	2.85
2006/2007	129	31	TM/ETM+ (SLC off)	10	6.94
2008/2009	129	31	TM/ETM+ (SLC off)	19	5.71
2010/2012	129	31	TM/ETM+ (SLC off)	7	7.52
2012/2013	129	31	ETM+ (SLC off)/OLI	17	7.22
2014/2015	129	31	ETM+ (SLC off)/OLI	54	8.71
2000/2001	129	32	TM/ETM+	33	7.12
2002/2003	129	32	TM/ETM+	13	5.98
2004/2005	129	32	TM/ETM+ (SLC off)	21	8.33
2006/2007	129	32	TM/ETM+ (SLC off)	22	14.12
2008/2009	129	32	TM/ETM+ (SLC off)	27	8.99
2010/2012	129	32	TM/ETM+ (SLC off)	26	8.65
2012/2013	129	32	ETM+ (SLC off)/OLI	30	6.82
2014/2015	129	32	ETM+ (SLC off)/OLI	53	6.01
2000/2001	128	31	TM/ETM+	25	4.50
2002/2003	128	31	TM/ETM+	8	1.87
2004/2005	128	31	TM/ETM+ (SLC off)	17	5.47
2006/2007	128	31	TM/ETM+ (SLC off)	17	10.32
2008/2009	128	31	TM/ETM+ (SLC off)	14	7.29
2010/2012	128	31	TM/ETM+ (SLC off)	14	8.56
2012/2013	128	31	ETM+ (SLC off)/OLI	12	3.87
2014/2015	128	31	ETM+ (SLC off)/OLI	49	9.91
2000/2001	128	32	TM/ETM+	50	6.72
2002/2003	128	32	TM/ETM+	42	6.84
2004/2005	128	32	TM/ETM+ (SLC off)	52	6.47
2006/2007	128	32	TM/ETM+ (SLC off)	50	10.57
2008/2009	128	32	TM/ETM+ (SLC off)	41	12.90
2010/2012	128	32	TM/ETM+ (SLC off)	32	8.77
2012/2013	128	32	ETM+ (SLC off)/OLI	35	6.74

Table 6.3 – continued from previous page

Time period	Path	Row	Sensor	Number of images	Mean cloud coverage (%)
2014/2015	128	32	ETM+ (SLC off)/OLI	59	9.67

Table 6.4: All Landsat images used in this chapter for computing the spectral-temporal metrics for delineating forest areas on the Central Loess Plateau.

Time period	Path	Row	Sensor	Number of images	Mean cloud coverage (%)
2000/2001	128	34	TM/ETM+	28	9.57
2002/2003	128	34	TM/ETM+	12	9.24
2004/2005	128	34	TM/ETM+ (SLC off)	22	10.85
2006/2007	128	34	TM/ETM+ (SLC off)	18	11.32
2008/2009	128	34	TM/ETM+ (SLC off)	20	14.59
2010/2012	128	34	TM/ETM+ (SLC off)	13	5.99
2012/2013	128	34	ETM+ (SLC off)/OLI	12	7.52
2014/2015	128	34	ETM+ (SLC off)/OLI	48	8.28
2000/2001	128	35	TM/ETM+	16	9.88
2002/2003	128	35	TM/ETM+	8	3.54
2004/2005	128	35	TM/ETM+ (SLC off)	12	13.01
2006/2007	128	35	TM/ETM+ (SLC off)	12	11.56
2008/2009	128	35	TM/ETM+ (SLC off)	14	8.70
2010/2012	128	35	TM/ETM+ (SLC off)	11	1.45
2012/2013	128	35	ETM+ (SLC off)/OLI	10	5.97
2014/2015	128	35	ETM+ (SLC off)/OLI	36	12.04
2000/2001	127	34	TM/ETM+	20	4.23
2002/2003	127	34	TM/ETM+	16	1.98
2004/2005	127	34	TM/ETM+ (SLC off)	23	4.38
2006/2007	127	34	TM/ETM+ (SLC off)	18	11.84
2008/2009	127	34	TM/ETM+ (SLC off)	22	16.07
2010/2012	127	34	TM/ETM+ (SLC off)	12	3.76
2012/2013	127	34	ETM+ (SLC off)/OLI	16	10.88
2014/2015	127	34	ETM+ (SLC off)/OLI	44	9.32
2000/2001	127	35	TM/ETM+	17	8.39
2002/2003	127	35	TM/ETM+	13	8.47
2004/2005	127	35	TM/ETM+ (SLC off)	15	5.50
2006/2007	127	35	TM/ETM+ (SLC off)	20	9.76

Table 6.4 – continued from previous page

Time period	Path	Row	Sensor	Number of images	Mean cloud coverage (%)
2008/2009	127	35	TM/ETM+ (SLC off)	17	5.07
2010/2012	127	35	TM/ETM+ (SLC off)	19	7.10
2012/2013	127	35	ETM+ (SLC off)/OLI	17	7.31
2014/2015	127	35	ETM+ (SLC off)/OLI	38	8.87
2000/2001	126	34	TM/ETM+	30	5.64
2002/2003	126	34	TM/ETM+	21	5.79
2004/2005	126	34	TM/ETM+ (SLC off)	25	7.85
2006/2007	126	34	TM/ETM+ (SLC off)	20	10.42
2008/2009	126	34	TM/ETM+ (SLC off)	18	6.29
2010/2012	126	34	TM/ETM+ (SLC off)	12	10.34
2012/2013	126	34	ETM+ (SLC off)/OLI	17	5.29
2014/2015	126	34	ETM+ (SLC off)/OLI	41	5.87
2000/2001	126	35	TM/ETM+	20	3.77
2002/2003	126	35	TM/ETM+	8	5.24
2004/2005	126	35	TM/ETM+ (SLC off)	17	5.13
2006/2007	126	35	TM/ETM+ (SLC off)	18	9.40
2008/2009	126	35	TM/ETM+ (SLC off)	21	13.64
2010/2012	126	35	TM/ETM+ (SLC off)	12	7.07
2012/2013	126	35	ETM+ (SLC off)/OLI	15	10.22
2014/2015	126	35	ETM+ (SLC off)/OLI	41	9.17

Table 6.5: All Landsat images used in this chapter for computing the spectral-temporal metrics for delineating urban areas on the North China Plain.

Time period	Path	Row	Sensor	Number of images	Mean cloud coverage (%)
2000/2001	125	36	TM/ETM+	18	5.94
2002/2003	125	36	TM/ETM+	11	10.16
2004/2005	125	36	TM/ETM+ (SLC off)	13	3.02
2006/2007	125	36	TM/ETM+ (SLC off)	18	10.44
2008/2009	125	36	TM/ETM+ (SLC off)	23	8.37
2010/2012	125	36	TM/ETM+ (SLC off)	12	6.63
2012/2013	125	36	ETM+ (SLC off)/OLI	19	12.31
2014/2015	125	36	ETM+ (SLC off)/OLI	36	12.27
2000/2001	124	36	TM/ETM+	18	8.47

Table 6.5 – continued from previous page

Time period	Path	Row	Sensor	Number of images	Mean cloud coverage (%)
2002/2003	124	36	TM/ETM+	12	7.91
2004/2005	124	36	TM/ETM+ (SLC off)	18	7.76
2006/2007	124	36	TM/ETM+ (SLC off)	13	9.62
2008/2009	124	36	TM/ETM+ (SLC off)	16	7.39
2010/2012	124	36	TM/ETM+ (SLC off)	14	8.14
2012/2013	124	36	ETM+ (SLC off)/OLI	22	8.07
2014/2015	124	36	ETM+ (SLC off)/OLI	28	13.12
2000/2001	123	36	TM/ETM+	25	9.54
2002/2003	123	36	TM/ETM+	10	0.01
2004/2005	123	36	TM/ETM+ (SLC off)	32	9.17
2006/2007	123	36	TM/ETM+ (SLC off)	21	8.26
2008/2009	123	36	TM/ETM+ (SLC off)	22	10.54
2010/2012	123	36	TM/ETM+ (SLC off)	15	8.06
2012/2013	123	36	ETM+ (SLC off)/OLI	12	6.10
2014/2015	123	36	ETM+ (SLC off)/OLI	29	7.83

6.3.2 Creating Spectral-temporal Landsat Metrics

Using the pre-processed surface reflectance layers, various spectral, multi-spectral, and spectral-temporal features were computed. As highlighted in section 6.1, spatially continuous spectral-temporal metrics from dense intra-annual Landsat time series proved to be reliable features for land cover/use differentiation as they capture the salient phenological information as shown in Figure 6.4. In contrast to the MODIS acquisition plan, Landsat imagery are temporally inconsistent due to cloud contamination and acquisition strategy, which make a direct delineation of phenological metrics difficult. To overcome this limitation, simple intra-annual metrics from all available Landsat scenes were derived, which are able to extract seasonal information without sequential timing. In this research, five statistical metrics, the percentiles of 10 %, 25 %, 50 %, 75 %, and 90 %, were derived from all cloud/cloud shadow free TM, ETM+, and OLI observations for five reflectance bands (Table 6.1). The omission of the minimum and maximum should reduce the potential influence of noise. In addition, five percentile statistics were computed: the NDVI and the Normalized Difference Built-up Index (NDBI) as proxy for built-up areas, which is defined as follows (Zha et al., 2003):

$$(6.1) \quad NDBI = \frac{(SWIR - NIR)}{(SWIR + NIR)}$$

Further, percentile differences (90 % – 10 % and 75 % – 25 %) for each band and multi-spectral

index were calculated. Besides the spectral metrics, the feature space consists of various textural information that consider spatial relationship of pixels. Based on the gray-level-co-occurrence matrix (GLCM), the *variance*, *contrast*, *homogeneity*, and *entropy* were computed by applying a local 3 by 3 spatial window (Haralick et al., 1973). The entire classification input feature set counts 69 multi-temporal and textural features.

6.3.3 Collection of Stable Reference Data Sets

A key point in multi-temporal land cover change analysis using automated or semi-automated classification procedure is the derivation of a reliable and time-consistent reference data set, which reduces possible semantic bias and manual data sampling requirements (Congalton and Green, 2009; Fortier et al., 2011). The automated adaptive signature generalization (AASG) algorithm from Gray and Song (2013) proved to be a reliable and efficient sampling technique for performing multi-temporal land cover change analysis on regional geographical scales (Gray and Song, 2013; Shao and Liu, 2014; Stow et al., 2014; Dannenberg et al., 2016). AASG is a simple change detection technique and works under the assumption that the majority of pixels remain stable between the reference and target image on large geographical scales. Stable pixels are identified as those, which fall within an interval of a predefined standard deviation. Subsequently a spatial filter kernel reduced the effect of image co-registration and edge effects. Thus only core and pure pixels retain as potential stable sampling sites (Figure 6.6).

Table 6.6: The gray-level-co-occurrence matrix (GLCM) metrics used in this study as defined by Haralick et al. (1973), where $P(i, j)$ is the element i, j of the normalized symmetrical GLCM and G the number of gray levels in the image.

GLCM metric	Equation	Description
variance	$\sum_{i=0}^{G-1} \sum_{j=0}^{G-1} (i - \mu)^2 P(i, j)$	Measures the dispersion of the values around the mean
contrast	$\sum_{n=0}^{G-1} n^2 \{ \sum_{i=1}^G \sum_{j=1}^G P(i, j) \},$ $ i - j = n$	Measures the local variations in the gray-level-co-occurrence matrix
homogeneity	$\sum_{i=0}^{G-1} \sum_{j=0}^{G-1} \{P(i, j)\}^2$	Measures the closeness of the distribution of elements in the GLCM to the GLCM diagonal
entropy	$-\sum_{i=0}^{G-1} \sum_{j=0}^{G-1} P(i, j) \log(P(i, j))$	Measures the disorder of an image

Table 6.7: Number of training/validation pixels for each region.

Focus region	Training pixels	Validation pixels
Qinghai-Tibet Plateau (Min)	41,456	10,364
Inner Mongolia (Ag)	67,208	16,802
Loess Plateau (Fo)	80,827	20,206
Central China Plain (Ur)	70,764	16,983

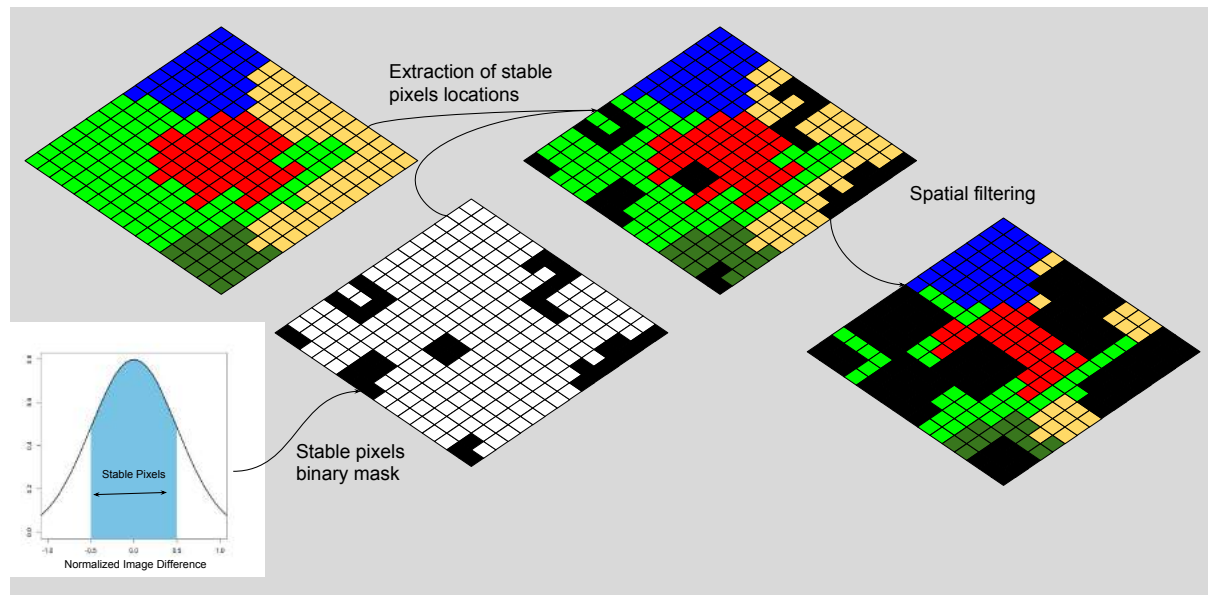


Figure 6.6: Schematic overview about identifying of stable pixels locations.

In this study, temporally stable samples were extracted from the bi-annual composites between 2000 and 2015. The first step involves the computation of several per pixel temporal difference images from consecutive time steps for each band n :

$$(6.2) \quad \Delta I = I_{1,n} - I_{2,n}$$

Then, stable pixels that fall into the following interval were selected:

$$(6.3) \quad \mu_c \pm c \cdot \sigma_c$$

where μ is the mean and σ represents the standard deviation. The constant c defines the interval width and was set to 0.5, which has been determined as a suitable value by prior testing. Then, spatial filtering procedure using a 3x3 pixel majority filter was applied, to remove erroneous transition pixels from marginal areas. Only all intersecting stable pixels binaries were retained for further reference sample selection.

The final step includes an unsupervised classification step for each focus region to delineate spectrally and spatially 5-8 homogeneous region specific classes. Subsequently, 10,000 points per class were distributed using stratified random sampling to ensure unbiased distribution of samples across the area with a minimum distance of 1,500 m to avoid spatial autocorrelation (Congalton and Green, 2009). As a minimum sampling unit, objects covering at least 3x3 contiguous pixels were generated. Finally, the samples were assigned with a class specific ID by visually cross-checking the objects against the Landsat archive and available VHR provided in Google Earth.

Only this step requires manual labor. The reference data set was further supported by integrating the ground truth measures derived from the three week field campaign conducted in 2016 (see section 4.3 on page 58).

6.3.4 Classification and Validation Strategy

The classification and validation procedure follows basically the approach as described in section 5.2.4 on page 75. Using the mono-temporal stable-pixels reference data set, RF classifiers were employed to delineate annual thematic maps for each focus region, based on spatial-temporal and textural metrics. Again, RF models were built with 300 individual trees and *mrtv* parameter was set to default value (\sqrt{p}). Boruta considered all variables as important (Kursa and Rudnicki, 2010). For each two-year time step and each focus region individual RF models were generated, summing up to 32 models. As training input served a 70 % split of the reference data set, the remaining 30 % for validation. By means of OA, kappa statistics, and class-wise UA and PA, the quality of each classified image was assessed. The amount of training and validation data can be viewed in Table 6.7.

6.4 Results

The results in this chapter are presented as follows: in the first step, the land cover dynamics and trends that have occurred since 2000 in the four thematic foci regions (mining, agriculture, ecological restoration, urban sprawl) are described in detail and quantitatively and qualitatively assessed. The thematic and spatial quality of each classification product is revealed by means of OA, UA, PA, kappa (κ) value, as well as Shannon entropy. Further, the variable importance of the feature space for each region is highlighted.

6.4.1 Expanding Mining Activities in Haibei (Qinghai Province)

The results reveal three expanding mining sites along the Datong River, which are known as the Muli coalfields as displayed in Figure 6.7. These open mining casts have been developed within a nature reserve, the Qinghai Qilian Mountains Nature Reserve. Mining excavations commenced in 2004 in the western part, followed by regions further east. By the year 2015, more than 30 km² of pristine alpine meadows vanished (Figure 6.8). With more than 23 km², the Jiangcang mine is found to be the most extensive and earliest developed coal mine, located in the very west of Haibei, close to Datong's source. The two remaining coal sites with 6.5 km² and 1.7 km², respectively, have developed since 2006 (Figure 6.7, B), but their spatial extent remained stable since 2010, whereas Jaingcang still disseminates (Figure 6.7, A). Despite a digging ban issued by the Chinese Ministry of Environmental Protection, local coal companies ignored these restrictions and continued with coal expansion (Xu et al., 2012). The classification results even reveal an accelerating trend in annual mining excavation activities. While 2.5 to 3.5 km² of land was transformed every two years between 2004 and 2010, this figure increased to more than 9 km² in 2015. This trend is worrisome

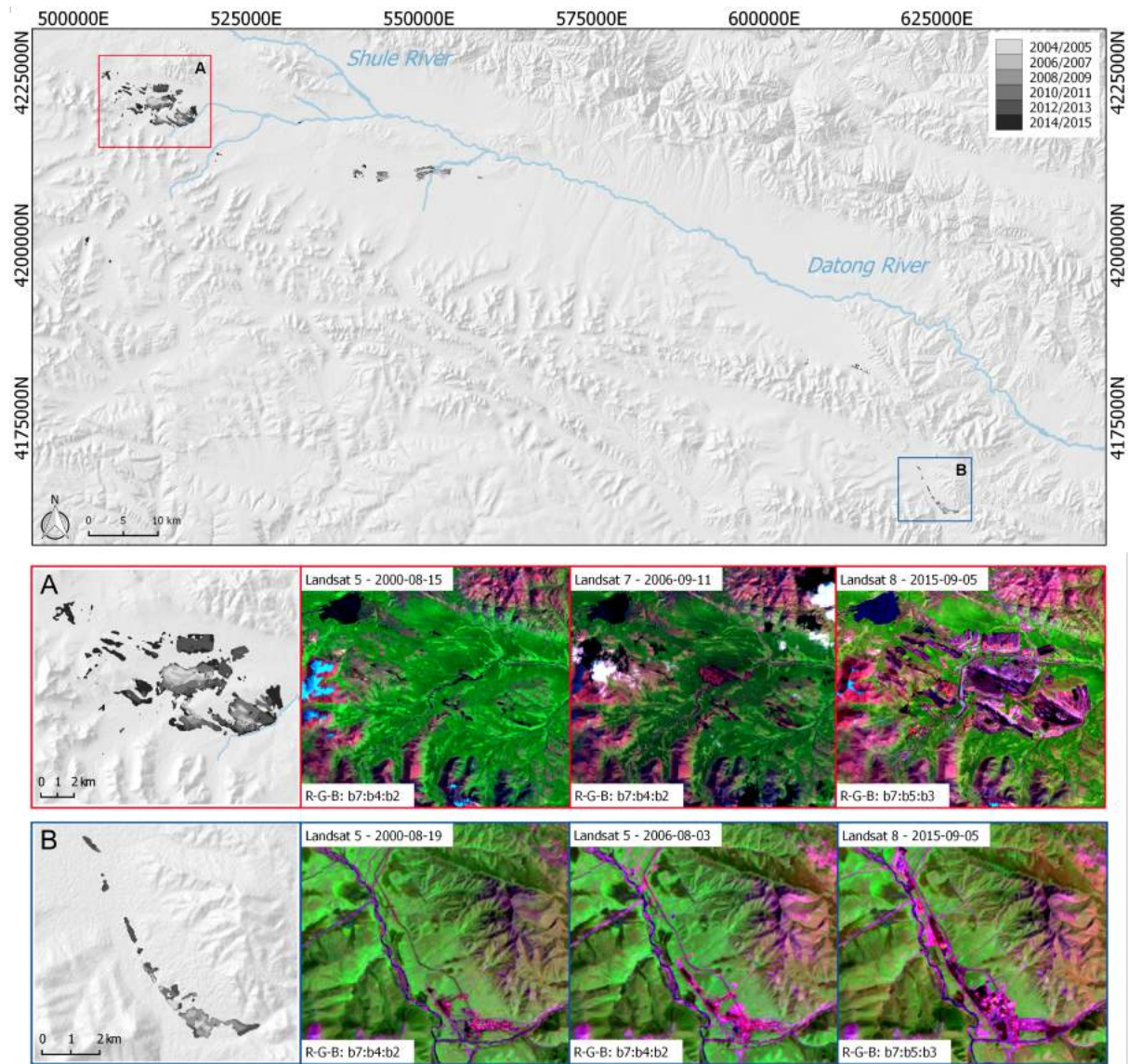


Figure 6.7: Classification and change detection results of open cast mining areas in Haibei Prefecture in Qinghai Province. Framed areas in red (A) and blue (B) illustrate regions with significant mining expansion.

as massive quantities of coal (around 3.5 billions tons) and gas hydrates are expected to lie under the Qinghai-Tibet Plateau and could trigger further mining operations (Zhu et al., 2010). However, the Chinese government has undertaken massive investments in renewable energies and overall coal production slows down (see Figure 3.3 on page 32 in chapter 3) and could lead to decelerating mining activities in near future.

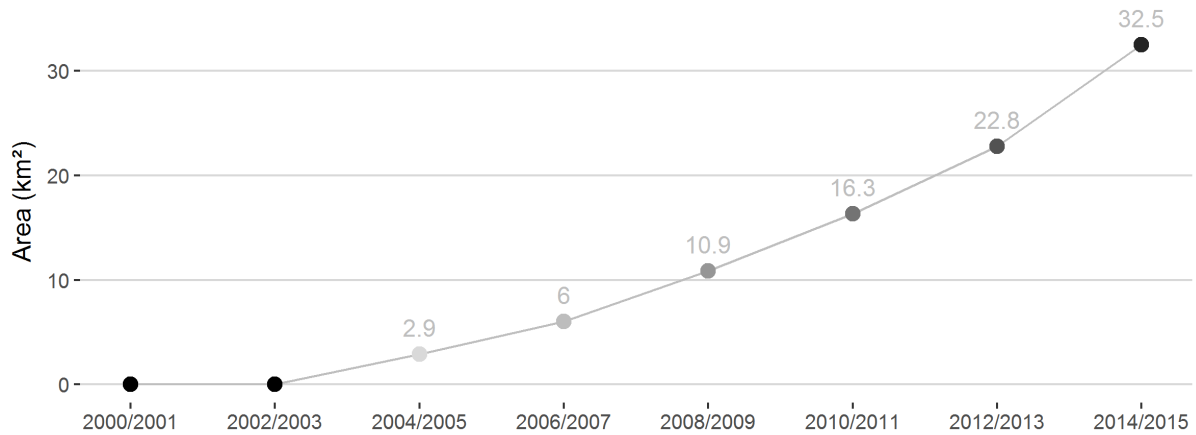


Figure 6.8: Temporal development of mining areas in Haibei between 2000 and 2015 (km²).

6.4.2 Agricultural Dynamics in the Hetao Irrigation District

Agriculture, as one of the major land cover facets in the Yellow River Basin, covers more than 20 % of the basin's landscape (see results from chapter 5) of which a major part is irrigated. Within the Hetao Irrigation District no clear tendency in agricultural development can be obtained between the years 2000 and 2015 (Figure 6.9). In 2000, around 9,000 km² were cultivated for agricultural purposes, which peaked in 2006 with covering around 10,000 km². The interannual variations ranged between 0.5 % and 5 %. Despite no significant trend tendency in absolute values (Figure 6.10), there are certainly local spatial dynamics, which become more obvious when investigating smaller scales as depicted in the two subsets in Figure 6.9 A and B. An increase in cropping area can be obtained particularly at peripheral regions of Hetao, where new fields proliferated towards the adjacent Gobi desert. Figure 6.9 A highlights the spatial-temporal development of center pivot irrigation systems, where such circular areas significantly have spread since 2006. Further north, similar agricultural expansion into desert was present at the foothills of the Yin Mountains. The enlargement has mainly been achieved by massive developments of irrigation facilities. Southwards in the Kubuqi Desert, small patches of agricultural land have emerged at groundwater-fed oasis. Furthermore, wetlands at the Wuliangshu Lake have been converted to agriculture or aquaculture.

While peripheral areas in Hetao have expanded towards deserts, declining trends appeared in the district's central part. Urbanization and the accompanied infrastructure development are meant to be the main drivers, as agriculture has vanished in the immediate vicinity to urban structures. This is illustrated in Figure 6.9 B, where cropland shrinks radially around Bayan Nur. This radial shrinkage can be observed across all major cities embedded in the Hetao Irrigation District. A further reason for declining agriculture is attributed to soil salinization. The prevailing arid climate conditions and geology make this region susceptible for salinization processes, further exacerbated by unsustainable water management resulting in degraded soils and declining yields.

Consequently, impoverished farming families have abandoned their parcels as they can not longer meet costs from agricultural business. A further spatial-temporal dynamic phenomenon has occurred on the Yellow River banks, where farmers grow crops within the diked floodplains and rotate fields according to the annual water level (Figure 6.9 B, lower right).

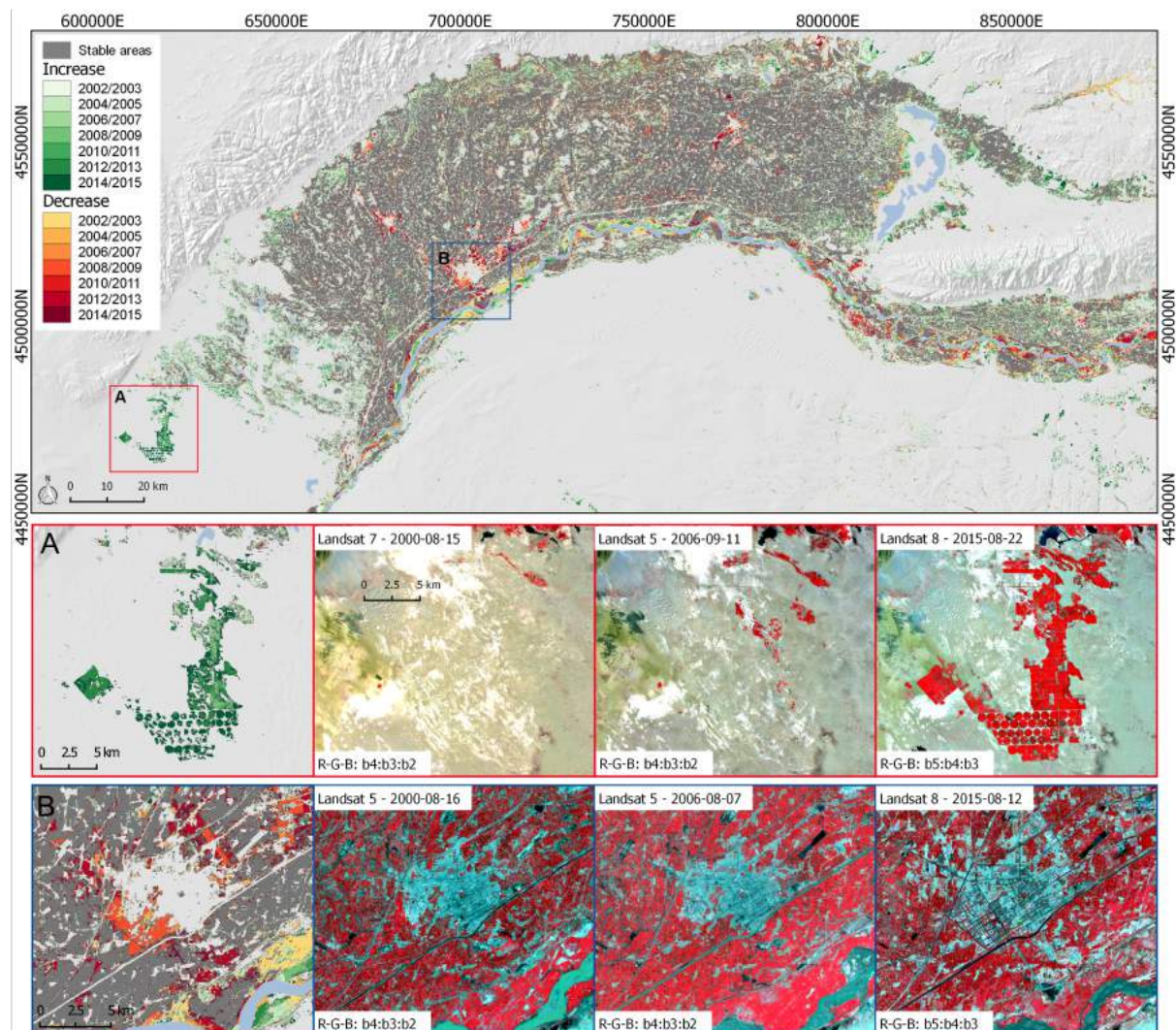


Figure 6.9: Classification and change detection results for agricultural areas in the Hetuo Irrigation District in Inner Mongolia from 2000 and 2015. Framed areas mark regions with significant increase (A in red) and decrease (B in blue) of cropland.

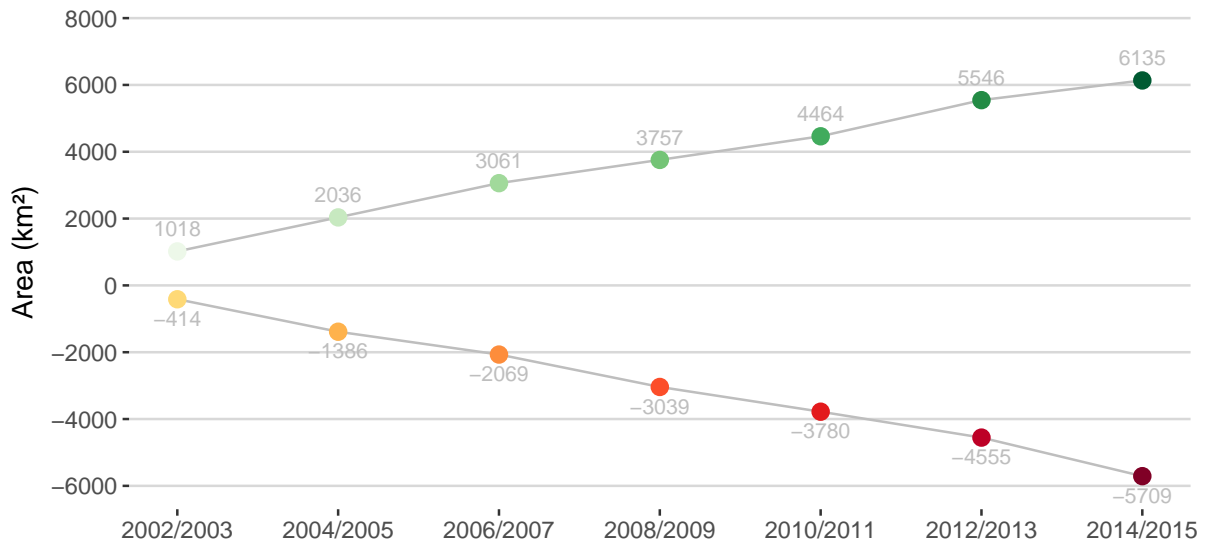


Figure 6.10: Temporal development of agricultural areas between 2000 and 2015 in Hetao (km²).



(a) Large scale soil salinization in Hetao Irrigation District



(b) Flood irrigated crop fields



(c) Abandoned agricultural field with a center pivot



(d) Sprawling urban areas on the North China Plain near Xi'an

Figure 6.11: Landscape features across the Yellow River Basin (photographs taken by Christian Wohlfart in April 2016).

6.4.3 Conservation Activities on the Central Loess Plateau

The applied Landsat based classification approach using spectral-temporal and textural metrics also works successfully for forest delineation in a spatially complex and heterogeneous landscape. The aforementioned conservation activities (*GfG* or *Watershed Rehabilitation Program*) have resulted in a remarkable increase of forested areas, previously non-vegetated or used for agriculture (Figure 6.12). Since 2000 forest covered areas have expanded from 26,000 km² to 33,000 km², equivalent to a 44 % increase. Prior to the year 2000, the Ziwuling and Yunwu Mountains in Shanxi and the Lu Liang Mountains at the eastern margins (Shaanxi Province) of the basin have remained on the Central Loess Plateau. Overall, forest areas have grown by approximately 9,000 km², while 1,700 km² disappeared between 2000 and 2015 (Figure 6.13). This is reflected in a steady increase of the total number of forest patches, which accumulated from 121,913 to 147,506 patches (Table 6.8). The mean patch area also did grow from around 200,000 to 240,000 km². The majority of afforestation happened in the Wugim, Zhidan, Ansai, Zichang, Yanchuan, and Yanchang districts. The spatio-temporal dynamics of the latter are exemplary depicted in subfigure A of Figure 6.12. There, forest patches occurred in 2000 only along river banks and had gradually extended until 2015 covering now large parts of the district. Trees that were planted include native species such as Chinese fir (*Cunninghamia Lanceolata*), Chinese red pine (*Pinus massoniana*), but also tree species for commercial purposes, such as walnut, chestnut, and orchard species (Zhou et al., 2007; Delang and Wang, 2013). Interannual forest growth ranged from 200 km² (2004/2005) to almost 1,900 km² (2006/2007) with a mean annual increase of 1,100 km². This value is very close to the statistical data provided by the Chinese government, where forests grew annually by 1,043 km² in Shaanxi province (NBS, 2015). Tree patches were mainly planted on gulch slopes to stabilize the highly erosive soils to minimize the loss of valuable fertile soils as obtained from Table 6.8. Around 80 % of the entire restoration occurred on slopes between 15° and 25°; the remaining 20 % on slopes are even exceeding 25°. Forest loss mainly at the margins of the Ziwuling and Yunwu Mountains, where forest patches were displaced by agriculture, infrastructure development, and urban expansion. The latter is exemplary illustrated in subfigure B of Figure 6.12, where the city of Yan'an expanded.

Table 6.8: Forest landscape patches.

Time period	Number of patches	Mean patch area (m ²)	Conversion on slopes		
			< 15°	15 - 25°	> 25°
2000/2001	121,913	203,491	1.4	85.1	13.5
2002/2003	126,245	204,992	1.7	84.4	13.8
2004/2005	126,230	214,520	1.9	94.5	13.6
2006/2007	127,980	214,893	2.1	93.4	14.4
2008/2009	132,922	231,114	1.5	93.1	14.4
2010/2011	133,094	235,183	1.3	92.2	15.4
2012/2013	140,033	236,236	1.3	91.6	16.1
2014/2015	147,506	242,113	1.5	91.1	16.3

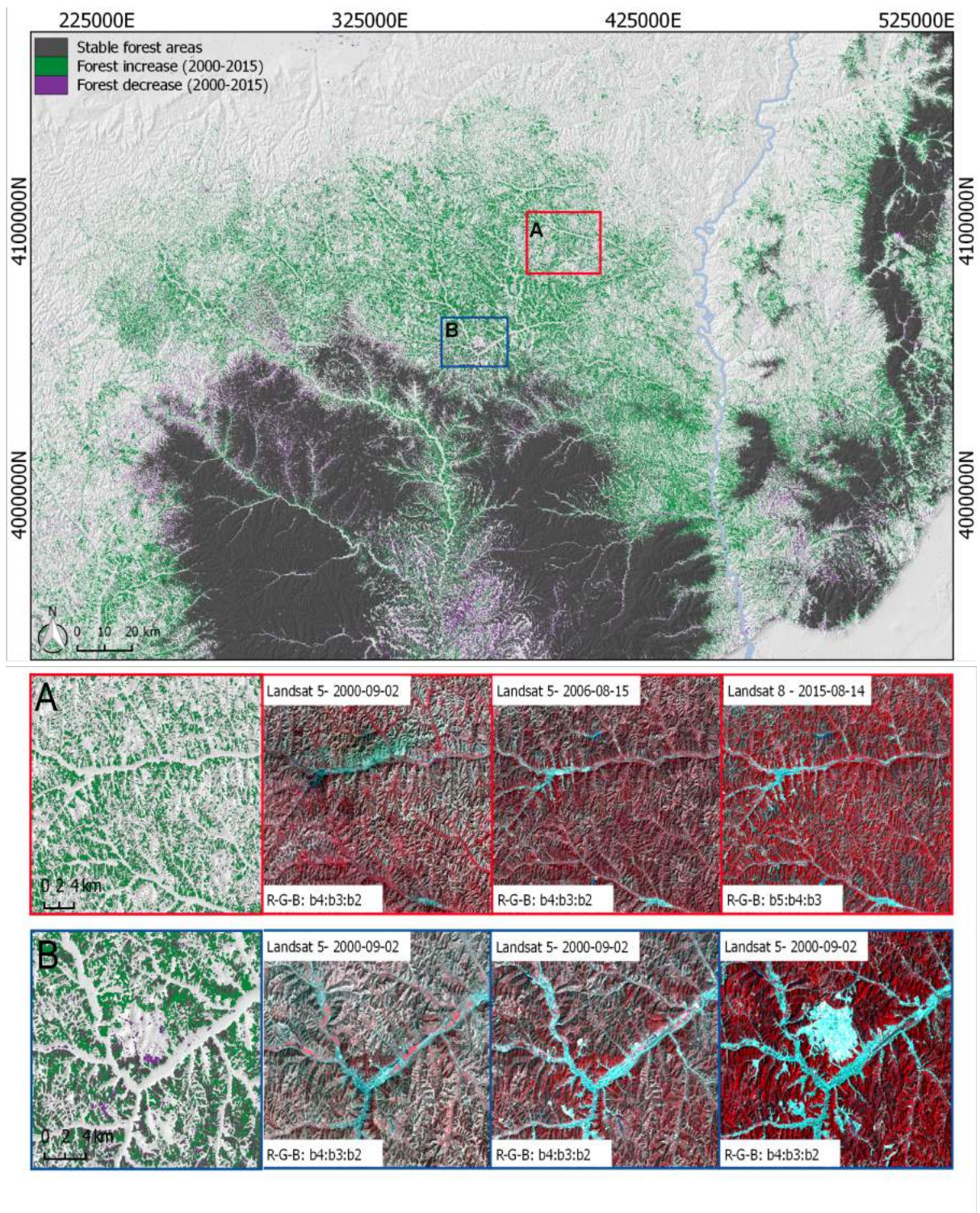


Figure 6.12: Classification and change detection results of forest areas on the Central Loess Plateau between 2000 and 2015. Framed areas mark regions where afforestation (A - in red) and deforestation (B - in blue) have occurred.



Figure 6.13: Temporal development of forest areas between 2000 and 2015 on the Central Loess Plateau (km²).

6.4.4 Urban Sprawl in the Central Plain Metropolitan Region

The Yellow River Basin faces an increasing population flow towards the metropolitan regions (see Figure 3.3 on 32), which requires new forms of housing and infrastructure. The tremendous spatial expansion of built-up areas is depicted in Figure 6.14. This massive construction was initialized by the Chinese government jointly with commercial partners to foster building development for urbanizing millions of people. Since 2000, urban and peri-urban areas in the Central Plain Metropolitan Region have sprawled from 3,650 km² to almost 5,000 km², which is equivalent to a 25 % growth (Figure 6.14). Within the metropolitan region, Zhengzhou (capital of Henan) marks a national hub for finance, trade, and heavy as well as high-tech industry that covers with 480 km² around 10 % of the Central Plain Metropolitan Region as can be seen in subset A of Figure 6.14. Further, Zhengzhou has the largest spatial absolute and relative growth with 180 km² and 7 %, respectively, amongst all major cities including Luoyang and Kaifeng. The first sprawled from 140 km² to 210 km², the latter from 74 km² to 121 km². The relative change is even larger in peri-urban areas with annual growth rates exceeding 10 %. Exemplary for peri-urban development, urban structures in the Weishi District (see subset in B of Figure 6.14) almost doubled from 59 km² to 107 km² (Figure 6.15). The Central Plain Metropolitan Region is embedded on the fertile Yellow River floodplains and cities are surrounded by agrarian fields. Therefore, urban sprawl was mainly achieved by converting agricultural fields but also riparian wetland ecosystems. China has eased relocation policies to attract rurals more to cities and has invested massive resources in infrastructure and housing. The World Bank predicts a continued migrating population into cities for the next decades (World Bank, 2014).

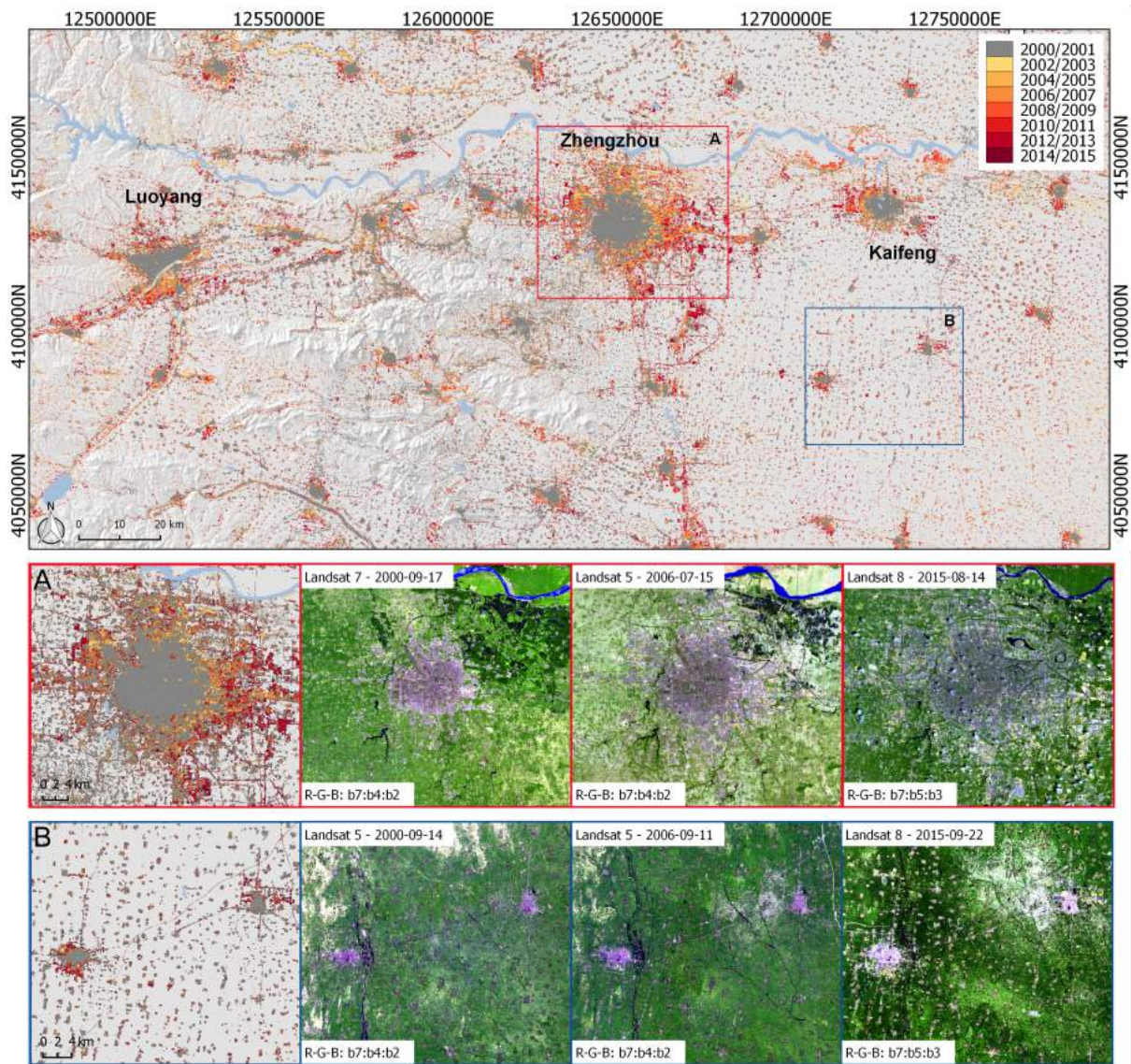


Figure 6.14: Classification and change detection results for the North China Plain Metropolitan Region in Henan Province from 2000 and 2015. Framed areas highlight regions with significant urban and built-up increase in the city of Zhengzhou (A) and in the Weishi District (B).

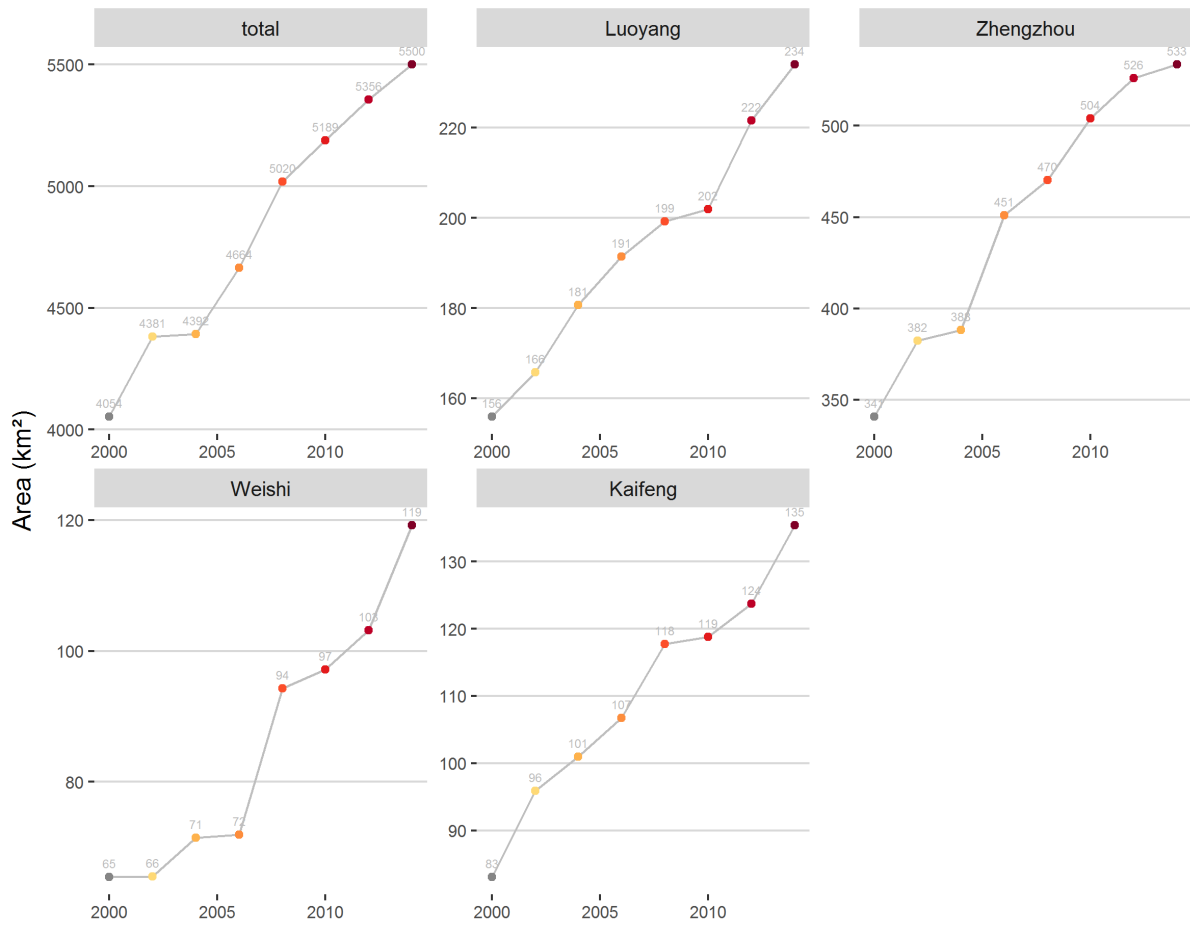


Figure 6.15: Temporal development of urban and built-up areas between 2000 and 2015 of the North China Plain Metropolitan Region and selected cities (km²).

6.4.5 Thematic Quality and Variable Importance

The accuracies for all individual classifications of each focus region are summarized in Table 6.9 and reveal overall accuracies in a high range from 90 % to 98 % and kappa (κ) coefficients of 0.86 - 0.96. Similar to section 5.2.4 on page 5.2.4 in the previous chapter 5, the concept of entropy to illustrate spatial uncertainty was again used. Class-wise entropy values for each year is displayed in Figure 6.16; the complementary spatial distribution can be found in the Figures 6.18, 6.19, 6.20, 6.21.

The delineation of mining areas and agricultural areas achieved highest reliability with mean overall accuracies across all time steps of almost 97 % (κ : 0.92) and 96 % (κ : 0.90), respectively. The classification results for forested areas on the heterogeneous Loess Plateau and the ambiguous urban land cover types on the North China Plain experienced slightly lower overall mean accuracies of around 94 % (both κ around 0.88). Same pattern follows the entropy in Figure 6.16, where mining and agricultural areas experienced lower uncertainties being classified. The spatially heterogeneous Loess Plateau forest patches reveal higher entropy values together with the spectrally complex urban environment. A notable dent in accuracy across all thematic classes is obvious for the time step 2012/2013, where the decommissioning of Landsat 5 end of 2011 and the SLC failure of Landsat 7 caused a decrease in data density in those years (see Figure 6.3).

The 20 most relevant predictor variables were derived from each RF classification of each focus region delineating mining, agriculture, forest, and urban classes (Figure 6.17). For mining areas

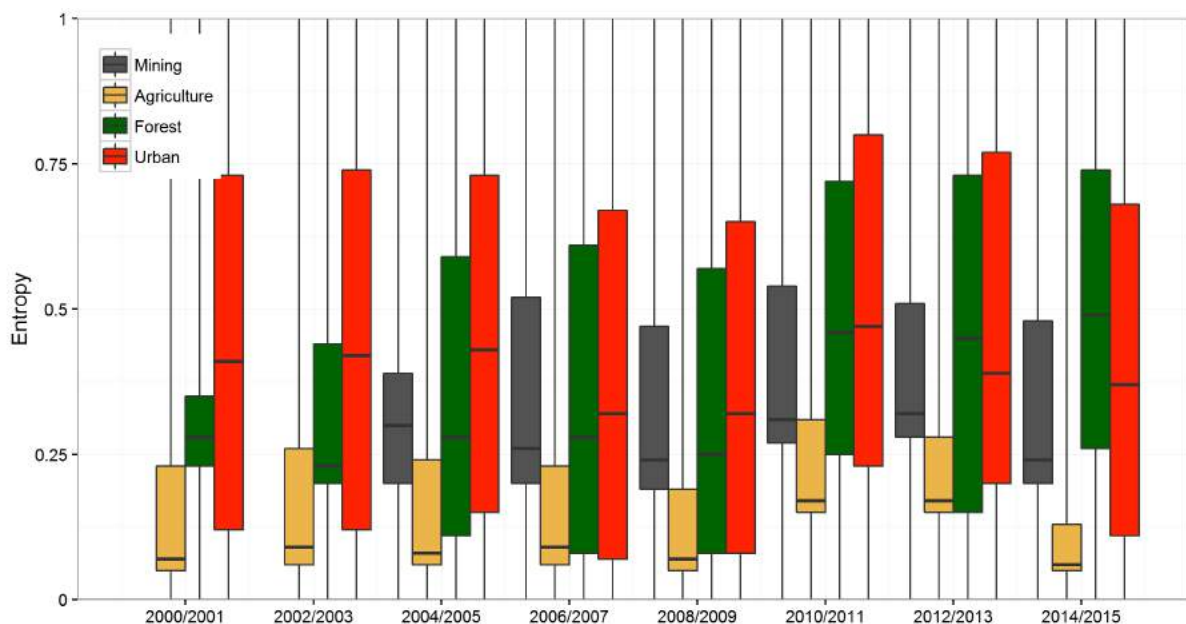


Figure 6.16: Classification and change detection results for the North China Plain Metropolitan Region in Henan Province from 2000 and 2015. Framed areas highlight regions with significant urban and built-up increase in the city of Zhengzhou (A) and in the Weishi District (B).

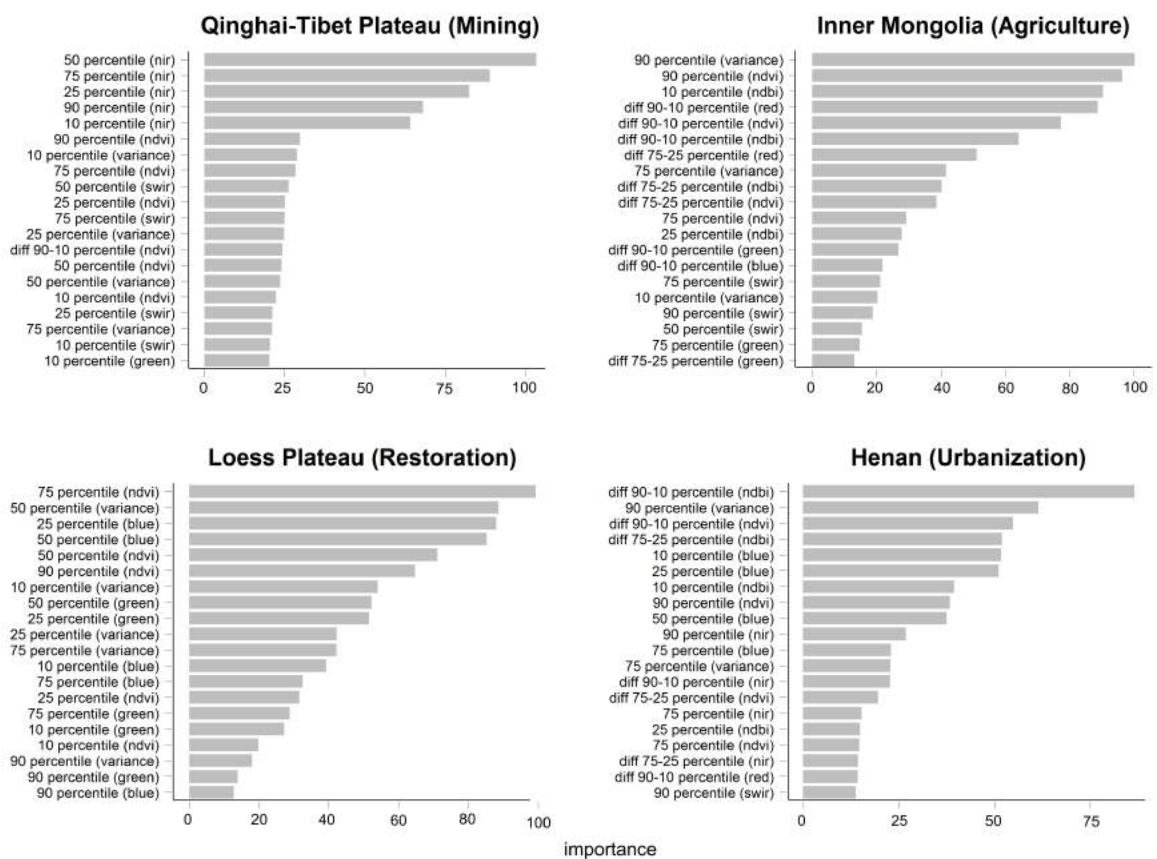


Figure 6.17: Median importance of the 20 most important features used in all RF models for each focus region.

particularly the NIR band percentiles contained the most explaining information, followed by NDVI and SWIR percentiles, whereas for vegetated classes such as agriculture and forests NDVI and NDVI texture metrics tend to have major influence. For the Hetao Irrigation District, where also urban areas are present, the NDBI play the major role in class separation. Logically, NDBI and NDVI percentiles are considered to be an important variable for delineating urban areas in the Central Plain Metropolitan Region. Further, high relevance was attributed to texture variables, particularly for the GLCM variance.

Table 6.9: Classification accuracies (%) for each thematic classes (M = Mining; nM = non Mining; A = Agriculture; nA = non Agriculture; F = Forest, nF = non Forest; U = Urban; nU = non Urban).

Region	Time period	Overall accuracy	Kappa	User's accuracy		Producer's accuracy	
				M	nM	M	nM
Mining	2000/2001	98.03	0.96	98.09	97.98	97.75	98.28
	2002/2003	98.17	0.96	97.82	98.29	98.09	98.05
	2004/2005	97.73	0.95	97.71	97.76	97.51	97.94
	2006/2007	97.23	0.94	97.23	97.08	96.76	97.50
	2008/2009	95.15	0.89	95.50	96.77	96.44	97.74
	2010/2011	95.12	0.89	92.92	95.14	96.85	98.12
	2012/2013	96.51	0.86	95.09	97.06	96.85	97.28
	2014/2015	97.74	0.95	97.92	97.58	97.41	98.05

Region	Time period	Overall accuracy	Kappa	User's accuracy		Producer's accuracy	
				A	nA	A	nA
Agriculture	2000/2001	95.72	0.89	98.04	92.85	94.44	97.45
	2002/2003	95.15	0.88	97.08	92.85	94.19	96.38
	2004/2005	94.35	0.88	91.70	97.50	97.75	90.82
	2006/2007	94.16	0.87	94.12	94.20	95.31	92.76
	2008/2009	98.21	0.96	98.83	97.42	97.99	98.49
	2010/2011	94.70	0.88	95.20	94.14	94.91	94.47
	2012/2013	98.17	0.96	98.61	97.60	98.13	98.22
	2014/2015	97.02	0.95	97.29	96.68	97.39	96.55

Region	Time period	Overall accuracy	Kappa	User's accuracy		Producer's accuracy	
				F	nF	F	nF
Forest	2000/2001	97.74	0.95	98.09	97.47	96.93	98.43
	2002/2003	91.87	0.86	91.12	91.78	90.55	98.03
	2004/2005	97.44	0.95	97.21	97.11	96.66	98.12
	2006/2007	96.79	0.93	97.12	96.45	95.91	97.55
	2008/2009	94.08	0.89	94.14	94.02	93.34	94.75
	2010/2011	96.85	0.94	96.98	96.25	95.70	97.13
	2012/2013	90.83	0.85	90.60	91.03	89.64	91.87
	2014/2015	97.28	0.95	97.79	97.76	96.27	97.14

Region	Time period	Overall accuracy	Kappa	User's accuracy		Producer's accuracy	
				U	nU	U	nU
Urban	2000/2001	93.45	0.86	92.77	93.92	92.77	93.92
	2002/2003	94.37	0.88	94.09	94.55	94.09	94.55
	2004/2005	94.73	0.89	94.08	95.17	94.08	95.17
	2006/2007	93.35	0.83	88.88	95.93	88.86	95.93
	2008/2009	95.86	0.91	95.30	96.24	95.30	96.24
	2010/2011	96.19	0.92	95.07	96.98	95.07	96.98
	2012/2013	93.63	0.92	94.84	92.17	94.84	92.17
	2014/2015	94.73	0.89	93.56	95.55	93.56	95.55

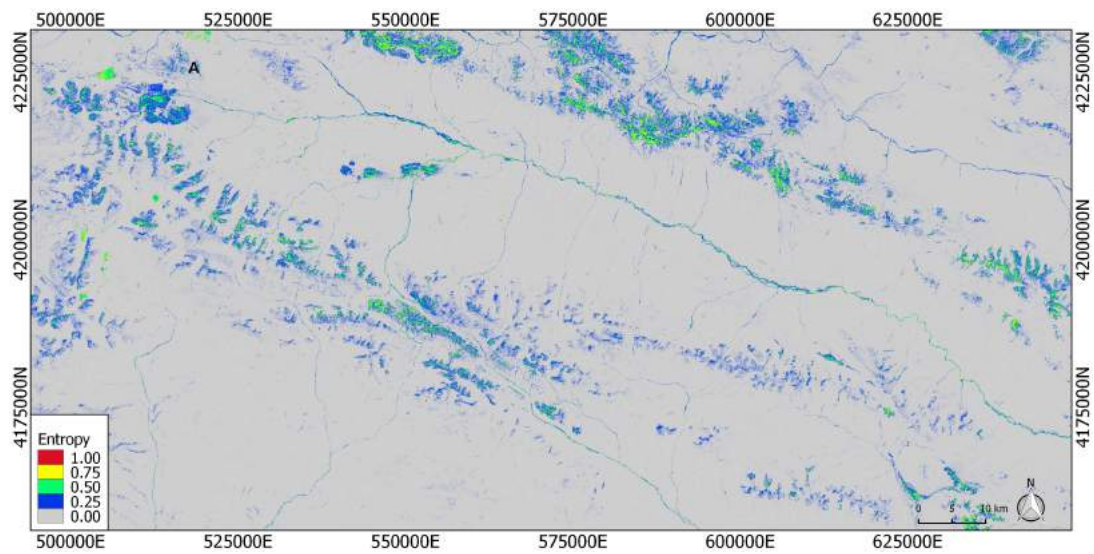


Figure 6.18: Mean entropy values of all RF classifications for the Haibei Prefecture on the Qinghai Tibet Plateau between 2000 and 2015.

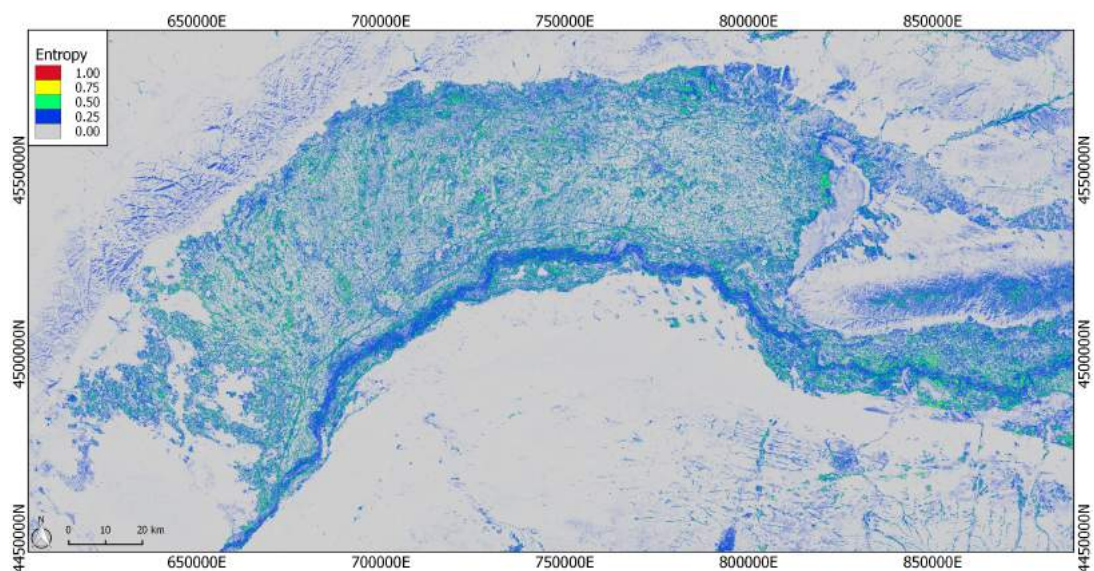


Figure 6.19: Mean entropy values of all RF classifications for the Hetao Irrigation District between 2000 and 2015.

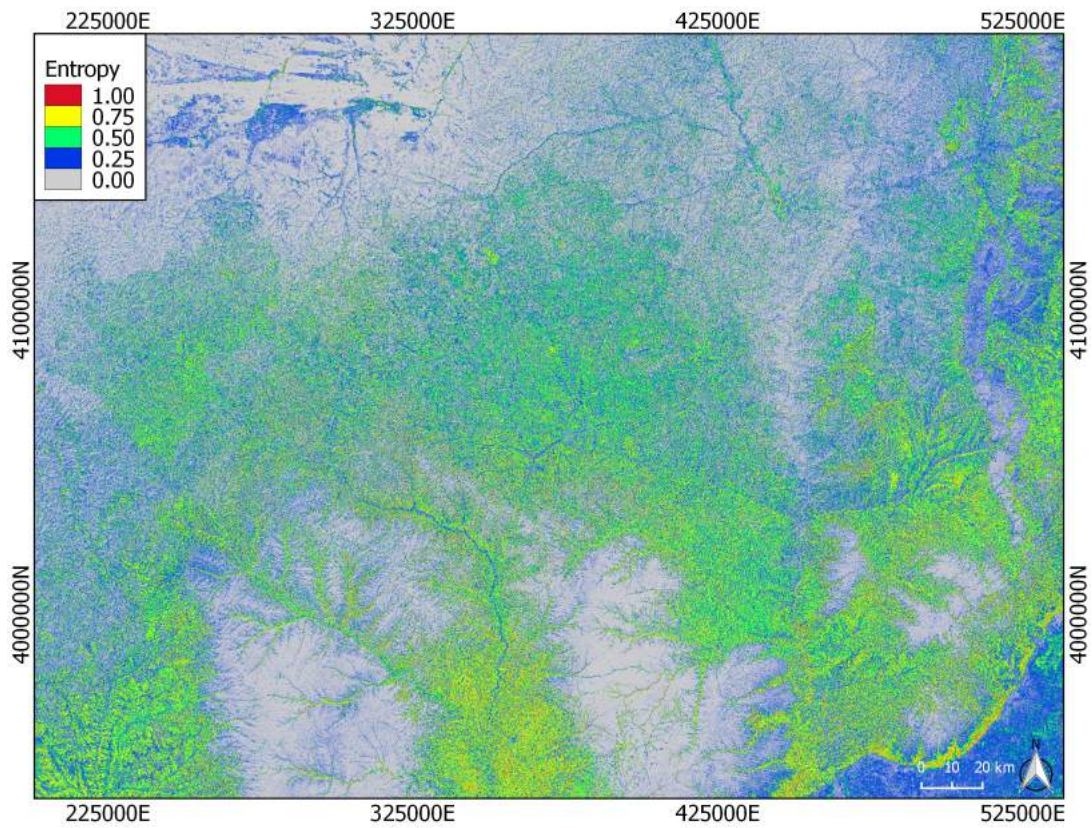


Figure 6.20: Mean entropy values of all RF classifications for the Central Loess Plateau between 2000 and 2015.

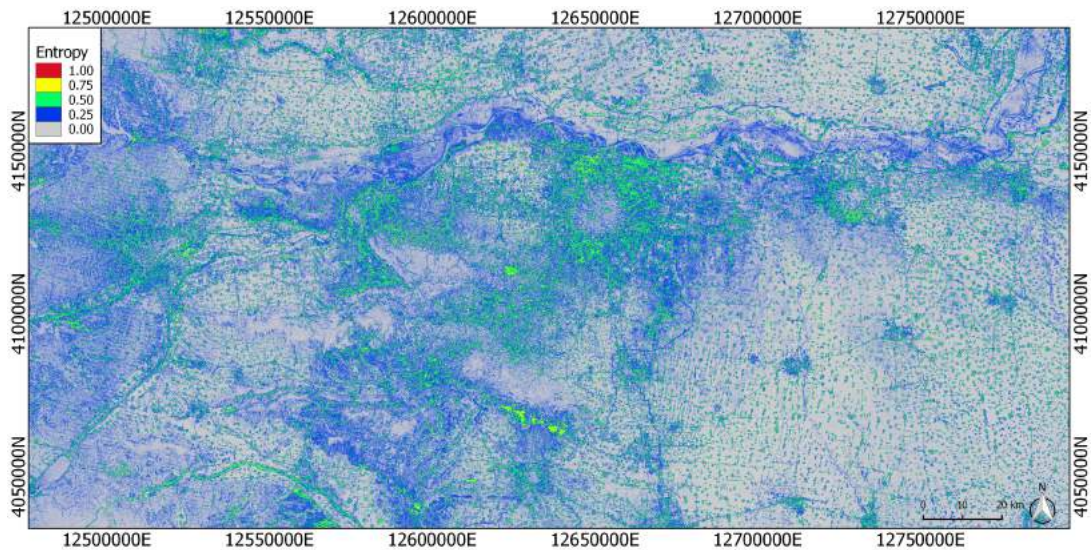


Figure 6.21: Mean entropy values of all RF classifications for the North China Plain Metropolitan Region between 2000 and 2015.

6.5 Discussion

To representing the rapid and complex spatial dynamics of a coupled human-environmental system adequately, such as the Yellow River Basin, there is need for consistent land surface information at high spatial and temporal scales. The novel applied classification approach of multi-spectral, spectral-temporal, and textural features combined with a stable-pixels reference data set provides to be an reliable scheme to separate various inherently complex land cover classes in an almost automated fashion. The results presented in this chapter reveal high magnitudes of land cover change dynamics requiring spatial monitoring at annual time steps to fully understand the underlying factors. This study covers the most significant facets of *Global Change* processes shaping China's environment and provides novel insights about the contemporary socio-economic development.

6.5.1 Land Cover Dynamics Across the Four Foci Regions

Despite the relative small spatial effect, **mining operations** on the Qinghai-Tibet Plateau pose great direct threat on the local prevailing ecosystem, along with severe regional impacts on water quality and global carbon budget. Still, China generates 69 % of its energy on coal resources contributing massively to global carbon emissions (Song and Kuenzer, 2014; NBS, 2015). However, since the production peak in 2013, domestic coal output stagnates and has even dwindled, while the capacity and investments of renewable energies stemming from wind and solar energy has increased making China to the worldwide leading investor in renewable energies (UNEP, 2016). This trend is not reflected on the Qinghai-Tibet Plateau, where coal mining activities continue, even accelerate. The results in this thesis are worrisome, as this sensitive region encompasses alpine grass- and wetland ecosystems in a permafrost environment holding large carbon stocks (Cheng and Wu, 2007). Degrading and disappearing permafrost wetlands and the subsequent release of carbon emissions can substantially contribute to global warming (MacDougall et al., 2012).

In section 3.2.4 of chapter 3, the challenging task of sustaining food security and self-sufficiency was already illustrated. In view of this, major efforts towards a more efficient and intensified **agricultural production** of crops were taken by applying more fertilizers and pesticides in conjunction with modern machineries and irrigation facilities (Ju et al., 2004). The classification results reveal stable area for crop fields since 2000, while production of agricultural commodities increased by approximately 25 % in Hetao (NBS, 2015). However, this rapid agrarian intensification has its downside on environment and society. Unsustainable crop production and increasing water logging fosters soil degradation by salinization processes deterring agricultural production. Soil salinity was found to pose real constraints to agricultural productivity and the economic livelihoods of Chinese farmers (Li et al., 2014a). Once soils are heavily salt affected, this process is difficult to revert. Remote sensing based analyses by Wu et al. (2008b) and Yu et al. (2010) show that around 50 % of Hetao's cropping fields are affected by saline soils, of which 10 % are considered as heavy saline and usually left abandoned by local farmers. To counteract this loss of

arable land, new fields have been developed at the marginal areas of Hetao with massive technical effort, but often in areas highly susceptible to salinization processes.

The initiation of the PES schemes (*GfG* and *NFCP*) across the Yellow River Basin in the late 1990s aimed to restore lost ecosystem functions including carbon sequestration, soil retention, and hydrological services together with sustainable agricultural production (see section 3.3 of chapter 3). The *GfG* has a significant bearing on the **ecological restoration** of degraded land and **poverty alleviation** in soil erosion prone Loess Plateau. For China, this program was the first attempt to introduce market-based initiatives. Its great success for China can serve as model for other developing countries to combat deteriorating ecosystems and alleviate poverty (Delang and Wang, 2012). The classification results reveal major afforestation activities on slopes $> 15^\circ$ as targeted by the *GfG* policy to reduce silt quantities reaching the Yellow River, mainly stemming from sloped farming (Xu et al., 2006a; Uchida et al., 2007). Such areas are mostly impoverished land with poor water supply and fertility, serious soil and water erosion threats as well as low and unstable yields. Hence, *GfG* has had no significant impact on national grain security and has not produced a significant impact on the equilibrium of supply and demand for grain nationwide (Xu et al., 2006b). Besides the achievements in improving the deteriorating ecological conditions, remarkable social benefits have been made. Around one third of the farmer's households in the participating provinces is engaged in the *GfG* Programme and received either grain, produced elsewhere, or direct financial compensation to cover the opportunity costs for transforming their fields (Uchida et al., 2005). It specifically supported the traditional way of extensive cultivation with little harvest and to readjust the inappropriate land-use structure. By the end of the program (end of 2016), a total of 49 billion USD (431.8 billion Yuan) had been invested (Delang and Zhen, 2015). Being successful in terms of sediment retention and rural poverty alleviation, *GfG* falls short in restoring local and regional biodiversity pattern (Hua et al., 2016). The newly established forests often contain only one single species or compositionally simple mixed forests and do not level up with the biodiverse pattern of native forests with higher compositional and structural diversity (Lindenmayer et al., 2006; Brockerhoff et al., 2008). This poses unforeseen local ecological and economic risks (Summers et al., 2015). A further future key issue will be the successful continuation and maintenance of established ecosystems, once payment ceased.

China's urbanization scale and pace continues at an unprecedented rate. If current trend holds, urban population will have exceeded one billion by the year 2030 (World Bank, 2014). The large urban-rural disparities have created massive migration movement towards cities as urban environments provide better perspectives for employment, education, lower transition costs, and health infrastructure. However, China has avoided some of the challenges associated with such urban agglomeration, where social inequity, pollution, and "ghost cities" (such as Ordos New Town in Inner Mongolia) emerged as a result of poor and inefficient urban development strategies (Gong et al., 2012; Zheng et al., 2017). While many urban dwellers have improved their social and economic situation, others suffer from unemployment and urban poverty due to unaffordable housing prices. Together with international partners such as the World Bank, the

Development Research Center of China's State Council has worked and is still working jointly to develop urbanization models towards a more efficient and long-term sustainable urbanized China (World Bank, 2014).

6.5.2 Land Cover Mapping Approach and Accuracies

The high range of overall accuracies and the low class-wise uncertainty has proved the superiority of spatio-temporal and textural information for land cover separation. The superiority of interannual metrics from dense Landsat time series imagery substantially enhances the discrimination of spatially and temporally ambiguous land cover types compared to single-date imagery, which only represents a specific phenological state within a year. The reliability of such multi-temporal Landsat approaches was proved by several studies for different regions delineating forest (Hansen et al., 2014; Müller et al., 2016), agriculture dominated areas (Müller et al., 2015), or urban environments (Schneider, 2012; Li et al., 2015).

The successful application of stable-pixels reference data sets on regional scales was proved by Gray and Song (2013). This method overcomes the challenges stemming from radiometric and phenological differences amongst multi-temporal scenes, which lead to semantic misinterpretation when classifiers are interpreted independently (Kim et al., 2014; Dannenberg et al., 2016).

A proper accuracy assessment of land cover change maps is a challenging task. In this thesis, the accuracy assessment was conducted on each individual classification, which is a common practice in remote sensing-based change detection analysis (Foody, 2002; Strahler et al., 2006). What is missing in this accuracy assessment, is the computation of quantitative metrics derived from the confusion matrix, such as area-weighted metrics and confidence intervals are useful measures to expand the quality of change detection analyses (Olofsson et al., 2013). Here, I only applied the measures overall accuracy, user's accuracy, producer's accuracy or the kappa coefficient (Foody, 2002; Stehman and Czaplewski, 1998; Congalton and Green, 2009), which are standard measures for thematic accuracy assessment. Furthermore, the introduction of change classes for accuracy assessment would give a better picture of the prevailing quality of the derived land cover maps as suggested by Olofsson et al. (2014).

6.5.3 Outlook

The multi-temporal information are key variables to support local and regional decision making processes for sustainable land management strategies. It can be expected that further landscape modifications will continue, despite China's recent economic slow-down. Therefore, continued future research on the Yellow River Basin land surface dynamics is crucial. In doing so, the applied analytic approach will profit from forthcoming satellite missions (Landsat 9, Sentinel-2 constellation) to further enhance data continuity with even higher temporal frequencies. Further, the current Landsat Global Archive Consolidation (LGAC) initiative seeks for archived imagery at all international ground stations, which would substantially enhance the capacity for mapping and monitoring historic land change in China further back in time (Wulder et al., 2016).

6.6 Summary

- ❶ This chapter presented an extended land cover change analysis of four land cover types across the Yellow River Basin between 2000 and 2015 by using dense Landsat TM/ETM+/OLI time series stacks.
- ❷ The semi-automated final classification procedure (with RF) was based on multi-spectral, spectral-temporal, and textural features combined with a stable pixels reference dataset, a novel and unique methodological combination.
- ❸ Thematic and spatial quality yielded high accuracies above 90 % overall accuracies across all thematic classes.
- ❹ Mining operations on the Qinghai-Tibet Plateau have commenced in 2004 and continue to expand resulting in a total loss of 30 km² of mainly sensitive alpine grassland. Despite a domestic slow-down of coal demand, mining excavations have been accelerated in the most recent years.
- ❺ Agricultural land in Hetao, the largest irrigation network in the Yellow River Basin, shows localized spatial dynamics. At marginal district areas new cropping fields were developed by constructing new canals and irrigation facilities. At the same time, farmers abandoned their fields as a result of large-scale soil salinization.
- ❻ The highly erosive Central Loess Plateau has experienced a remarkable regrowth of forest areas. Since 2000, national and international conservation incentives planted trees covering a total area of around 9000 km². Forest loss occurred mainly in the vicinity of the Ziwuling and Yunwu Mountains due to urban and agricultural expansion.
- ❼ Urbanization is one of the most prominent land cover change types in the Yellow River Basin. The North China Plain Metropolitan Region has sprawled from 3,650 km² to almost 5,000 km² with annual growth rates exceeding 10 %.

SYNTHESIS AND OUTLOOK

Global Change is one of the most important concerns of the 21st century and has a deep impact on the sustainable development of regional and local systems (Ye and Dong, 2010; Zhou et al., 2015). By 2030, China is expected to be world's largest economy accompanied with increasing affluence and growing consumption and competition for scarce water and land resources (World Bank, 2016; International Monetary Fund, 2017). This makes the transition of economic development towards sustainability a challenging task. As a national hub for economic development, the Yellow River Basin is a generic example how such a resource intense socio-economic development has resulted in large-scale changes of land surface characteristics and impacted environmental features and processes. It has already reached a critical state where nature's self-regulating abilities are undermined and threatening human well-being. There is an urgent need to identify the past temporal and spatial variability of land change patterns on which a better understanding of the causal drivers of change can be drawn. To meet the challenges of a rapid changing environment, observations from the surface with remote sensing tools yield new insights in recent and historic land cover change dynamics at various spatial and temporal scales. Based on such information products, new strategies emphasizing on a more integrative and sustainable management framework can evolve to coordinate water and land land resources in the Yellow River Basin.

In this context, this dissertation provides new perspectives of land cover change dynamics that have occurred during the last decades across the second largest watershed in China - the Yellow River Basin. The Yellow River Basin is a unique study region for several reasons. Long-term and intense anthropogenic activities have transformed this region into a human-dominated and degraded landscape, which remains understudied by the scientific community. Precise and up-to-date information about spatial and temporal dynamics of land change is lacking. Therefore, the main objective of this thesis was to give a detailed and consistent picture of the regional characterization of the prevailing land surface cover and its dynamics, which was based on multi-

source remote sensing time series with a specific local focus on the most prominent land change types.

The main objectives defined in this thesis were presented in three core chapters. In the following, each objective, which was formulated in the Chapter 1 on page 12, are addressed and concluded to contribute to the main objective of this thesis.

Objective 1

Determining the current and most pressing social-ecological challenges affecting the Yellow River Basin and developing a possible governance model towards a more sustainable and holistic management.

In chapter 3 of this thesis, a sound review was provided about current and possible future social-ecological challenges affecting the Yellow River Basin. This area is characterized by a long coupled human-environment interrelationship and thus an illustrative case study region of how anthropogenic activities have altered a river ecosystem leading to a large scale degraded landscape. Recently, this long relationship has been dramatically intensified triggered by tremendous socio-economic evolution throughout the basin. However, many years of intensive economic development and natural resource exploitation have had their downside. Land reclamation for agricultural and industrial purposes, dam and reservoir construction, the extraction of natural resources, water and environmental pollution, combined with climate change, have greatly affected the natural dynamic conditions of the river. These dynamics have imposed serious new environmental and social problems hampering a regional sustainable development in the basin. To tackle these complex and often interlinked challenges, more holistic and multi dimensional management perspectives are required for the Yellow River Basin to increase overall resilience for environment and society. Due to China's cultural heritage, strong vertical top-down and command-driven policies are attempted to resolve the arising problems in the past. But this approach has its limits. Indeed, the capacity of traditional top-down policies in dealing with simple and linear challenges is high, but remains insufficient when it comes to more complex and multi-scale social-ecological tasks. They also fail in aligning interests of local communities, which in turn show little to no interests in following national governance and undermine their implementation. A paradigm shift towards more flexible, market-based incentives, and bottom-up solutions is becoming more frequent, but the degree, scope and impact is still limited. It is the task of a strong and proper designed YRCC to coordinate all involved stakeholders and balance the different interests, with mutual benefits, also those of poorer locals, should not be determined by political and provincial constrains. An effective integrated river basin management also demands basin-wide precise and consistent information about biophysical, environmental, and socio-economic situations, which are either difficult to access or fragmented, inconsistent or outdated. The establishment of a common data platform, e.g. operated by the YRCC, could be a powerful tool for data handling and sharing, on which decision making can be based on.

Objective 2

Building a comprehensive land cover picture of the Yellow River Basin to determine the current land surface characteristics and the most dynamic processes that have influenced the entire basin.

The pathway towards an integrated river basin management for solving the multi-fold social-ecological problems requires precise up-to-date multi-temporal information about the spatial component of the Yellow River Basin. In view of this, chapter 5 of this thesis presented a “wall-to-wall” picture about land cover characteristics and its dynamics from the complete last decade based on high-temporal continuous MODIS time series. The semi-automated classification approach used the principle of intra-annual phenology that allows for a clear separation of different land cover types. Despite the spatially complex and heterogeneous land cover structure, which includes a wide range of different land cover entities, the regional-adapted Yellow River Basin LC has achieved high thematic accuracies. The derived multi-temporal maps allow for the spatial depiction of trends and recent land change across the basin. Results have revealed tremendous land cover change dynamics since 2003 triggered by recent socio-economic evolution, such as growing economy, increasing urbanization, agricultural expansion and intensification, and various land use policies that had been initiated in the past decades. Perhaps the most obvious dynamic trend was detected on the central part of the Loess Plateau, where ecological restoration activities revitalized a degraded environment, which resulted in an overall “greening” of the landscape. The China-wide urbanization tendency was also reflected in the change detection analysis in the Yellow River Basin, where urban areas have sprawled on surrounding lands, transforming agriculture and natural forms of vegetation. Besides, dynamic processes have affected agricultural encroachment and expanding mining excavations. This study clearly exemplifies the necessity of regional-adapted land cover maps when comparing them to global products. Regional maps better address local heterogeneities and specific local characteristics of the land surface characteristics due to their regional optimization of data preprocessing, reference and *in-situ* data collection for training and validation, model tuning as well as post classification.

However, the tessellated landscape structure (e.g. Loess Plateau) and spatial complexity thematic classes (e.g. urban) require mapping efforts on higher spatial detail. Therefore, this analysis can be seen as a preliminary study to the research conducted in chapter 6 of this thesis. Nevertheless, the basin-wide land cover change products hold great potential for climate, hydrology, or biodiversity modelers.

Objective 3

Detailed spatio-temporal change detection analysis of the most prominent land cover dynamics across the Yellow River Basin related to mining, agriculture, forest, and urban areas.

Based on the previously gained results, chapter 6 extended the land cover change analysis at finer spatial and temporal scales to provide information related to mining, agriculture, forest, and urban areas, the most prominent land cover change types across the basin. Adequately representing the fast and complex dynamics of a coupled human-environment system needs consistent land surface information at high spatial and temporal scales. The medium resolution MODIS sensor is not sufficient in dealing with heterogeneous landscape types requiring mapping at higher spatial detail. China's tremendous socio-economic development has fostered dynamics at such a high rate of change, which required annual monitoring to fully understand the underlying drivers of change. In this chapter, Landsat time series, served as backbone remote sensing data. This sensor balances the trade-offs between spatial and temporal resolution, geographical coverage, and the long availability of archived data. Unfortunately, the analysis was temporally restricted to a time span between 2000 and 2015, as the amount of Landsat data was not sufficient to create reliable high quality time series stacks. The utilization of phenology-derived features facilitated the delineation of different land cover across the heterogeneous Yellow River landscape. Due to the temporal irregularity, the direct delineation of phenological metrics with Landsat imagery is limited. To overcome this obstacle various spectral-temporal metrics were derived, which are able to extract the inherent seasonal trajectories across different land cover entities without the necessity of sequential timing. All available TM, EMT+, OLI imageries between 2000 and 2015 were acquired to compute annual spatially contiguous spectral-temporal and textural metrics on which mining, agriculture, forests, and urban structures were discretely classified. This semi-automated classification approach was combined with a single "stable-pixels" reference data set, which proved to be a reliable and efficient sampling technique for performing multi-temporal land cover classification. These novel land cover maps provide new insights in local and regional spatio-temporal dynamics of the most predominant land cover change types in the Yellow River Basin in light of contemporary *Global Change* processes. Albeit slowed, the intense socio-economic development concomitant with urbanization, industrialization and extraction of natural resources still dominates the current land surface dynamics often at the expenses of environment and society creating complex social-ecological challenges in the basin (see chapter 3 on page 3.2). Basin-wide there is an increasing population flow towards the metropolitan regions, which has boosted the urbanization scale and pace at unprecedented rates. The results of this thesis reveal the most apparent landscape dynamics on the Loess and Ordos Plateau. There, the worldwide largest conservation projects (e.g. the *GfG* or *NFCP* programs or the *Loess Plateau Watershed Rehabilitation Program*) have transformed a heavily and large-scale degraded landscape into an ecologically vital region to recreate lost ecosystem functions, such as carbon sequestration, hydrological services, and soil retention. These projects also emphasized social aspects and aimed to support local farming structures and improve the living and working conditions to reduce the increased impoverishment in rural areas. As one of the most important crop production zones in China, agriculture is the dominant landscape feature across the basin, covering one third of the entire area. A rising urbanized and more affluent society requires higher food products. Food security as a major concern, might become increasingly unstable. Due to the process of rapid modernization, significant portions of arable land has been lost, largely in the most fertile alluvial

regions (e.g. Central Plain Metropolitan Region or the Yellow River Delta), where urbanization and industrialization have flourished. Also the progressive degradation of water and land resources has fostered farmers to abandon their arable land.

Towards an Integrated Monitoring Framework

River basins are complex holistic social-ecological systems comprising various nested components of hydrological, ecological, institutional, or socio-economic dimensions, which are linked with each other and function at various scales in space and time. The strong interrelation of such components require new holistic and participatory approaches such as an *Integrated River Basin Management* (IRBM) to understand and integrate the needs of all competing users across sectors within a given physical, climatic, and ecological context (Qureshi et al., 2002; Bandaragoda and Babel, 2010; Evers, 2016). Traditional approaches usually emphasize on sectors or disciplines (e.g. hydrology, agriculture, urban, ecology) and aim at specific objectives. Such sector-oriented management perspectives are still practiced across the Yellow River Basin leading often to

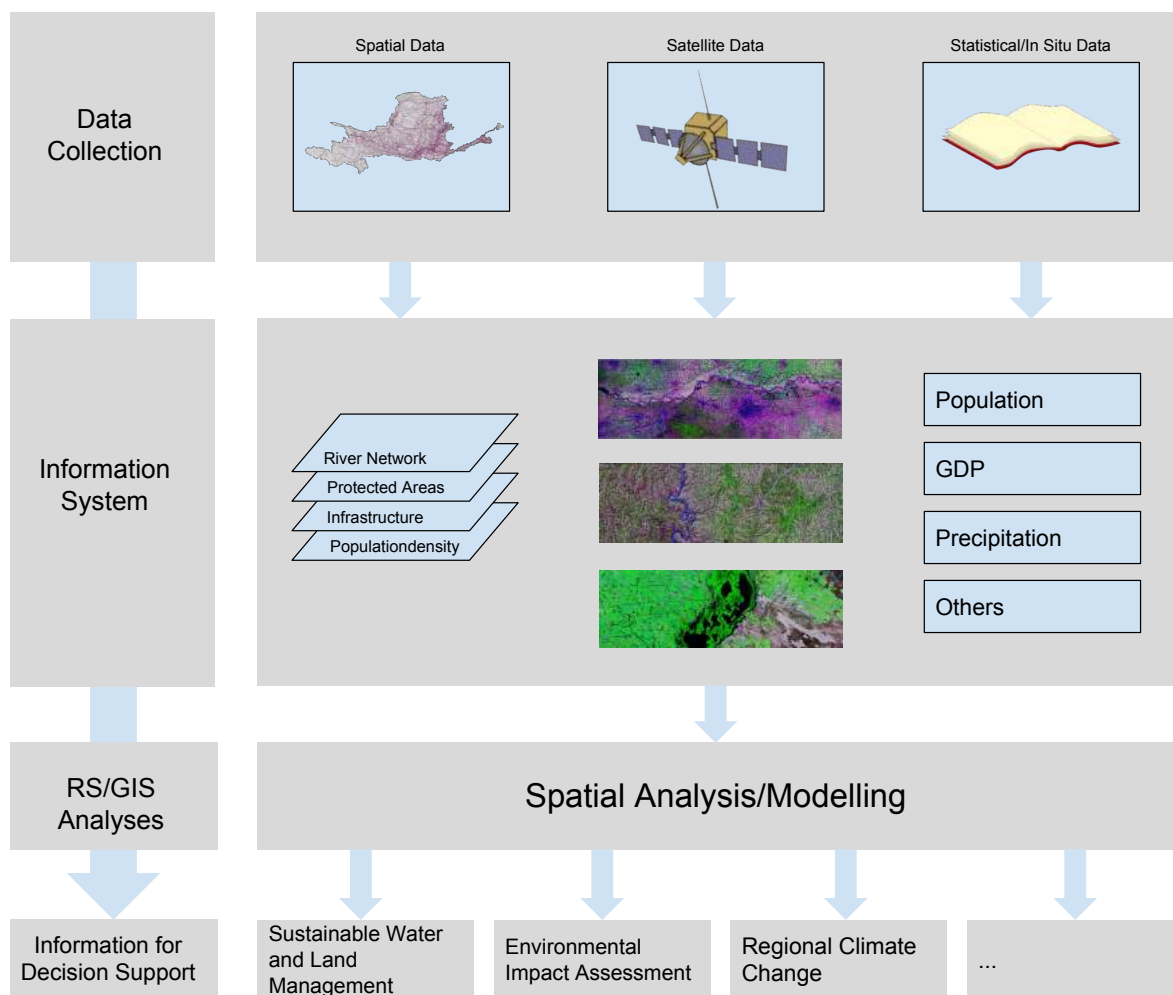


Figure 7.1: Methodological framework for a decision support system.

a series of different contradicting approaches, viewpoints, and outputs. The proposed river basin governance framework (Figure 3.10) - introduced in chapter 3 on page 3.4 - integrates the vertical and horizontal dimensions that ideally incorporates all different needs and the behavior of all actors to address the complex issues. In order to built up such a multi-disciplinary framework for sustaining a long-term sustainable development, there is a strong need of a geospatial perspective of all components in the basin. The recent advent of information technology for handling large volume of digital data has altered the scope for providing information products. The implementation of a common inter- and transdisciplinary geographical information system (GIS) database for the entire Yellow River Basin, which features the integration of spatial (e.g. land cover) and non-spatial (socio-economic statistics) data types, could give added value products for decision making (Figure 7.1).

This integrated database could potentially be mandated to the YRCC, where the information flow is harmonized and provided to management agencies, policy makers or researchers to elaborate possible management scenarios. This thesis is a first step to gain a generic knowledge about spatio-temporal land surface processes across the basin, which pinpoint hotspot locations of change. The applied regionally adapted methodologies in an almost automated fashion have delivered substantial and novel land cover perspectives, which are needed to understand the drivers and impacts of change. Satellite remote sensing is entering a new era, in which a multitude of space-borne sensors continually acquires data over the earth's surface. The applied methodology is sensor independent and will profit from forthcoming satellite missions (Landsat 9, Sentinel constellation).

BIBLIOGRAPHY

A

- Adelabu, S., Mutanga, O., and Adam, E. (2015). Testing the reliability and stability of the internal accuracy assessment of random forest for classifying tree defoliation levels using different validation methods. *Geocarto International*, 30(7):810–821.
- Allan, S. (2007). Erlitou and the formation of chinese civilization: Toward a new paradigm. *The Journal of Asian Studies*, 66(2):461–496.
- Anderies, J. M., Janssen, M. A., and Ostrom, E. (2004). Framework to analyze the robustness of social-ecological systems from an institutional perspective. *Ecology and Society*, 9:1–18.
- Arino, O., Bicheron, P., Achard, F., Latham, R., Witt, R., and Weber, J. (2008). GLOBCOVER - the most detailed portrait of Earth. *European Space Agency Bulletin*, 136:25–31.

B

- Bai, Y., Feng, M., Jiang, H., Wang, J., Zhu, Y., and Liu, Y. (2014). Assessing consistency of five global land cover data sets in China. *Remote Sensing*, 6(9):8739–8759.
- Ban, N. C., Mills, M., Tam, J., Hicks, C. C., Klain, S., Stoeckl, N., Bottrill, M. C., Levine, J., Pressey, R. L., Satterfield, T., and Chan, K. M. A. (2013). A social-ecological approach to conservation planning: Embedding social considerations. *Frontiers in Ecology and the Environment*, 11(4):194–202.
- Bandaragoda, D. J. and Babel, M. S. (2010). Institutional development for IWRM: An international perspective. *International Journal of River Basin Management*, 8(3-4):215–224.
- Barnes, W. L., Xiong, X., and Salomonson, V. V. (2003). Status of terra MODIS and aqua MODIS. *Advances in Space Research*, 32(11):2099–2106.
- Barnett, J., Webber, M., Wang, M., Finlayson, B., and Dickinson, D. (2006). Ten key questions about the management of water in the Yellow River basin. *Environmental management*, 38(2):179–88.
- Barrow, C. J. (1998). River basin development planning and management: A critical review. *World Development*, 26(1):171–186.

- Bartholomé, E. and Belward, A. S. (2005). GLC2000: a new approach to global land cover mapping from Earth observation data. *International Journal of Remote Sensing*, 26(9):1959–1977.
- Bennett, E., Carpenter, S. R., and Caraco, N. (2001). Human impact on erodable phosphorus and eutrophication: A global perspective. *Bios*, 51:227 – 234.
- Berk, A., Bernstein, L., Anderson, G., Acharya, P., Robertson, D., Chetwynd, J., and Adler-Golden, S. (1998). MODTRAN cloud and multiple scattering upgrades with application to AVIRIS. *Remote Sensing of Environment*, 65(3):367 – 375.
- Berkes, F. and Folke, C. (1998). *Linking social and ecological systems: Management practices and social mechanism for building resilience*. Cambridge University Press, Cambridge UK.
- Bi, X., Wang, B., and Lu, Q. (2011). Fragmentation effects of oil wells and roads on the Yellow River Delta, North China. *Ocean & Coastal Management*, 54(3):256–264.
- Bicheron, P., Defourny, P., Brockmann, C., Schouten, L., Vancutsem, C., Huc, M., Bontemps, S., Leroy, M., Achard, F., Herold, M., Ranera, F., and Arino, O. (2010). GLOBCOVER - Products description and validation report. Technical report.
- Binder, C. R., Hinkel, J., Bots, P. W. G., and Pahl-Wostl, C. (2013). Comparison of frameworks for analyzing social-ecological systems. *Ecology and Society*, 18(4).
- Blanco, E. (2011). A social-ecological approach to voluntary environmental initiatives: The case of nature-based tourism. *Policy Sciences*, 44(1):35–52.
- Blanco, P. D., Colditz, R. R., Saldaña, G. L., Hardtke, L. A., Llamas, R. M., Mari, N. A., Fischer, A., Caride, C., Aceñolaza, P. G., del Valle, H. F., Lillo-Saavedra, M., Coronato, F., Opazo, S. A., Morelli, F., Anaya, J. A., Sione, W. F., Zamboni, P., and Arroyo, V. B. (2013). A land cover map of Latin America and the Caribbean in the framework of the SERENA project. *Remote Sensing of Environment*, 132:13 – 31.
- Boden, T. A., Marland, G., and Andres, R. J. (2016). Global, regional, and national fossil-fuel CO₂ emissions. Technical report, Carbon Dioxide Information Analysis Center, Oak Ridge National Laboratory, U.S. Department of Energy, Oak Ridge, Tennessee, USA.
- Borruso, L., Esposito, A., Bani, A., Ciccazzo, S., Papa, M., Zerbe, S., and Brusetti, L. (2017). Ecological diversity of sediment rhizobacteria associated with *Phragmites australis* along a drainage canal in the Yellow River watershed. *Journal of Soils and Sediments*, 17(1):253–265.
- Boxer, B. (2001). Contradictions and challenges in China’s water policy development. *Water International*, 26(3):335–341.
- Brakenridge, G. R. (2016). Global active archive of large flood events.
- Breiman, L. (2001). Random Forests. *Machine Learning*, 45(1):5–32.

- Brockerhoff, E. G., Jactel, H., Parrotta, J. A., Quine, C. P., and Sayer, J. (2008). Plantation forests and biodiversity: oxymoron or opportunity? *Biodiversity and Conservation*, 17(5):925–951.
- Broich, M., Hansen, M. C., Potapov, P., Adusei, B., Lindquist, E., and Stehman, S. V. (2011). Time-series analysis of multi-resolution optical imagery for quantifying forest cover loss in Sumatra and Kalimantan, Indonesia. *International Journal of Applied Earth Observation and Geoinformation*, 13(2):277 – 291.
- Brundtland, G., Khalid, M., Agnelli, S., Al-Athel, S., Chidzero, B., Fadika, L., Hauff, V., Lang, I., Shijun, M., Morino de Botero, M., Singh, M., Okita, S., and Others, A. (1987). *Our Common Future ('Brundtland report')*. Oxford Paperback Reference. Oxford University Press, USA.

C

- Cai, X. (2008). Water stress, water transfer and social equity in Northern China-implications for policy reforms. *Journal of environmental management*, 87(1):14–25.
- Cai, X. and Rosegrant, M. W. (2004). Optional water development strategies for the Yellow River Basin: Balancing agricultural and ecological water demands. *Water Resources Research*, 40(8):n/a–n/a.
- Carr, E. R., Wingard, P. M., Yorty, S. C., Thompson, M. C., Jensen, N. K., and Roberson, J. (2007). Applying DPSIR to sustainable development. *International Journal of Sustainable Development & World Ecology*, 14(6):543–555.
- Chan, J. C.-W. and Paelinckx, D. (2008). Evaluation of random forest and adaboost tree-based ensemble classification and spectral band selection for ecotope mapping using airborne hyper-spectral imagery. *Remote Sensing of Environment*, 112(6):2999–3011.
- Chen, J., Chen, J., Liao, A., Cao, X., Chen, L., Chen, X., He, C., Han, G., Peng, S., Lu, M., Zhang, W., Tong, X., and Mills, J. (2015). Global land cover mapping at 30 m resolution: A POK-based operational approach. *Journal of Photogrammetry and Remote Sensing*, 103:7 – 27. Global Land Cover Mapping and Monitoring.
- Chen, J., He, D., and Cui, S. (2003). The response of river water quality and quantity to the development of irrigated agriculture in the last 4 decades in the Yellow River Basin, China. *Water Resources Research*, 39(3):n/a–n/a.
- Chen, L., Wei, W., Fu, B., and Lu, Y. (2007). Soil and water conservation on the Loess Plateau in China: Review and perspective. *Progress in Physical Geography*, 31(4):389–403.
- Chen, Y., Syvitski, J. P. M., Gao, S., Overeem, I., and Kettner, A. J. (2012). Socio-economic impacts on flooding: A 4000-year history of the Yellow River, China. *Ambio*, 41(7):682–98.
- Chen, Y.-F., Liu, Y.-S., Wang, J., Yan, J.-P., and Guo, X.-D. (2009). Land use changes of an aeolian-loessial soil area in northwest China: Implications for ecological restoration. *Pedosphere*, 19(3):356–361.

- Cheng, G. and Wu, T. (2007). Responses of permafrost to climate change and their environmental significance, Qinghai-Tibet Plateau. *Journal of Geophysical Research: Earth Surface*, 112(F2):n/a–n/a.
- CIESIN (2005). Gridded Population of the World, Version 3 (GPWv3): Population Density Grid, Future Estimates.
- Clapp, F. G. (1922). The Hwang Ho, Yellow River. *Geographical Review*, 12(1):1–18.
- Clark, M. L., Aide, T. M., Grau, H. R., and Riner, G. (2010). A scalable approach to mapping annual land cover at 250 m using MODIS time series data: A case study in the Dry Chaco ecoregion of South America. *Remote Sensing of Environment*, 114(11):2816 – 2832.
- Clark, M. L., Aide, T. M., and Riner, G. (2012). Land change for all municipalities in Latin America and the Caribbean assessed from 250-m MODIS imagery (2001–2010). *Remote Sensing of Environment*, 126:84 – 103.
- Colditz, R., Schmidt, M., Conrad, C., Hansen, M., and Dech, S. (2011). Land cover classification with coarse spatial resolution data to derive continuous and discrete maps for complex regions. *Remote Sensing of Environment*, 115(12):3264 – 3275.
- Colditz, R. R., na, G. L. S., Maeda, P., Espinoza, J. A., Tovar, C. M., Hernández, A. V., no Benítez, C. Z., López, I. C., and Ressler, R. (2012). Generation and analysis of the 2005 land cover map for Mexico using 250 m MODIS data. *Remote Sensing of Environment*, 123:541 – 552.
- Congalton, R. G. (1991). A review of assessing the accuracy of classifications of remotely sensed data. *Remote Sensing of Environment*, 37(1):35–46.
- Congalton, R. G. and Green, K. (2009). *Assessing the accuracy of remotely sensed data: Principles and practices*. CRC Press, Boca Raton.
- Coppin, P., Jonckheere, I., Nackaerts, K., Muys, B., and Lambin, E. (2004). Digital change detection methods in ecosystem monitoring: A review. *International Journal of Remote Sensing*, 25(9):1565–1596.
- Cui, B., Yang, Q., Yang, Z., and Zhang, K. (2009). Evaluating the ecological performance of wetland restoration in the Yellow River Delta, China. *Ecological Engineering*, 35(7):1090–1103.
- Cui, B.-L. and Li, X.-Y. (2011). Coastline change of the Yellow River estuary and its response to the sediment and runoff (1976–2005). *Geomorphology*, 127(1-2):32–40.
- CWRC (2016). Changjing Water Reports.

D

- Daily, G. (1997). *Nature's Services: Societal Dependence on Natural Ecosystems*. Island Press.
- Daily, G. C., Söderqvist, T., Aniyar, S., Arrow, K., Dasgupta, P., Ehrlich, P. R., Folke, C., Jansson, A., Jansson, B.-O., Kautsky, N., Levin, S., Lubchenco, J., Mäler, K.-G., Simpson, D., Starrett, D., Tilman, D., and Walker, B. (2000). The value of nature and the nature of value. *Science*, 289(5478):395–396.
- Dannenbergh, P. M., Hakkenberg, R. C., and Song, C. (2016). Consistent classification of Landsat time series with an improved automatic adaptive signature generalization algorithm.
- Daofeng, L., Chunhui, L., Fanghua, H., and Zheng, L. (2004). Complex vegetation cover classification study of the Yellow River Basin based on NDVI data. In *IGARSS 2004. 2004 IEEE International Geoscience and Remote Sensing Symposium*, volume 5, pages 3360–3363 vol.5.
- Das, T., Haldar, S., Das Gupta, I., and Sen, S. (2014). River bank erosion induced human displacement and its consequences. *Living Reviews in Landscape Research*, 8.
- Defourny, P., Kirches, G., Brockmann, C., Boettcher, M., Peters, M., Bontemps, S., Lamarche, C., Schlerf, M., and Santoro, M. (2014). Land cover CCI Product User Guide Version 2. UCL-Geomatics: Louvain, Belgium.
- DeFries, R. S., Foley, J. A., and Asner, G. P. (2004). Land-use choices: Balancing human needs and ecosystem function. *Frontiers in Ecology and the Environment*, 2(5):249–257.
- Defries, R. S., Hansen, M., Townshend, J. R. G., and Sohlberg, R. (1998). Global land cover classifications at 8 km spatial resolution: The use of training data derived from Landsat imagery in decision tree classifiers. *International Journal of Remote Sensing*, 19(16):3141–3168.
- Defries, R. S. and Townshend, J. R. G. (1994). NDVI-derived land cover classifications at a global scale. *International Journal of Remote Sensing*, 15(17):3567–3586.
- Delang, C. O. (2016). *China's Water Pollution Problems*. Tay.
- Delang, C. O. and Wang, W. (2012). Chinese forest policies in the age of decentralisation (1978 – 1997). *International Forestry Review*, 14(1).
- Delang, C. O. and Wang, W. (2013). Chinese forest policy reforms after 1998: The case of the natural forest protection program and the slope land conversion program. *International Forestry Review*, 15(3):290–304.
- Delang, C. O. and Zhen, Y. (2015). *China's Grain for Green Program: A review of the largest ecological restoration and rural development program in the world*. Springer International Publishing.

- DeVries, B., Verbesselt, J., Kooistra, L., and Herold, M. (2015). Robust monitoring of small-scale forest disturbances in a tropical montane forest using Landsat time series. *Remote Sensing of Environment*, 161:107 – 121.
- Di Gregorio, A. (2005). *Land Cover Classification Scheme (LCCS), version2: Classification Concepts and User Manual*. FAO Environmental and Natural Resources Services, No. FAO. Rome. 208p.
- Dinar, A., Rosegrant, M. W., and Meinzen-Dick, R. (1997). *Water allocation mechanisms: Principles and examples*. The World Bank.
- Dong, L., Wang, W., Ma, M., Kong, J., and Veroustraete, F. (2009). The change of land cover and land use and its impact factors in upriver key regions of the Yellow River. *International Journal of Remote Sensing*, 30(5):1251–1265.

E

- Eatwell, J., Milgate, M., and Newman, P. (1989). *Social Economics*. The New Palgrave. Palgrave Macmillan UK.
- Eisfelder, C. and Kuenzer, C. (2015). *Remote Sensing Time Series*, chapter Investigating fourteen years of net primary productivity based on remote sensing data for China, pages 269 – 288. Springer International Publishing, Cham, Switzerland.
- Esch, T., Marconcini, M., Felbier, A., Roth, A., Heldens, W., Huber, M., Schwinger, M., Taubenböck, H., Müller, A., and Dech, S. (2013). Urban footprint processor - fully automated processing chain generating settlement masks from global data of the TanDEM-X mission. *IEEE Geoscience and Remote Sensing Letters*, 10(6):1617–1621.
- Evers, M. (2016). Integrative river basin management: Challenges and methodologies within the german planning system. *Environmental Earth Sciences*, 75(14):1085.

F

- Falkenmark, M. and Widstrand, C. G. (1992). *Population and water resources: A delicate balance*. Population bulletin. Population Reference Bureau.
- FAO (1996). Rome declaration on world food security and world food summit plan of action. World Food Summit 13-17 November 1996, Rome.
- Feng, J., Wang, T., Qi, S., and Xie, C. (2005). Land degradation in the source region of the Yellow River, northeast Qinghai-Xizang Plateau: Classification and evaluation. *Environmental Geology*, 47(4):459–466.
- Feng, K., Siu, Y. L., Guan, D., and Hubacek, K. (2012). Assessing regional virtual water flows and water footprints in the Yellow River Basin, China: A consumption based approach. *Applied Geography*, 32(2):691–701.

- Feng, X., Fu, B., Lu, N., Zeng, Y., and Wu, B. (2013). How ecological restoration alters ecosystem services: An analysis of carbon sequestration in China's Loess Plateau. *Scientific Reports*, 3:2846.
- Fernandes, R., Fraser, R., Latifovic, R., Cihlar, J., Beaubien, J., and Du, Y. (2004). Approaches to fractional land cover and continuous field mapping: A comparative assessment over the BOREAS study region. *Remote Sensing of Environment*, 89(2):234–251.
- Foley, J. A., Costa, M. H., Delire, C., Ramankutty, N., and Snyder, P. (2003). Green surprise? how terrestrial ecosystems could affect Earth's climate. *Frontiers in Ecology and the Environment*, 1(1):38–44.
- Foley, J. A., DeFries, R., Asner, G. P., Barford, C., Bonan, G., Carpenter, S. R., Chapin, F. S., Coe, M. T., Daily, G. C., Gibbs, H. K., Helkowski, J. H., Holloway, T., Howard, E. A., Kucharik, C. J., Monfreda, C., Patz, J. A., Prentice, I. C., Ramankutty, N., and Snyder, P. K. (2005). Global consequences of land use. *Science*, 309(5734):570–574.
- Folke, C., Hahn, T., Olsson, P., and Norberg, J. (2005). Adaptive governance of social-ecological systems. *Annual Review of Environment and Resources*, 30(1):441–473.
- Foody, G. M. (2002). Status of land cover classification accuracy assessment. *Remote Sensing of Environment*, 80(1):185 – 201.
- Fortier, J., Rogan, J., Woodcock, C. E., and Runfola, D. M. (2011). Utilizing temporally invariant calibration sites to classify multiple dates and types of satellite imagery. *Photogrammetric Engineering & Remote Sensing*, 77(2).
- Franklin, S. E., Ahmed, O. S., Wulder, M. A., White, J. C., Hermosilla, T., and Coops, N. C. (2015). Large area mapping of annual land cover dynamics using multitemporal change detection and classification of Landsat time series data. *Canadian Journal of Remote Sensing*, 41(4):293–314.
- Friedl, M., McIver, D., Hodges, J., Zhang, X., Muchoney, D., Strahler, A., Woodcock, C., Gopal, S., Schneider, A., Cooper, A., Baccini, A., Gao, F., and Schaaf, C. (2002). Global land cover mapping from modis: algorithms and early results. *Remote Sensing of Environment*, 83(1-2):287 – 302. The Moderate Resolution Imaging Spectroradiometer (MODIS): a new generation of Land Surface Monitoring.
- Friedl, M. A., Sulla-Menashe, D., Tan, B., Schneider, A., Ramankutty, N., Sibley, A., and Huang, X. (2010). MODIS Collection 5 global land cover: Algorithm refinements and characterization of new datasets. *Remote Sensing of Environment*, 114(1):168 – 182.
- Fritz, S. and See, L. (2008). Identifying and quantifying uncertainty and spatial disagreement in the comparison of global land cover for different applications. *Global Change Biology*, 14(5):1057–1075.

Fritz, S., See, L., and Rembold, F. (2010). Comparison of global and regional land cover maps with statistical information for the agricultural domain in Africa. *International Journal of Remote Sensing*, 31(9):2237–2256.

Fu, G., Chen, S., Liu, C., and Shepard, D. (2004). Hydro-climatic trends of the Yellow River Basin for the last 50 years. *Climatic Change*, 65:149–178.

G

Gao, P., Niu, X., Wang, B., and Zheng, Y. (2015). Land use changes and its driving forces in hilly ecological restoration area based on GIS and RS of Northern China. *Scientific Reports*, 5:11038.

Gassert, F., Luo, T., Shiao, T., and Luck, R. (2013). Yellow River Study. Working Paper. Washington, DC: World Resources Institute.

Gessner, U., Machwitz, M., Conrad, C., and Dech, S. (2013). Estimating the fractional cover of growth forms and bare surface in savannas: A multi-resolution approach based on regression tree ensembles. *Remote Sensing of Environment*, 129:90 – 102.

Gessner, U., Machwitz, M., Esch, T., Tillack, A., Naeimi, V., Kuenzer, C., and Dech, S. (2015). Multi-sensor mapping of west african land cover using modis, ASAR and TanDEM-X/TerraSAR-X data. *Remote Sensing of Environment*, 164:282 – 297.

Ghose, B. (2014). Food security and food self-sufficiency in China: from past to 2050. *Food and Energy Security*, 3(2):86–95.

Gislason, P. O., Benediktsson, J. A., and Sveinsson, J. R. (2006). Random Forests for land cover classification. *Pattern Recognition Letters*, 27(4):294–300.

Gómez, C., White, J. C., and Wulder, M. A. (2016). Optical remotely sensed time series data for land cover classification: A review. *{ISPRS} Journal of Photogrammetry and Remote Sensing*, 116:55 – 72.

Gómez, C., White, J. C., Wulder, M. A., and Alejandro, P. (2014). Historical forest biomass dynamics modelled with landsat spectral trajectories. *{ISPRS} Journal of Photogrammetry and Remote Sensing*, 93:14 – 28.

Gong, P., Liang, S., Carlton, E. J., Jiang, Q., Wu, J., Wang, L., and Remais, J. V. (2012). Urbanisation and health in China. *Lancet*, 379(9818):843–852.

Goodwin, N. R., Coops, N. C., Wulder, M. A., Gillanders, S., Schroeder, T. A., and Nelson, T. (2008). Estimation of insect infestation dynamics using a temporal sequence of Landsat data. *Remote Sensing of Environment*, 112(9):3680 – 3689.

Gray, J. and Song, C. (2013). Consistent classification of image time series with automatic adaptive signature generalization. *Remote Sensing of Environment*, 134:333–341.

- Griffiths, M. (2002). The European Water Framework Directive: An approach to integrated river basin management. Technical Report 5, European Commission.
- Griffiths, P., Kuemmerle, T., Baumann, M., Radeloff, V. C., Abrudan, I. V., Lieskovsky, J., Munteanu, C., Ostapowicz, K., and Hostert, P. (2014). Forest disturbances, forest recovery, and changes in forest types across the Carpathian ecoregion from 1985 to 2010 based on Landsat image composites. *Remote Sensing of Environment*, 151:72–88.
- Griffiths, P., van der Linden, S., Kuemmerle, T., and Hostert, P. (2013). A pixel-based Landsat compositing algorithm for large area land cover mapping. *IEEE Journal of Selected Topics in Applied Earth Observations and Remote Sensing*, 6(5):2088–2101.
- Guo, J. and Gong, P. (2016). Forest cover dynamics from Landsat time-series data over Yan'an City on the Loess Plateau during the Grain for Green Project. *International Journal of Remote Sensing*, 37(17):4101–4118.
- Guo, W. Q., Yang, T. B., Dai, J. G., Shi, L., and Lu, Z. Y. (2008). Vegetation cover changes and their relationship to climate variation in the source region of the Yellow River, China, 1990 – 2000. *International Journal of Remote Sensing*, 29(7):2085–2103.
- Guobin, L. (1999). Soil conservation and sustainable agriculture on the Loess Plateau: Challenges and prospects. *Ambio*, 28(8):663–668.

H

- Habron, G. (2003). Role of adaptive management for watershed councils. *Environmental Management*, 31(1):0029–0041.
- Hansen, M. C., DeFries, R. S., Townshend, J. R. G., Carroll, M., Dimiceli, C., and Sohlberg, R. A. (2003). Global percent tree cover at a spatial resolution of 500 meters: First results of the MODIS Vegetation Continuous Fields algorithm. *Earth Interactions*, 7(10):1–15.
- Hansen, M. C., Defries, R. S., Townshend, J. R. G., and Sohlberg, R. (2000). Global land cover classification at 1 km spatial resolution using a classification tree approach. *International Journal of Remote Sensing*, 21(6-7):1331–1364.
- Hansen, M. C., Egorov, A., Potapov, P. V., Stehman, S. V., Tyukavina, A., Turubanova, S. A., Roy, D. P., Goetz, S. J., Loveland, T. R., Ju, J., Kommareddy, A., Kovalsky, V., Forsyth, C., and Bents, T. (2014). Monitoring conterminous United States (CONUS) land cover change with Web-Enabled Landsat Data (WELD). *Remote Sensing of Environment*, 140:466–484.
- Hansen, M. C. and Loveland, T. R. (2012). A review of large area monitoring of land cover change using Landsat data. *Remote Sensing of Environment*, 122:66–74.

- Hansen, M. C., Potapov, P. V., Moore, R., Hancher, M., Turubanova, S. A., Tyukavina, A., Thau, D., Stehman, S. V., Goetz, S. J., Loveland, T. R., Kommareddy, A., Egorov, A., Chini, L., Justice, C. O., and Townshend, J. R. G. (2013). High-resolution global maps of 21st-century forest cover change. *Science*, 342(6160):850–853.
- Hao, F., Zhang, X., Ouyang, W., Skidmore, A., and Toxopeus, A. G. (2012). Vegetation NDVI linked to temperature and precipitation in the upper catchments of Yellow River. *Environmental Modeling & Assessment*, 17(4):389–398.
- Haralick, R. M., Shanmugam, K., and Dinstein, I. (1973). Textural features for image classification.
- Hermosilla, T., Wulder, M. A., White, J. C., Coops, N. C., and Hobart, G. W. (2015). An integrated Landsat time series protocol for change detection and generation of annual gap-free surface reflectance composites. *Remote Sensing of Environment*, 158:220 – 234.
- Herold, M., Mayaux, P., Woodcock, C., Baccini, A., and Schmullius, C. (2008). Some challenges in global land cover mapping: An assessment of agreement and accuracy in existing 1 km datasets. *Remote Sensing of Environment*, 112(5):2538 – 2556. Earth Observations for Terrestrial Biodiversity and Ecosystems Special Issue.
- Hijmans, R. J., Cameron, S. E., Parra, J. L., Jones, P. G., and Jarvis, A. (2005). Very high resolution interpolated climate surfaces for global land areas. *International Journal of Climatology*, 25(15):1965–1978.
- Houghton, R. A. (2003). Revised estimates of the annual net flux of carbon to the atmosphere from changes in land use and land management 1850 – 2000. *Tellus B*, 55(2):378–390.
- Hu, Y., Maskey, S., and Uhlenbrook, S. (2012). Trends in temperature and rainfall extremes in the Yellow River source region, China. *Climatic Change*, 110(1-2):403–429.
- Hua, F., Wang, X., Zheng, X., Fisher, B., Wang, L., Zhu, J., Tang, Y., Yu, D. W., and Wilcove, D. S. (2016). Opportunities for biodiversity gains under the world's largest reforestation programme. *Nature Communications*, 7:12717.
- Huang, C., Goward, S. N., Masek, J. G., Thomas, N., Zhu, Z., and Vogelmann, J. E. (2010). An automated approach for reconstructing recent forest disturbance history using dense Landsat time series stacks. *Remote Sensing of Environment*, 114(1):183 – 198.
- Huete, A., Didan, K., Miura, T., Rodriguez, E. P., Gao, X., and Ferreira, L. G. (2002). Overview of the radiometric and biophysical performance of the MODIS vegetation indices. *Remote Sensing of Environment*, 83(1–2):195–213.
- Hui, F. and Haijun, H. (2004). Spatial-temporal changes of tidal flats in the Huanghe River Delta using Landsat TM/ETM+ images. *Journal of Geographical Sciences*, 14(3):366–374.

Hui, Y., Zheng, M., Liu, Z., and Gao, L. (2009). Distribution of polycyclic aromatic hydrocarbons in sediments from Yellow River Estuary and Yangtze River Estuary, China. *Journal of Environmental Sciences*, 21(12):1625–1631.

I

International Monetary Fund (2017). *World Economic Outlook (WEO) Update: A shifting global economic landscape*.

IPCC (2013). *Climate Change 2013 - The Physical Science Basis: Working Group I Contribution to the Fifth Assessment Report of the IPCC*. Cambridge University Press, Cambridge, UK and New York, NY, USA.

Irons, J. R., Dwyer, J. L., and Barsi, J. A. (2012). The next Landsat satellite: The Landsat data continuity mission. *Remote Sensing of Environment*, 122:11 – 21. Landsat Legacy Special Issue.

IUCN (2015). The IUCN Red List of threatened species. Version 2015.2.

IUCN and UNEP-WCMC (2015). The World Database on Protected Areas (WDPA).

J

Jiang, Y., Dong, W., Yang, S., and Ma, J. (2008). Long-term changes in ice phenology of the Yellow River in the past decades. *Journal of Climate*, 21(18):4879–4886.

Jönsson, P. and Eklundh, L. (2002). Seasonality extraction by function fitting to time-series of satellite sensor data.

Jönsson, P. and Eklundh, L. (2004). TIMESAT – a program for analyzing time-series of satellite sensor data. *Computers & Geosciences*, 30(8):833–845.

Ju, X., Liu, X., Zhang, F., and Roelcke, M. (2004). Nitrogen fertilization, soil nitrate accumulation, and policy recommendations in several agricultural regions of China. *Ambio*, 33(6):300–305.

Justice, C. O., Townshend, J. R. G., Vermote, E. F., Masuoka, E., Wolfe, R. E., Saleous, N., Roy, D. P., and Morisette, J. T. (2002). An overview of MODIS Land data processing and product status. *Remote Sensing of Environment*, 83(1-2):3–15.

Justice, C. O., Vermote, E., Townshend, J. R. G., Defries, R., Roy, D. P., Hall, D. K., Salomonson, V. V., Privette, J. L., Riggs, G., Strahler, A., Lucht, W., Myneni, R. B., Knyazikhin, Y., Running, S. W., Nemani, R. R., Wan, Z., Huete, A. R., van Leeuwen, W., Wolfe, R. E., Giglio, L., Muller, J., Lewis, P., and Barnsley, M. J. (1998). The Moderate Resolution Imaging Spectroradiometer (MODIS): Land remote sensing for global change research. *IEEE Transactions on Geoscience and Remote Sensing*, 36(4):1228–1249.

K

- Kennedy, R. E., Cohen, W. B., and Schroeder, T. A. (2007). Trajectory-based change detection for automated characterization of forest disturbance dynamics. *Remote Sensing of Environment*, 110(3):370 – 386.
- Kennedy, R. E., Yang, Z., and Cohen, W. B. (2010). Detecting trends in forest disturbance and recovery using yearly Landsat time series: 1. LandTrendr – Temporal segmentation algorithms. *Remote Sensing of Environment*, 114(12):2897 – 2910.
- Kidder, T. R. and Liu, H. (2014). Bridging theoretical gaps in geoarchaeology: Archaeology, geoarchaeology, and history in the Yellow River valley, China. *Archaeological and Anthropological Sciences*, 2:1–18.
- Kim, D.-H., Sexton, J. O., Noojipady, P., Huang, C., Anand, A., Channan, S., Feng, M., and Townshend, J. R. (2014). Global, Landsat-based forest-cover change from 1990 to 2000. *Remote Sensing of Environment*, 155:178–193.
- Kiptala, J., Mohamed, Y., Mul, M., Cheema, M., and der Zaag, P. V. (2013). Land use and land cover classification using phenological variability from MODIS vegetation in the Upper Pangani River Basin, Eastern Africa. *Physics and Chemistry of the Earth*, 66:112 – 122. Putting Science into Practice.
- Klein, I., Gessner, U., and Kuenzer, C. (2012). Regional land cover mapping and change detection in Central Asia using MODIS time-series. *Applied Geography*, 35(1–2):219 – 234.
- Knauer, K., Gessner, U., Fensholt, R., Forkuor, G., and Kuenzer, C. (2017). Monitoring agricultural expansion in Burkina Faso over 14 years with 30 m resolution time series: The role of population growth and implications for the environment. *Remote Sensing*, 9(2).
- Kovalskyy, V. and Roy, D. (2013). The global availability of Landsat 5 TM and Landsat 7 ETM + land surface observations and implications for global 30 m Landsat data product generation. *Remote Sensing of Environment*, 130:280 – 293.
- Kuenzer, C. (2007). Water pollution, scarcity and distribution challenges. Technical report, BusinessForum China.
- Kuenzer, C., Campbell, I., Roch, M., Leinenkugel, P., Tuan, V., and Dech, S. (2013). Understanding the impact of hydropower developments in the context of upstream – downstream relations in the Mekong river basin. *Sustainability Science*, 8(4):565–584.
- Kuenzer, C., Leinenkugel, P., Vollmuth, M., and Dech, S. (2014a). Comparing global land-cover products - Implications for geoscience applications: an investigation for the trans-boundary Mekong Basin. *International Journal of Remote Sensing*, 35(8):2752–2779.

- Kuenzer, C., Ottinger, M., Liu, G., Sun, B., Baumhauer, R., and Dech, S. (2014b). Earth observation-based coastal zone monitoring of the Yellow River Delta: Dynamics in China's second largest oil producing region over four decades. *Applied Geography*, 55:92–107.
- Kuenzer, C., Ottinger, M., Wegmann, M., Guo, H., Wang, C., Zhang, J., Dech, S., and Wikelski, M. (2014c). Earth observation satellite sensors for biodiversity monitoring: Potentials and bottlenecks. *International Journal of Remote Sensing*, 35(18):6599–6647.
- Kursa, M. B. and Rudnicki, W. R. (2010). Feature selection with the Boruta package. *Journal of Statistical Software*, 36(11):1–13.

L

- Lambin, E. F. and Geist (2006). *Land use and land cover change. Local processes and global impacts*. Springer International Publishing.
- Lambin, E. F., Geist, H. J., and Lepers, E. (2003). Dynamics of land-use and land-cover change in tropical regions. *Annual Review of Environment and Resources*, 28(1):205–241.
- Lambin, E. F., Turner, B. L., Geist, H. J., Agbola, S. B., Angelsen, A., Bruce, J. W., Coomes, O. T., Dirzo, R., Fischer, G., Folke, C., George, P. S., Homewood, K., Imbernon, J., Leemans, R., Li, X., Moran, E. F., Mortimore, M., Ramakrishnan, P. S., Richards, J. F., Skånes, H., Steffen, W., Stone, G. D., Svedin, U., Veldkamp, T. A., Vogel, C., and Xu, J. (2001). The causes of land-use and land-cover change: Moving beyond the myths. *Global Environmental Change*, 11(4):261–269.
- Lawler, A. (2009). Beyond the Yellow River: How China became China. *Science*, 325(5943):930–935.
- Lebel, L., Nikitina, E., Pahl-Wostl, C., and Knieper, C. (2013). Institutional fit and river basin governance: A new approach using multiple composite measures. *Ecology and Society*, 18(1).
- Leinenkugel, P., Kuenzer, C., Oppelt, N., and Dech, S. (2013). Characterisation of land surface phenology and land cover based on moderate resolution satellite data in cloud prone areas – A novel product for the Mekong Basin. *Remote Sensing of Environment*, 136(0):180–198.
- Leinenkugel, P., Wolters, M. L., Kuenzer, C., Oppelt, N., and Dech, S. (2014). Sensitivity analysis for predicting continuous fields of tree-cover and fractional land-cover distributions in cloud-prone areas. *International Journal of Remote Sensing*, 35(8):2799–2821.
- Li, G. (2005). *Maintaining the healthy life of the Yellow River*. Yellow River Conservancy Press, Zhengzhou.
- Li, G., Wei, H., Han, Y., and Chen, Y. (1998a). Sedimentation in the Yellow River delta, part I: Flow and suspended sediment structure in the upper distributary and the estuary. *Marine Geology*, 149(1-4):93–111.

- Li, G., Wei, H., Yue, S., Cheng, Y., and Han, Y. (1998b). Sedimentation in the Yellow River delta, part II: Suspended sediment dispersal and deposition on the subaqueous delta. *Marine Geology*, 149(1-4):113–131.
- Li, J., Pu, L., Han, M., Zhu, M., Zhang, R., and Xiang, Y. (2014a). Soil salinization research in china: Advances and prospects. *Journal of Geographical Sciences*, 24(5):943–960.
- Li, L., Friedl, M. A., Xin, Q., Gray, J., Pan, Y., and Frolking, S. (2014b). Mapping crop cycles in China using MODIS-EVI time series. *Remote Sensing*, 6(3):2473–2493.
- Li, X., Cheng, G., Jin, H., Kang, E., Che, T., Jin, R., Wu, L., Nan, Z., Wang, J., and Shen, Y. (2008). Cryospheric change in China. *Global and Planetary Change*, 62(3–4):210–218.
- Li, X., Gong, P., and Liang, L. (2015). A 30-year (1984-2013) record of annual urban dynamics of Beijing City derived from Landsat data. *Remote Sensing of Environment*, 166:78–90.
- Li, X.-l., Brierley, G., Shi, D.-j., Xie, Y.-l., and Sun, H.-q. (2012). *Ecological protection and restoration in Sanjiangyuan National Nature Reserve, Qinghai Province, China - Perspectives on environmental management and technology in Asian river basins*. Springer Netherlands, Dordrecht.
- Li, X. W., Huang, S., ren Li, J., Xu, M., and Song, X. (2007). The study of wetlands change in Yellow River delta based on RS and GIS. In *2007 IEEE International Geoscience and Remote Sensing Symposium*, pages 4607–4610.
- Liang, P. and Yang, X. (2016). Landscape spatial patterns in the maowusu (mu us) sandy land, northern china and their impact factors. *Catena*, 145:321 – 333.
- Liang, S., Ge, S., Wan, L., and Xu, D. (2012). Characteristics and causes of vegetation variation in the source regions of the Yellow River, China. *International Journal of Remote Sensing*, 33(5):1529–1542.
- Liaw, A. and Wiener, M. (2002). Classification and regression by randomforest. *R News*, 2(3):18–22.
- Lieberthal, K. and Lampton, D. (1992). *Bureaucrazy, politics, and decision making in post-Mao China*. Berkeley University Press.
- Lillesand, T. and Kiefer, R. (2000). *Remote sensing and image interpretation*. John Wiley & Sons., New York, USA.
- Lindenmayer, D., Franklin, J., and Fischer, J. (2006). General management principles and a checklist of strategies to guide forest biodiversity conservation. *Biological Conservation*, 131(3):433 – 445.
- Liu, J., Li, Z., Zhang, X., Li, R., Liu, X., and Zhang, H. (2013). Responses of vegetation cover to the Grain for Green Program and their driving forces in the He-Long region of the middle reaches of the Yellow River. *Journal of Arid Land*, 5(4):511–520.

- Liu, L., Zhang, B., and Bi, J. (2012). Reforming China's multi-level environmental governance: Lessons from the 11th Five-Year Plan. *Environmental Science & Policy*, 21(0):106–111.
- Lohmar, B., Wang, J., Rozelle, S., Huang, J., and Dawe, D. (2003). Water problems and hydrological research in the Yellow River and the Huai and Hai River basins of China. Technical report, U.S. Department of Agriculture, Agriculture Information Bulletin Number 782, Washington DC.
- Loucks, C. J., Zhi, L., Dinerstein, E., Dajun, W., Dali, F., and Hao, W. (2003). The giant pandas of the Qinling Mountains, China: a case study in designing conservation landscapes for elevational migrants. *Conservation Biology*, 17(2):558–565.
- Loveland, T. R., Reed, B. C., Brown, J. F., Ohlen, D. O., Zhu, Z., Yang, L., and Merchant, J. W. (2000). Development of a global land cover characteristics database and IGBP DISCover from 1 km AVHRR data. *International Journal of Remote Sensing*, 21(6-7):1303–1330.
- Lu, D., Mausel, P., Brondízio, E., and Moran, E. (2004). Change detection techniques. *International Journal of Remote Sensing*, 25(12):2365–2401.

M

- MacDougall, A. H., Avis, C. A., and Weaver, A. J. (2012). Significant contribution to climate warming from the permafrost carbon feedback. *Nature Geosci*, 5(10):719–721.
- Mack, B., Leinenkugel, P., Kuenzer, C., and Dech, S. (2017). A semi-automated approach for the generation of a new land use and land cover product for Germany based on Landsat time-series and Lucas in-situ data. *Remote Sensing Letters*, 8(3):244–253.
- Macklin, M. G. and Lewin, J. (2015). The rivers of civilization. *Quaternary Science Reviews*, 114:228 – 244.
- Matson, P. A., Parton, W. J., Power, A. G., and Swift, M. J. (1997). Agricultural intensification and ecosystem properties. *Science*, 277(5325):504–509.
- Mattiuzzi, M. (2016). *MODIS: MODIS Acquisition and Processing*. R package version 0.10-34/r510.
- Maxwell, S. K., Schmidt, G. L., and Storey, J. C. (2007). A multi-scale segmentation approach to filling gaps in Landsat ETM+ SLC-off images. *International Journal of Remote Sensing*, 28(23):5339–5356.
- McCallum, I., Obersteiner, M., Nilsson, S., and Shvidenko, A. (2006). A spatial comparison of four satellite derived 1 km global land cover datasets. *International Journal of Applied Earth Observation and Geoinformation*, 8(4):246 – 255.
- Meng, E., Hu, R., Shi, X., and Zhang, S. (2006). *Maize in China: Production systems, constraints, and research priorities*. International Maize and Wheat Improvement Center (CIMMYT), El Batán, Mexico.

- Miao, C., Ni, J., and Borthwick, A. G. (2010). Recent changes of water discharge and sediment load in the Yellow River basin, China. *Progress in Physical Geography*, 34(4):541–561.
- Miao, C., Ni, J., Borthwick, A. G., and Yang, L. (2011). A preliminary estimate of human and natural contributions to the changes in water discharge and sediment load in the Yellow River. *Global and Planetary Change*, 76(3-4):196–205.
- Miao, C. Y., Yang, L., Chen, X. H., and Gao, Y. (2012). The vegetation cover dynamics (1982 – 2006) in different erosion regions of the Yellow River Basin , China. *Land Degradation and Development*, 71(October 2010):62–71.
- Millennium Ecosystem Assessment (2005). *Ecosystems and human well-being: general synthesis*. Island Press, Washington DC.
- Milliman, J. D. and Meade, H. (1983). World-wide delivery of river sediment to the oceans. *The Journal of Geology*, 91(1):1–21.
- Milliman, J. D., Qin, Y. S., and Ren, M.-E. (1987). Mans influence on the erosion and transport of sediment by Asian rivers: the Yellow River (Huanghe) example. *Journal of Geology*, 95:751–762.
- Miyamoto, M., Parid, M. M., Aini, Z. N., and Michinaka, T. (2014). Proximate and underlying causes of forest cover change in peninsular malaysia. *Forest Policy and Economics*, 44:18 – 25.
- Moss, T. (2004). The governance of land use in river basins: Prospects for overcoming problems of institutional interplay with the EU water framework directive. *Land Use Policy*, 21(1):85 – 94.
- Müller, H., Griffiths, P., and Hostert, P. (2016). Long-term deforestation dynamics in the Brazilian Amazon - Uncovering historic frontier development along the Cuiabá - Santarém highway. *International Journal of Applied Earth Observation and Geoinformation*, 44:61–69.
- Müller, H., Rufin, P., Griffiths, P., Barros Siqueira, A. J., and Hostert, P. (2015). Mining dense Landsat time series for separating cropland and pasture in a heterogeneous Brazilian savanna landscape. *Remote Sensing of Environment*, 156:490–499.
- Myint, T. (2003). Democracy in global environmental governance: issues, interests, and actors in the Mekong and Rhine. *Indiana Journal of Global Legal Studies*, 10:287–314.

N

- Nagendra, H., Lucas, R., Honrado, J. P., Jongman, R. H. G., Tarantino, C., Adamo, M., and Mairota, P. (2013a). Remote sensing for conservation monitoring: Assessing protected areas, habitat extent, habitat condition, species diversity, and threats. *Ecological Indicators*, 33(0):45–59.
- Nagendra, H., Reyers, B., and Lavorel, S. (2013b). Impacts of land change on biodiversity: Making the link to ecosystem services. *Current Opinion in Environmental Sustainability*, 5(5):503 – 508.

Nakayama, T. (2011). Simulation of the effect of irrigation on the hydrologic cycle in the highly cultivated Yellow River Basin. *Agricultural and Forest Meteorology*, 151(3):314–327.

NBS (2015). China Statistical Database of the National Bureau of Statistics of China.

Ni, J. (2011). Impacts of climate change on Chinese ecosystems: Key vulnerable regions and potential thresholds. *Regional Environmental Change*, 11(1):49–64.

O

Ojima, D. S., Galvin, K. A., and Turner, B. L. (1994). The global impact of land-use change. *BioScience*, 44(5):300–304.

Olofsson, P., Foody, G. M., Herold, M., Stehman, S. V., Woodcock, C. E., and Wulder, M. A. (2014). Good practices for estimating area and assessing accuracy of land change. *Remote Sensing of Environment*, 148:42 – 57.

Olofsson, P., Foody, G. M., Stehman, S. V., and Woodcock, C. E. (2013). Making better use of accuracy data in land change studies: Estimating accuracy and area and quantifying uncertainty using stratified estimation. *Remote Sensing of Environment*, 129:122 – 131.

Olson, D. M., Dinerstein, E., Wikramanayake, E. D., Burgess, N. D., Powell, G. V. N., Underwood, E. C., D'amico, J. A., Itoua, I., Strand, H. E., Morrison, J. C., Loucks, C. J., Allnutt, T. F., Ricketts, T. H., Kura, Y., Lamoreux, J. F., Wettengel, W. W., Hedao, P., and Kassem, K. R. (2001). Terrestrial ecoregions of the world: A new map of life on earth. *BioScience*, 51(11):933–938.

Ongley, E. D. (2009). The Yellow River: Managing the unmanageable. *Water International*, 25:2(June 2013):37–41.

Ongley, E. D. and Wang, X. (2004). Transjurisdictional water pollution management in China: The legal and institutional framework. *Water International*, 29(3):270–281.

Ostrom, E. (2009). A general framework for analyzing sustainability of social-ecological systems. *Science*, 325(5939):419–422.

Ottinger, M., Kuenzer, C., Liu, G., Wang, S., and Dech, S. (2013). Monitoring land cover dynamics in the Yellow River Delta from 1995 to 2010 based on Landsat 5 TM. *Applied Geography*, 44:53–68.

P

Parrott, L., Chion, C., Gonzales, R., and Latombe, G. (2012). Agents, individuals, and networks: Modeling methods to inform natural resource management in regional landscapes. *Ecology and Society*, 17(3).

Peel, M. C., Finlayson, B. L., and McMahon, T. A. (2007). Updated world map of the Köppen-Geiger climate classification. *Hydrology and Earth System Sciences*, 11(5):1633–1644.

Peng, J., Chen, S., and Dong, P. (2010). Temporal variation of sediment load in the Yellow River basin, China, and its impacts on the lower reaches and the river delta. *Catena*, 83(2-3):135–147.

Piao, S., Ciais, P., Huang, Y., Shen, Z., Peng, S., Li, J., Zhou, L., and Liu, H. (2010). The impact of climate change on water resources and agriculture in China. *Nature*, 467:43–51.

Q

Qureshi, A. S., Hussain, A., and Makin, I. (2002). Integrated database development for river basin management: An example from Rechna Doab. IWMI Working Papers H035618, International Water Management Institute.

R

R Core Team (2016). *R: A language and environment for statistical computing*. R Foundation for Statistical Computing, Vienna, Austria.

Ran, L. and Lu, X. X. (2012). Delineation of reservoirs using remote sensing and their storage estimate: an example of the Yellow River basin, China. *Hydrological Processes*, 26(8):1215–1229.

Ran, Y., Li, X., and Lu, L. (2010). Evaluation of four remote sensing based land cover products over China. *International Journal of Remote Sensing*, 31(2):391–401.

Richter, R. (2007). *Atmospheric/topographic correction for satellite imagery*. ATCOR-2/3 user guide. ATCOR-2/3 User Guide, Version 6.3.

Ringler, C., Cai, X., Wang, J., Ahmed, A., Xue, Y., Xu, Z., Yang, E., Jianshi, Z., Zhu, T., Cheng, L., Yongfeng, F., Xinfeng, F., Xiaowei, G., and You, L. (2010). Yellow River basin: Living with scarcity. *Water International*, 35(5):681–701.

Rockstrom, J., Steffen, W., Noone, K., Persson, A., Chapin, F. S., Lambin, E. F., Lenton, T. M., Scheffer, M., Folke, C., Schellnhuber, H. J., Nykvist, B., de Wit, C. A., Hughes, T., van der Leeuw, S., Rodhe, H., Sorlin, S., Snyder, P. K., Costanza, R., Svedin, U., Falkenmark, M., Karlberg, L., Corell, R. W., Fabry, V. J., Hansen, J., Walker, B., Liverman, D., Richardson, K., Crutzen, P., and Foley, J. A. (2009). A safe operating space for humanity. *Nature*, 461(7263):472–475.

Rudel, T. K., Schneider, L., Uriarte, M., Turner, B. L., DeFries, R., Lawrence, D., Geoghegan, J., Hecht, S., Ickowitz, A., Lambin, E. F., Birkenholtz, T., Baptista, S., and Grau, R. (2009). Agricultural intensification and changes in cultivated areas, 1970 – 2005. *Proceedings of the National Academy of Sciences*, 106(49):20675–20680.

S

- Savitzky, A. and Golay, M. J. E. (1964). Smoothing and differentiation of data by simplified least squares procedures. *Anal. Chem.*, 36(8):1627–1639.
- Schneider, A. (2012). Monitoring land cover change in urban and peri-urban areas using dense time stacks of Landsat satellite data and a data mining approach. *Remote Sensing of Environment*, 124:689–704.
- Scholz, R. W., Binder, C. R., and Lang, D. J. (2011). The HES framework. In Scholz, R. W., editor, *Environmental literacy in science and society*, pages 453–462. Cambridge University Press.
- Sedano, F., Gong, P., and Ferráo, M. (2005). Land cover assessment with MODIS imagery in southern African Miombo ecosystems. *Remote Sensing of Environment*, 98(4):429 – 441.
- Shao, Z. and Liu, C. (2014). The integrated use of DMSP-OLS nighttime light and MODIS data for monitoring large-scale impervious surface dynamics: A case study in the Yangtze River Delta. *Remote Sensing*, 6(10).
- Shi, H. and Shao, M. (2000). Soil and water loss from the Loess Plateau in China. *Journal of Arid Environments*, 45(1):9–20.
- Siebert, S., Portmann, F. T., and Döll, P. (2010). Global patterns of cropland use intensity. *Remote Sensing*, 2(7):1625–1643.
- Small, C., Pozzi, F., and Elvidge, C. (2005). Spatial analysis of global urban extent from DMSP-OLS night lights. *Remote Sensing of Environment*, 96(3–4):277 – 291.
- Song, X., Ravesteijn, W., Frostell, B., and Wennersten, R. (2010). Managing water resources for sustainable development: The case of integrated river basin management in China. *Water Science and Technology*, 61(2):499–506.
- Song, X., Yang, G., Yan, C., Duan, H., Liu, G., and Zhu, Y. (2009). Driving forces behind land use and cover change in the Qinghai-Tibetan Plateau: A case study of the source region of the Yellow River, Qinghai Province, China. *Environmental Earth Sciences*, 59(4):793–801.
- Song, Z. and Kuenzer, C. (2014). Coal fires in china over the last decade: A comprehensive review. *International Journal of Coal Geology*, 133:72 – 99.
- Starvins, R. N. (2000). Market based environmental policies. In Portney, P. N. and Stavins, R. N., editors, *Public Policies for Environmental Protection*, pages 31–77. Resources of the Future, Washington DC.
- Steffen, W., Crutzen, P. J., and McNeill, J. R. (2007). The Anthropocene: Are humans now overwhelming the great forces of nature. *AMBIO: A Journal of the Human Environment*, 36(8):614–621.

- Stehman, S. V. (2009). Sampling designs for accuracy assessment of land cover. *International Journal of Remote Sensing*, 30(20):5243–5272.
- Stehman, S. V. and Czaplewski, R. L. (1998). Design and analysis for thematic map accuracy assessment: Fundamental principles. *Remote Sensing of Environment*, 64(3):331 – 344.
- Stow, D. A., Shih, H.-C., and Coulter, L. L. (2014). Discrete classification approach to land cover and land use change identification based on Landsat image time sequences. *Remote Sensing Letters*, 5(10):922–931.
- Strahler, A. H., Boschetti, L., Foody, G. M., Friedl, M. A., Hansen, M. C., Herold, M., Morisette, J. T., Stehman, S. V., and Woodcock, C. E. (2006). Global land cover validation: Recommendations for evaluation and accuracy assessment of global land cover maps.
- Summers, D. M., Bryan, B. A., Nolan, M., and Hobbs, T. J. (2015). The costs of reforestation: A spatial model of the costs of establishing environmental and carbon plantings. *Land Use Policy*, 44:110 – 121.
- Syvitski, J. P. M., Kettner, A. J., Overeem, I., Hutton, E. W. H., Hannon, M. T., Brakenridge, G. R., Day, J., Vorosmarty, C., Saito, Y., Giosan, L., and Nicholls, R. J. (2009). Sinking deltas due to human activities. *Nature Geosci*, 2(10):681–686.

T

- Tang, Q., Oki, T., Kanae, S., and Hu, H. (2008). A spatial analysis of hydro-climatic and vegetation condition trends in the Yellow River basin. *Hydrological Processes*, 458(October 2007):451–458.
- Tao, F., Hayashi, Y., Zhang, Z., Sakamoto, T., and Yokozawa, M. (2008). Global warming, rice production, and water use in China: Developing a probabilistic assessment. *Agricultural and Forest Meteorology*, 148(1):94–110.
- Tao, F. and Zhang, Z. (2013). Climate change, wheat productivity and water use in the North China Plain: A new super-ensemble-based probabilistic projection. *Agricultural and Forest Meteorology*, 170:146–165.
- Tateishi, R., Uriyangqai, B., Al-Bilbisi, H., Ghar, M. A., Tsend-Ayush, J., Kobayashi, T., Kasimu, A., Hoan, N. T., Shalaby, A., Alsaadeh, B., Enkhzaya, T., Gegentana, and Sato, H. P. (2011). Production of global land cover data - GLCNMO. *International Journal of Digital Earth*, 4(1):22–49.
- Thompson, S. D., Nelson, T. A., White, J. C., and Wulder, M. A. (2015). Mapping dominant tree species over large forested areas using Landsat best-available-pixel image composites. *Canadian Journal of Remote Sensing*, 41(3):203–218.
- Tilman, D., Fargione, J., Wolff, B., D'Antonio, C., Dobson, A., Howarth, R., Schindler, D., Schlesinger, W. H., Simberloff, D., and Swackhamer, D. (2001). Forecasting agriculturally driven global environmental change. *Science*, 292(5515):281–284.

- Tisdell, C. (2009). Economic reforms and openness in China: China's policies in the last 30 years. *Economic Analysis & Policy*, 39:271–294.
- Tucker, C. J. (1979). Red and photographic infrared linear combinations for monitoring vegetation. *Remote Sensing of Environment*, 8(2):127 – 150.
- Turner, J. (2005). River basin governance in China. *China Environmental Series*, 7:106 – 110.
- Turner, W. R., Brandon, K., Brooks, T. M., Costanza, R., da Fonseca, G. A. B., and Portela, R. (2007). Global conservation of biodiversity and ecosystem services. *BioScience*, 57(10):868.

U

- Uchida, E., Xu, J., and Rozelle, S. (2005). Grain for green: Cost-effectiveness and eustainability of china's conservation set-aside program. *Land Economics*, 81(2):247–264.
- Uchida, E., Xu, J., Xu, Z., and Rozelle, S. (2007). Are the poor benefiting from China's land conservation program? *Environment and Development Economics*, 12(4):593–620.
- UNDP (1999). China Human Development Report 1999: Transition and the state. Technical report, United Nations Development Programme, New York: Oxford University Press.
- UNEP (2016). Global trends in renewable engery investment 2016. Technical report, United Nations Environmental Programme, Frankfurt School of Finance & Management.

V

- Varis, O. and Vakkilainen, P. (2001). China's 8 challenges to water resources management in the first quarter of the 21st Century. *Geomorphology*, 41(2–3):93–104.
- Vitousek, P. M. (1994). Beyond global warming: Ecology and Global Change. *Ecology*, 75(7):1861–1876.
- Vogelmann, J. E., Tolk, B., and Zhu, Z. (2009). Monitoring forest changes in the southwestern United States using multitemporal Landsat data. *Remote Sensing of Environment*, 113(8):1739 – 1748.

W

- Wang, H., Gao, J., Ren, L.-L., Kong, Y., Li, H., and Li, L. (2012a). Assessment of the red-crowned crane habitat in the Yellow River Delta Nature Reserve, East China. *Regional Environmental Change*, 13(1):115–123.
- Wang, H., Yang, Z., Saito, Y., Liu, J. P., and Sun, X. (2006). Interannual and seasonal variation of the Huanghe (Yellow River) water discharge over the past 50years: Connections to impacts from ENSO events and dams. *Global and Planetary Change*, 50(3–4):212 – 225.

- Wang, H., Yang, Z., Saito, Y., Liu, J. P., Sun, X., and Wang, Y. (2007). Stepwise decreases of the Huanghe (Yellow River) sediment load (1950 – 2005): Impacts of climate change and human activities. *Global and Planetary Change*, 57(3-4):331–354.
- Wang, J., Liu, Y., and Liu, Z. (2013). Spatio-temporal patterns of cropland conversion in response to the “Grain for Green Project” in China’s Loess hilly region of Yanchuan County. *Remote Sensing*, 5(11):5642–5661.
- Wang, M., Qi, S., and Zhang, X. (2012b). Wetland loss and degradation in the Yellow River Delta, Shandong Province of China. *Environmental Earth Sciences*, 67(1):185–188.
- Wang, S., Ding, C., and Liu, J. (2009). Landscape evolution in the Yellow River Basin using satellite remote sensing and GIS during the past decade. *International Journal of Remote Sensing*, 30(21):5573–5591.
- Wang, S., Fu, B., Piao, S., Lu, Y., Ciais, P., Feng, X., and Wang, Y. (2016). Reduced sediment transport in the Yellow River due to anthropogenic changes. *Nature Geosci*, 9(1):38–41.
- Wang, X.-j., Zhang, J.-y., He, R.-m., Amgad, E., Sondoss, E., and Shang, M. (2011). A strategy to deal with water crisis under climate change for mainstream in the middle reaches of Yellow River. *Mitigation and Adaptation Strategies for Global Change*, 16(5):555–566.
- Webber, M., Barnett, J., Wang, M., Finlayson, B., and Dickinson, D. (2008). The Yellow River in transition. *Environmental Science & Policy*, 11(5):422–429.
- Wei, J., Zhou, J., Tian, J., He, X., and Tang, K. (2006). Decoupling soil erosion and human activities on the Chinese Loess Plateau in the 20th century. *CATENA*, 68(1):10–15.
- Wen, D., Zhang, F., Zhang, E., Gao, C., and Han, Z. (2009). Outline of the Yellow River basin, China. *Bulletin of the Geological Survey of Japan*, 60:9–18.
- White, J. C., Wulder, M. A., Hobart, G. W., Luther, J. E., Hermosilla, T., Griffiths, P., Coops, N. C., Hall, R. J., Hostert, P., Dyk, A., and Guindon, L. (2014). Pixel-based image compositing for large-area dense time series applications and science. *Canadian Journal of Remote Sensing*, 40(3):192–212.
- Williams, D. L., Goward, S., and Arvidson, T. (2006). Landsat: Yesterday, today, and tomorrow. *Photogrammetric Engineering & Remote Sensing*, 72(10):1171–1178.
- Wohlfart, C., Bevanda, M., Hornig, N., Leutner, B., and Wegmann, M. (2016a). Field data for remote sensing data analysis. In Wegmann, M., Leutner, B., and Dech, S., editors, *Remote sensing and GIS for ecologists using open source software*, chapter Field data for remote sensing data analysis, pages 136 – 149. Pelagic Publishing.
- Wohlfart, C., Kuenzer, C., Chen, C., and Liu, G. (2016b). Social-ecological challenges in the Yellow River basin (China): A review. *Environmental Earth Sciences*, 75(13):1–20.

- Wohlfart, C., Liu, G., Huang, C., and Kuenzer, C. (2016c). A river basin over the course of time: Multi-temporal analyses of land surface dynamics in the Yellow River Basin (China) based on medium resolution remote sensing data. *Remote Sensing*, 8(3).
- Wohlfart, C., Mack, B., Liu, G., and Kuenzer, C. (2017). Multi-faceted land cover and land use change analyses in the yellow river basin based on dense landsat time series: Exemplary analysis in mining, agriculture, forest, and urban areas. *Applied Geography*, 85:73 – 88.
- Wohlfart, C., Wegmann, M., and Leimgruber, P. (2014). Mapping threatened dry deciduous dipterocarp forest in South-East Asia for conservation management. *Tropical Conservation Science*, 7(4):597–613.
- Woodcock, C. E., Allen, R., Anderson, M., Belward, A., Bindschadler, R., Cohen, W., Gao, F., Goward, S. N., Helder, D., Helmer, E., Nemani, R., Oreopoulos, L., Schott, J., Thenkabail, P. S., Vermote, E. F., Vogelmann, J., Wulder, M. A., and Wynne, R. (2008). Free access to Landsat imagery. *Science*, 320(5879):1011 LP – 1011.
- World Bank (2014). Urban China: Towards efficient, inclusive, and sustainable urbanization. Technical report, World Bank, Washington DC.
- World Bank (2016). World Development Indicators Database.
- Wu, B., Wang, Z., and Li, C. (2004). Yellow River Basin management and current issues. *Journal of Geographical Sciences*, 14(50239040):29–37.
- Wu, C. S., Yang, S. L., and Lei, Y.-p. (2012). Quantifying the anthropogenic and climatic impacts on water discharge and sediment load in the Pearl River (Zhujiang), China (1954 – 2009). *Journal of Hydrology*, 452–453(0):190–204.
- Wu, J., Vincent, B., Yang, J., Bouarfa, S., and Vidal, A. (2008a). Remote sensing monitoring of changes in soil salinity: A case study in Inner Mongolia, China. *Sensors (Basel, Switzerland)*, 8(11):7035–7049.
- Wu, Q., Hou, Y., Yun, H., and Liu, Y. (2015). Changes in active-layer thickness and near-surface permafrost between 2002 and 2012 in alpine ecosystems, Qinghai–Xizang (Tibet) Plateau, China. *Global and Planetary Change*, 124:149–155.
- Wu, W., Shibasaki, R., Yang, P., Ongaro, L., Zhou, Q., and Tang, H. (2008b). Validation and comparison of 1 km global land cover products in China. *International Journal of Remote Sensing*, 29(13):3769–3785.
- Wulder, M. A., White, J. C., Loveland, T., Woodcock, C., Belward, A., Cohen, W. B., Fosnight, E. A., Shaw, J., Masek, J. G., and Roy, D. P. (2016). The global Landsat archive: Status, consolidation, and direction. *Remote Sensing of Environment*, 185:271–283.
- Wulder, M. A., White, J. C., Masek, J. G., Dwyer, J., and Roy, D. P. (2011). Continuity of Landsat observations: Short term considerations. *Remote Sensing of Environment*, 115(2):747–751.

X

- Xia, C. and Pahl-Wostl, C. (2012). The development of water allocation management in the Yellow River Basin. *Water Resources Management*, 26(12):3395–3414.
- Xia, X., Zhou, J., and Yang, Z. (2002). Nitrogen contamination in the Yellow River Basin of China. *Journal of Environmental Quality*, 31.
- Xie, Y., Sha, Z., and Yu, M. (2008). Remote sensing imagery in vegetation mapping: A review. *Journal of Plant Ecology*, 1(1):9.
- Xu, H. (1999). Environmental policy and rural industrial development in China. *Research in Human Ecology*, 6(2):72–80.
- Xu, J., Yin, R., Li, Z., and Liu, C. (2006a). China's ecological rehabilitation: Unprecedented efforts, dramatic impacts, and requisite policies. *Ecological Economics*, 57(4):595 – 607.
- Xu, J., Zhang, Z., Liu, W., and McGowan, P. J. K. (2012). A review and assessment of nature reserve policy in China: Advances, challenges and opportunities. *Oryx*, 46(04):554–562.
- Xu, X., Lin, H., and Fu, Z. (2004). Probe into the method of regional ecological risk assessment: A case study of wetland in the Yellow River Delta in China. *Journal of Environmental Management*, 70(3):253–262.
- Xu, Z., Xu, J., Deng, X., Huang, J., Uchida, E., and Rozelle, S. (2006b). Grain for Green versus grain: Conflict between food security and conservation set-aside in China. *World Development*, 34(1):130 – 148.

Y

- Yan, C., Song, X., Zhou, Y., Duan, H., and Li, S. (2009). Assessment of aeolian desertification trends from 1975's to 2005's in the watershed of the Longyangxia Reservoir in the upper reaches of China's Yellow River. *Geomorphology*, 112(3-4):205 – 211.
- Yancheva, G., Nowaczyk, N. R., Mingram, J., Dulski, P., Schettler, G., Negendank, J. F. W., Liu, J., Sigman, D. M., Peterson, L. C., and Haug, G. H. (2007). Influence of the intertropical convergence zone on the East Asian monsoon. *Nature*, 445(7123):74–77.
- Yang, D. and Ishidaira, H. (2010). Profile of the Yellow River Basin. In Kusuda, T., editor, *The Yellow River - Water and Life*, pages 5–24. World Scientific Publishing, Singapore.
- Yang, D., Li, C., Hu, H., Lei, Z., Yang, S., Kusuda, T., Koike, T., and Musiaka, K. (2004). Analysis of water resources variability in the Yellow River of China during the last half century using historical data. *Water Resources Research*, 40(6):W06502.
- Yang, Y., Xiao, P., Feng, X., and Li, H. (2017). Accuracy assessment of seven global land cover datasets over China. *ISPRS Journal of Photogrammetry and Remote Sensing*, 125:156 – 173.

- Ye, D. and Dong, W. (2010). Coordinated research on orderly human activity to cope with global climate change - our thoughts and recommendations. *Advances in Climate Change Research*, 1(1):46 – 48.
- Ye, Q. and Glantz, M. H. (2005). The 1998 Yangtze Floods: The use of short-term forecasts in the context of seasonal to interannual water resource management. *Mitigation and Adaptation Strategies for Global Change*, 10(1):159–182.
- YRCC (2015). Yellow River Water Resources Bulletins.
- Yu, L. (2002). The Huanghe (Yellow) River: A review of its development, characteristics, and future management issues. *Continental Shelf Research*, 22(3):389–403.
- Yu, L. (2006). The Huanghe (Yellow) River: Recent changes and its countermeasures. *Continental Shelf Research*, 26(17–18):2281–2298.
- Yu, R., Liu, T., Xu, Y., Zhu, C., Zhang, Q., Qu, Z., Liu, X., and Li, C. (2010). Analysis of salinization dynamics by remote sensing in Hetao Irrigation District of North China. *Agricultural Water Management*, 97(12):1952 – 1960. Salinity Management in China.
- Yue, T. X., Liu, J. Y., Jørgensen, S. E., and Ye, Q. H. (2003). Landscape change detection of the newly created wetland in Yellow River Delta. *Ecological Modelling*, 164(1):21–31.
- Yue, T. X., Xu, B., and Liu, J. Y. (2004). A patch connectivity index and its change in relation to new wetland at the Yellow River Delta. *International Journal of Remote Sensing*, 25(21):4617–4628.

Z

- Zha, Y., Gao, J., and Ni, S. (2003). Use of normalized difference built-up index in automatically mapping urban areas from TM imagery. *International Journal of Remote Sensing*, 24(3):583–594.
- Zhai, J., Liu, R., Liu, J., Huang, L., and Qin, Y. (2015). Human-induced landcover changes drive a diminution of land surface albedo in the loess plateau (china). *Remote Sensing*, 7(3):2926–2941.
- Zhai, P., Yu, R., Guo, Y., Li, Q., Ren, X., Wang, Y., Xu, W., Liu, Y., and Ding, Y. (2016). The strong El Niño of 2015/16 and its dominant impacts on global and China's climate. *Journal of Meteorological Research*, 30(3):283–297.
- Zhang, J., Lu, H., Gu, W., Wu, N., Zhou, K., Hu, Y., Xin, Y., and Wang, C. (2012). Early mixed farming of millet and rice 7800 years ago in the middle Yellow River region, China. *PLOS ONE*, 7(12):1–8.
- Zhang, J., Wen Huang, W., and Chong Shi, M. (1990). Huanghe (Yellow River) and its estuary: Sediment origin, transport and deposition. *Journal of Hydrology*, 120(1–4):203–223.

- Zhang, K.-m. and Wen, Z.-g. (2008). Review and challenges of policies of environmental protection and sustainable development in China. *Journal of Environmental Management*, 88(4):1249–1261.
- Zhang, Q., Xu, C.-y., Becker, S., and Jiang, T. (2006). Sediment and runoff changes in the Yangtze River basin during past 50 years. *Journal of Hydrology*, 331(3–4):511–523.
- Zhang, Z., Wang, X., Zhao, X., Liu, B., Yi, L., Zuo, L., Wen, Q., Liu, F., Xu, J., and Hu, S. (2014). A 2010 update of national land use/cover database of china at 1:100000 scale using medium spatial resolution satellite images. *Remote Sensing of Environment*, 149:142 – 154.
- Zhang, Z., Xu, H., and Wang, R. (2005). *The formation of Chinese civilization - An archaeological Perspective*. Yale University and New World Press.
- Zhao, D., Kuenzer, C., Fu, C., and Wagner, W. (2008). Evaluation of the ERS scatterometer-derived soil water index to monitor water availability and precipitation distribution at three different scales in China. *Journal of Hydrometeorology*, 9(3):549–562.
- Zhao, G. X., Lin, G., and Warner, T. (2004). Using Thematic Mapper data for change detection and sustainable use of cultivated land: a case study in the Yellow River delta, China. *International Journal of Remote Sensing*, 25(13):2509–2522.
- Zhao, T., Xu, H., He, Y., Tai, C., Meng, H., Zeng, F., and Xing, M. (2009). Agricultural non-point nitrogen pollution control function of different vegetation types in riparian wetlands: A case study in the Yellow River wetland in China. *Journal of Environmental Sciences*, 21:933–939.
- Zhen, L. and Zhang, H. (2011). Payment for ecosystem services in China: An overview. *Living Reviews*, 5.
- Zheng, Q., Zeng, Y., Deng, J., Wang, K., Jiang, R., and Ye, Z. (2017). “Ghost cities” identification using multi-source remote sensing datasets: A case study in Yangtze River Delta. *Applied Geography*, 80:112 – 121.
- Zhou, D., Lin, Z., and Liu, L. (2012). Regional land salinization assessment and simulation through cellular automaton-markov modeling and spatial pattern analysis. *Science of The Total Environment*, 439:260 – 274.
- Zhou, H., Van Rompaey, A., and Wang, J. (2009). Detecting the impact of the “Grain for Green” program on the mean annual vegetation cover in the Shaanxi province, China using SPOT-VGT NDVI data. *Land Use Policy*, 26(4):954–960.
- Zhou, S., Yin, Y., Xu, W., Ji, Z., Caldwell, I., and Ren, J. (2007). The costs and benefits of reforestation in Liping County, Guizhou Province, China. *Journal of Environmental Management*, 85(3):722 – 735. Carbon Sequestration In China’s Forest Ecosystems.
- Zhou, W.-L., Jin, N., Lin, Z., and Wu, G.-X. (2015). From global change to future earth in china. *Advances in Climate Change Research*, 6(2):92 – 100. Special issue on advances in Future Earth research.

- Zhou, Z. C., Shangguan, Z. P., and Zhao, D. (2006). Modeling vegetation coverage and soil erosion in the Loess Plateau Area of China. *Ecological Modelling*, 198(1–2):263–268.
- Zhu, Y., Zhang, Y., Wen, H., Lu, Z., Jia, Z., Li, Y., Li, Q., Liu, C., Wang, P., and Guo, X. (2010). Gas hydrates in the Qilian Mountain permafrost, Qinghai, northwest China. *Acta Geologica Sinica - English Edition*, 84(1):1–10.
- Zhu, Z., Cai, X., Giordano, M., Molden, D., Hong, S., Zhang, H., Lian, Y., Li, H., Zhang, X., and Xue, Y. (2003). Yellow River Comprehensive Assessment Yellow River Comprehensive Assessment: Basin features and issues. Technical report, International Water Management Institute, Colombo.
- Zhu, Z., Giordano, M., Cai, X., and Molden, D. (2004). The Yellow River Basin: Water accounting, water accounts, and current issues. *Water International*, 29(1):2–10.
- Zhu, Z., Wang, S., and Woodcock, C. E. (2015). Improvement and expansion of the Fmask algorithm: Cloud, cloud shadow, and snow detection for Landsats 4–7, 8, and Sentinel 2 images. *Remote Sensing of Environment*, 159:269–277.
- Zhu, Z. and Woodcock, C. E. (2012). Object-based cloud and cloud shadow detection in Landsat imagery. *Remote Sensing of Environment*, 118:83–94.
- Zhuo, L., Mekonnen, M. M., Hoekstra, A. Y., and Wada, Y. (2016). Inter- and intra-annual variation of water footprint of crops and blue water scarcity in the Yellow River basin (1961–2009). *Advances in Water Resources*, 87:29–41.

Christian Wohlfart

curriculum vitæ

Persönliche Daten

Geburtsdatum **26. August 1985**
in Bad Kissingen, Deutschland

Nationalität **Deutsch**

Ausbildung

- 2013 – 2017 **Dissertation**, Deutsches Zentrum für Luft- und Raumfahrt (DLR) in Kooperation mit der Universität Würzburg und SLU (Sachverständigenbüro für Luftbildauswertung und Umweltfragen)
'The Yellow River Basin in Transition - Multi-faceted Land Cover Change Analysis in the Yellow River Basin in the Context of Global Change Using Multi-sensor Remote Sensing Imagery'
- 2010 – 2013 **M.Sc. Global Change Ecology**, *Universität Bayreuth*, im Elitenetzwerk Bayern, *Abschlussnote: 1.2*
Thesis: 'Mapping tropical dry forest in South East Asia using a continuous cover approach'
Fokus: Erdbeobachtung, Ökosystemdienstleistungen, räumliche Statistik, Zeitserienanalysen
- 2007 – 2010 **B.Sc. Geoökologie**, *Universität Bayreuth*, *Abschlussnote: 1.9*
Thesis: 'Frost hardiness of Pinus nigra as influenced by local adaption, summer drought and summer warming'
Fokus: Biogeographie, GIS, Winterökologie, Statistik
- 2006 **Abitur**, *Rhön-Gymnasium Bad Neustadt*, **Prüfungsfächer:** Geographie, Mathematik, Chemie, Englisch

Berufserfahrung und Praktika

- seit 2017 **Wissenschaftlicher Angestellter**, *Deutsches Zentrum für Luft- und Raumfahrt (DLR)*, Wessling, Deutschland
- Jul 2016 – 2017 **Wissenschaftlicher Angestellter**, *Sachverständigenbüro für Luftbildauswertung und Umweltfragen (SLU)*, München, Deutschland
- Mär – Jul 2012 **Praktikum**, *Smithsonian Conservation Biological Institution (SCBI)*, Front Royal, USA
- Jul – Sep 2011 **Praktikum**, *Deutsches Zentrum für Luft- und Raumfahrt (DLR)*, *Deutsches Fernerkundungsdatenzentrum (DFD)*, Wessling, Deutschland
- 2007 – 2012 **Studentische Hilfskraft**, *Universität Bayreuth*, Deutschland
- Aug – Sep 2007 **Praktikum**, *OPUS (Ökologische Planungen, Umweltstudien und Service)*, Bayreuth, Deutschland

Bahnhofstr. 1 – 83673 Bichl – Germany

☎ +49 (171) 5816950 • 📞 +49 (8856) 9378238

✉ christian.wohlfart@gmx.de • in Christian Wohlfart • 🐦 cwohlfart

1/3

Computerkenntnisse

Betriebssysteme	Mac OS X, Windows, Solaris, Linux
Office Software	Microsoft Word/Excel/Power Point, L ^A T _E X, LibreOffice
Bild- und Datenanalyse	Quantum Gis, ArcGIS, GRASS GIS, GDAL, ENVI, Erdas Imagine
Programmierung	R Statistical Programming, Bash, HTML, Python
Datenbanken	PostGis, SQLite

Sprachkenntnisse

Deutsch	Muttersprache
Englisch	Verhandlungssicher
Französisch	Grundkenntnisse

Science Schools und Workshops

- 2015 **Spatio-temporal data analyses using free and open source software**, Matera, Italien
- 2012 **An introduction to bayesian modeling for ecologists**, Bayreuth, Deutschland
- 2011 **Summer school of biodiversity of islands in face of climate change**, La Palma, Spanien
- 2010 **CBD Workshop**, Bayreuth, Deutschland

Publikationen

- 2018 Wessel, B., Huber, M., **Wohlfart, C.**, Marschalk U., Kosmann, D., Roth, A.: Accuracy assessment of the global TanDEM-X Digital Elevation Model with GPS data. *ISPRS Journal of Photogrammetry and Remote Sensing*, 139, 171 –182.
- 2017 Da Ponte, E., Mack, B., **Wohlfart, C.**, Rodas, O., Fleckenstein, M., Oppelt, Natascha, Dech, S., Kuenzer, C.: Assessing Forest Cover Dynamics and Forest Perception in the Atlantic Forest of Paraguay, Combining Remote Sensing and Household Level Data. *Forests*, 8, 389.
- 2017 **Wohlfart, C.**, Mack, B., Liu, G., Kuenzer, C.: Multi-faceted land cover and land use change analyses in the Yellow River Basin based on dense Landsat time series: Exemplary analysis in mining, agriculture, forest, and urban areas. *Applied Geography*, 85, 73 – 88.
- 2016 **Wohlfart, C.**, Liu, G., Chong, H., Kuenzer, C.: A river over the course of time – multi-temporal analyses of land surface dynamics in the Yellow River basin (China) based on medium resolution remote sensing data. *Remote Sensing*, 8, 2 – 25.
- 2015 **Wohlfart, C.**, Kuenzer, C, Cui, C., Liu, G.: Socio-ecological challenges in the Yellow River Basin (China): a review. *Environmental Earth Sciences*, 75(13).
- 2015 Ziegler, S., Fa, J.E., **Wohlfart, C.**, Streit, B., Jacob, S., Wegmann, M.: Mapping bushmeat hunting pressure in Central Africa. *Biotropica*, 48(3).

Bahnhofstr. 1 – 83673 Bichl – Germany

☎ +49 (171) 5816950 • 📞 +49 (8856) 9378238

✉ christian.wohlfart@gmx.de • in Christian Wohlfart • 🐦 cwohlfart

2/3

- 2014 **Wohlfart, C.**, Wegmann, M., Leimgruber, P.: Mapping threatened dry deciduous dipterocarp forest in South-east Asia for conservation management. *Tropical Conservation Science*, 7: 597 - 613.
- 2014 Irl, D. H. S., Steinbauer, M. J., Epperlein, L., Harter, D. E. V., Jentsch, A., Paetz, S., **Wohlfart, C.**, Beierkunlein, C.: The Hitchhiker's guide to island endemism: biodiversity and endemic perennial plant species in roadside and surrounding vegetation. *Biodiversity and Conservation*, 23: 2273 - 2287.
- 2012 Kreyling, J., Wiesenberg, G.L.B., Thiel, D., **Wohlfart, C.**, Huber, G., Walter, J., Jentsch, A., Konnert, M., Beierkuhnlein, C.: Cold hardiness of *Pinus nigra* Arnold as influenced by geographic origin, warming, and extreme summer drought. *Environmental and Experimental Botany*, 78, 99 - 108.

Buchbeiträge

- 2016 **Wohlfart, C.**, Bevarna, M., Hornig, N., Leutner, B., Wegmann, M.: Field data for remote sensing data analysis. *in book: Remote Sensing and GIS for ecologists*, Pelagic Publishing.
- 2016 Verbesselt, J., Leutner, B., **Wohlfart, C.**, Wegmann, M.: Time series analyses. *in book: Remote Sensing and GIS for ecologists*, Pelagic Publishing.